UNIVERSIDAD NACIONAL DE COLOMBIA

INFLUENCE OF CONCRETE MATERIAL TIME-DEPENDENCY AND TEMPERATURE ON THE PERFORMANCE OF A COFFERDAM STRUCTURE BRACED WITH REINFORCED CONCRETE RING BEAMS

Alejandro Velásquez Pérez

Universidad Nacional de Colombia

Facultad de Minas, Departamento de Ingeniería Civil

Medellín, Colombia

2016

INFLUENCE OF CONCRETE MATERIAL TIME-DEPENDENCY AND TEMPERATURE ON THE PERFORMANCE OF A COFFERDAM STRUCTURE BRACED WITH REINFORCED CONCRETE RING BEAMS

Alejandro Velásquez Pérez

Research thesis presented as partial requirement to obtain the title of:

Magister en Ingeniería Geotécnica

Director:

David G. Zapata Medina, Ph.D.

Codirector:

Luis G. Arboleda Monsalve, Ph.D.

Research line:

Urban excavations

Universidad Nacional de Colombia

Facultad de Minas, Departamento de Ingeniería Civil

Medellín, Colombia

2016

A mis padres y hermano, por su amor y apoyo.

Acknowledgments

I want to thank my family, my dad Juan Diego Velásquez, my mom Luz Victoria Pérez, and my brother Mauricio Velásquez for the constant support and comprehension during this process.

Also, I want to thank my professors and guiders through this process David G. Zapata, and Luis G. Arboleda, without them this would be an impossible task. Their help, guidance, patience and support were always well received to achieve this goal. Also my friend and college Andrés Felipe Uribe, who constantly help me with the goals of this investigation.

I also want to thank the constant support of my bosses and friends: Bernardo Vieco, and Pedro Salvá and special mention to my friends and colleagues in study and work who were always with me in this process: Jaime Mercado, Marisol Salvá Ramírez, Carellys Vergara and Luis Villegas.

Lastly my sincere gratitude to my dear friends that always been there for me with their support and comprehension: Santiago Botero, Nicolás Céspedes, Andrés Ortega, and Sebastián Portillo.

Abstract

The lateral load resisting system of tall buildings is often made of reinforced concrete shear walls that are constructed using a cofferdam structure. The term cofferdam, often used in offshore applications, is employed in this research as a temporary watertight structure made of steel sheet piles and internally braced with steel or reinforced concrete ring beams to retain the surrounding soil. The soil removal inside of the cofferdam, necessary to install the foundations of the concrete core in rock or competent soil, is typically performed following a bottom-up excavation sequence. The performance of these type of systems in urban environments is critical as excessive excavation-induced ground movements can lead to significant damage of adjacent infrastructure.

In this research, concrete material time-dependent and temperature-dependent effects of shrinkage, creep, and aging of concrete ring beam bracings are shown to have contributed to the lateral deformations of an urban cofferdam built for a structure that was projected as the tallest building in America. It is shown that because of the very low stiffness of perimeter steel sheet piles, the performance of these cofferdams is highly influenced by the quality control and adequate curing of the concrete material of the ring beams used as the internal lateral bracing system of the cofferdam. It is also shown with actual performance data how the sequence and timing of cycles of excavation and lateral bracing highly impacted the performance.

The concrete material time-dependent effects presented in this research have not been incorporated as an integral part of the analysis and design of these temporary structures in urban environments and ignoring these effects conceal the fundamental reason for the resulting lateral deformations of these structures.

Keywords: Cofferdam, bottom-up construction, field performance, concrete time-effects, concrete temperature-effects

Resumen

Los sistemas de contención para cargas laterales de edificios altos son comúnmente hechos con muros de concreto construidos a partir de ataguías. Las ataguías son normalmente usadas para aplicaciones costeras, la empleada en esta investigación fue usada como una estructura temporal impermeable construida con tablestacas de acero y arriostrada internamente por anillos de acero o concreto reforzado para soportar el suelo alrededor. El proceso de excavación dentro de la ataguía necesario para instalar las fundaciones del núcleo rígido de concreto en roca o suelo competente, es típicamente realizado a partir de una excavación descendente-ascendente. El desempeño de este tipo de estructura en un ambiente urbano es crítico, pues movimientos del suelo alrededor inducidos por la excavación pueden llevar a daños significativos en estructuras cercanas.

En esta investigación se muestran como los efectos en el tiempo y de la temperatura del concreto: contracción, repteo y madurez han contribuido a deformaciones laterales en una ataguía urbana construida para el edificio proyectado como el más alto de América. Se muestra como por la baja rigidez del tablestacado perimetral de acero, las deformaciones de la ataguía son altamente dependientes del control de calidad y del curado del concreto reforzado empleado para el arrostramiento interno con anillos perimetrales. También se presenta con instrumentación de campo como la secuencia constructiva y los tiempos de los ciclos de excavación impactaron altamente el desempeño de la estructura.

Los efectos del concreto, dependientes del tiempo y la temperatura que son tratados en esta investigación no son tenidos en cuenta de forma integral en los análisis y durante la etapa de diseño, ignorar estos efectos es la principal razón de las deformaciones laterales resultantes de estas estructuras.

Palabras clave: ataguía, construcción descendente-ascendente, desempeño en campo, efectos del tiempo del concreto, efectos de la temperatura del concreto

Table of Contents

Lists of Figures

Pág.

Lists of Tables

Lists of symbols

$(f'_c)_{28}$	Concrete compressive strength at 28 days
$(f'_c)_t$	Concrete compressive strength with time in days
$(\varepsilon_{sh})_t$	Concrete shrinkage strain at any time
$(\varepsilon_{sh})_u$	Ultimate shrinkage strain coefficient
a	Air content in concrete mix expressed in percentage
A_c	Is the cross sectional area of the structural member
B	Width of a cell of cellular cofferdam on vertical shear failure
B_e	Excavation width
c	content of cement in *kg/m³*
c'	Intercept cohesion Mohr-Coulomb failure criterion
C_a	Adhesion between soil and steel sheet pile
D	Embedment depth
d	Time variable in days
d_e	Depth of the reinforcement ring
D_e	Internal diameter of the cofferdam
D_s	Ground surface settlement influence range
E	Activation energy in *J/mol* - compressive strength-maturity
E_c	Concrete modulus of elasticity
E_{ci}	Modulus of elasticity in MPa for concrete at 28 days
$E_{ci}(t)$	Variation of modulus of elasticity with time in days
E_{co}	Constant equal to 2.15 x 10^4 MPa
E_{ct}	Development of concrete modulus of elasticity with time
E_r	Modulus of elasticity of the retained medium
E_s	Young modulus of the soil
E_w	Young modulus of the wall
f	Steel friction coefficient
$F.S.$	Factor of safety against basal heave
f'_c	Concrete compressive strength
f_{ck}	Compressive strength below which 5% of strength measurements
f_{cm}	Concrete compressive strength at 28 days
$f_{cm}(t)$	Average concrete compressive as a function of time

f_{cmo}	Constant equal to 10 MPa
$FoS_{bearing}$	Factor of safety against bearing capacity
FoS_{int}	Factor of safety against interlock strength
FoS_{pull}	Factor of safety against pull-out
$FoS_{sliding}$	Factor of safety against sliding failure
FoS_{vs}	Factor of safety on shear failure on a vertical plane
g_{ct}	Is a constant taken as 0.043
H	height of the cell
h	Is 2Ac/u is the notional size of the structural member, mm
h_0	Equal to 100 mm
H_1	Height of water above the base
H_e	Excavation depth
H_p	Distance below the dredge line
H_T	Wall total height
H_t	Lateral distance with settlement influence
H_w	Wall height to the dredge line
I	Moment of inertia per unit length of the wall
i_c	Inclination factor
I_v	Moment of inertia about the vertical axis
k	coefficient that depends on the stiffness of the retained medium
k_0	Lateral earth pressure coefficient at-rest
k_a	Active earth pressure coefficient
k_c	Rate constant for concrete strength-maturity, initial slope of strength-age curve
k_e	Earth pressure coefficient (according to the case)
k_p	Passive earth pressure coefficient
L	Distance between centerlines of adjacent cells
M	Applied bending moment
M_o	Net overturning moment
M_{pen}	Resting moment on the sheet pile against the push
N_c	Bearing capacity factor
P	Lateral earth pressure
P'_a	Active earth pressure
P_d	Pressure difference of the inboard sheeting
p_{max}	Maximum pressure over sheet piles
P'_p	Passive earth pressure
P_s	Resultant horizontal force

p_T	Interlock tension
Q	Ultimate load on the centerline
Q_p	Pull-out reaction force by overturning moment
Q_s	Shear stress through a cofferdam cell fill
Q_u	Pull-out capacity of sheet piles
qu	Ultimate bearing capacity
r	radius after the rotation of a cellular cofferdam
R	Relative stiffness ratio
r_0	Original radius
r_c	Sheet piles radius cell
R_c	Cofferdam radius
R_g	Universal gas constant
RH	Relative humidity of the ambient
RH_0	is a relative humidity of the ambient constant 100%
R_p	Resistance to penetration
s	Slump of the concrete mix in mm
S	Compressive strength at time *t*
s_c	Coefficient that depends on the type of concrete for compressive strength, 0.2 for rapid hardening high strength cements, 0.25 for normal and rapid hardening cements, and 0.38 for slowly hardening cement
s_f	Interlock shear resistance
S_H	Horizontal element spacing
S_i	Ground settlement
s_s	Cell fill shear strength
s_T	Total shearing resistance
s_u	Undrained shear strength
S_u	Limit compressive strength
S_V	Vertical element spacing
S_w	Surface settlement behind the wall
t	Time in days
T	Temperature in °C
t_0	Age of concrete at loading for creep
T_0	Temperature equal to 1°C
t_1	Constant equal to 1 day
T_c	Average concrete temperature in °C for a given time interval
t_e	Equivalent age at reference curing temperature
t_i	Maximum interlock pressure
T_i	Interlock strength
t_{la}	Loading time in days not less than 7

t_{max}	Maximum connecting pressure between neighboring cells
T_r	Reference temperature usually equal to 20 or 23 °C
t_s	Age of concrete at the beginning of shrinkage
t_T	Age time adjusted by temperature
u	Perimeter of the member in contact with the atmosphere
v/s	Volume-to-surface in mm
V_s	Volume in the displacement zone
v_t	Concrete creep at a given time t
v_u	Ultimate creep coefficient
W	gravity forces (include weight)
w	Concrete unit weight
W_u	Ultimate radial wailing load
z	Depth
α	Constant based on element size
α'	Constant type of concrete vary from 0.05 to 9.25
$\alpha_{sT}(T)$	Temperature dependent coefficient which replace the product of $350(h/h_0)^2$, $h_0=100mm$ and T_0
β	Concrete curing method vary from 0.67 to 0.98
β_c	Coefficient that describes the development of creep with time
$\beta_c\ (t\text{-}t_0)$	Development of creep coefficient with time
$\beta_{cc}(t)$	Coefficient variable function of concrete age
$\beta_E\ (t)$	Concrete modulus of elasticity variable with time
$\beta_{H,T}$	Temperature dependent coefficient which replace β_H
$\beta_{RH,T}$	Temperature dependent coefficient which replace β_{RH}
β_s	Coefficient to describe development of shrinkage with time
β_{sc}	Coefficient that depends on the type of cement
γ	Soil unit weight
γ'	Submerged unit weight
γ_e	effective unit weight of soil in contact with sheet pile
γ_s	Average unit weight of the soil
δ	Friction coefficient between steel sheet piles and soil
Δf	Is a constant of 8 MPa
$\delta_{H(max)}$	Lateral maximum deformation
δ_{hm}	Horizontal maximum displacement
Δt	Time interval in hours for equivalent age at reference curing temperature
Δt_i	Interval of time in days for a temperature in °C
Δu	Out of balance water pressure
$\delta_{v(max)}$	Maximum settlement deformation

$\varepsilon_{cc}\,(t,t_0)$	Concrete creep strains
$\varepsilon_{cs}\,(t,t_s)$	Shrinkage strain with time
ε_{cso}	Notional shrinkage coefficient
θ	Angle between the joint and the centerline of the cofferdam
θ'	Rotation angle of a cellular cofferdam
λ	Is the relative humidity
σ'_a	Undrained active pressure
σ'_h	Horizontal effective stress
σ'_p	Undrained passive pressure
σ'_v	Vertical effective stress
τ	Shear stress developed at the failure surface
τ_f	Soil shear strength at failure surface
$\phi(t,\, t_0)$	Concrete creep coefficient
ϕ_0	Notional creep coefficient
ϕ_{RH}	Creep coefficient dependent of relative humidity
$\phi_{RH,T}$	Temperature dependent coefficient which replace φ_{RH}
Ψ	Ratio of fine aggregates from the total aggregates in percentage from the total weight
Ψ'	Creep constant in function of the element shape
ϕ'	Drained internal friction angle

Chapter 1

1. Introduction

Urban construction is becoming increasingly common as the global population concentrates in urban areas. It is expected to reach 70% of the world population by the year 2050 (ITACUS 2011). This requires to modernize the cities, and develop their infrastructure using better designs, engineering solutions and construction methods. As space in congested and highly populated zones is very limited, the construction and modernization of buildings and infrastructure generally involves the use of underground space, resulting in significant excavation depths and soil removal.

Excavations are perhaps one of the most complicated soil-structure interaction problems. Their design and construction are complex as excavation-induced ground movement can affect neighboring structures yielding them unserviceable and in some cases causing their collapse. Additionally, nowadays project planning requires excavation works to be shorter and more efficient. Then, combined types of construction using top-down and bottom-up excavations sequences are becoming popular as excavation activities are removed from the critical path of the construction project. However, the available design and analysis methodologies for these combined excavation methods do not show a good correlation with field observations. The differences can be associated with construction activities not taken into account during the design process and simplified model idealizations that assumed concrete as an invariable material neglecting time and temperature effects. Not to mention the importance of soil behavior that requires the use of

an “advance” constitutive soil model that can reproduce the characteristic incremental non-linear response of geomaterials.

Current construction methods for high rise buildings combine a temporary cofferdam structure with top-down excavation techniques. The cofferdam is built following a bottom-up sequence using sheet piles as the retaining wall. The main purpose of the temporary cofferdam is to support the building rigid concrete core in deep competent soil. The building basement area is then constructed using a top-down methodology propping a perimeter slurry wall with the basement floor slabs. As abovementioned, this method presents significant benefits in construction times, but it also has some disadvantages as additional ground movements related to the inherent nature of the cofferdam construction are generated. Among them are the slack in the sheet pile interlock connection, the coupling between steel ring beams and the perimeter sheet pile wall, and concrete time-dependent and temperature effects when concrete ring beam are used. These phenomena are conventionally not taken into account during the design and analysis of this type of structures.

This research presents two cofferdam case histories located in the loop area of Chicago, IL. The first case is the One Museum Park West (OMPW) project which involves the construction of a 53-story skyscraper combining top-down and bottom-up techniques. For this project a 15-m-deep and 24.25-m-wide temporary cofferdam propped by segmental steel ring beams was constructed. The second case was projected to be the highest building in America with a total height of 610 m. However, at the date only the temporary cofferdam, needed to build the rigid central core, was completed. The cofferdam is approximately 33.2-m-wide and 23.4-m-deep and was laterally supported by seven reinforced concrete ring beams. These two case histories provide a unique opportunity to compare side by side their measured performance and evaluate the differences resulting from using a cofferdam braced with steel circular props or reinforced concrete ring beams.

Despite of using advance constitutive soil models for excavation analysis and design and considering well-sized structural elements, there are always additional ground-movements to those obtained in the analysis of urban excavations (Arboleda-Monsalve 2015). This research tries to quantify ground movements arising from concrete time-dependent effects such as creep and shrinkage; temperature effects which affect the concrete resistance and stiffness. Additionally, the classical approach used in the state-of-

the-practice assuming the concrete as a linear-elastic material no affected by time or temperature is evaluated. In general, the scope of this research is to provide design and construction recommendations to allow mitigate ground movements around cofferdam excavations, and reach a more similar setting between what is computed and what is constructed.

Objectives of the research

The objective of this research is to evaluate and quantify ground movements around cofferdams structures braced by concrete ring beams taking into account the coupled effects of the retaining system, soil mass, temperature and concrete creep and shrinkage.

The specific objectives of this work included:

- Identify the main characteristics of the excavation system (design, structure and construction techniques), as well as the sub-soil conditions.
- Analyze the actual performance by construction stages through field instrumentation.
- Compare two case histories with registered field performance, one with steel reinforcements and the other braced with concrete ring beams located 2.5 km away one from the other with similar geological and geotechnical conditions.
- Analyze the time and temperature concrete effect in the performance of the cofferdam stage by stage, comparing its results with a linear analysis.

Content of Thesis

Chapter 2 presents a technical background of the main aspects of the research, including earth pressures, excavation support systems, bottom-up excavation technique, main aspects of cofferdam design and concrete fundamental time and temperature effects.

Chapter 3 presents the main geological and geotechnical characteristics of the case histories, details the construction sequence and shows the recorded field performance for both cases.

Chapter 4 presents principal aspects of concrete behavior according to the CEB-FIP model code of 1990, the ACI 209 of 1997 and the maturity recommendations from ASTM applied to the reinforced concrete ring beams used to support a cofferdam. These models

pretend to explain the nonlinear behavior of concrete in time used to make back-analyses evaluations of the excavation performance presented in Chapter 5.

Chapter 5 presents the analyses of the cofferdam with and without the concrete time-dependency and temperature-dependency effects, next to the field instrumentation and a comparison discussion between the two case histories.

Chapter 6 summarizes the results and presents the conclusions of the thesis.

Chapter 2

2. Technical Background

This chapter presents a brief description of lateral earth pressures theory and a general overview of different excavation methodologies and earth support systems making a detailed summary of cofferdams characteristics and describing its design and construction procedures. Then, the p-y method for modeling lateral load versus deformation of soils is described as it is used in the analyses with a discrete spring model presented in chapter 5.

The excavation deformation analysis methods are presented and a description of different field instrumentation sensors and excavation monitoring systems. This chapter finishes with a description of concrete as an engineering material describing its advantages and disadvantages for the construction of cofferdams is presented in light of its time and temperature dependency effects.

2.1. Overview of Lateral Earth Pressure Theory

Apparent earth pressure diagrams are used to design excavation support systems without taking into account the construction type and process (Zapata-medina 2007). Those diagrams are used in practice for sizing elements of retaining systems including embedment depth of walls, lateral bracing spacing and capacity, and wall general stiffness. For those earth pressure conditions to be reached, different deformation magnitudes must occur in the soil behind and in front of the retaining structure. For example, Figure 1 (Budhu 2010) presents the soil mass behind the wall transitioning from an at-rest earth pressure

condition to and active pressure condition caused by a small rotation in the wall. The soil mass in front of the wall passes from an at-rest condition to a passive pressure induced by a larger rotation. The at-rest earth pressure represents the initial condition state of soils corresponding to the undeformed situation.

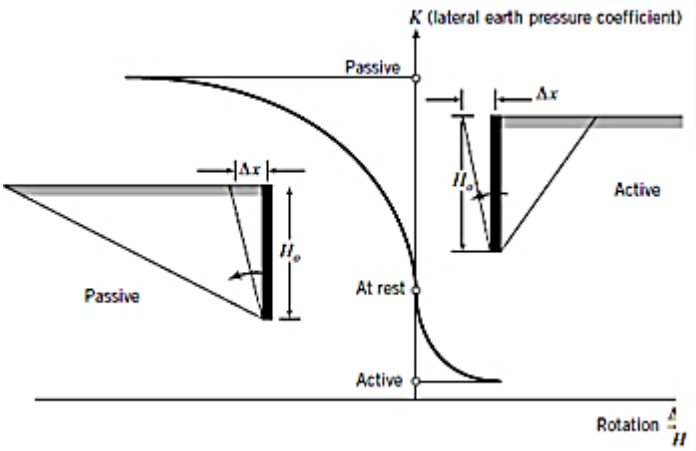

Retained soil	Stress state	Approximate displacement, Δx
Coarse-grained	Active	$0.001H_o$, (T, R)
	Passive	$0.05H_o$, (T) $> 0.1H_o$, (R)
Fine-grained	Active	$0.004H_o$, (T, R)
	Passive	unknown

T = translation, R = rotation

Figure 1. Rotation required to mobilize active and passive earth pressure states. After (Budhu 2010).

- **At-Rest Earth Pressures**

The at-rest conditions exist when a retaining structure when no lateral deformation is developed (Braja M. 1987). If one knows the vertical effective stress at a given depth, the following relation express the lateral earth pressure at-rest:

$$k_0 = {\sigma'_h}/{\sigma'_v} \tag{1}$$

Where k_0 is the lateral earth pressure coefficient for at-rest conditions; σ'_h, and σ'_v are the horizontal and vertical effective stresses, respectively.

The most widely used in practice relationship to determine the k_0 coefficient is the one presented by Jaky (1944) applicable for normally consolidated soils. If soils are preloaded, the overconsolidation ratio plays an important role in the determination of this coefficient and variations to the following expression are proposed (Robert Holtz ; William Kovacs 1986).

$$k_0 = 1 - \sin\phi' \tag{2}$$

where ϕ' is the drained friction angle.

- **Rankine Earth Pressures**

Rankine (1857) presented a simplified solution for lateral earth pressures in retaining structures. This theory is based on plastic equilibrium assuming isotropic and homogenous soil conditions, zero friction between the wall and the soil, and that the failure surface and backfilled surfaces are planar (Zapata-medina 2007).

Consider Figure 2 and the abovementioned assumptions, in initial conditions there will be no shear stresses since friction between the wall and the soil does not exist, so the initial conditions represented in the Mohr's circle will be a circle contained within the failure envelope. As the wall moves away from the soil, the vertical effective stresses in the soil will remain constant and the horizontal stress will decrease until the lateral earth pressure reaches the active earth pressure growing the circle until it reaches the failure envelope.

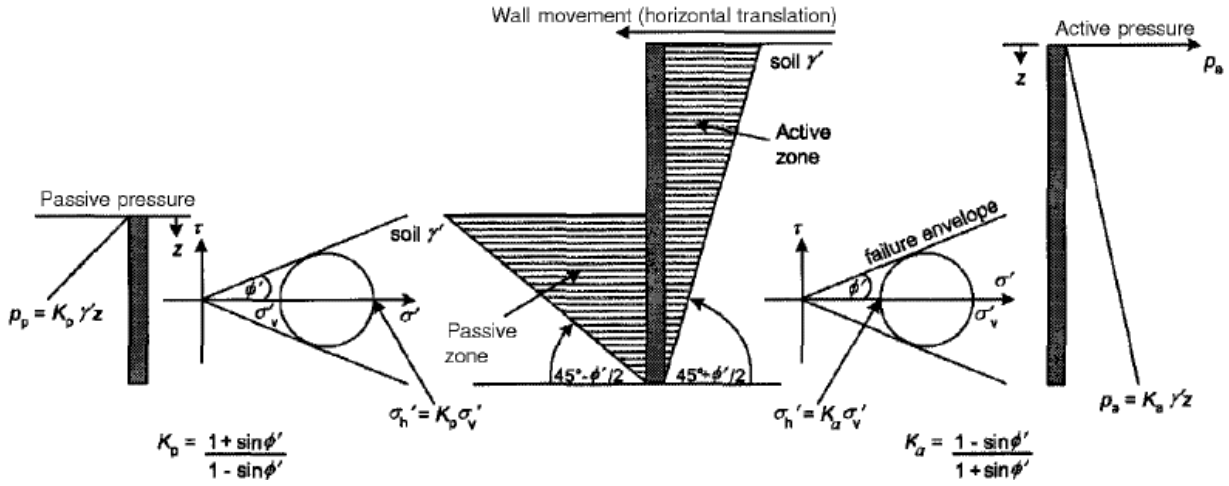

Figure 2. Active and passive earth pressures distribution according to Rankine. After (CIRIA C580 2003).

The active earth pressure magnitude can be defined as.

$$P'_a = k_a \gamma z - 2c\sqrt{k_a} \tag{3}$$

where $k_a = tan^2(45° - {\phi'}/{2})$, γ is the unit weight of the soil, z is the depth, and c is the cohesion intercept from the Mohr-Coulomb failure criterion. Also, considering the assumptions and by geometric considerations, it can be shown that the surface angle behind the wall is.

The total pressure behind the wall can be calculated with these considerations and taking into account the water pressure if there is any. Considering the Rankine earth pressure theory, a wall in its original condition without yielding the soil in front will be subjected to at-rest conditions with a vertical effective stress and a horizontal effective stress, in the Mohr's circle it will be apart from the failure envelope. But ones the retaining wall is pushed against the soil the vertical effective stress will remain the same and the horizontal will increase, finally the horizontal stress will be greater than the vertical ones the circle touches the failure envelope and that will be the passive earth pressure. It's important to mention that for this case the major principal stress will be the horizontal and the minor principal stress will be the vertical, this condition is illustrated in Figure 2.

The passive earth pressure can be estimated as follows.

$$P'_p = \gamma z k_p + 2c\sqrt{k_p} \tag{4}$$

where $k_p = tan^2(45° + {\phi'}/{2})$, γ is the unit soil weight, z is the soil depth and c is the cohesion intercept. As mentioned before, the inclined angle between the horizontal and the passive surface can be estimated by geometry as follows.

In case that in the bottom of the excavation was water its pressure must be added to the one computed as presented in expression (4). Both cases presented above are the expressions used for long term conditions. When evaluating undrained conditions, the following expressions can be used:

Active case $$\sigma'_a = \sigma'_v k_a - 2s_u \tag{5}$$

Passive case $$\sigma'_p = \sigma'_v k_p + 2s_u \tag{6}$$

where $\phi' = 0$ as the analysis is in short-term conditions, then $k_a = k_p = 1$ and S_u is the undrained shear strength.

- **Apparent Earth Pressure Diagrams**

As exposed by (FHWA 1999), Peck's apparent earth pressure diagrams were presented by Terzaghi and Peck for the first time in 1967 and later only by Peck in 1969 to provide conservative loads for strut design. Those loads can only be used for the design of the bracing system. Those diagrams represent envelope pressures back-calculated by Terzaghi and Peck from field measurements of struts loads in internally braced excavations. Those diagrams were developed from case histories for relatively uniform soil conditions. The earliest measurements were made in the 1930's from drained loadings in sands for the Berlin and New York subways (Terzaghi et al. 1996). The other two cases were developed for undrained loadings in stiff to hard clays, and for undrained loadings in soft to medium clays. Those measurements were made in excavations in which undrained conditions prevail.

The apparent earth pressure diagrams resulting from these case histories are presented in Figure 3. For the case of predominantly sandy soils (Figure 3 (a)), the k_a coefficient must be calculated according to Rankine earth pressure theory and separate water pressures. For predominant clayey conditions, the stability number $N_s = \frac{\gamma H}{S_u}$ must be evaluated. When N_s is greater than 6, the soft to medium clay diagram is applicable. The stiff-to-hard fissured clay diagram can be used when N_s is equal or lower than 4.

In the figure, the variable H represents the excavated depth. The apparent earth pressure diagrams and should not be used to estimate true earth pressure or calculate flexural stresses over the retaining walls.

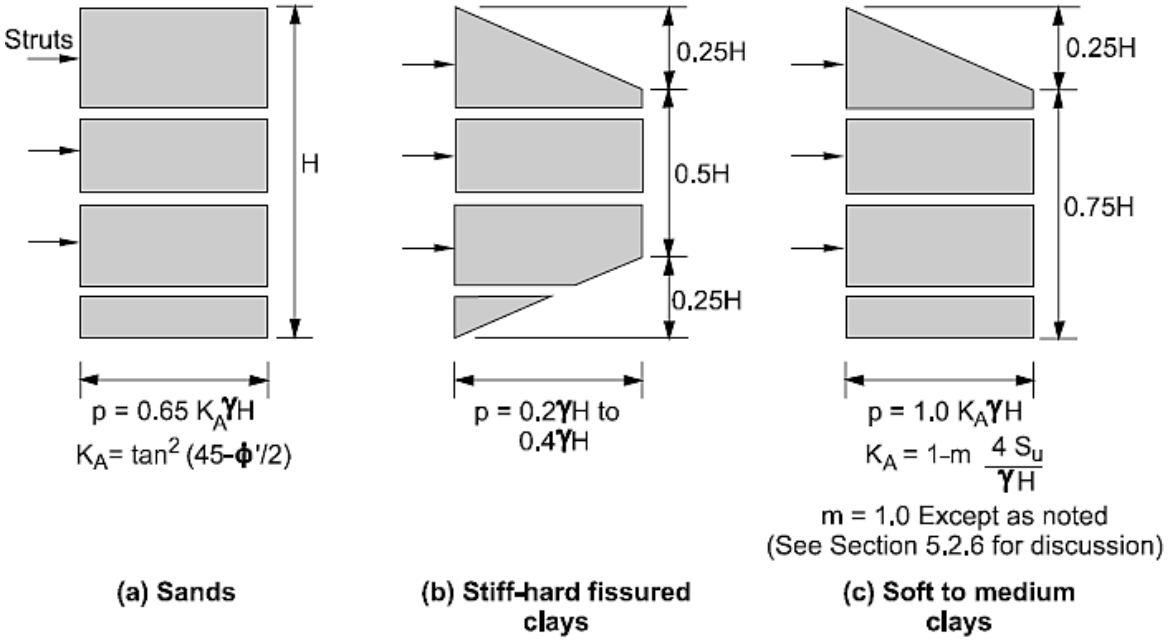

Figure 3. Terzaghi and Peck apparent earth pressure. (a) Drained envelope for sandy soils, (b) undrained envelope for stiff to hard fissured clays, and (c) envelope for soft to medium clays. After (FHWA 1999).

Layered soils are typical in practice. For those cases, there are modifications to the general earth apparent diagrams as presented in (Terzaghi et al. 1996) and more recently by (Ou 2006). These authors present the dominant soil alternative and the equivalent cohesion concept. The former mostly used for sandy soils and the latter for predominant clayey soils.

It is worth mentioning that even though some of the evaluated case histories had excavation depths larger than 20 m as presented in (Terzaghi et al. 1996) for the Civic Center subway station in Los Angeles, the apparent earth pressure diagrams may be used for excavation depths of 10 m or less as recommended by (Ou 2006). This is because the upper zone is at times prestressed or preloaded with cross-lot bracings which prevents undesirable deformations. These methods were established more than 40 years ago from empirical back-analyses when the constructions methods were simpler and the excavations depths were much less than those currently performed. According to the same author for deep excavations, the finite element methods or even beam analyses on elastic foundation stand out as alternative methods that can be readily used in practice.

2.2. Excavation Methods and Earth Support Systems

For the construction of basements using deep excavations, it is necessary to implement different types of support systems and construction techniques. Factors like economic feasibility, the availability of technology and access of construction equipment, and the location and subsurface conditions play an important role in the definition of the type of excavation support system. Different structural systems can be employed in the construction of deep excavations, including prefabricated piles, secant or tangent piles, sheet piles, or diaphragm walls. Those elements based on the construction methodology can be braced with cross-lot bracings or with anchors made post-tensioned tendons or bars (Ou 2006). The construction can also be advanced using full open cut methods, zoned excavation methods, or island techniques if the surrounding areas allow those types of constructions.

In urban excavations limited deformation are an important issue, due to neighboring structures. The excavation factors that affect wall deflections during an excavation process can be grouped into three categories according to (Kung 2009) as follows, and must be always be taken into account when selecting a retaining structure and an excavation technique.

Inherent factors:

- Stratigraphy: geotechnical conditions as soil stress history, strength stiffness, permeability and other characteristics that may induced large deflections over a retaining structure.
- Site environment: neighboring building and infrastructures, which mainly condition the limit soil horizontal and vertical movements and in some cases the construction procedure.

Design-related factors:

- Properties of retaining system: wall and braces or anchors stiffness, the higher the stiffness the lower the retaining structure deflections.
- Excavation geometry: Depth and width of the excavation as well as the wall embedment.
- Strut prestress: This factor is employed to assure an immediate connection between the strut and the wall in order to avoid installation movements.

- Ground improvement: methods, such as jet grouting and deep mixing among other, used to increase soil strength and stiffness.

Construction-related factors:

- Construction methods: commonly used top-down method, bottom-up method and anchored walls method.
- Over-excavation: when the excavation is performed between struts levels and beyond the next one in order to be installed.
- Prior construction: such as sheet pile driving or the initial excavation used to diaphragm walls.
- Construction of concrete floor slabs: every concrete time and temperature effect that may affect the retaining system, such as creep and shrinkage.
- Duration of the construction sequence: time required to complete the construction of struts and slabs. If it is too short the material may not be ready to withstand the imposed pressures and if the time is too large and the material behind the wall is clay, additional wall deflections may occur due to consolidation, changes of excess pore water pressure, or creep.
- Workmanship: always poor workmanship quality and mistaken procedures may lead to higher deflections of the wall.

Now days, according to the design related and construction factors two types of excavation construction sequences are typically used for urban excavations, to reach an efficient construction process and limited lateral and vertical deformations in the surroundings. A bottom-up sequence in which the excavation is performed first followed by the installation of foundations and construction of the superstructure or a top-down procedure in which deep foundations and the perimeter wall are installed first, followed by the installation of the basement topmost slab structurally connected to the perimeter pile wall and thereafter the excavation is developed in a top-down fashion. In this method, the construction of the basements and the superstructure is performed simultaneously and the basements slabs serve as the main lateral bracing system of the perimeter excavation support system (Ou 2006).

2.2.1. Bottom-up sequence of excavation

In this procedure, struts or anchors in front of the retaining wall are needed at different depths to retain the earth and water pressure behind the wall. As mentioned by (Ou 2006) these systems are generally made of soldier piles, sheet piles or diaphragm walls as the perimeter support system. Struts, wales, and corner braces are used to stiffen the excavation support system and resist the earth and water pressures. At time, depending upon the width of the excavation, additional temporary internal posts are required. Although the central posts may impact the efficiency of the excavation, this is one of the most common systems used in deep excavations. This system is illustrated in Figure 4. The following is the typical construction procedure of a braced excavation following a bottom-up sequence:

1. Construction of the perimeter retaining wall.
2. Installation of the central posts.
3. First stage of soil removal (excavation).
4. Installation of wales and struts between the wall and internal posts. If necessary, preloading of the struts for deformation control purposes.
5. Repeat sequence of excavation and installation of bracings until the final excavation elevation is reached.
6. Construction of the foundation system.
7. Strut removal as they are being replaced by basements slabs following a bottom-up sequence of construction.

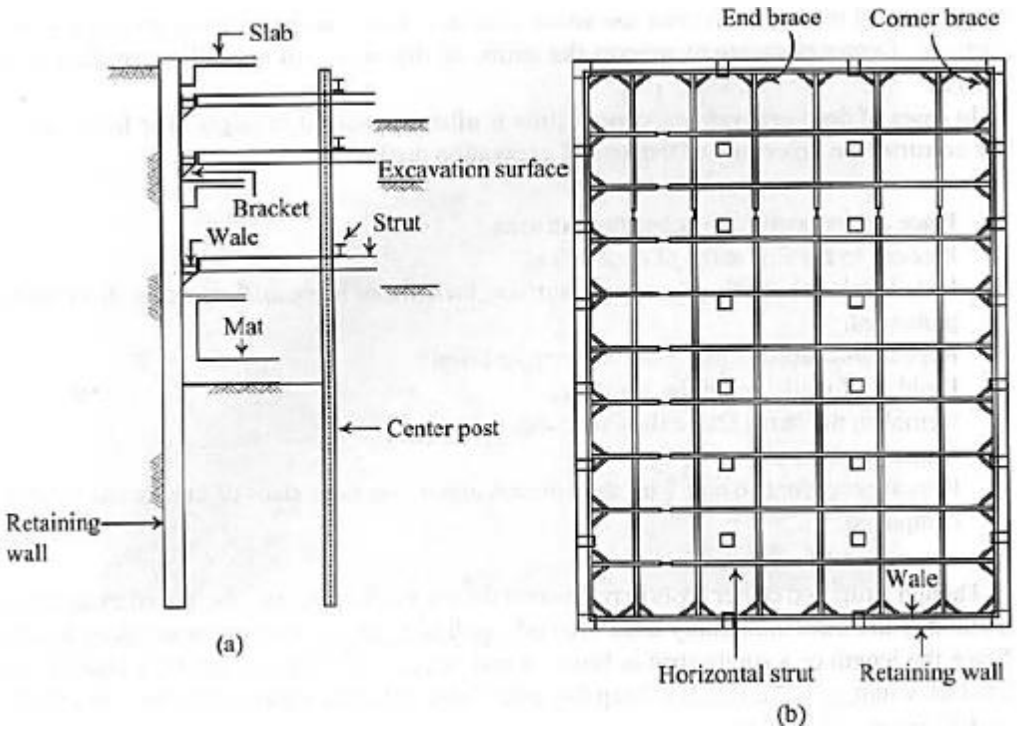

Figure 4. Braced excavation built following a bottom up sequence, (a) typical cross section and (b) typical plan view. After (Ou 2006).

2.2.2. Top-down sequence of excavation

This methodology is illustrated in Figure 5 and consists on the construction of permanent basement slabs to simultaneously sustain earth and pressures and serve as the permanent basement slabs of the main structure. The basement slabs are constructed from the ground surface until the bottom of the excavation is reached. Deep foundations and structural columns are typically installed in the original ground surface. This technique is limited only to structures supported on deep foundations. The construction time can be reduced significantly and the stiffness of the slabs that act as bracing system decreases the resulting wall deformations limiting the impact on the adjacent infrastructure.

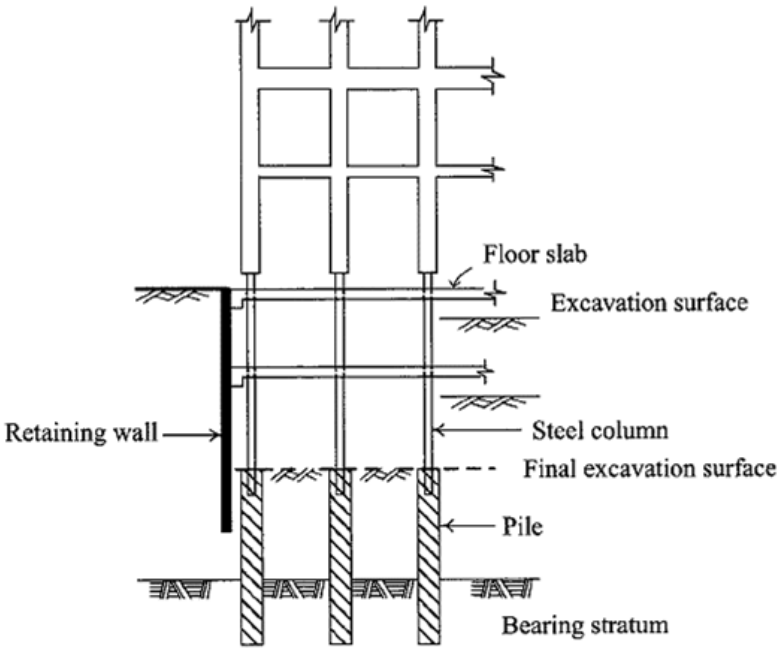

Figure 5. Braced excavation built following a top-down sequence. After (Ou 2006).

The typical construction process is outlined as follows:

1. Construction of the perimeter wall. Typically used diaphragm walls, tangent or secant pile walls.
2. Construction of deep foundations from the original ground surface.
3. First excavation stage.
4. Installation of the first basement slab.
5. Construction of the first floor slab.
6. Excavation with low clearance equipment to reach the second excavation level and installation of the second basement slab while construction of the superstructure advances.
7. The process is repeated until the bottom of the excavation is reached.

2.3. Design and Construction of Urban Cofferdams

2.3.1. Definitions

A cofferdam in this thesis presented as a temporary structure, usually used to keep water outside a close working area, for example a cofferdam is normally built for the construction of piers, embankments and bridges, in this last one, the foundation structures

in middle of the river or the sea can be performed first by driving sheet piles in the site and then by pumping the water of the working area outside while the excavation is done (Murthy 2007).

There are several types of cofferdams according to (Murthy 2007) and are presented ahead.

1. Cantilever sheet pile. Profitable when the structure height is not large, these types of cofferdams are susceptible to damages by leakage and water flows, due to the flexibility.
2. Braced cofferdams. Economical for small to moderate depths, also susceptible to damages by leakage and water flows. An example is shown in Figure 6.
3. Earth embankments. Without height limit, but the construction area must be bigger and the construction requires more time.
4. Double-wall cofferdam. Suitable for moderate excavation depths.
5. Cellular cofferdams. These can always be used for deep excavations in big areas, usually used to provide water barriers.

According to (Packshaw 1962) a cofferdam must accomplish at least with the following aspects.

- The walls of the cofferdam or the bracings must support the loads and stresses imposed on them.
- Cofferdams aren´t entirely impermeable structures, the dry zone must be controlled with pumping.
- It must be possible to reach the desirable cut level without having a uncontrolled flow into the dam or heave problems in the bottom.
- The walls deflections must be tolerable, so there will not be any problem in the future with the internal structure.
- The walls must have overall stability against unbalanced earth pressures or ground movements.

Nowadays, cofferdams are not only use in off shore applications and embankments constructions, they are also used in deep urban excavations, with the purpose to accelerate

the process by pulling apart the construction of the central concrete core while the periphery structures are been built (Finno et al. 2014).

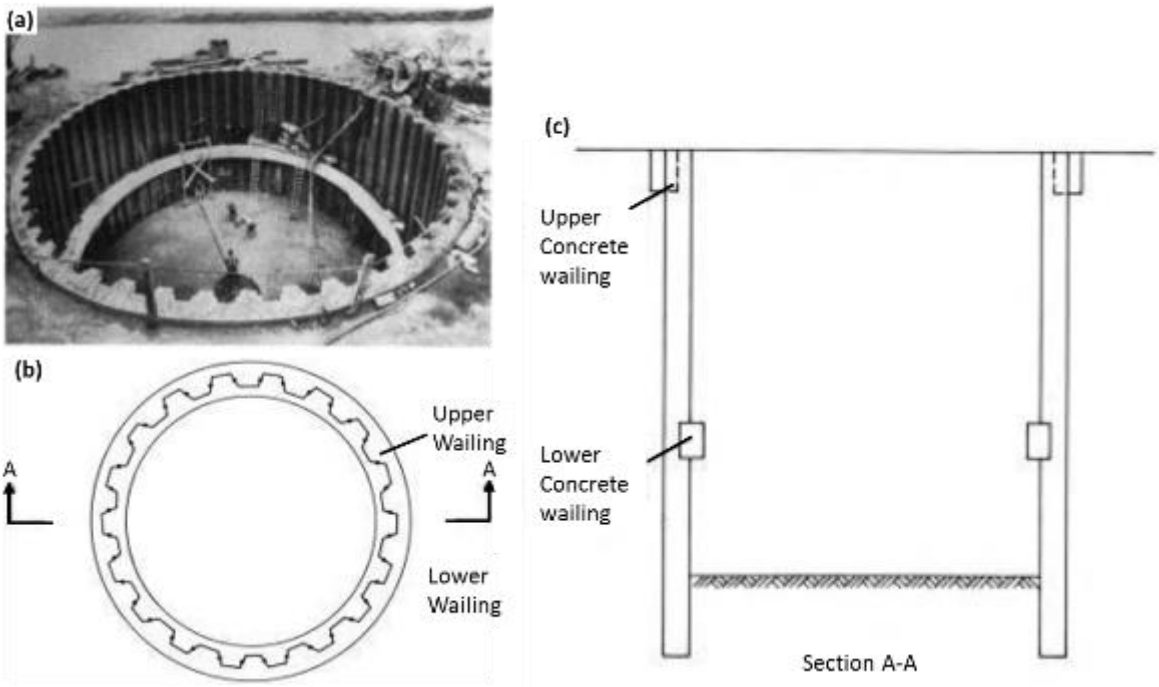

Figure 6. Braced cofferdam, (a) picture, (b) plant view, (c) Section view. After (Puller 1996).

From Figure 6 a typical braced cofferdam and its structural elements can be appreciated, for example, in the picture the vertical principal containing structure are sheet piles, the most commonly used, but other types of retaining structures like diaphragm wall can be used. Also, the bracing elements are shown, in this occasion concrete reinforcements were employed, other commonly used type are steel prefabricated wailings. These ones must be installed to support earth pressures at recommended design levels.

According to (Puller 1996) to select the type of cofferdam one must know the geotechnical site conditions, the depth of compacted soil or rock, and the water retaining level. When the principal objective is to control deformations and reach a very stiffness structure the selection must be a circular cofferdam, which works with compression stresses and in compensated conditions. Also, reinforced with circular ring beams to add strength and stiffness to the structure.

The ring beam type selection in circular cofferdams has some advantages and disadvantages, the principal advantage of a prefabricated steel one is that, it can be installed and the excavation can be performed immediately while the concrete one must wait for the proper concrete cured time (Puller 1996), but the concrete one helps to control more the structure deformations, because is poured right in the sheet pile (or the retaining element) without generating a gap between elements, however, the sheet piles cannot be reused again.

It is also important to mention, that circular cofferdams must be subjected to similar earth and water pressures in all the perimeter, to avoid structural problems and failures (Puller 1996).

The possible causes of failure for braced cofferdams are presented by (Puller 1996), they vary according to the structure geometry and site conditions. The principal causes are the following.

- Failure for no consideration of water levels variations due to seasonal effect, or drastic changes in flow conditions.
- The no consideration of flooding valves when they are necessary.
- Variations in the ground conditions assumed in the design and the one reveal during the excavation.
- Failure at no controlling the excavation levels to those recommended in the designs.
- Failure produced by insufficient o inadequate lateral restraints.
- Unauthorized strut removal or substitution.
- Uncontrolled water ingress through separated interlocks to the inside zone.
- Ill-fitting interlocks that causes eccentrics loads.

Overall failure is most likely to occur due to inadequate strutting or insufficient sheet pile embedment, rather than excessive flexural sheet pile deformation (Puller 1996).

According to (Packshaw 1962) the causes of failure are almost invariable according to soil type below the formation level, concluding that soil failure is due to insufficient passive resistance or changes in its properties by changes in stress conditions.

By the other hand, (Puller 1996) listed the following as the principal causes of base failures.

- In permeable soils, blow may occur due to inadequate cut-off of the flow or to excessive pumping, that may mobilize the perimeter piles due to not enough passive resistance, generating a progressive collapse by transference of excessive stresses.
- In permeable soils an upward flow may decreases the passive resistance at the bottom of the excavation, generating an overload of the last ring beam and a possible failure.
- Variations in loading, may not only test the strength and stiffness of the braced elements, but can also increase deformations that may transfer overloads to the lowest ring beam until generate failure.
- In soft clays excavate below the critical depth may deflect the piling inwards.
- In clays the water pressure below the bottom may cause and uplift failure.

The same author mention that workmanship quality is also very important and that this factor may cause failure and even collapse, and present an example of a cofferdam constructed in the Thames river in London, where, the lowest ring beam was installed in a mistaken level and generated a progressive failure of the entire system.

2.3.2. Cofferdam design

The braced cofferdam design requires to consider a tolerance in the installation of sheet piles and sufficient space for the internal reinforcements, these ones must comply a satisfactory state in limit equilibrium analysis (Puller 1996). By the other hand, when an allowable service state must be required, the calculations must be performed be taking into account the permissible deformations of the structure, these deformations will be the decisive parameter that finally define the structure dimensions, the reinforcements sections and the used materials.

Cofferdams design like any other soil-structure interaction structure, the design must meet all the minimal standards, with a complete survey exploration, a good soil characterization and an allowable design methodology. For example, manuals and normative book like (CIRIA C580 2003) recommends a checklist of the minimum activities

that must be accomplish to fulfill a complete geotechnical work for the design of retaining structures, like in this case a cofferdam.

According to the stratigraphic conditions of the site, the design should be performed in drained or undrained conditions, also by taking into account the service time of the structure (Puller 1996). Also, the same authors mention the following *"… For application of total stress, undrained analysis is therefore valid only for a very short period after the application of load to the cofferdam sheeting and support, but the period for full dissipation of excess pore pressure may vary from days to months. In these circumstances the designer's best option will probably lie in the use of undrained analysis in homogeneous clays, particularly soft clays, using effective stress parameters as a check. The use of effective stress analysis without a total stress analysis would then be reserved for areas of good soil drainage, laminated soils or strata of shallow depth, and analysis made at the end of a long construction period or for later permanent work phase." (Puller 1996).*

- **Design**

For the design limit equilibrium methods, can be used as for cantilever or tie walls, which obtain from satisfactory factors of safety for internal and external stability analysis. These analyses must be performed in a limit state between acting and resistant forces. Checking internal stability, collapsing, overturning, sufficient embedment depth, structure resistance against sliding, basal heave (in soft soils), bottom uplift (impermeable soils) (Puller 1996). These modes of failures are presented in Figure 7.

Then, the structural elements like sheet piles, wales, struts, bracers and anchors, must be sized, and their materials selected. For this stage to methods can be applied according to (Puller 1996), allowable stresses and limit state. The first one takes into account design stresses by decreasing ultimate stresses by a factor, by the other hand, the second one, applied factors to the loads from which gets major stresses used to size the elements and the materials properties. It is important to mention that the materials quality with time effects due to environment conditions must be take into account, for example steel corrosion.

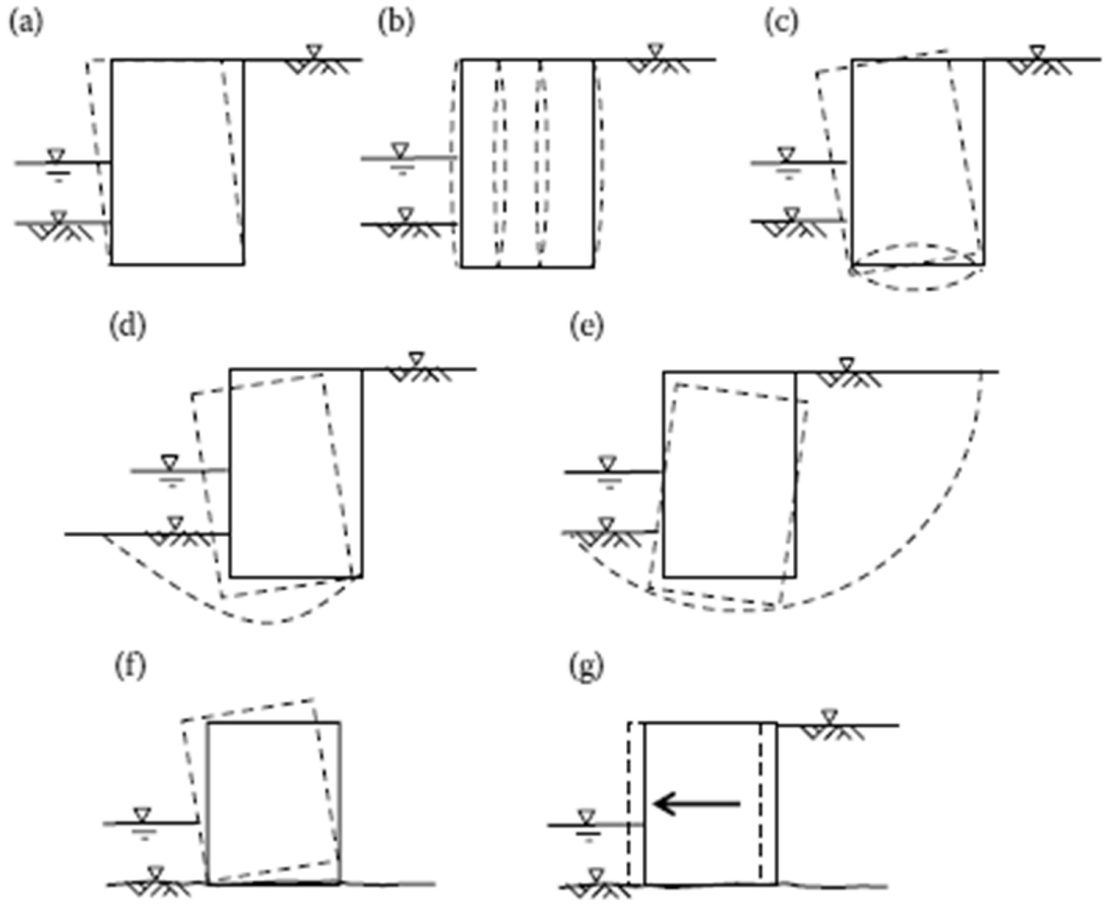

Figure 7. Cofferdam modes of failure. (a) Shear failure within the fill, (b) Sheet interlock failure, (c) Tilting on base rupture surface, (d) Bearing capacity failure, (e) Global stability, (f) Rotation about the toe, (g) Sliding on the base. After (Clayton et al. 2014).

As presented by (IQBAL 2009) in his thesis, currently there are five guidelines commonly used for the design of cellular cofferdams, The aspects can be applied according to the type of cofferdam and the site in which is constructed, they are necessarily to check for cellular cofferdams, but only some can be applicable to braced in urban cofferdam. The existing design consideration are listed ahead as presented by (Clayton et al. 2014) and then each topic is summarized and illustrated.

- Interlock strength of sheet-piles
- Internal shear failure within the cell
    - Vertical shear failure
    - Horizontal shear failure
    - Sheet pile penetration capacity

- External instability
  - Sliding failure
  - Bearing failure
  - Overturning failure
  - Seepage failure

- **Interlock strength of sheet piles**

According to (IQBAL 2009) and his historical cases of failure review this is the principal cause of failure. To determine the maximum interlock forces, the soil and water pressure acting against the sheet pile must be estimated. As expressed by the same author the lateral soil pressure is considered to increase with depth, calculated by multiplying with an overburden lateral earth pressure coefficient, therefore the pressure at a depth H can be expressed as.

$$P = k_e \sigma'_v + \Delta u \tag{7}$$

where the coefficient k_e can estimated by the methods abovementioned or can be assumed equal to 0.5 suggested by (US Army Corps of Engineers 1989), σ'_v is the effective vertical stress and Δu is the out of balance water pressure. The pressure distribution was originally assumed as proposed by Terzaghi to act over the cell wall as presented in Figure 8 (a), but nowadays the diagram distribution is assumed as presented in Figure 8 (b) with maximum pressure at $0.75H$ after being modified by TVA Engineers guidelines (1957) assuming that the pressure in the base is equal to zero as if the structure was supported in rock, the same assumption can be made for soil (clay or sands) with sufficient embedment (IQBAL 2009). The same author also mention that these assumptions were tested in cofferdams over rock and soil and the results were found applicable to both cases.

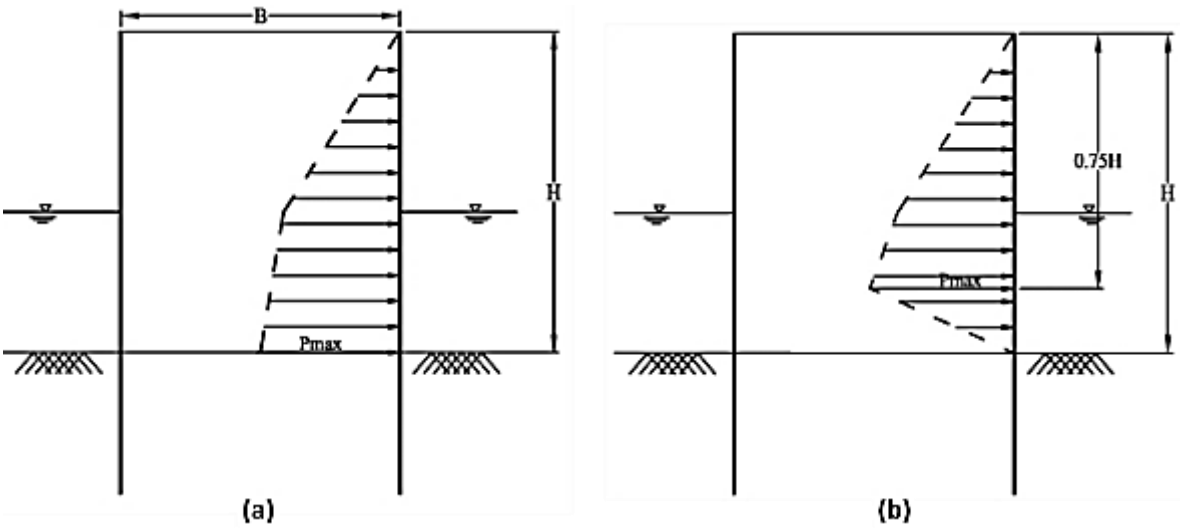

Figure 8. Fill pressure acting on the wall of the cell (a) Terzaghi proposal, (b) Actually used diagram. After (IQBAL 2009).

Once, the pressure is estimated, the interlock tension can be computed as.

$$t_i = p_{max} r \tag{8}$$

where, t_i is the maximum interlock pressure, p_{max} is the maximum pressure over the sheet pile and r is the radius of the cell.

The maximum connecting pressure between neighboring cells is defined as.

$$t_{max} = p * L * \sec\theta \tag{9}$$

where, L is the distance between centerlines of adjacent cells and θ is the angle between the joint and the centerline of the cofferdam, subtended at the center of the cell.

Then, the factor of safety against interlock strength failure can be estimated as follows.

$$FoS_{int} = \frac{T_i}{t_{max}} \tag{10}$$

where T_i is the interlock strength of the sheet piles.

- **Internal shear failure within the cell**

This analysis is performed to check for excessive deflections or rotations of the cells when they are caused by internal shear failure of the soil as first notice by Terzaghi (1944). For this purpose, vertical and a horizontal shear planes are assumed and factors of safety against them are calculated.

- **Vertical plane shear failure**

Terzaghi (1944) suggested that because of the cells flexibility, the fill is more likely to fail for shear stress. As explained by (Clayton et al. 2014), Terzaghi proposed a methodology were the applied shear stress is compare to the available shear stress on a vertical plane through the center of the cell fill. The shear force acting on a plane can be calculated from an assumed triangular pressure distribution like the one presented in Figure 9.

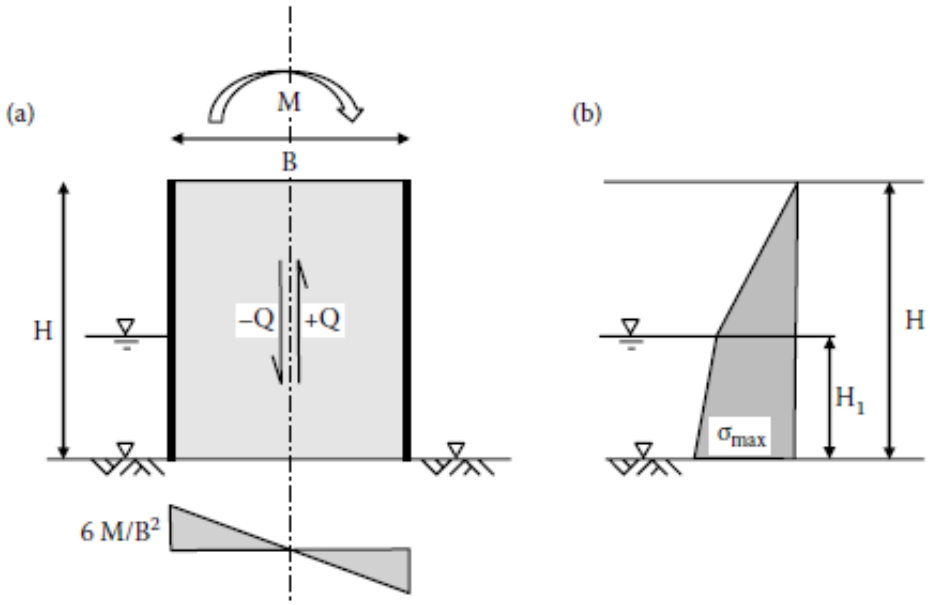

Figure 9. Vertical shear stress through a cofferdam cell fill, (a) Applied bending moment and contact stresses, (b) Earth pressure profile. After (Clayton et al. 2014).

For an applied bending moment, M, acting on a cell of width B, the contact stresses on the base can vary as presented in Figure 9 from $6M/B^2$ to $-6M/B^2$, and therefore the shear stress can be estimated as.

$$Q_s = {}^{3M}/_{2B} \tag{11}$$

The shear resistance is the resultant from the sheet pile interlock sliding resistance plus the shear strength of the fill. The fill shear strength can be estimated as the effective lateral pressure multiplied by the effective friction angle using the centerline earth pressure distribution proposed by Terzaghi and illustrated in Figure 10 (b), and the resultant horizontal force P_s can be computed as.

$$P_s = \frac{1}{2}\gamma K(H - H_1)^2 + \gamma K H_1(H - H_1) + \frac{1}{2}\gamma' K H_1^2 \tag{12}$$

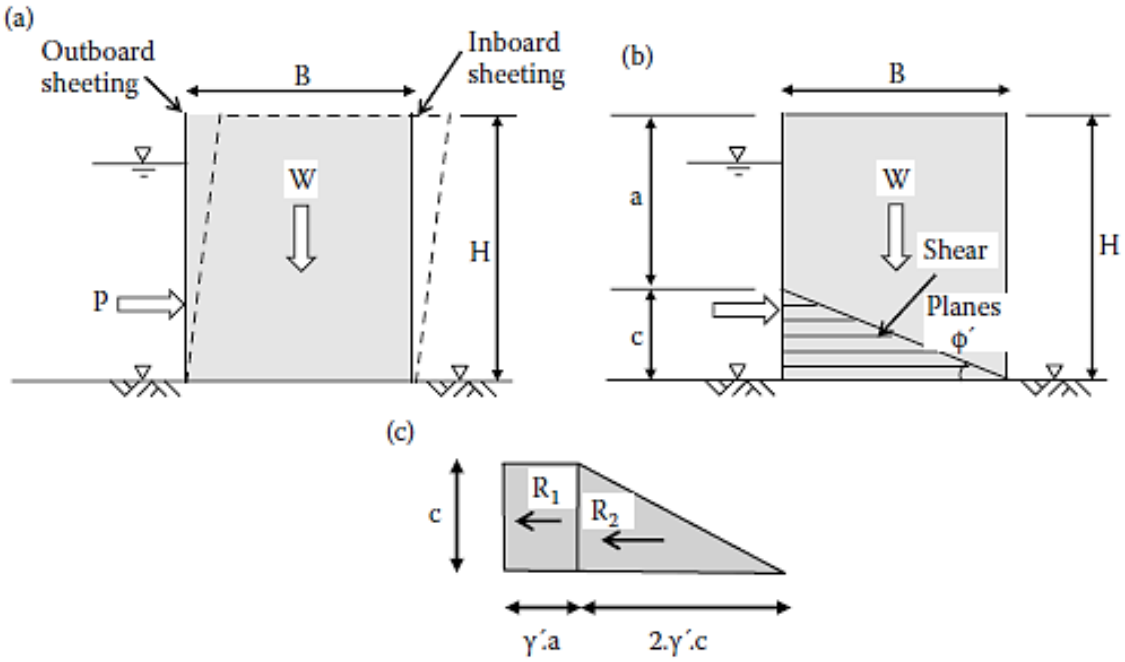

Figure 10. Horizontal shear resistance in a cofferdam, (a) applied forces on the cell, (b) Resisting wedge, (c) Resulting pressure diagram. After (Clayton et al. 2014).

where, H is the height of the cell, H_1 is the height of water above the base, γ is the unit weight of cell backfill above water, γ' is the submerged unit weight $(\gamma - \gamma')$ of the backfill under water, K is the earth pressure coefficient.

According to the formulation above-mentioned the cell fill shear strength can be calculated as.

$$S_s = P_s \tan \phi' \tag{13}$$

By the other hand, the interlock shear resistance can be estimated from the tension interlock P_T calculated above and the steel friction coefficient (f).

$$S_f = f P_T \tag{14}$$

Finally, the total shearing resistance S_T will be the sum of (13) and (14).

For cofferdams founded on rock, sand and stiff clay, the factor of safety on shear failure on a vertical plane, will be the division of the total shear strength (S_T) by the ultimate load on the centerline (Q). For cofferdams supported over soft clay the following expression must be used (Clayton et al. 2014).

$$FoS_{vs} = \frac{P_d r_c f \left(\frac{B}{L}\right)\left(\frac{L+0.25B}{L+0.50B}\right)}{M} \tag{15}$$

where, P_d is the pressure difference of the inboard sheeting, r_c is the radius of the cell, f is the coefficient of steel friction (0.3), B is the effective width of the cell, L is the distance between centerlines of adjacent cells and M is the net overturning moment.

- **Horizontal plane shear failure**

As suggested by (IQBAL 2009), the horizontal shear failure can be calculated as suggested by (Cummings 1957). Where the fill inside of the cofferdam offered resistance in form of a wedge with an angle equal to the fill internal friction angle. The shear resistance force can be calculated from Figure 10 (c) as show in equation (16).

As an additional comment, the diagram proposed by Cummings is justified on case histories records, particularly in the USA.

$$R_T = R_1 + R_2 = \gamma' B H \tan \varphi' \tag{16}$$

Substituting

$$H = a + c \tag{17}$$

$$\tan \varphi' = \frac{c}{B} \tag{18}$$

Finally, the expression Cummings recommended is.

$$R_T = R_1 + R_2 = ac\gamma' + c^2\gamma' \tag{19}$$

The resisting moment above the base of the cell can be calculated as

$$M = R_1 \frac{c}{2} + R_2 \frac{c}{3} = \frac{ac^2\gamma'}{2} + \frac{c^3\gamma'}{3} \tag{20}$$

Also, the horizontal shear resistance provided by the sheet pile interlock can be added to the resistance forces and estimated as

$$M_f = P_T f B \tag{21}$$

Then, the resisting moment against horizontal shear failure is sum of (20) and (21), and the factor of safety against failure will be

$$F = \frac{M + M_f}{M_o} \tag{22}$$

where, M_o is the net overturning moment.

- **Penetration capacity of sheet piles**

The overturning moment, generate a pull-out action over the external (outboard) sheet piles, while the inboard are subjected to push in pressures. The (US Army Corps of Engineers 1989) proposed an equilibrium method that later (IQBAL 2009) presented again in his thesis as the following.

- The pull-out capacity of sheet piles can be calculated as.

$$Q_u = \left(\frac{1}{2} k_a \gamma_e D^2 \tan \delta\right) \tag{23}$$

where, Q_u is the ultimate pull out capacity, k_a is the coefficient of active earth pressure, γ_e effective unit weight of soil in contact with the sheet pile, D is the embedment depth, $\tan\delta$ is the friction coefficient between steel sheet piles and soils presented in Table 1 and Table 2.

Table 1. Friction angle between sheet piles against soils. Adapted from (US Army Corps of Engineers 1989).

Steel sheet piles Against the following soils	$\tan\delta$
Clean gravel, gravel-sand mixtures, well-graded rock fill with spalls	0.40
Clean sand, silty sand-gravel mixture, single size hard rock	0.30
Silty sand, gravel or sand mixed with silt or clay	0.25
Fine sandy silt, non-plastic silt	0.20

When the pull-out capacity is going to be checked on clay, the following equation must be used

$$Q_u = C_a D Perimeter \tag{24}$$

where, C_a is the adhesion between the soil and the steel sheet pile, this value can be taken from Table 2.

The factor of safety against pull out in the outboard sheet piles, can be estimated as.

$$FoS_{pull} = \frac{Q_u}{Q_p} \tag{25}$$

where, Q_p is the pull-out reaction force generated by the overturning moment.

Table 2. Ultimate friction factor and adhesion. Adapted from (NAVFAC 1971).

Interface material	Friction factor	Friction angle
Steel sheet piles against the following soils:		
1. Clean gravel, gravel-sand mixtures, well-graded rock fill with spalls	0.4	22
2. Clean sand, silty sand-gravel mixture, single site hard rock fill	0.3	17
3. Silty sand, gravel or sand mixed with silt or clay	25	14
4. Fine sandy silt, non-plastic silt	0.2	11
Interface material (cohesive soils)	**Adhesion (kPa)**	
1. Very soft cohesive soil (0 -12 kPa)	0	12
2. Soft cohesive soil (12 - 24 kPa)	12	24
3. Medium stiff cohesive soil (24 -48 kPa)	24	36
4. Stiff cohesive soil (48 - 96 kPa)	36	45
5. Very stiff cohesive soil (96 - 192 kPa)	45	62

- Penetration of inboard sheet piles.

The resisting moment on the sheet piles against the push in of inboard can be estimated using the following expression.

$$M_{pen} = (P_T \tan\delta)D \tag{26}$$

where, P_T is the interlock pressure, and finally the factor of safety against penetration of the inboard piles will be.

$$FoS_{pen} = \frac{M_{pen}}{M_o} \tag{27}$$

- **External stability analyses**

As mentioned before, the external analyses must check: the sliding failure, the bearing failure, the overturning failure, and for serviceability sheet pile penetration failure and seepage.

- **Sliding failure**

(Gallant 2011) explained this failure as the evaluation of the horizontal forces that will drive the cofferdam away compare with the shear resistance force along the bottom. The same author also mentioned that when a cofferdam without an

embedment depth is evaluated, the resistance force is given be the friction within the fill and the foundation material, and if the cofferdam is founded over sand the seepage forces must be consider in the analysis.

The other case to be analyzed will be with a structure with embedment depth where the passive pressure will resist the driving translation forces. As sheet piles are not rigid structures, so the passive resistance will only develop to the fixity point as reference by (Schroeder and Maitland 1979) saying that a shear distortion will occur before a translation failure happen, this mechanism is illustrated in Figure 11.

(IQBAL 2009) mentioned that the factor of safety against sliding failure can be calculated as.

$$FoS_{sliding} = \frac{\tau_F}{\tau} \tag{28}$$

where, τ_F is the soil shear strength at the failure surface and τ shear stress developed at the failure surface. This calculation only satisfy the equilibrium of forces, the moment equilibrium must be analyzed separately. The uplift pressure caused by seepage water should be take into account for a complete analyses, also for temporary analyses in cohesive soils where tension cracks can be develop, this issue must be added into the calculations.

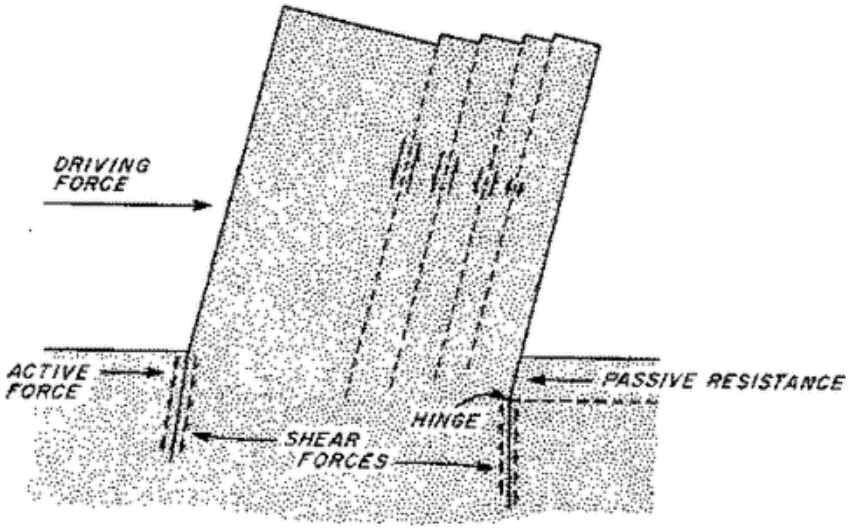

Figure 11. Failure mechanism by vertical shear due to horizontal force. After (Schroeder and Maitland 1979).

- **Bearing capacity failure**

This failure can result in excessive rotation and sinking of the entire structure, especially for cofferdams constructed in soft cohesive soils where the bearing capacity must be checked, (Lacroix et al. 1970) recommended for this computation the use of ultimate bearing capacity equation proposed by Meyerhof 1963.

$$q_u = S_u N_c i_c \tag{29}$$

where S_u is the undrained shear strength, N_c is the bearing capacity factor and i_c is the inclination factor.

For the vertical load (Gallant 2011) expressed that in most cases the width of the cofferdam is too long, so any eccentricity load can be negligible, and the load can be estimated only by the weight in the occupation area.

However, the pressure due to overturning moment can be calculated based on the diagram in Figure 9 (a), and therefore the factor of safety against bearing capacity can be calculated as.

$$FoS_{bearing} = \frac{q_u}{\left(\frac{W}{B} + \frac{6M}{B^2}\right)} \tag{30}$$

(Lacroix et al. 1970) indicated that the factor of safety should be at least of 2 and always complemented by overall stability analysis, especially when there is presence of weaker soils under the founded soil.

- **Overturning stability failure**

Several proposes were made by Pennoyer (1934) and Terzaghi (1944), however, (Hansen 1953), discussed their assumptions, and said that the internal failure was kinematically inadmissible, and that the earth pressure coefficient must be much higher in practice than the one used in calculations.

Hansen, suggested an involving overall rotation under the center of the cell, with a circular rupture surface passing through the toe as presented in Figure 12. For cofferdams founded on rock the failure circular is consider to be concave downward,

but in soils the two cases may happen in function of the sheet pile embedment. For shallow embedment, the circular failure will be concave downward as presented in Figure 12 (a), for structures with deeper embedment the failure surface is in opposite direction concave upward as in Figure 12 (b). For greater embedment depths, the plastic hinge over the sheet piles must be consider as mentioned before.

Later, (Ovensen 1962) suggested a modified failure surface from the one proposed by Hansen with a log spiral form as shown in Figure 13, he mentioned that Hansen method is extreme. Ovensen method is as follows.

$$r = r_0 e^{\theta' \tan \phi'} \tag{31}$$

where, r_0 is the radius at the start of the log spiral, r is the radius after the rotation θ' about the center of the log spiral and ϕ' is the soil angle of internal friction.

For the equilibrium method, a number of failure surfaces must be considered in the analyses in search of the on with the minimum factor of safety.

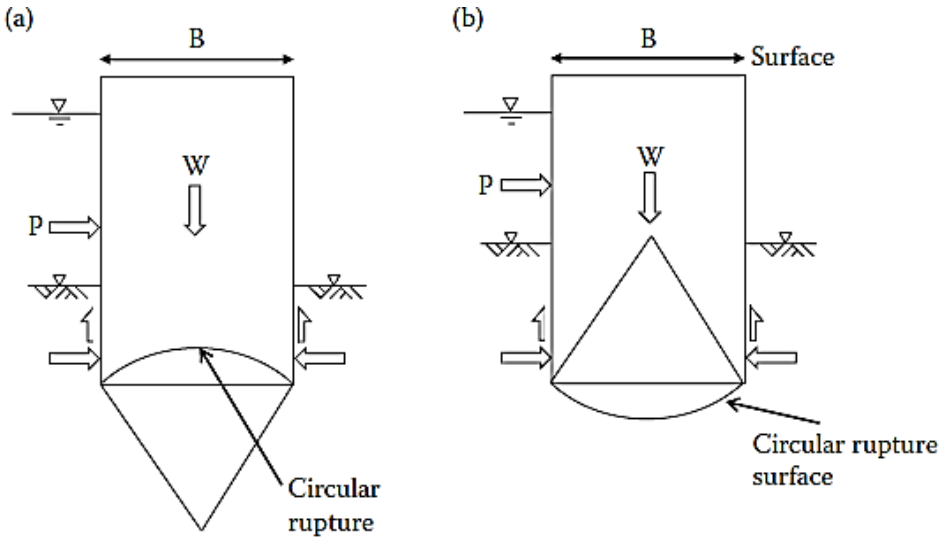

Figure 12. (Hansen 1953) method. (a) Shallow sheet-pile driving depth, (b) Deeper sheet-pile depth. After (Clayton et al. 2014).

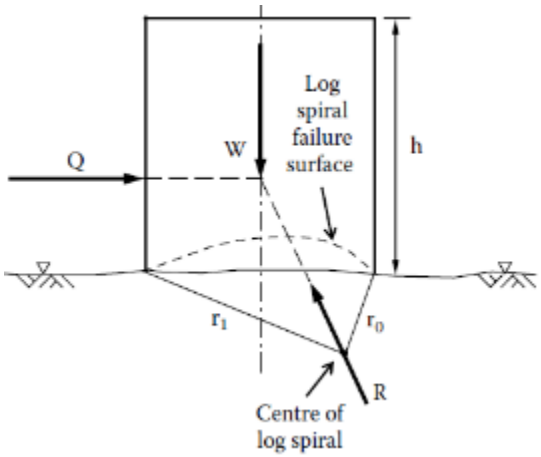

Figure 13. Hansen Modified failure surface. After (Clayton et al. 2014).

Clayton et al. (2014) recommended the following procedure to estimate the stability moment:

1. Draw the cofferdam to scale, as shown in Figure 13.

2. Compute the external (Q) and gravity (W) forces acting over the cofferdam and above the rupture line.

3. Plot an arbitrary log spiral through the toes of the inboard and outboard sheet piles. Locate the center (pole) of the log spiral and the resultants of Q and W

4. Take moment about the pole as.

$$F = \frac{M_{stabilising}}{M_{driving}} \tag{32}$$

5. Draw a number of other log spiral, with the same center for different values of r_0.

6. Calculate the factor of safety for each surface.

7. Plot the factor of safety as a function of the radius r_0, of the log spirals. If none of factors of safesty are equal or less than 1, then the structure is stable.

- **Sheet pile penetration**

When the embedment is constructed in soft materials, excessive penetration can be reached from a sinking effect. Terzaghi (1944) suggested that an embedment D must be checked on the unloaded side of the structure and must be of $D = {}^{2H}/_{3}$ when this issue is a concern. The resistance to penetration can be evaluated as:

$$R_p = 2\left(\frac{1}{2}\gamma' K D^2 \tan\delta + \frac{2}{3}c\right) \tag{33}$$

where δ is the angle of friction between the soil and the sheet pile, these values are presented in Table 1, c is the effective cohesion intercept. This friction resistance must be considered in both sides of the sheet piles. According to (Lacroix et al. 1970) The adhesion should not exceed 1.5 ksf.

- **Sheet pile penetration**

Terzaghi (1944) suggested that an embedment of $D = {}^{2H}/_{3}$ should mitigate these effects, but a flow net should be developed to understand the head loss across the structure, as the one presented in Figure 14.

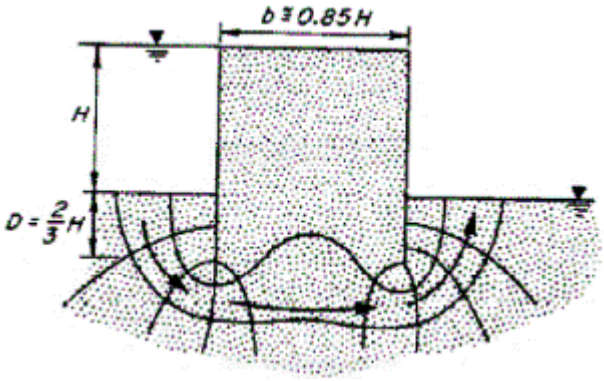

Figure 14. Typical cofferdam flow net. After (Schroeder and Maitland 1979).

(Lacroix et al. 1970) suggested three major problems. The first is the formation of a pipe caused by internal erosion, the second issue is the possibility of a quick sand condition where the head pressure is able to lift the soil, and the third concern

is the passive resistance reduced due to vertical stress decrease generated by an upward gradient in the passive zone.

The piping could generate voids, causing settlement of the structure, the uplift may cause and excessive bottom heave and failure at the toe, causing movements on the structure, finally the reduction of the passive resistance could generate an excessive shear distortion of the sheet piles.

All these concerns must be checked with a flow net and factors of safety.

- **Additional comments for Urban braced cofferdams**

Urban cofferdams are constructed below soil and groundwater, commonly used as temporary structures for infrastructure and urban development projects. The construction procedure and the geometric alternatives vary according to the soil conditions such as the presence of rock, soft soils, and the water table level (Puller 1996).

The cost of the cofferdam is proportional to the size and shape, been more efficient the circular and the rectangular shape, this also condition the type of strut or props that must be employed, and always taking into account the space require in the inside for the permanent structure in place.

Puller, suggests that in case of soft soils a lower strut must be used next to the bottom cut, to help avoid a failure due to lack of passive resistance.

About the quality of workmanship (Puller 1996) says "*it is essential that load is transferred efficiently from soil to sheeting to wailing to strutting, without any doubt as to the direction of the transfer. The principal reasons for failure of sheeted cofferdams are poor workmanship in connections causing insecure transfer of load, inadequate strut section, inadequate embedment of the sheeting and overload due to inadequate allowance for surcharge loading. These modes of failure should never be forgotten".*

- **Cofferdams sheet piles**

The sheet piling is selected according to its flexion capacity and strength, needed to support earth and water pressures, and taking into account the driving permissibility considering toe and head possibly damages.

In granular soils without large blocks or gravel, the factor that determines the driving of sheet piling is friction between the ground and the steel, while on cohesive soils is the adhesion factor. For this there are tables and correlation that help the designer to select the type of sheet pile based on the N value from the SPT, the soil internal friction angle, the undrained shear strength among others (Puller 1996).

- **Cofferdams ground anchors**

The use of anchors as a reinforcement of a cofferdam depends on the embedment soil where the anchor is going to be installed, soft soils as clays must be avoid instead gravels and sand strata are ideal for this use. Also should be consider the use of the neighbor soil and future structures in the zone.

The anchors purpose is to transfer the arriving loads on the sheet piles to a fixed length beyond the theoretical failure surface, where the contact between the cement slurry and the soil can resist the stresses. Generally, there are four types of anchors, according to the type of use, time of service, methodology of filling or injection. Additionally, their design can be performed with empirical or semi-empirical methods, from typical values of vertical and horizontal spacing, as well, as for the free and fixed lengths.

- **Cofferdams tremied plugs and grouted bases**

According to (Puller 1996) when there are permeable strata the bottom can be seal with concrete plugs avoiding the flow of water into the inside of the cofferdam due to differences between the water table and the bottom of the excavation. The concrete plug weight is greater than the pressure difference and can also be helped with injections that may reduce the flow and if they are constructed with vertical reinforcement can increase the capacity of the plug by assuming tensile forces. The same author mention that this concrete plug can serve the dual function of reducing

the sheeting moment and reducing the stresses over the lower bracer working as an additional one.

In other cases, only injections could be used in the bottom, forming a curtain around the bottom area, and assuming a dual purpose, reducing the permeability and anchoring the ground to a lower stiffness material if they are constructed for this work with vertical reinforcement.

- **Cofferdams bracings**

The first step is the design of the wailing needed to transfer loads in an uniform way to the struts or anchors. The principal characteristic of these elements is that they should be perfectly set over the sheet pile and located at the reinforcement level. The wailing can be constructed with reinforcement or with prefabricated steel profiles, which may even be used in pairs to add stiffness (Puller 1996). In Figure 15 a schematically braced excavation is shown, in the figure the wales are presented over the sheet pile and denoted as “Wale”.

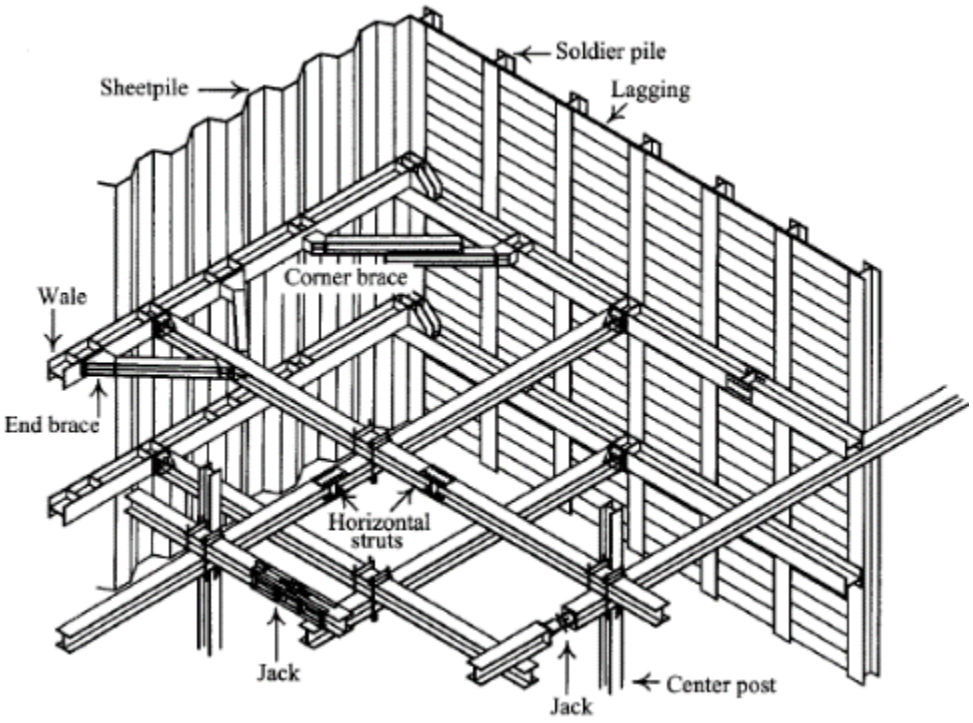

Figure 15. Typical structural components of a braced excavation. After (Ou 2006).

The other principal element is the strut, for this element special precautions must be taken avoiding failures for buckling or insufficient strength, otherwise a collapse for excessive buckling may occur.

According to Puller the workmanship quality plays a fundamental role in the behavior of the strut work, because of redundancy and installation quality. A bad process, an error or an element failure could trigger a progressive failure, especially if it is the lower level of reinforcement and the structure has a minimum embedment, which means a practical full stability dependency over the last strut.

Additionally, for the strut design and distribution the minimum space for an efficient excavation process must be taking into account, so the construction will not be affected. A typical minimum space range for this purpose is between 4 and 6 m as suggested by Puller.

For the construction of struts various materials can be employed. However, the more efficient is the use of steel pipes, due to its void content (less weight), to its high resistance to buckling and compressive strength. In Figure 15 struts with an “I” profile are shown. The ideal installation is perpendicular to the wailing.

(Puller 1996) says that the structural design of these elements can be performed with a limit state of loads and if load factors are mobilized is not necessary to use additional factors. The same author also recommends to always compare the result with empirical methodologies. As an additional comment if steel is going to be used in the design the thermal changes should be taken into account.

To the selection of the vertical spacing between wailings, the first concept to be considered must be the elements strength and then the space require for the construction sequence, for example is a double height construction can be performed or the space should be sacrifice and the procedure performed in simple heights.

- **Circular Urban cofferdams**

The great advantage of these systems is the net compressive forces generated inside of the excavation, due to their circular shape, enabling the possibility of using perimeter reinforcements that don´t occupy the working area. However, for this to happen the soil and water pressures around the cofferdam should be uniform.

For these systems, different construction methodologies and structural elements can be employed. In addition, Puller (1996) suggests that the estimation of the radial load can be calculated by the expression recommended by Timoshenko and Goodier and presented as:

$$W_u = \frac{KE_r I_v}{{R_c}^3 x 10^5} \tag{34}$$

where, W_u is the ultimate radial wailing load, k is the coefficient that depends on the stiffness of the retained medium, for cofferdams in water a common value is 3, this value should be major when the medium stiffness is increased. However, for soils is common to use the same value and a reduction factor of 2 for and admissible radial resistance, R_c is the cofferdam radius and I_v is the moment of inertia about the vertical axis.

Alternatively CIRIA according to (Puller 1996), determines an empirical relationship based on the level of the reinforcement ring and the diameter of the cofferdam to estimate the stiffness of the bracing where $d_e = D_e/35$, where d_e is the depth of the reinforcement ring and D_e is the internal diameter of the cofferdam.

(Puller 1996) proposed an empirical relationship from the cofferdam diameter, for the use of wailings, this relation is shown in Table 3 and warns that caution should be taken when using perimeter reinforcement and there are not uniform stresses at each level around the cofferdam.

Commonly the vertical reinforcement of circular cofferdam is built using sheet piles or diaphragm walls. The advantage of diaphragm walls is that can reach great depths and can be installed in soils where sheet piles can not be driving, even this type of wall can support compressive stresses when they are built with an acceptable verticality and properly connected with all segments, i.e., a construction with high quality workmanship. So it is always recommended to consider horizontal reinforcement to make a redundant system with temporary struts or with permanent slabs (in case of a top-down construction).

Table 3. Admissible load for braced circular cofferdam. Adapted from (Puller 1996).

D, diameter of cofferdam (m)	Size of wailing *d* x *b* (mm)				
	450 x 300	600 x 400	750 x 500	900 x 600	1050 x 700

	six 20 mm dia. Bars	ten 20 mm dia. Bars	ten 25 mm dia. Bars	fourteen 25 mm dia. Bars	twelve 32 mm dia. Bars
5	280	500			
10	140	250	390		
15	90	165	260	375	
20		125	195	280	380
25			155	225	305
30				185	255
35					215

Based on:
(i) Permissible compressive stress in concrete not to exceed 5-2 N/mm^2.
(ii) Wailing load (in kN/m) = 1-5EI/10$^5R^3$; E = Young's modulus, for concrete E = 13800 N/mm^2, I = moment of inertia about xy axis (cm^4), R = cofferdam radius (m).
(iii) Depth of wailing d to be no less that D/35.
(iv) Need to check tension in waling beam if sheet piles distort under load and concentrate load on top and bottom of wailing beam.

In case of using sheet piles, the installation can be faster and in some cases the elements reused, but its low rigidity requires the use of bracers so the deformations can be controlled.

2.3.3. Typical cofferdam construction

Normally off shore construction procedure for cellular cofferdam is as exposed by (IQBAL 2009) and is presented as follows. Some of these steps vary depending of the type of cofferdam and the place where is constructed.

1. The sheet piles are fixed in place and driven into their design depth.
2. When the cell is complete, the excavation within the cell is made, this procedure must be done under balanced water to avoid movement towards the inside of the cell, and by using temporary bracing system at needed levels.

Until this point a regular cofferdam (or one cell of a cellular cofferdam) will be done to perform the necessary work. For a cellular cofferdam in off shore conditions the procedure continuous as follows.

3. Once the excavation is complete a fill compacted in layers is constructed inside the cells while they are tied between them.

4. Once the cofferdam structure is completed with all the cells filled with compacted soil, the water can be removed to reach a dry work zone.
5. The berm (commonly needed in off shore applications) can be constructed underwater or ones the dry zone is reached, depending on the design conditions (undrained or drained case).
6. When the cut base is reached with the appropriate excavation-bracing sequence and the water is pumped out of the cofferdam, the temporary use of this structure is completed and the area can be used to the next construction activity, normally the construction of the foundation structures.

2.3.4. Cofferdam safety precaution

As mentioned by (Santhosh et al. 2014) in their publication and as seen in common excavation constructions, the safety aspect is a very important concern, since during the construction, workers will be exposed to the hazard of sudden collapse or flooding. To control safety potential problems every part should be of suitable design, construction, sufficient strength and capacity material.

Every construction stage should provision the adequate access, light, ventilation and attention for safety practices, and each stage must meet the design hypothesis without departing from the recommendations, so the field performance must be as similar to the design estimations as possible, and every possible misbehavior can be repair as soon as detected.

2.4. P-Y Model for Soils

The p-y methodology was used for the back-analysis of the Chicago Downtown Cofferdam so this title contains a brief description of the methodology to contextualize the reader.

As an introduction (FHWA 2010) defined this methodology as: a criteria to associate the soil mobilized resistance as a nonlinear force – displacement relation. There are several theoretical bases for this design technique, however, most of the principles are based on empirical relations from in-situ experiments (load tests). Therefore, the authors explain that the used of the p-y curves must be under their limitations and with a complete understood of the models characteristics.

- **P-y curves for clays**

As explained by (Reese et al. 2002), Matlock (1970) and Reese et al. (1975) hardly researched the stiffness (ε_{50}) of the material with the in-situ experimental response of clays, and they concluded that this parameter is an important one to compute the deflection response under a lateral load. Matlock (1970) found from laboratory tests that ε_{50} values may vary from 0.02 to 0.005 for normally and overconsolidated clays with different undrained shear strength.

When there is absence of data this parameter could be selected from Table 4 by knowing the magnitude of undrained shear strength (S_u), due that ε_{50} is the strain that correspond to S_u.

Table 4. Values of ε_{50} for stiff clays. Adapted from (Reese et al. 2002).

Consistency of clay	Average value of kPa	$\boldsymbol{\varepsilon_{50}}$
Soft	<48	0.020
Medium	48-96	0.010
Stiff	96-192	0.005

As briefly explained by (FHWA 2010) Matlock (1970) and Welch and Reese (1972), proposed polynomial models for the nonlinear soil response to lateral loads, these conceptual models are presented in Figure 16. Figure 16 (a) is the one proposed for soft clays, Figure 16 (b) is the one used for stiff clay in the presence of water.

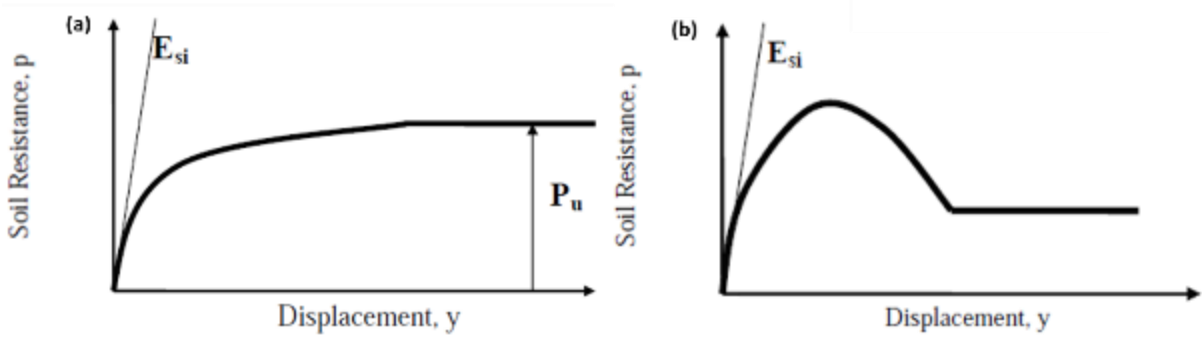

Figure 16. Conceptual p-y curves. (a) Soft to medium cohesive soil. (b) Stiff clay. Taken from (FHWA 2010).

For clays the input that most significantly affects the p-y curve response is the undrained shear strength, which can be directly related with the ultimate soil resistance and the soil modulus, therefore are tables and correlations like Table 5 that correlate S_u with the lateral

stiffness of the clay. Brown et al. (2010) recommends that the engineers using p-y curves must perform the analyses with ranges of values of S_u and ε_{50} so a sensitivity of the analyses can be understand. In case of the stiff case the curve according to (Reese et al. 2002) were proposed for stiff clay exposed to free water or near the ground surface where a resistance degradation can occur, it is also applicable below groundwater conditions.

Table 5. Soil Modulus Parameter for clay. Adapted from (Reese et al. 2002).

	Average undrained shear strength		
	50-100	100-200	300-400
k (static), MN/m^3	135	270	540
k (cyclic), MN/m^3	55	110	540

For sands the model, is based in an initial linear stiffness followed by a polynomial model as the one presented in Figure 17.

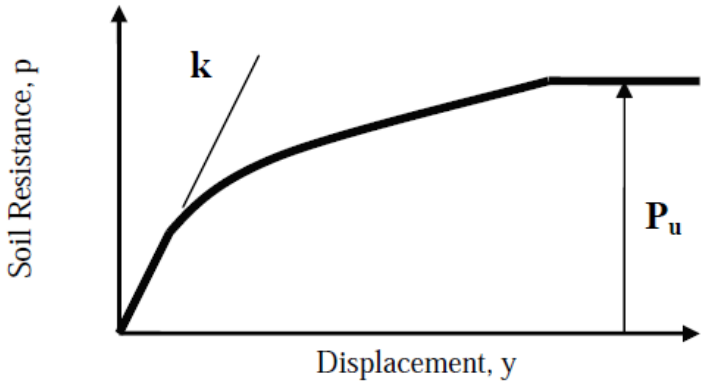

Figure 17. Conceptual p-y curve for cohesionless soil. Taken from (FHWA 2010).

In this case of sands the most relevant parameter is the initial modulus value k, which directly affects the initial linear response, this parameter value is based on the relative density of the sand, taking into account the effect in dry or submerged conditions. Additionally, the ultimate resistance is function of the internal friction angle and the vertical stress. But the most relevant parameter is the modulus value k, these were suggested by (Reese et al. 2005), and are presented in Table 6.

Table 6. Soil modulus for sand. Taken from (FHWA 2005).

Relative Density	**Loose**		**Medium**		**Dense**	
	(kPa/m)	(lb/in^3)	(kPa/m)	(lb/in^3)	(kPa/m)	(lb/in^3)
Submerged Sand	5430	20	16300	60	33900	125
Sand above W.T.	6790	25	24430	90	61000	225

2.5. Soil-structure spring models

When a complete analysis is required to estimate pressures, internal forces, movements that may affect near structures a soil-structure interaction model can be performed.

A spring model is an alternative from several types of analyses that can be performed where the soil is replaced by discrete springs like the example presented in Figure 18.

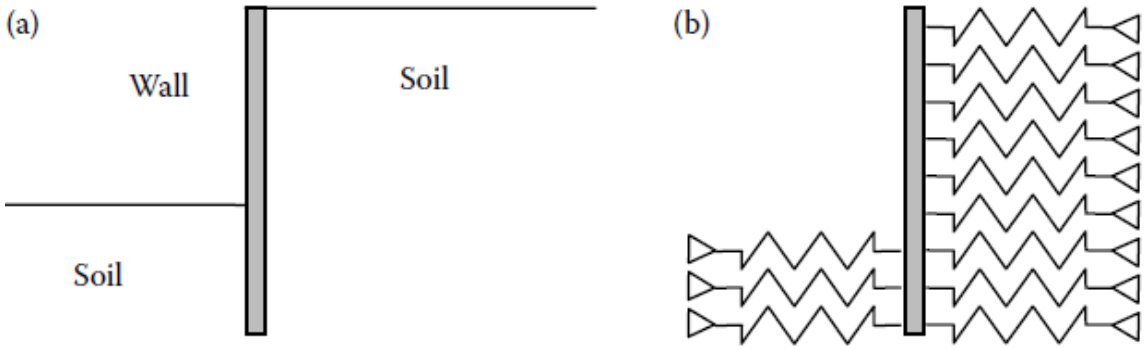

Figure 18. Discrete soil-structure spring model. After (Clayton et al. 2014).

This methodology was employed in the back-analyses for the Chicago Downtown Cofferdam.

As mentioned by (Clayton et al. 2014) method consist in idealizing the soil in contact with a structure as linear spring. There are alternatives for applied this as a force-displacement spring or as a pressure-displacement spring, these relations are controlled with a modulus of elasticity k and the idealization that soil is a homogeneous, isotropic linear elastic material. Therefore, the definition of the k magnitude is very important, knowing that is not entirely correct to assume this value as constant for a material subjected to different stress levels. Notwithstanding this the model has proven to be practical useful for geotechnical problems.

For horizontal problems (i.e. retaining structures) k is the modulus of subgrade reaction, or the horizontal methodology proposed by Matlock and Reese (1960), the p-y curves initially oriented for laterally-loaded piles. This last one can be used to eliminate the linearity of the model, and in analytical solutions these p-y curves can be used varying with depth to improve the results.

The greater limitation of this solution is that as refined as the model can be it cannot model movements in the surrounding ground, away from the soil structure interface (Clayton et al. 2014).

For reliable result a full discretization of the soil-structure interaction must be performed by replacing continuous functions with discrete approximations. The procedure typically

begins with balance in-situ stress distribution over the retaining structure, and then the excavation process from the top to the bottom is modeled, this procedure must be as similar as the real construction sequence will be. Initially the springs will start at zero and will be removed by levels in the inside of the excavation generating load imbalance, making the other springs deform as they take additional load to reach equilibrium for each excavation stage. If a structural element is going to be used, they can be simulated by additional springs. Also (Clayton et al. 2014) mentioned that is a long-term condition is going to be modeled the softening can be performed by decreasing the spring stiffness.

The principal output of this type of simulation is the wall displacement.

2.6. Deformation Analyses with simplified techniques

2.6.1. General ground movement pattern for braced excavations

Excavation procedures always generate lateral movements and settlements in the surrounding ground. It is necessary to estimate the magnitude of these deformations, so damage in adjacent structures can be avoid and in extreme cases collapse due to excessive deformation. These movements are closely related to soil and ground water conditions, the retaining structure stiffness and the construction stages (Zapata-medina 2007).

(Clough and O'Rourke 1990) established a general pattern of ground deformations for braced excavation according to the excavation stages as shown in Figure 19. The first stage is a cantilever movement that happened after the installation of the vertical retaining support and the excavation to the first level, generating a settlement with a triangular distribution behind the wall. Typical of flexible structures with zero restraining forces next to the initial ground level.

Then, to reach deeper levels a horizontal support must be installed to avoid excessive displacements, with these step a deeper cumulative displacement occurs, as illustrated in Figure 19 (b), also if the wall is not fixed in the toe into a stiff enough soil the cumulative displacement may be larger and behind the wall the triangular shape tend to change its distribution into a concave shape.

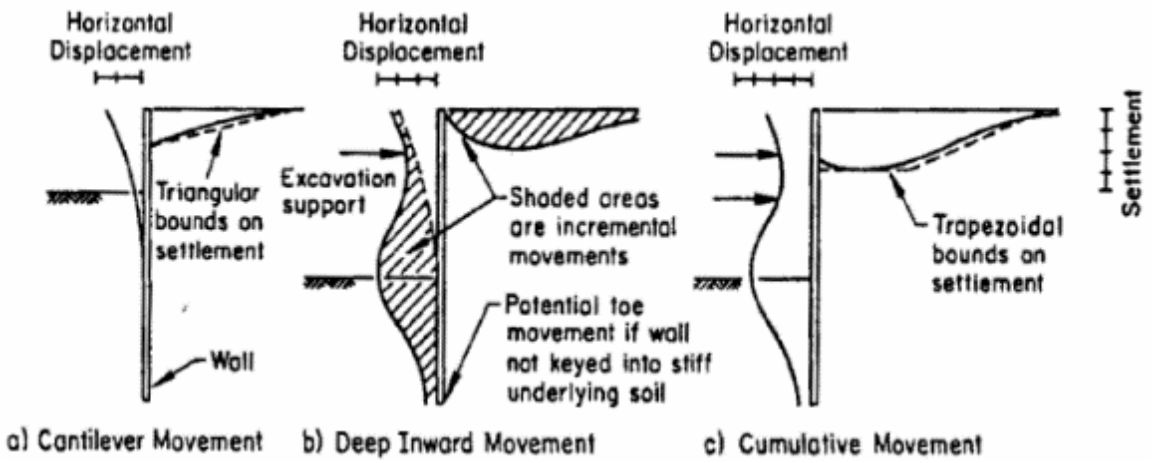

Figure 19. Typical scheme of ground movements for braced excavation systems. After (Clough and O'Rourke 1990).

Finally, if the excavation continuous, additional struts or braces should be installed to restrain the movement and reach a cumulative displacement as the one presented in Figure 19 (c) where, a combination of cantilever wall behavior next to the surface and braced excavation trend around the bottom is achieved. Also, a trapezoidal bound settlement shape behind the wall is very likely to occur.

A similar behavior was reported by (Ou 2006), where he made an explanation with the schematic illustration presented in Figure 20 with different stiffness levels. The first sequence (a), (b) and (c) represent a braced excavation system with high stiffness supports, where the restraining elements control the horizontal displacements, generating a wall rotation about the contact point, and a deeper movement at the bottom cut level if the soil in the passive zone is not strong enough.

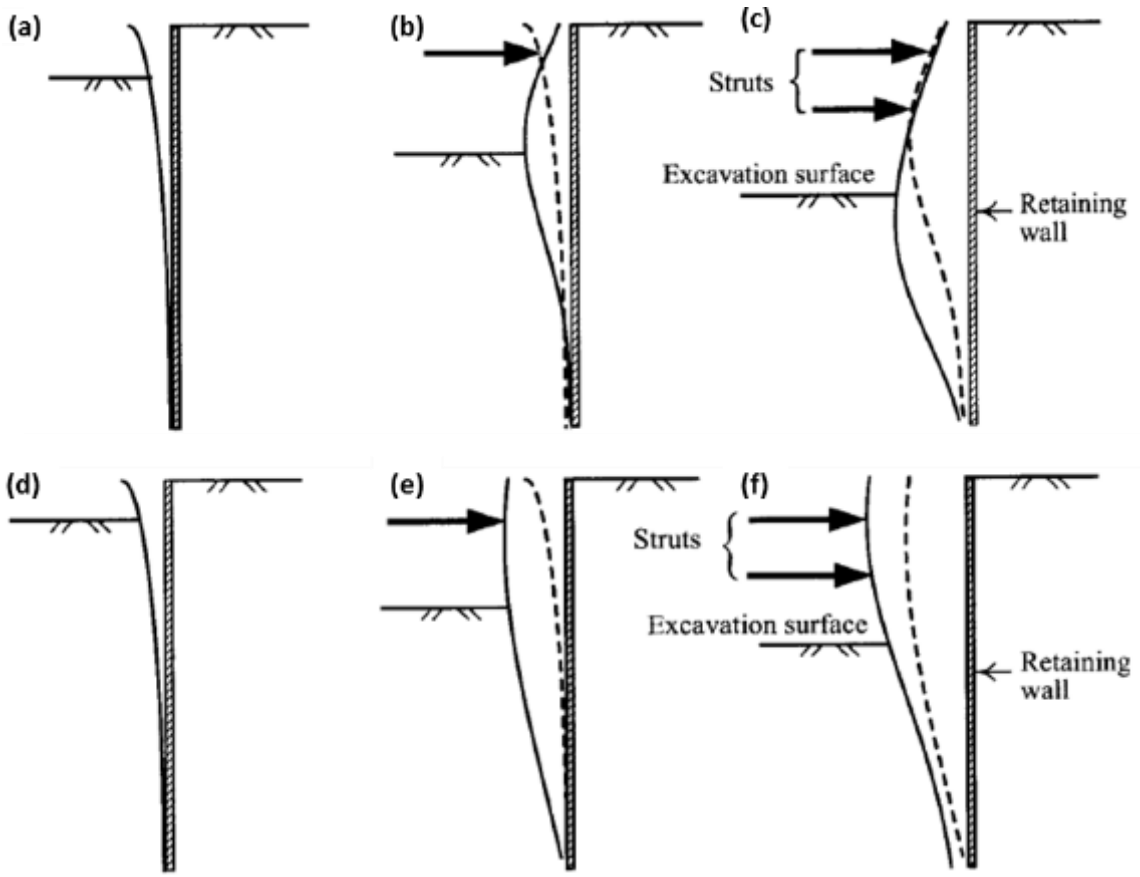

Figure 20. Difference between braced excavations with high stiffness struts (a) first stage of excavation, (b) second stage of excavation, (c) third excavation level and with low stiffness struts (d) first stage of excavation, (e) second stage of excavation (f) final stage of excavation. After (Ou 2006).

By the other hand, Figure 20 sequence (d), (e) and (f) shows an equal excavation stages with struts with lower stiffness. In this case the result is a lateral deformation more likely to a cantilever wall and the maximum displacement will be located next to the original surface.

2.6.2. Horizontal ground movement prediction due to excavation activities

When an excavation take place the initial stress conditions change, generating unbalance forces and displacements, these conditions must be equilibrated by the retaining structure, however, as presented before there are always different factors that affect the shape and magnitude of this horizontal displacements, (i) the excavation depth, (ii) surrounding soil and water conditions (iii) the wall and struts stiffness, (iv) the preload

magnitude, (v) excavation quality and sequence procedure and (vi) the surcharge magnitude. Also, the stability factor of safety indicates the magnitude of deformation, the greater the factor the smaller the horizontal displacement will be.

(Clough and O'Rourke 1990) describe the horizontal displacement due to basic excavation activities and divide the results by type of soil.

1. Horizontal movements in stiff clays, residual soils and sands. In these type of soils is usual that the basal heave stability is not an issue. And they found that with excavation support systems the maximum displacement is limited to 0.5% the excavation depth this is shown in Figure 21.

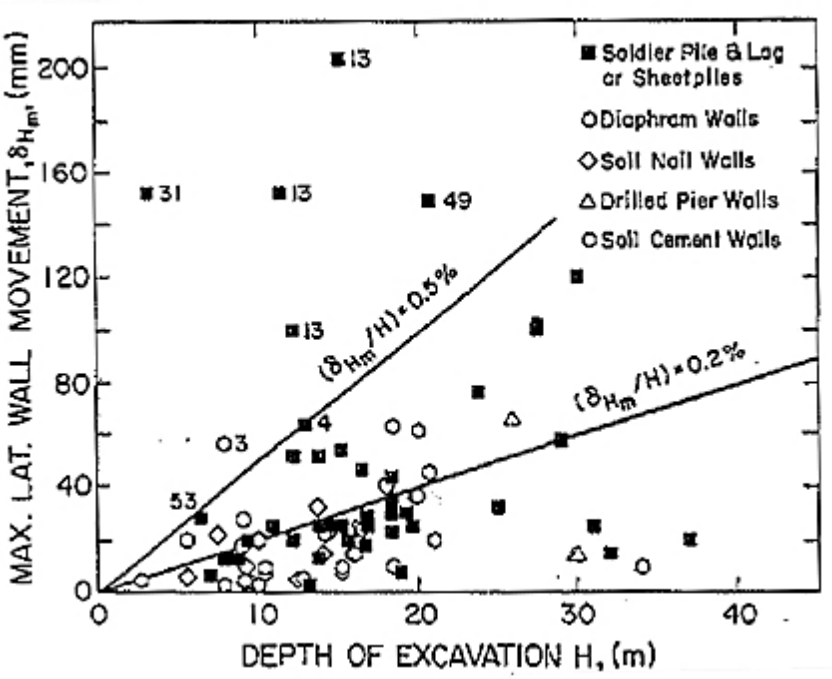

Figure 21. Maximum lateral movement for in-situ walls in stiff clays, residual soils and sands. After (Clough and O'Rourke 1990).

The chart from Figure 21 present points outside the regular data, according to each case history those were excavations influenced by additional factors (i.e. bad workmanship quality).

The conclusion is that the horizontal movements tend to an average value of 0.2% of the excavation height and that there is not a significant difference between the kinds of support system for the maximum displacement.

As an additional comment for these soils Clough and O'Rourke (1990) suggest "…*that in stiff soil environment variations in soil stiffness have a more profound effect on wall behavior than system stiffness."*

2. Horizontal movements in soft and medium clays. In this case the basal heave stability is a great concern and may dominate the deformation pattern. So Peck (1969) relate the behavior with soil stability number that directly affect the factor of safety against basal heave. Finally, they proposed the chart presented in Figure 22 that is also influenced by the structure stiffness and the struts spacing. Where δ_{hm} is the horizontal

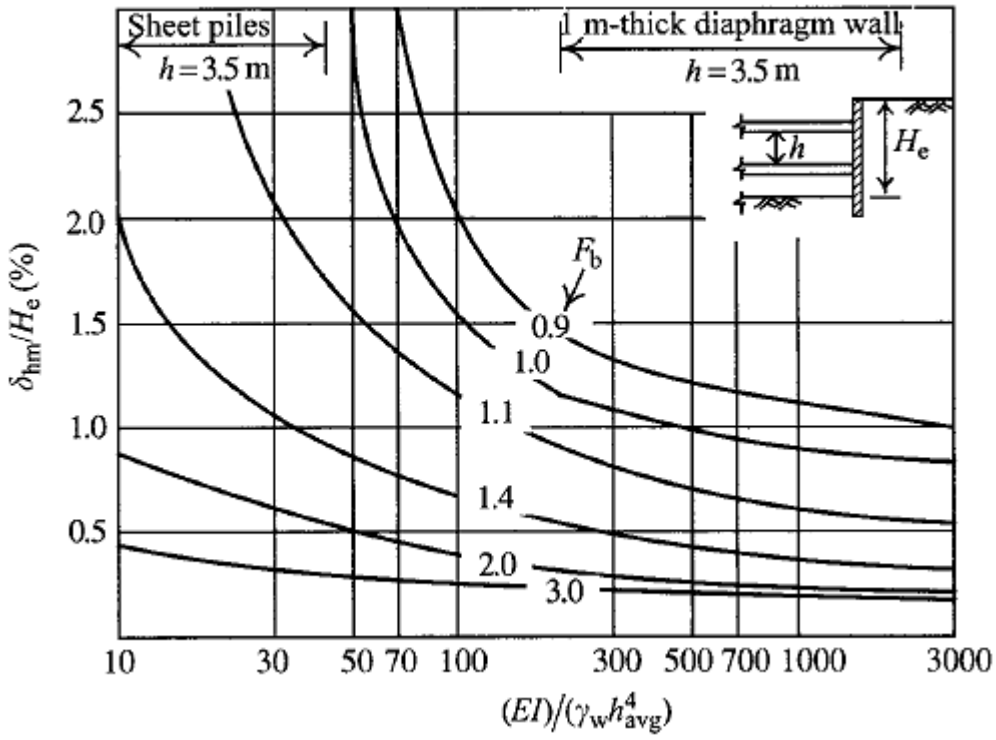

Figure 22. Curves to obtain maximum lateral wall movement or soil settlement for soft to medium clays. After (Ou 2006).

This chart shows that for low stiffness retaining structures like sheet piles with low factor of safety against basal heave (under 1.5) the lateral movement increase rapidly. But in other cases, it shows that high stiffness wall like diaphragm walls (1 m thick) with factors of safety against basal heave over 1.5 have lateral movements related with the excavation depth of approximately 0.5%: Showing consistency with Figure 21 when the basal heave is not an issue.

This chart is commonly used in practice to predict wall lateral deflections and surrounding ground settlements when the deformation conditions are primarily due to the excavation process.

More recent excavations devepoled in Tapei (Ou et al. 1993) allowed to confirme the correlations presented by (Clough et al. 1989), these evalutions are presented in Figure 23, where the lateral deformation increase with a linear correlation with the excavation depth.

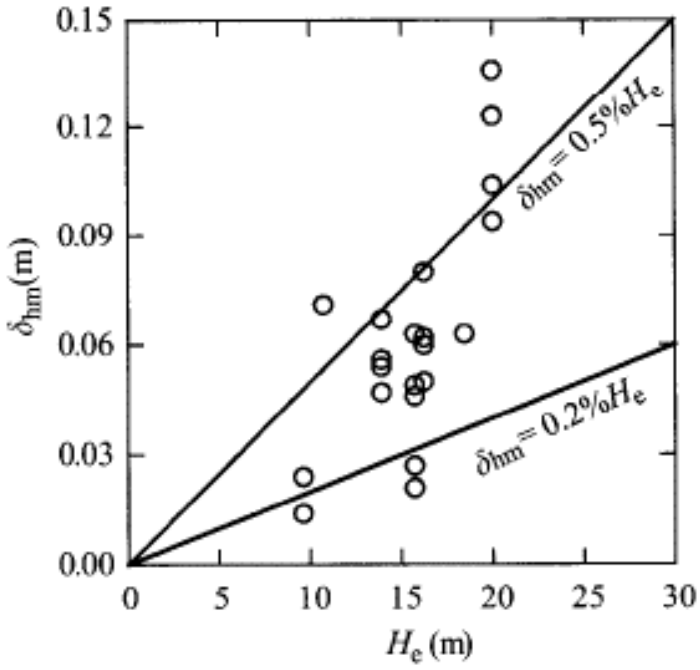

Figure 23. Relationship between lateral deformations on retaining wall vs. excavation depth. After (Ou 2006).

From the chart proposed by (Ou et al. 1993) the following equation was presented, where usually the upper limit is recommended for soft clay and the lower limit for sand, also an averga value can be used for alternating layers of clay and sand.

$$\delta_{hm} = (0.2 - 0.5\ \%)H_e \tag{35}$$

where, δ_{hm} is the horizontal maximum displacement and H_e the excavation depth.

Some cases may exceed the upper value, the common issue with those is that the they are influenced by additional factors, like heavily surcharges, artesians water pressures, structural elements with stiffness variations due to time and temperature effects, amound others.

(Bryson and Zapata-Medina 2012) presented a semi-empirical method to design excavations by taking inot account the retaining system stiffness to limit the excavation-induced ground movements.

They improved the chart presented by (Clough et al. 1989) (Figure 22) by adding an additional factor that represent a more realistic behavior of deep excavations, this factor relates the soil and retaining system stiffness and was called relative stiffness ratio R and is definied as.

$$R = \frac{E_s}{E_w}\frac{S_H S_V H_T}{I}\frac{\gamma_s H_e}{S_u} \tag{36}$$

where, E_s is the young modulus of the soil, E_w is the Young's modulus of the wall, I is the moment of inertia per unit length of the wall, S_H and S_V the horizontal and vertical support element spacing, H_T the total wall height, H_e the excavation depth, γ_s the average unit weight of the soil and S_u the undrained shear strength of the soil at the bottom cut.

Low values of R represent high stiffness walls like secant piles and diaphragms walls, high values represent flexible structures like sheet piles. From re-analyses of several case histories they reached the following equation that correlate the maximum lateral deformation wall height relation with the relative stiffness ratio and the factor of safety against basal heave.

$$\frac{\delta_{H(max)}}{H_T}(\%) = 0.275 x F.S.^{-0.9322}\, R^{(0.2585-0.0351 x F.S.)}. \tag{37}$$

where $\delta_{H(max)}$ is the lateral maximum deformation, H_T is the wall total height and $F.S.$ is the factor of safety against basal heave, that can be calculated using the Terzaghi modified procedure proposed by Ukritchon (2003), and presented in the following Figure 24 among the design chart proposed by (Bryson and Zapata-Medina 2012).

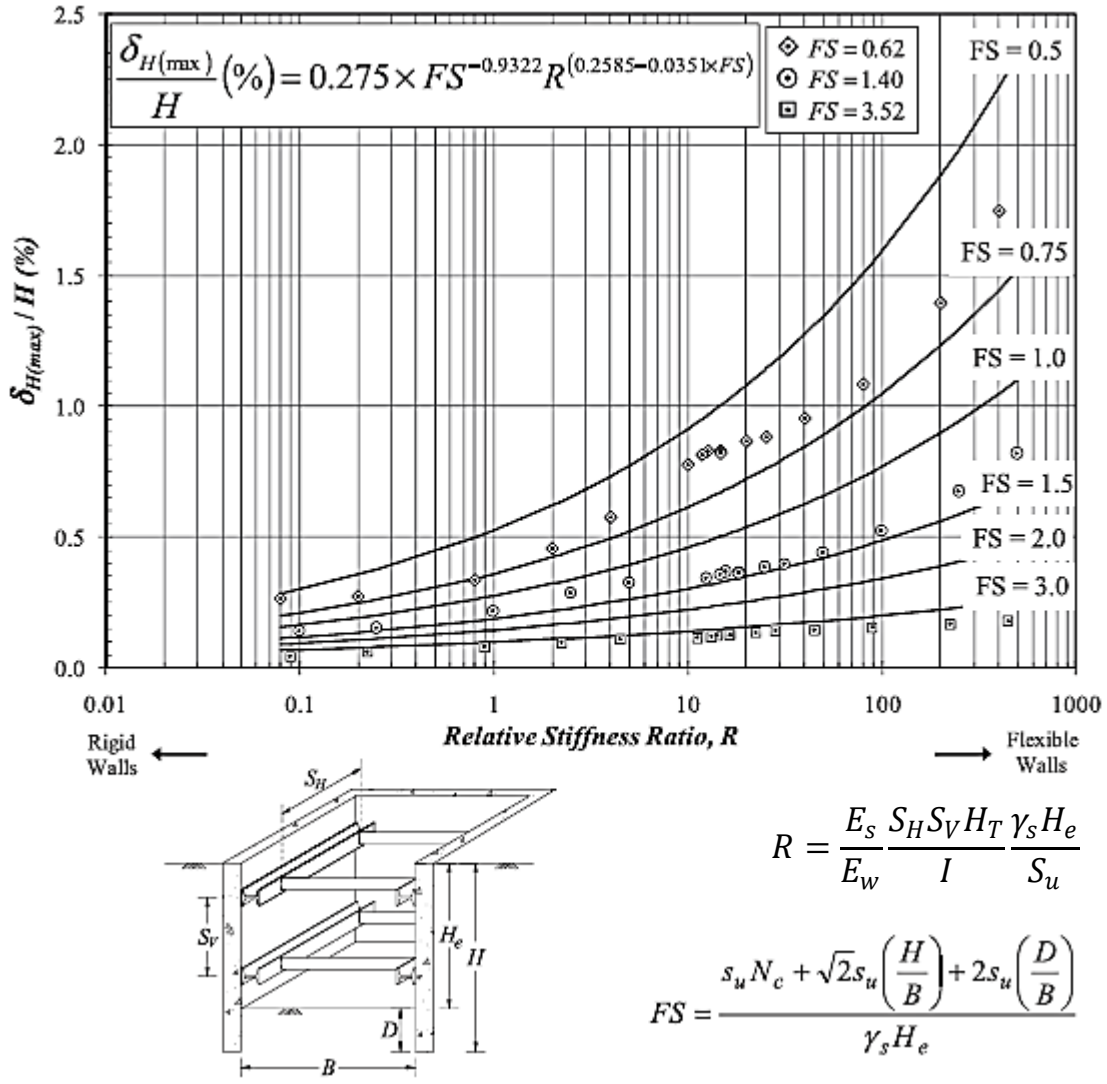

Figure 24. Design chart with relative stiffness ratio. After (Bryson and Zapata-Medina 2012).

This methodology perform much better than the one proposed by (Clough et al. 1989), as presented in Figure 25. Where also is shown how this methodology can predict small and large movements.

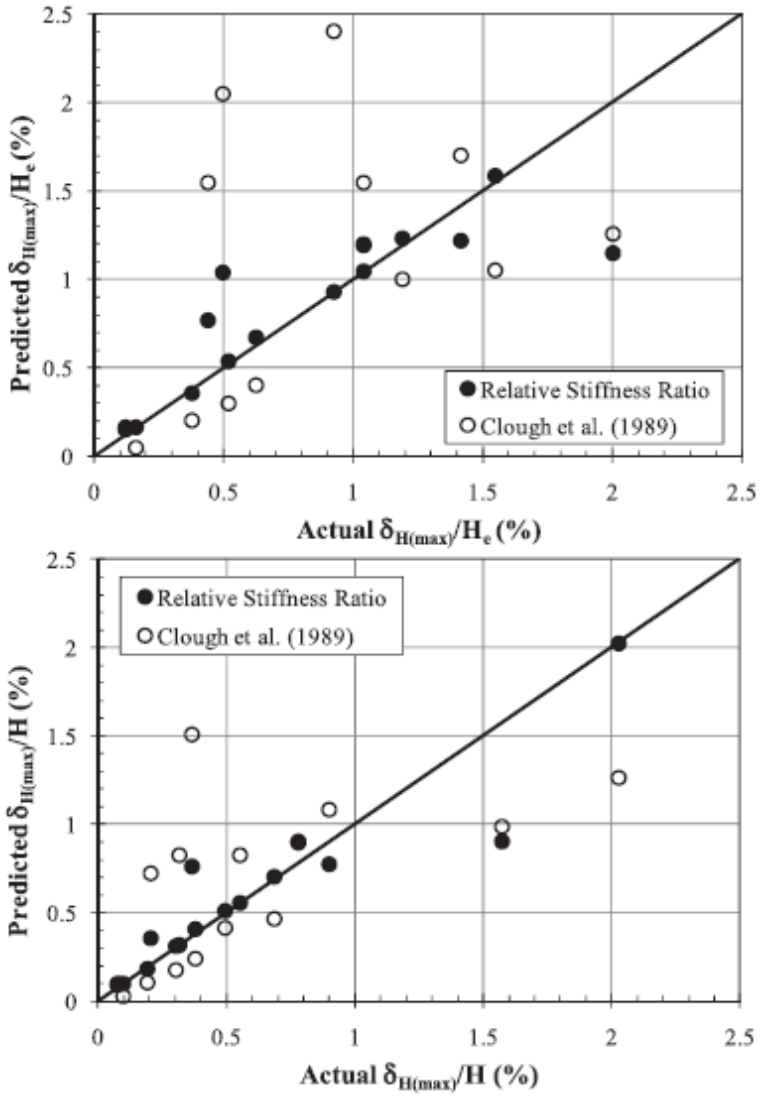

Figure 25. Comparison between methods to predict lateral wall deformation magnitude. After (Bryson and Zapata-Medina 2012).

Also, the authors proposed a relation between from case histories evaluation between the maximum lateral deformation and the maximum settlement without presenting a pattern or deformation distribution only the magnitude, this one can be estimated with the following equation.

$$\frac{\delta_{H(max)}}{H} = 0.9221\left(\frac{\delta_{V(max)}}{H}\right)^{0.7696} \tag{38}$$

where $\delta_{V(max)}$ is the maximum settlement deformation.

By applying this semi-empirical method in common practice the system stiffness can be design based on the allowable deformation for the surrounding structures. Compared with (Clough et al. 1989) methodology this one predicts better results because does not overpredict lateral deformations in soft clays and does not underpredicted horizontal displacements with medium to stiff clays.

2.6.3. Vertical ground movement prediction due to excavation activities

As mention before, when an excavation take place the initial in-situ stresses change. These changes generate deformations in the retaining structure and in the surrounding ground, the shape and magnitude are function as for the horizontal displacements of: the soil conditions, the excavation geometry, stability against basal heave, type and material of retaining wall, stiffness, preload magnitude and spacing of the used struts, construction techniques and workmanship quality (Zapata-medina 2007).

(Ou 2006) presented four of the most known empirical formulas to estimate ground movements induced by excavation procedures.

- **Peck's method**

Peck was the first one to introduce a correlation between the ground settlement behind the wall taking into account the distance and the excavation height for different types of soils. He created a correlation from case histories in Chicago and Oslo. The curves used to estimate the ground movement behind the wall is presented in Figure 26.

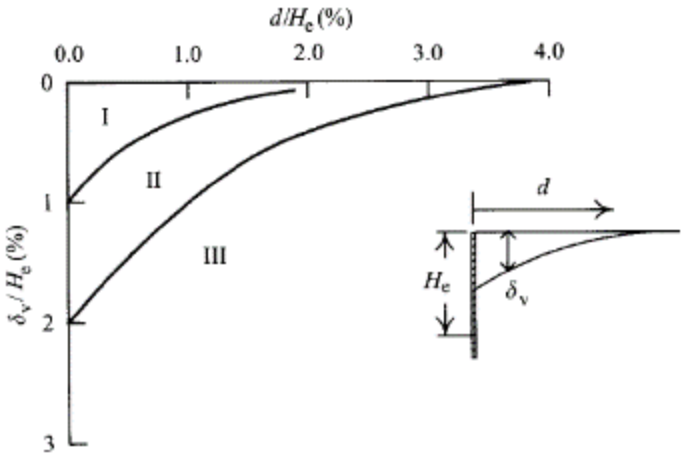

Figure 26. Peck´s method for ground settlement behind the wall. After (Ou 2006).

Peck classifies the soil in three types.

- Type I, sand and soft to stiff clay, average workmanship.
- Type II, very soft to soft clay. Limited depth of clay below the excavation bottom or significant depth of clay below the excavation bottom with $N_b < N_{cb}$
- Type III, very soft to soft clay located to a significant depth below the excavation bottom and $N_b \geq N_{cb}$.
  Where N_b is the stability number of the soil and N_{cb} is the critical stability number against basal heave.

Peck's method was created from case histories before 1969, its principal characteristics is that the curves for each type of soil are envelopes were the common retaining structures were sheet piles and soldier piles without taking into account currently diaphragm walls. So, this methodology is not always applicable, but is still common in today's practice.

- **Bowles's method**

(Bowles 1997) propose a methodology to estimate ground settlement behind a retaining structure after excavation activities. The procedure is as follows.

1. Estimate lateral wall deflections.
2. Form the wall deflections estimate the volume in the displacement zone V_s. Average end areas may be employed, as the trapezoidal formula, or the Simpson's one-third rule.
3. Compute the lateral distance with settlement influence, for this step the Caspe's (1966) method can be used.
   a) Compute wall height to the dredge line H_w.
   b) Then the distance below the dredge line H_p. If it is a cohesive soil $H_p = B_e$ where B_e is the excavation width, and if it is a cohesionless soil $H_p = 0.5B \tan\left(45 + \frac{\Phi}{2}\right)$.
   c) Then the ground surface settlement influence range D can be estimated as

$$H_t = H_w + H_p \tag{39}$$

$$D_s = H_t \, tan\left(45 - \frac{\Phi}{2}\right) \tag{40}$$

4. Compute the surface settlement behind the wall as.

$$S_w = \frac{2V_s}{D_s} \tag{41}$$

5. By assuming a parabolic variation, the ground settlement S_i can be estimated from D toward the wall as.

$$S_i = S_w \left(\frac{x}{D_s}\right)^2 \tag{42}$$

This methodology can be easily programmed into a spreadsheet, and with practical examples (Bowles 1997) illustrate that it's results are very similar to those obtained by Peck's envelopes.

- **Clough and O'Rourke's method**

They proposed their correlations also from case histories with different types of retaining walls and also restraining elements differentiating their results by behavior according to soil types.

1. Excavation in sand. They said that the data follow a triangular pattern with a maximum depth next to the wall decreasing with the distance. The maximum settle was less than 0.3% in relation with the excavation depth this pattern is presented in Figure 27.

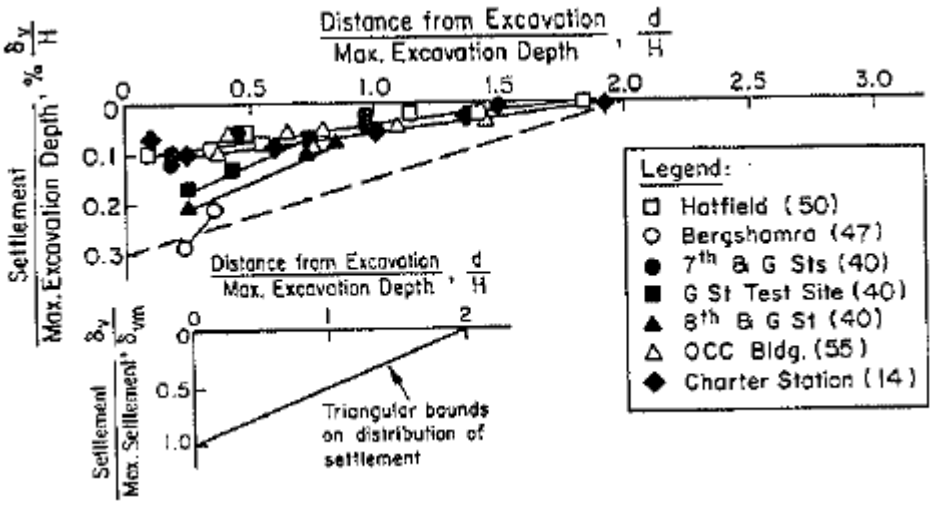

Figure 27. Measured settlement adjacent to excavations in sand. After (Clough and O'Rourke 1990).

2. Excavation in stiff to very hard clays. As presented before the maximum settlement was about 0.3% of the excavation height but with greater effect in the distance until 3 times the excavation depth. The pattern is triangular too. The horizontal displacement was related too with the distance from the excavation with the maximum excavation depth. The distribution pattern along the influence zone is presented in Figure 28.

   Shows a clear influence of the support stiffness acting over the wall when horizontal movements were measured. A low stiffness strut can duplicate the settlement measurements behind the structure in the same influence zone of 3 times the excavation depth.

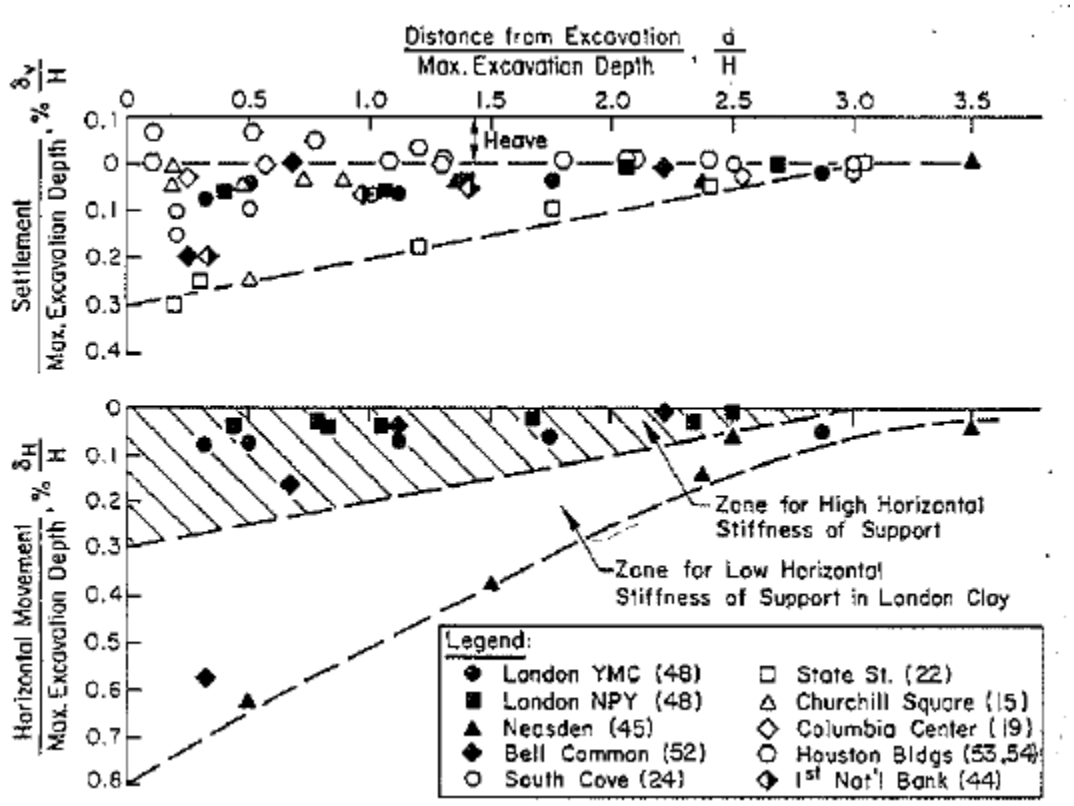

Figure 28. Measured settlement and horizontal displacement adjacent to excavations in stiff to very hard clay. After (Clough and O'Rourke 1990).

3. Excavations in soft to medium clay. In this case the (Clough and O'Rourke 1990) plotted a relation between the settlement and the maximum settlement against the relation between the distance from the excavation with the maximum excavation

depth, obtaining a trapezoidal envelope in which to zones are well defined, this deformation diagrams are presented Figure 29. The first zone is where the maximum magnitudes occurs between$0 \leq {}^{d}/_{H} \leq 0.75$. Then there is the transition zone where the maximum values decrease to negligible ones, located at $0.75 \leq {}^{d}/_{H} \leq 2.0$.

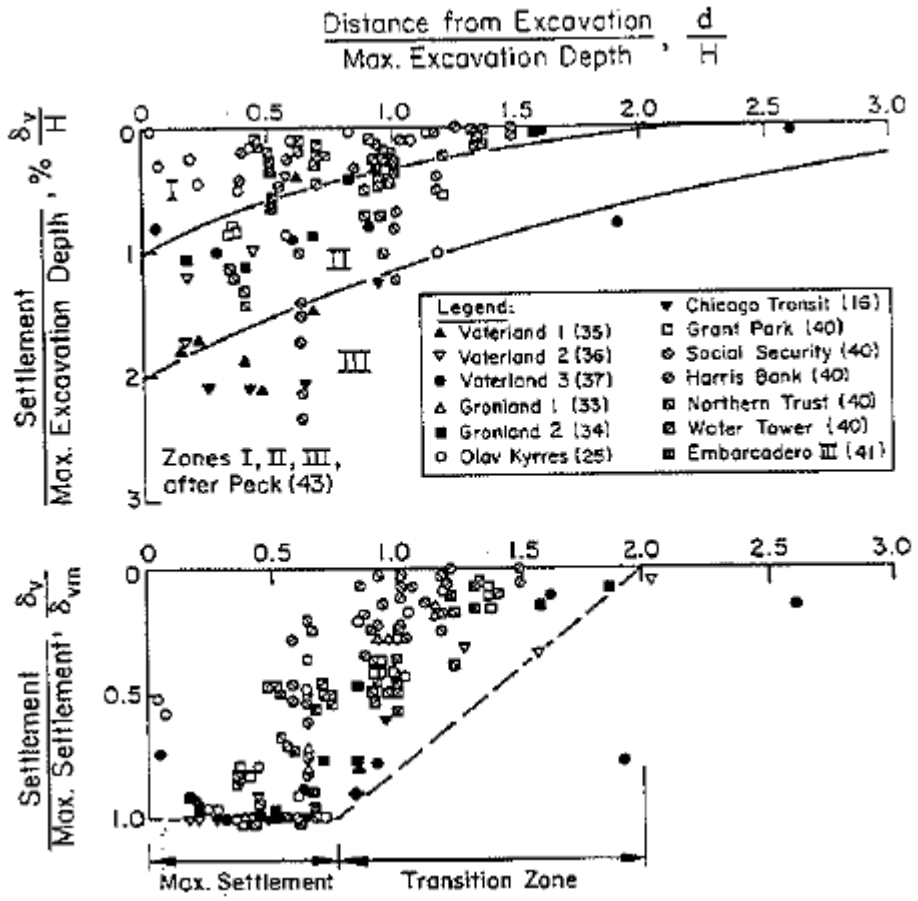

Figure 29. Measured settlement adjacent to excavations in soft to medium clay. After (Clough and O'Rourke 1990).

After all the observations (Clough and O'Rourke 1990) said that the minimum linear regression value they registered was for the soft to medium clay a was about $r^2 = 0.76$.

Then, they resume the soil ground settlement movement for each soil in dimensionless profiles in function with the excavation depth for a distance measured from the wall. These diagrams are presented in Figure 30 and correspond only to excavation activities, additional procedures as dewatering or deep foundations removal must be analyzed separately and

added. Also, poor workmanship quality was not taking into account so bad procedures may end in larger values than the ones estimated by the proposed diagrams.

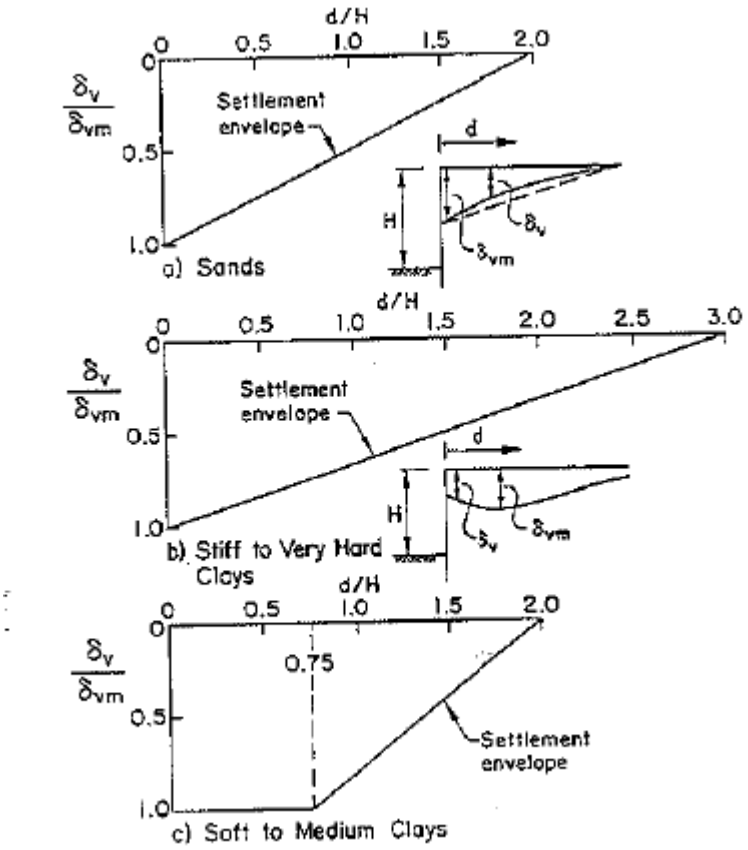

Figure 30. Dimensionless settlement profiles recommended for estimating the distribution of settlement adjacent to excavations in different soil types. After (Clough and O'Rourke 1990).

- **Ou and Hsieh's method**

They proposed to types of curves, the spandrel and the concave diagrams to predict ground surface settlement. These curves are based on observations of case histories and are presented in Figure 31.

They divided both diagrams in a primary influence zone (PIZ) and in a secondary influence zone (SIZ), the PIZ generate larger settlement and therefore cause more damage in adjacent structures, and instead the SIZ has less influence and in some cases can be negligible (Ou 2006).

The also established a simple process to estimate surface settlement behind the wall, the procedure is the following:

A. Compute the lateral displacement of the wall (δ_{hm})with any valid methodology.

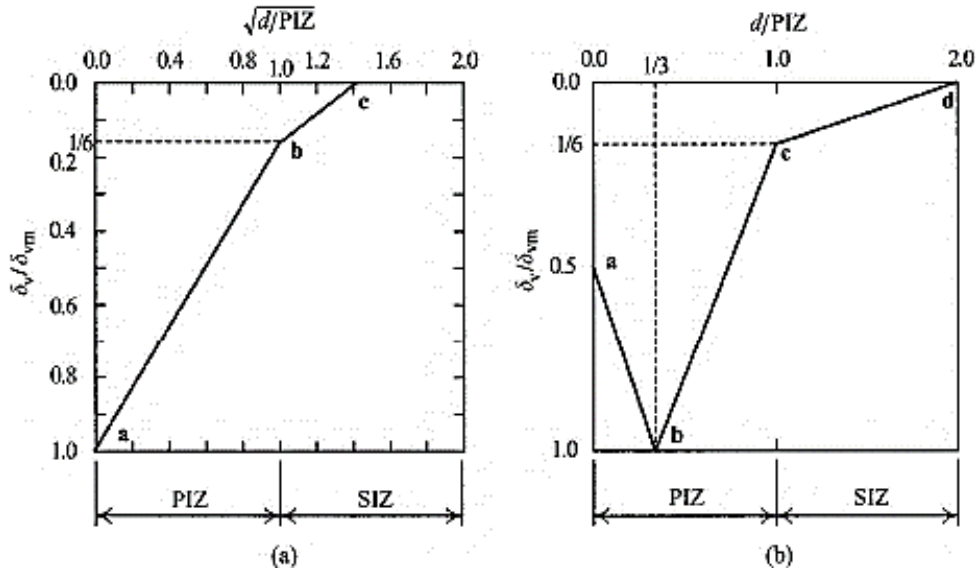

Figure 31. Ground settlement curves proposed by Ou and Hsieh (2000), (a) spandrel settlement profile, (b) concave settlement profile. After (Ou 2006).

B. With Figure 32 determine the type of ground settlement

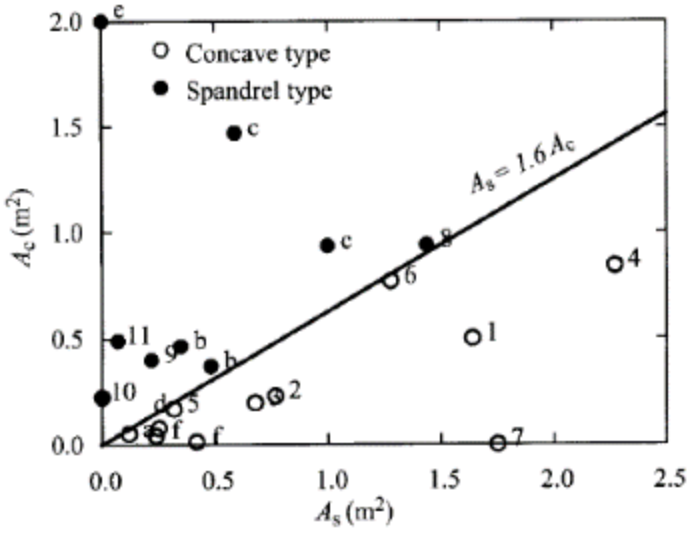

Figure 32. Relationship between the ground surface settlement pattern and the lateral wall deformation. After (Ou 2006).

where A_c is the deformation area of the cantilever component and A_s is the area of the total wall movement without the cantilever area. One relationship between these areas is $A_s \geq 1.6A_c$ when this happens the ground settlement will have a concave shape.

C. Estimate the maximum settlement value δ_{vm} with the relation presented in Figure 33.

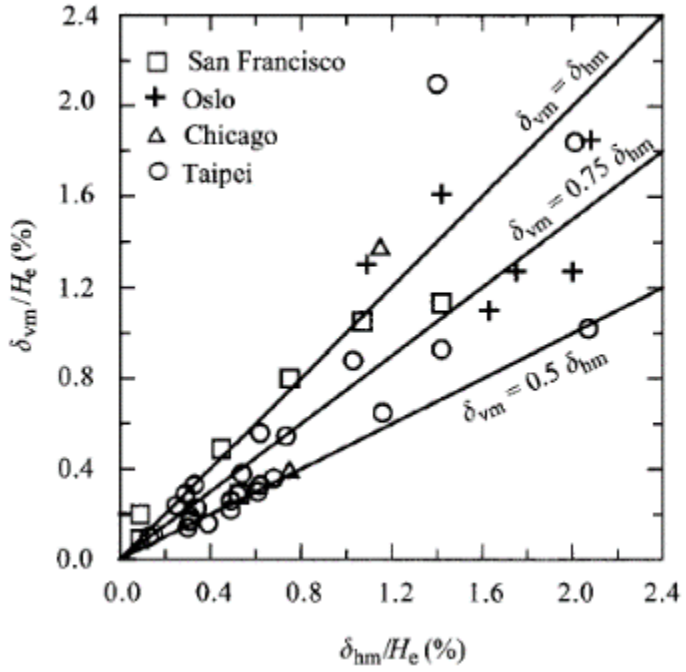

Figure 33. Maximum ground surface settlement vs maximum wall deflection (Ou et al. 1993). After (Ou 2006).

D. Finally, after knowing the maximum settlement and the deformation shape, estimate the other settlement magnitudes in different points of the settlement diagram with Figure 31.

2.7. Instrumentation and Monitoring Systems

Excavation necessities grow in urban areas as well as they grow in depth bringing with them problems in adjacent property damage and even in security. So monitoring systems can help study the excavation behavior as well as its safety conditions (Ou 2006). According to the same author the main objectives of monitoring an excavation are the following.

1. To ensure the safety if the excavation.
2. To ensure the safety of the surroundings.
3. To confirm the design conditions and the expected behavior.
4. To study the construction behavior in long-term conditions.
5. To supply factual material for legal judgment.

The objectives 3 and 4 are also specially used for academic purposes and research.

According also to (Ou 2006) For excavation purposes the common monitoring topics are

1. Movement of the structure or soil. Basically, lateral deformation of retaining structures, tilt of neighboring buildings, settlement in adjacent areas and heave or uplift of the excavation bottom.
2. Stress or strain of the structure or soil. Consist in struts loads and stress of the wall
3. Water pressure and level. These measurements consist on knowing the water pressure behind the excavation zone and on the retaining wall.

In this research were principally measured the soil and structure movement, for that reason ahead will be only describe the instruments employed for that purposes.

2.7.1. Ground settlement points

These are used behind the retaining structure and at different distances from the wall, with the purpose of making a contour settlement map with their information.

These points are commonly made of steel nails driven in the ground and later fixed with a datum point outside the influence of the excavation, the influence distance can be estimated using empirical deformation analysis, like the methods presented before. These nails must be directly installed in soil, because any type of structure normally has a higher stiffness and does not show a representative settlement value.

2.7.2. Inclinometers

This measurement is the most important one to inspect for security issues, and can be directly related with the settlement around the excavation, also the results can be used for academic purposes for the study of soil-structure interaction due to a construction procedure.

As mentioned by (Slope-Indicator 2006) in its manual, this system consist in an inclinometer casing, a plastic pipe (usually made from different kind of plastics) with vertical guidelines as the shown in Figure 34 (b), an inclinometer probe, and a control readout unit (cable and data-logger) presented in Figure 34 (a).

Figure 34. (a) Inclinometer system, (b) Inclinometer casing. After (Slope-Indicator 2006).

The installation commonly consist in making a perforation between 1 or 2 m behind the retaining structure, in this perforation is then installed the inclinometer casing with one of its guidelines perpendicular to the retaining wall line, the casing must be embedment under the retaining structure or the presume movement zone, as shown in Figure 35, then, the perforation is backfilling ensuring the containment of the casing pipe. After that, the reference reading is done with the inclinometer probe before any construction activity is performed and then additional control readings must be done to check the behavior of the excavation procedure or in other cases of a landslide stability.

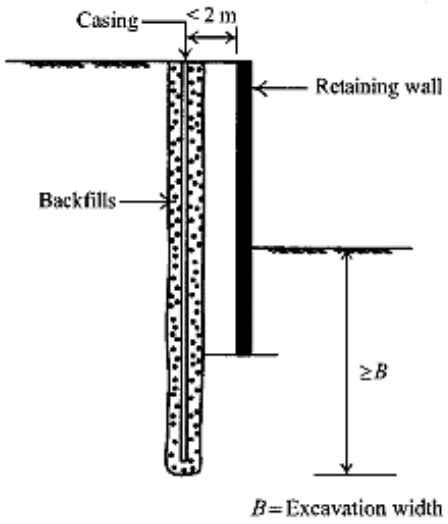

Figure 35. Schematic illustration of an inclinometer behind a retaining wall. After (Ou 2006).

The final result is a graphic of cumulative displacement vs. depth that with complementary graphics can illustrate the performance of the excavation with the constructions stages.

Normally, is assumed that the interpretation of field data is very simple, because modern software have the simplified the process. But There are two types of errors that can occur in a inclinometer survey, random and systematic, these errors and can easily guide to bad interpretations (Mikkelsen 2003).

Random error is the limited precision of the equipment, that cannot be corrected but in good practice can be tolerated.

Systematic errors can influence the results producing false indications of displacement. The potential of error must be checked always because it tends to be greater than real deformations. These errors are (i) Bias shift, (ii) rotation error, (iii) sensitivity drift and (iv) depth-control error. (i) and (ii) are simpler to check and correct by the checksum analyses, and the physical limitations of the sensor, (iii) is very rare to occur and detect, but is easy to correct, and (iv) is the most difficult to correct because it involve a physical phenomenon during the field measuring, that can be influenced by additional external factors like ground vertical movements (Mikkelsen 2003).

Always before presenting inclinometer analyses these errors must be corrected because further studies or actions can be taken based on these mistaken results.

2.7.3. Water pressure, piezometers

Basically there are three types of piezometers, that are commonly installed during the geotechnical exploration and complemented during the construction stage, where some of them can be built inside the retaining structures as a diaphragm wall (Ou 2006).

The basic installation is also called the Casagrande piezometer and it consist in a plastic pipe with a permeable surrounding made of porous stone or sand at the bottom, the rest of the length is backfilled within a seal of bentonite. When the pipe is finished, the water will flow inside the pipe and equal its pressure with the surrounding water table by reaching its level. Then this water level can be check with a level indicator. A schematic installation is shown in Figure 36.

The most important defect of the Casagrande piezometer is that is not applicable in clayey soils. So, there are another options like the pneumatic piezometer and the electronic piezometer. The pneumatic piezometer has almost the same installation process, the difference is that is a closed pipe than expressed the water pressure changes with a correlation with air pressure changes, this instrument is also illustrated in Figure 36.

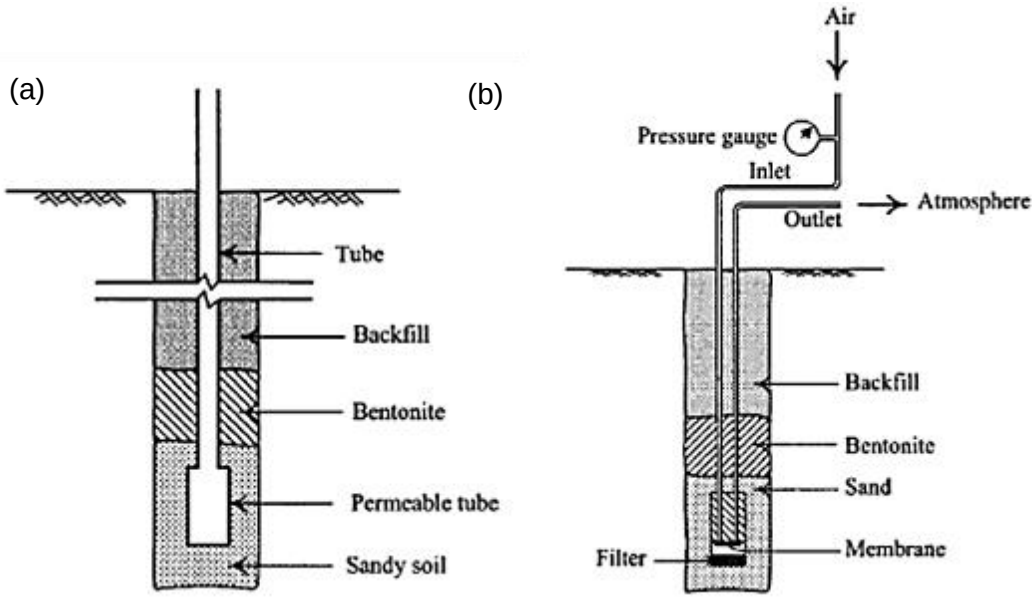

Figure 36. (a) Schematic configuration of an open standpipe piezometer, (b) Schematic illustration of a pneumatic piezometer. After (Ou 2006).

By the other hand, the electronic piezometer, uses a pressure cell isolated from earth pressure to check the water pressure at the installation level. It is installed in a similar way to the both piezometer abovementioned, with the difference that there is no pipe, in its place a signal wire is connected to the cell pressure at the bottom a to a readout data-logger. The principal advantage of this piezometer is that it can read real time information.

2.8. Concrete as Construction Material

Concrete is composed by two principal components, the hydrated cementitious paste and the granular aggregates, and as expected, it's response is governed by the properties of these two phases, where the hydrated cementitious paste put together the aggregates as the concrete loses moisture (Neville and Brooks 2010).

In order to obtain a good quality, the mixture is as important as the conditions of curing. Curing is the time in which the cementitious material link the aggregates as one material, developing in this process its strength and elasticity. This process is mainly influenced by the temperature and humidity, consequently these variables must be taken into account during design and construction (Neville and Brooks 2010). Also, these factors will influence time-dependent factors: creep and shrinkage, which affect the concrete element ones it starts to lose moisture.

These aspects will be theoretically review in this section. Starting with a briefly explanation of the curing process, then, describing the development of concrete strength and elasticity, the temperature influence in the concrete response, and creep and shrinkage characteristics, such as influence factors and development conditions. The numerical models that take into account the factors and hypothesis of each condition are presented later in chapter 4.

2.8.1. Curing

Normally during the construction process concrete must be constantly moist so a propping curing occurs with a correct hydration level by avoiding self-desiccation, so the maximum compressive and tensile strength can be achieved. In the other case, the hydration process will stop and the design strength will not be reached.

Preventing evaporation during the early stages also secure a good curing process this issue depends on the surrounding temperature, relative humidity and wind velocity. Therefore, the curing time cannot be established in a simple way. It must be considered according to temperature, relative humidity and elements geometry.

There are many ways of curing concrete principally depending on the site conditions, and the element size and shape. The most common procedure is wet curing method and it is more efficient when is a continuous supply of water instead of an intermittent supply. Another way if the concrete element surface/volume ratio is small, is to cover the castings in oil and wetting the forms and the element during hardening. An alternative curing method consists in using an impermeable membrane, waterproof paper, or plastic sheets, this will prevent evaporation but will not allow ingress of new water to relief the self-desiccation.

In summary, the most efficient method will be the one that allows the lowest loss of moisture. As mentioned above the most common procedure is the wet curing one, but it is often applied in an intermittent way leading to better results to the sealing procedure (Neville and Brooks 2010). This moisture changes and its consequences will be properly described in the following sections.

2.8.2. Development of Strength and Elasticity

Among many properties, strength is considered to be the most important characteristic of concrete, and this property generally gives direct information of other properties such as the elasticity modulus and the concrete quality. Strength is function of the cement paste, aggregates and the hydration process. At the end of the curing period the presence of discontinuities and pores significant affect the ultimate compressive strength.

As mention before, the concrete principal criteria is the ultimate strength, but in many cases a real criterion can be the limit strain that vary in a small range for different ultimate strength concretes, i.e. from $2x10^{-3}\ to\ 4x10^{-3}$ for 70 to 14 MPa concrete respectively. Also from unconfined compressive tests results it has been proved that the ultimate strength capacity can be correlated to the modulus of elasticity and the Poisson ratio, for that reason the (ASTM C469-02 2002) presents a standard method for estimation of these parameter and (ACI 1980) presented correlations for the modulus of elasticity from the ultimate compressive strength such as $E = 4700\sqrt{f'_c}, [MPa]$.

As abovementioned the strength and elasticity are time and temperature dependent parameters which start with low values and finally reach the design magnitudes, if the construction procedures satisfies the design hypothesis. (Westerberg 2008) mentioned that concrete strength depends on many factors, but principally on the chemical composition of the cementitious paste, its fineness and the characteristics of the aggregates. For example, concrete with very fine cement can rapidly increase strength but in the future will not have a great strength reserve. Instead, for concrete with less fines cement particles such as the ones used for older concrete usually with coarser particles may have slower short-term strength development but in the future will have very high strength reserve.

Concrete admixtures

These are used to improved concrete workability when there is the need to reduce the water/cement ratio while producing high strength concrete, or simply to directly produce very high strength concrete in the short-term. An example of using admixtures in concrete is presented in Figure 37 where moderate to high ultimate compressive strength such as 52 MPa can be reached in almost 24 hours with a high content of superplasticizer and a small ratio of water/cement content to improve workability.

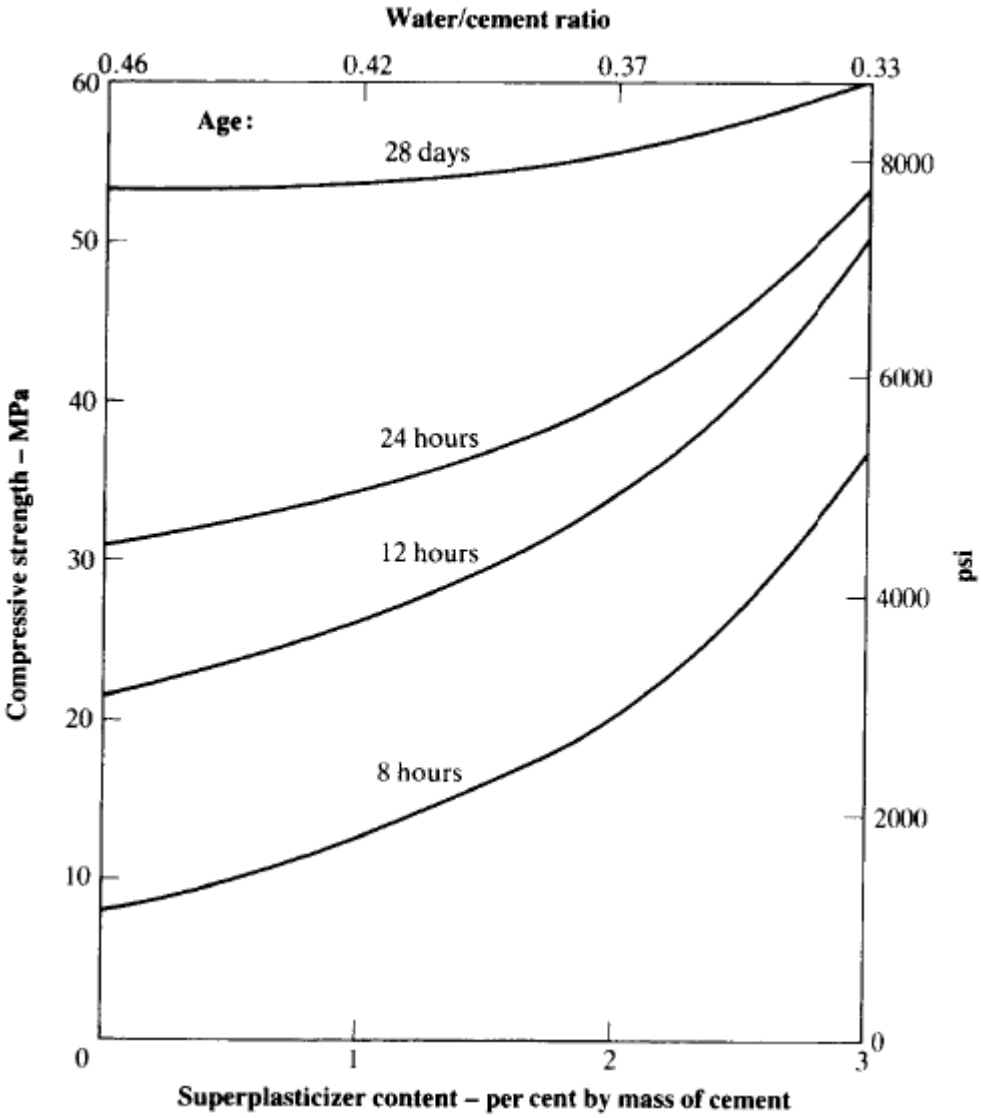

Figure 37. Influence of adding superplasticizer on early strength concrete. After (Neville and Brooks 2010).

Strength with additional effects

When there are second order effects like creep and shrinkage during early age concrete, it reaches little strength. Additionally, during early age deflections are not much influenced by creep or shrinkage, but near the end of the construction or service life, these effects can highly impact concrete deformations, making this a critical aspect, so for these cases this must be the design criteria by taking into account the incidence of elastic deformations, creep and shrinkage. Therefore the design will be restricted by two conditions, concrete strength at the beginning and deformations at the end (Westerberg 2008). The normal assumption in concrete design is to neglect these second order effects (creep and shrinkage) and use a constant compressive strength and elasticity. However, it is always important to consider these effects for deformations and strength capacity when the concrete is being designed for service during early age, and especially when deflections or distortions can affect neighboring structures.

2.8.3. Concrete Temperature Influence

- **Temperature precautions and protection**

During an experimental and analytic research performed by (Kim et al. 1998) they correlated concrete compressive strength with different curing-time and curing-temperature, and concluded that concrete specimens subjected to an early low temperature (5°C) had lower early strength but in the long term they can reach the same strength as specimens subjected to “normal” temperature (20°C). Probing that short-term concrete cured in lower temperature reach an affected strength by a slower hydration process. The relation of temperature and concrete strength is shown in Figure 38.

Basically, in the short-term the higher the temperature the higher the concrete strength but if the high temperature is approximately constant the long-term strength can be affected because a rapid hydration process due to high temperature does not allow a uniform distribution of the cement gel. In the other hand, the short-term result for lower the temperature is lower compressive strength, so for the long-term resistant precautions an protection method should be used so the hydration heat can be higher and the cementation process can be developed (Neville and Brooks 2010).

To reach a proper curing there are manuals and guidelines that presented procedures to concrete curing during different temperatures. In this case, cold weather curing will be

summarized. Cold weather for concreting is defined by (ACI 306R 2010) as any temperature below 4°C, and mentions that concrete may achieve the design magnitudes if it is properly produced, placed and protected against these cold temperatures. For these purposes design codes like (CEB-FIP 1993) and (ACI 209 1997) established equations that can take into account the low temperatures in concrete resistance parameters.

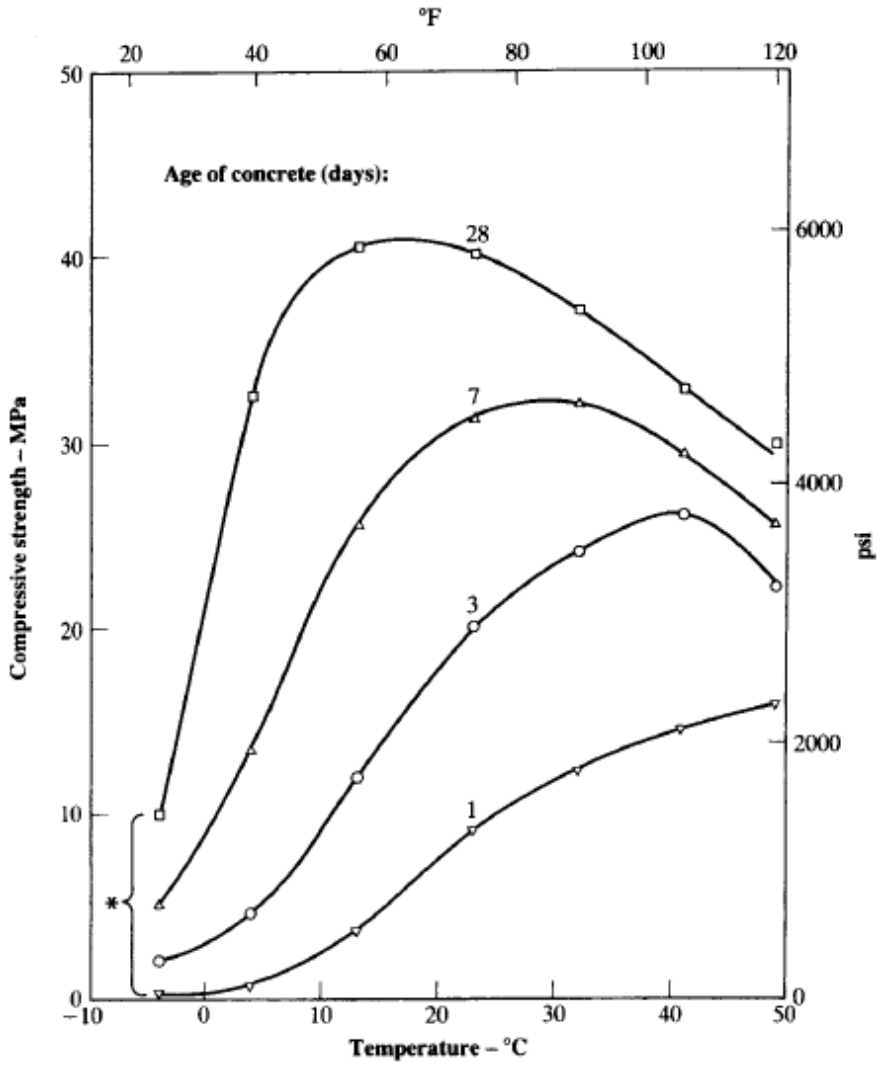

Figure 38. Influence of temperature on compressive strength for concrete cast al 4°C and cured at -4° from day 1. After (Neville and Brooks 2010).

(ACI 306R 2010) recommended a curing minimum temperature and a protection method to prevent freezing according to the element size and applicable to normal-weight concrete (Table 7). Also mentioned that it can take advantage of the situation because a properly protected concrete element in low temperatures can develop in the long-term greater ultimate strength and durability. The workability as well must be controlled

minimizing the bleeding during the curing period, because excessive bleeding can cause lower strength near the surface.

Table 7. Recommended concrete temperatures. Adapted from (ACI 306R 2010).

		Section size, minimum dimension			
		<12 in (300 mm)	12 to 36 in (300 to 900 mm)	36 to 72 in (900 to 1800 mm)	>72 in (1800 mm)
Line	Air temperature	**Minimum concrete temperature as placed and maintained**			
		55°F (13°C)	50°F (10°C)	45°F (7°C)	40°F (5°C)
1	-	**Minimum concrete temperature as mixed for indicated air temperature**			
2	Above 30°F (-1°C)	60°F (16°C)	55°F (13°C)	50°F (10°C)	45°F (7°C)
3	0 to 30°F (-18 to -1°C)	65°F (18°C)	60°F (16°C)	55°F (13°C)	50°F (10°C)
4	Below 0°F (-18°C)	70°F (21°C)	65°F (18°C)	60°F (16°C)	55°F (13°C)
5	-	**Maximum allowable gradual temperature drop in first 24 hours after end of protection**			
		50°F (28°C)	40°F (22°C)	30°F (17°C)	20°F (11°C)

The more massive the concrete structure the slower it loses heat, that's the reason Table 7 admits lower temperatures for bigger concrete elements. As an additional measure (ACI 306R 2010) recommends for seasonal variations to heat water and/or aggregates when there are lower temperatures than the ones presented in Table 7. By the other hand, the steel reinforcement and the formwork can also be heated with enclosures, electric blankets or heating systems recommended always that the concrete surface should always be over the freezing temperature, always avoiding frozen subgrades.

For low temperatures, concrete should always be protected, this protection can be provided by (i) mixture acceleration, (ii) insulation, (iii) heat systems, (iv) enclosures, (v) or a combination of the abovementioned. "*Effective protection allows the concrete to gain strength at a normal rate and prevents the concrete from early-age damage by freezing of the mixing water. Concrete can resist the effects of one freezing-and-thawing cycle as long as it is air-entrained, not exposed to an external water source, and has reached a compressive strength of approximately 3.5 MPa"* (ACI 306R 2010). To ensure this minimum strength the minimum protection time period must be as presented in Table 8 according to the lines of Table 7. This approximately agrees with what was found by (Kim et al. 1998) during their laboratory tests, that varying temperature after 3 days of curing does not seem have a significant effect on concrete strength.

Table 8. Length of protection for concrete placed during cold weather. Adapted from (ACI 306R 2010).

Line	Service condition	Protection period at minimum temperature indicated in Line 1 of Table 5.1, days	
		Normal-set concrete	Accelerated-set concrete
1	No load, not exposed	2	1
2	No load, exposed	3	2
3	Partial load, exposed	6	4
4	Full load	**Refer to Chapter 8	

*A day is a 24-hour period
**Look at: Guide to Cold Weather Concreting, Chapter 8-Protection for Structural Concrete Requiring Construction Supports (ACI 306R 2010).

The protection must be maintained until the desired maturity or strength is achieved. For air entrainment consideration, the protection must be placed until a minimum strength of 24.5 MPa.

When there is an early strength requirement, the admixture must be design for that and extension of the protection period beyond the minimum expressed in Table 8. For line 4 in Table 8 early full load concrete cylinders must be tested and the maturity method should be performed relating curing time and exposed temperature this procedure is briefly explained in the next title.

Maturity

The maturity method was developed to take into account the time and temperature effects on the concrete strength gain. According to (Carino and Lew 2001) there are several expressions to estimate in-place strength development but they are still fitting approximations than do not calculate with absolute precision the concrete behavior with time and temperature.

The maturity can be calculated from different expressions proposed by Nurse-Saul (1951), Freiesleben, Hansen and Pedersen (1977), this one allows the computation of an equivalent concrete age, as well as the one presented in the CEB-FIP (1993), (2010).

The special parameter that relates the maturity with the strength development with time is the *activation parameter*. This parameter varies according to the water/cement ratio between$30 - 60\ kJ/mol$. Then strength development relations where proposed to relate

maturity with strength in time, these relations are hyperbolic, exponential or logarithmic, and limited by the ultimate compressive strength in theory reached at 28 days.

By these formulations the in-place strength can be estimated by taking into account the temperature, and the activation energy form laboratory and field testing to calculate the concrete maturity and later relate the maturity with a strength development relation.

Later (Wade et al. 2006) reevaluated the maturity methods and the procedures recommended by ASTM and one of many recommendations was "*Strength estimations using the maturity method may not be accurate beyond 7 days of equivalent age"* Therefore precautions must be taken in this case.

2.8.4. Creep and Shrinkage

"Realistic prediction of concrete creep and shrinkage is of crucial importance for durability and long-time serviceability of concrete structures, and in some cases also for long-time stability and safety against collapse. Mispredictions of this phenomenon, which contribute to excessive deflections and cracking, have been one of the reasons for problems with longevity of the civil engineering infrastructure in all countries" (Bazant and Baweja 2001).

The prediction of creep and shrinkage is a very difficult task, because these phenomena are the result of physical and chemical factors that act in time during the concrete hardening and its service life. At the end the total deformation of a concrete element is the total due to strain induced by stress, shrinkage and creep as presented in Figure 39 (ACI 209.1R 2005).

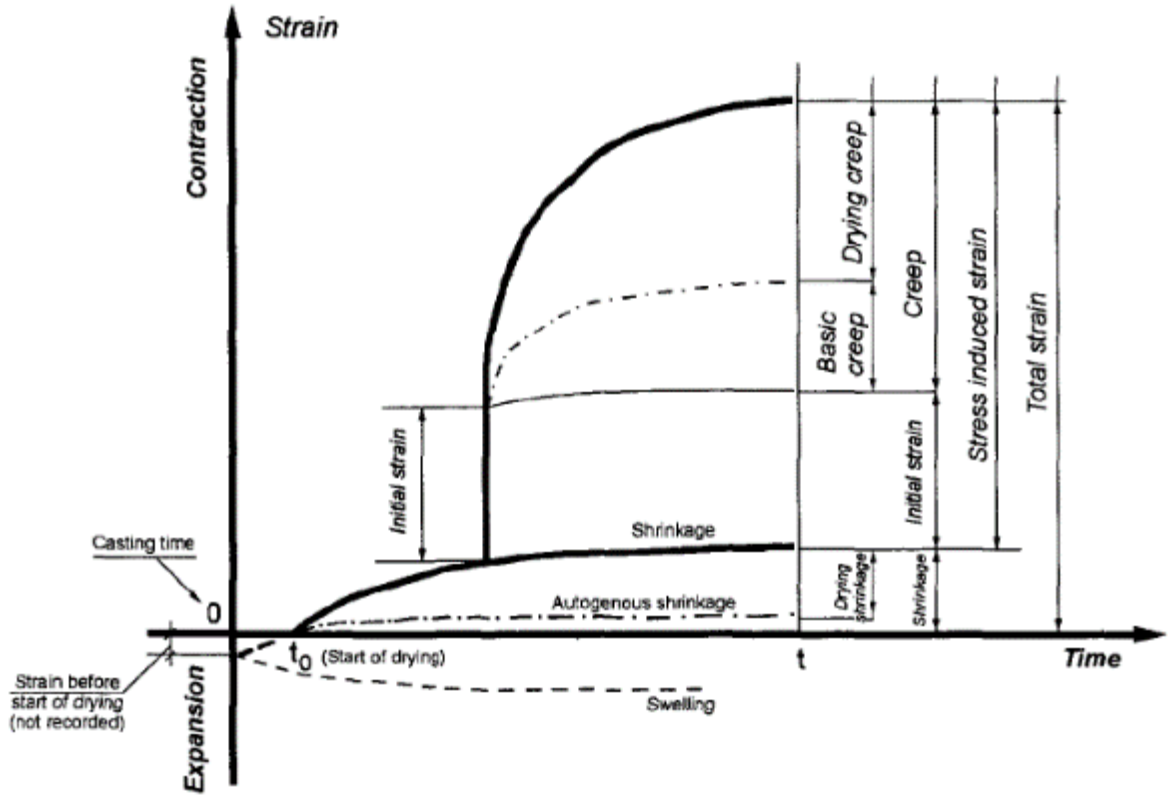

Figure 39. Strains, shrinkage and creep in time. After (ACI 209.1R 2005).

Figure 39 presents the total change in length per unit length of a concrete specimen subjected to a constant load with a constant temperature, dividing the total deformation by:

1. Autogenous shrinkage.
2. Drying shrinkage
3. Carbonation shrinkage (is not explicit in Figure 39).
4. Strain due to induced stress.
5. Basic creep.
6. Drying creep

As observed these two effects are additive in nature, i.e. they accumulate with the material normal deformation when subjected to stresses. So these effects can generate additional strains than the ones consider during the design process (ACI 209 1997).

These phenomena will theoretically be described in this section, and the formulation used to estimate shrinkage and creep proposed by (ACI 209 1997),(ACI 209 2008), and (CEB-FIP 1993) is presented in Chapter 4. Moreover there are approximate methodologies

that seek to predict the behavior of the concrete over time, these were adjusted by additional statistical methods in order to adjust to the variability of factors governing the performance of these effects in time (ACI 209 1997).

Creep

According to (ACI 209.1R 2005) creep represents the strains due to a constant load as a time-dependent effect, taking place after the initial elastic load. It can be several times larger than the elastic strains. Other authors as (Neville and Brooks 2010) mentioned that creep occurs at sustained load, by material fatigue or cyclic loads. Strictly is defined as the increase in deformation resulting of a constant effort happening after other time-dependent deformations such as shrinkage, swelling and expansion or contraction due to thermal changes. By another point of view, when a concrete element is restricted creep can be manifested by the loss of effort over time, seeing as a relaxation phenomenon. Creep under constant stress is shown in Figure 40.

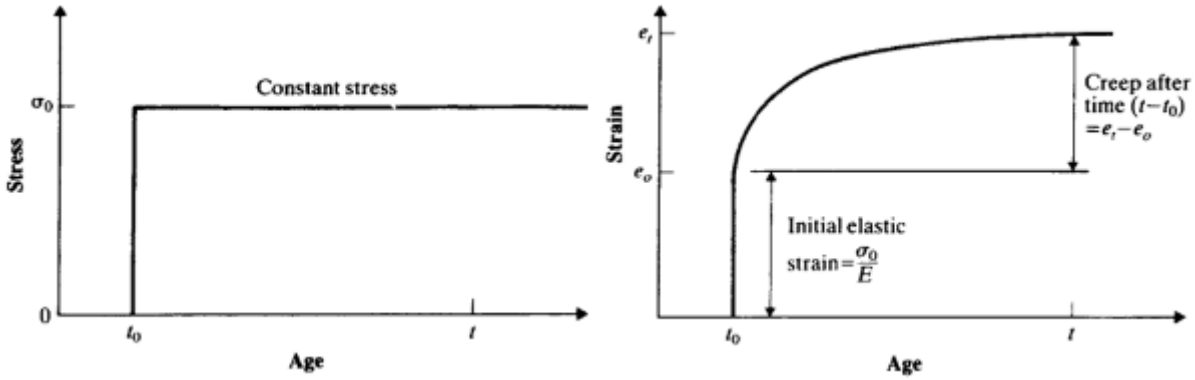

Figure 40. Creep under a constant stress. After (Neville and Brooks 2010).

The initial elastic strain is due to the application of load (initial elastic strain), and by maintining the effort during time, a non-linear creep is presented tending to remain consanst over a long period of time. If the element is discharged only the first linear elastic deformation will recover, while the other will remain.

The factor that ifluence the creep is the hardening of the cementitious paste, since the aggregates that make up the mixture defom to much greater efforts. Given the stiffness difference between the paste and the aggregates the main role of the last ones is to restrict the creep of the cementitious paste, for that reason the more rigid the aggregates the lowest the creep, likewise with the quantity of aggregates the greater the volumen of aggregates

the lower the resultant creep (Neville and Brooks 2010). The water/cement ratio also influences the creep, because this relationship is directly linked to the porosity of the mixture, but special attention should be taken with this aspect, if the water/cement ratio is reduced the resultant creep will decrease but the limit strength will behave as well.

The abovementioned are the internal factors that affect creep, however there are also external conditionss that influence over this phenomenos, the principal enviromental factor is the relative humidity, the lower the relative humidity the higher the creep will be. Also the creep is lower when the cured process is done at high temperatures. Never the less, by the creep definition itself the main factor over creep is the applied stress or load.

Due the many factors that affects creep, it is difficult to accurately estimate the amount of deformation produce by it. However (Neville and Brooks 2010) approximately known by observations that deformation by this factor based on a creep of 20 years may be expressed as.

- 25 % of 20 years creep occurs in the first 2 weeks.
- 50 % of 20 years creep occurs in the first 3 months.
- 75 % of 20 years creep occurs in the first year.

Some of creep effects consist in increasing the beams deflection, gradual transfer of load to the joint elements such as columns that can be traduced in additional deflections and lead to buckling. Creep decreases internal stresses resulting in a reduction of cracking and fracturing of the concrete element.

Shrinkage

Shrinkage is caused by the water loss due to evaporation or the hydration process causing volumetric strains. While the cement paste suffers a volumetric contraction due drying a volumetric change approximately of 1 % of the absolute volume of dry cement occurs, this phenomenon is known as plastic shrinkage, that produce superficial cracks due to tension forces, this is directly proportional to the evaporation process. Even when there is not water content changes autogenous shrinkage take place due to the hydration process, normally its magnitude can be negligible but with high strength concrete can be considerable.

A part of shrinkage deformation is irreversible and can be distinguished from the reversible part, this is presented in Figure 41.

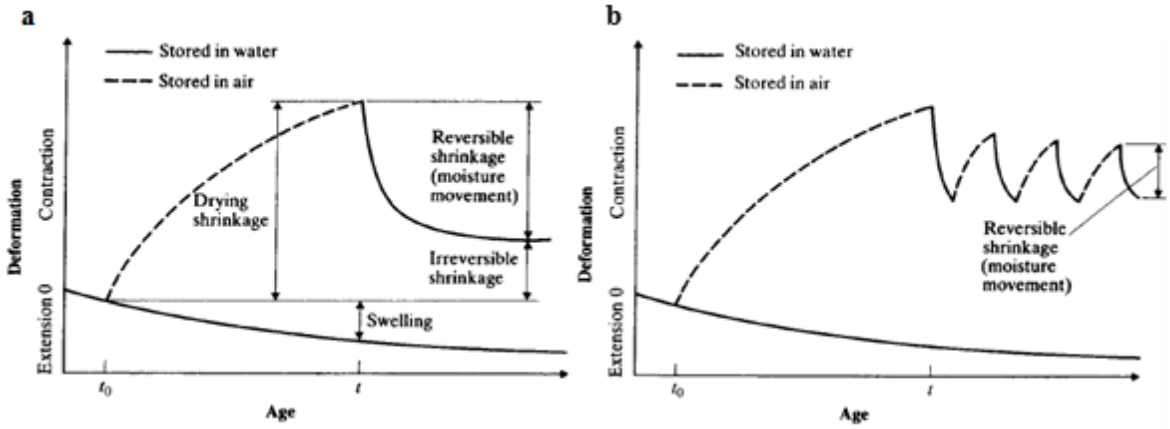

Figure 41. Deformation due to moisture changes in concrete. (a) Concrete dried and then re-saturated, (b) concrete dried and then subjected to cycles of wetting and drying (like common practice). After (Neville and Brooks 2010).

As illustrated in Figure 41, strain due shrinkage can be reestablished when the element is rehydrated. Situation (a) is a concrete first dried and then wetting in a single cycle where part of strain due to shrinkage is reversible and other volumetric change is generated by swelling. According to (Neville and Brooks 2010) in first place a expansion is produced by swelling but then the shrinkage is reduced and for usual range concrete the drying shrinkage strains represents almost the 70 %. Figure 41 (b) represent the same situation as (a), but with the difference that the wetting is applied in cycles with drying periods as common practice.

The irreversible shrinkage in concrete is dried and the element loses water located in the pores then due to a hydraulic gradient water get out of the element an a volumetric strain take place. An additional shrinkage process is also presented, is the carbonation shrinkage, which is the formation of insoluble calcium carbonate, this process is slower than drying shrinkage since it depends on the concrete permeability and the environmental relative humidity. Figure 42 shows the proportion of total shrinkage by drying a carbonation shrinkage. Also, shows the variation in function with the relative humidity.

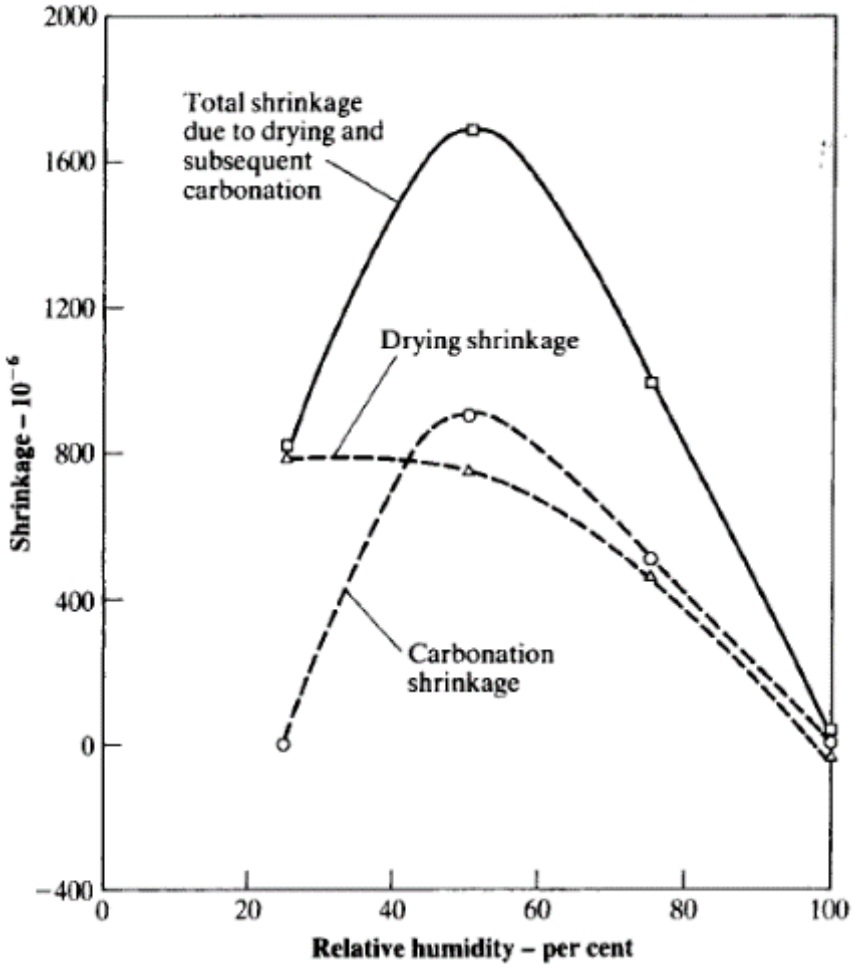

Figure 42. Drying and carbonation shrinkage of specimens at different relative humidity. After (Neville and Brooks 2010).

The carbonation shrinkage is important during the hardeing process of reinfocement concrete due that is the phenomeum that protects the steel from corrosion. Also these elements and the aggreates in the mixture can be the of huge inluence to control the shrinkage process because their stiffness can restrain the deformation, other influent factor is the water/cement ratio due that this control the porosity and direclty affects the permeablity that influence the carbonation shrinkage (Neville and Brooks 2010).

In general shrinkage decrease with time an according to observations established that it approximately behavies in the following way.

- 14 to 34 % of 20 years shrinkage occurs in 2 weeks.
- 40 to 80 % of 20 years shrinkage occurs in 3 months.

- 66 to 88 % of 20 years shrinkage occurs in 1 year.

Figure 43 Presents the variation of shrinkage in time subjected to different relative humidity.

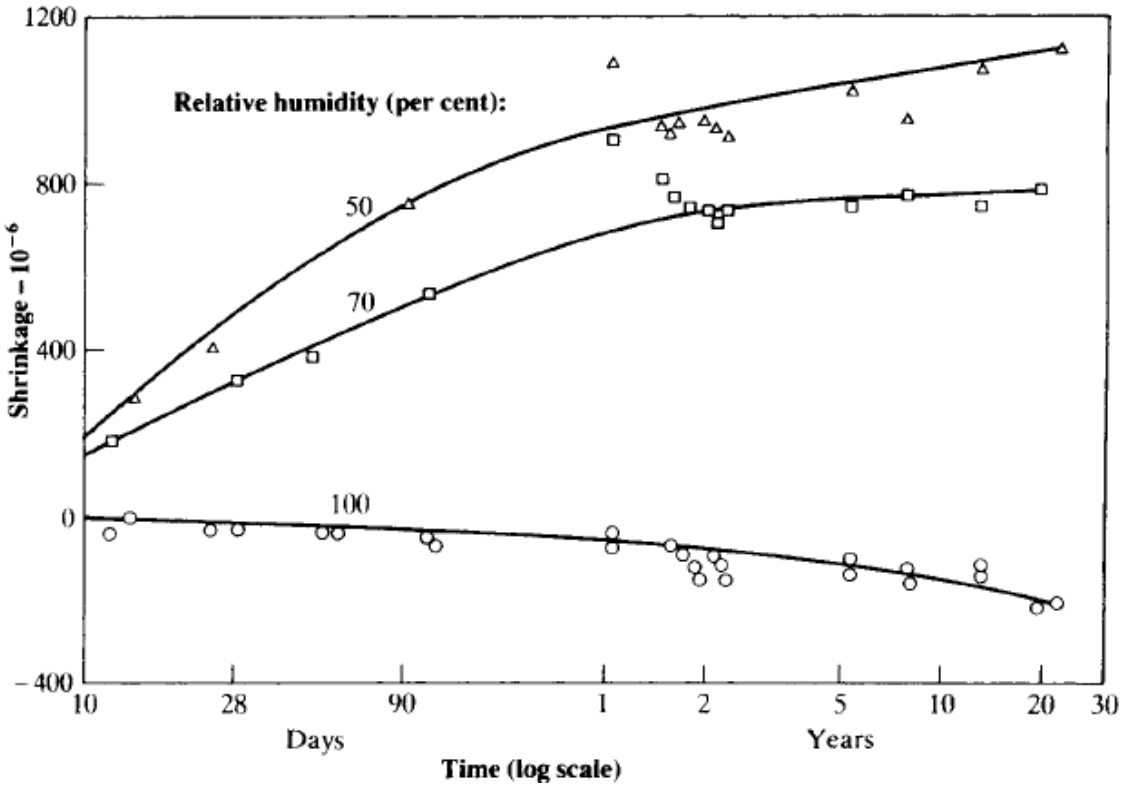

Figure 43. Relation between shrinkage with time and relative humidity. After (Neville and Brooks 2010).

Figure 43 shows how the shrinkage is highly influenced by relative humidity in the long-term, how high relative humidity causes minor shrinkage because it prevents great moisture changes and reduce the carbonation shrinkage. Its also shows that in time shrinkage tends to remain constant and for lower relative humidity the increment always decresae its strain ratio.

Chapter 3

3. Construction Procedures and Field Performance

This chapter presents a summary of the construction activities, sub-soil geotechnical conditions and field performance of two cofferdam case histories in Chicago, IL. The first case history is the One Museum Park West cofferdam (OMPW) and the second one is the construction of a cofferdam located 2.5 km from OMPW as shown in Figure 44.

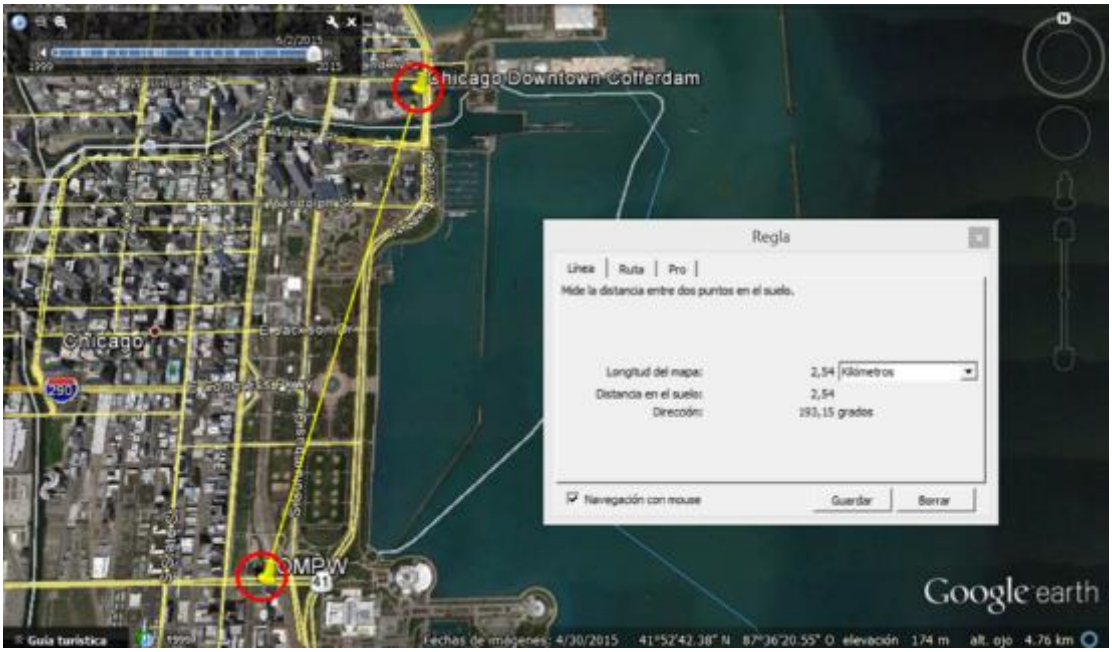

Figure 44. Urban location of OMPW and Chicago Downtown Cofferdam (Google Earth, 2016).

3.1 One Museum Park West (OMPW)

The OMPW project is located where the Lake Michigan shore meets the Field Museum campus in Chicago, IL. It is a 53-story skyscraper housing 298 residences constructed with a combination of top-down and bottom-up techniques. Nowadays, it is known as The Grant.

3.1.1. Construction procedures

The construction of the concrete central core was completed using a temporary cofferdam built with bottom-up procedures. The basement area was constructed using a top-down methodology propping a perimeter secant pile wall with the basements slabs. Today's structure is shown in Figure 45.

Figure 45. Today's view of OMPW (taken from Google Earth, 2016).

A schematic plan view of the project area is illustrated in Figure 46, structural elements such as the cofferdam, perimeter wall and foundation system are detailed in the figure.

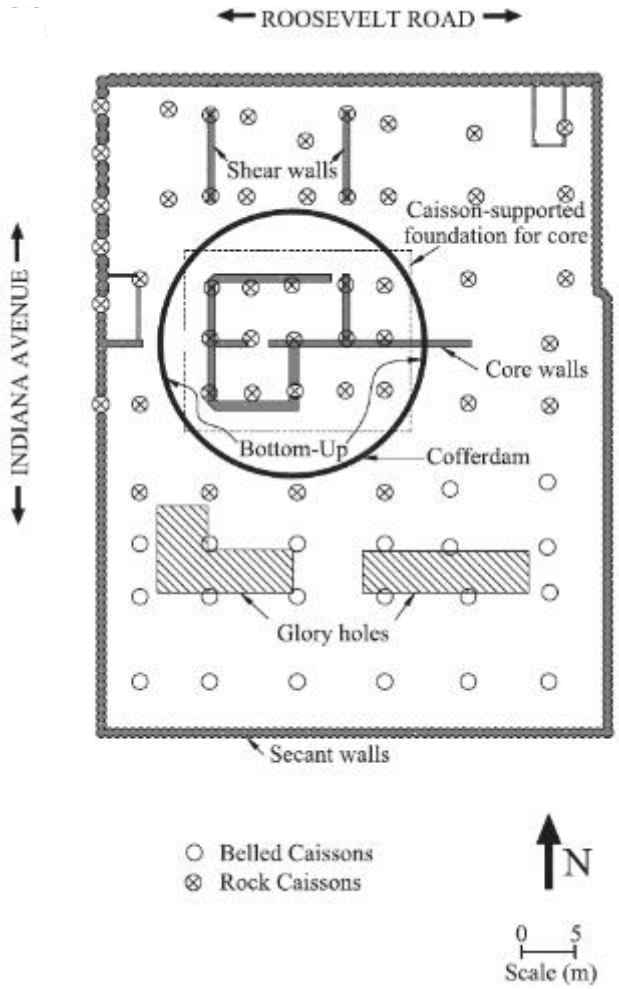

Figure 46. Schematic plan view of OMPW contentions and foundation systems. After (Arboleda-Monsalve 2014).

The underground constructive sequence followed three main stages. The first one was the installation of the perimeter secant pile wall, and the construction from the surface of the foundation caissons. Then, the temporary cofferdam was installed using a perimeter sheet pile wall braced with prefabricated steel ring beams following a bottom-up sequence. Once the bottom of the cofferdam was reached, the bottom caissons and the mat foundation were constructed and the central rigid core built. After that, the basements were constructed using top-down construction techniques.

Figure 47 shows in more detail the construction process abovementioned. The installation of the temporary cofferdam, of particular interest for this research, took place between days 360 and 529.

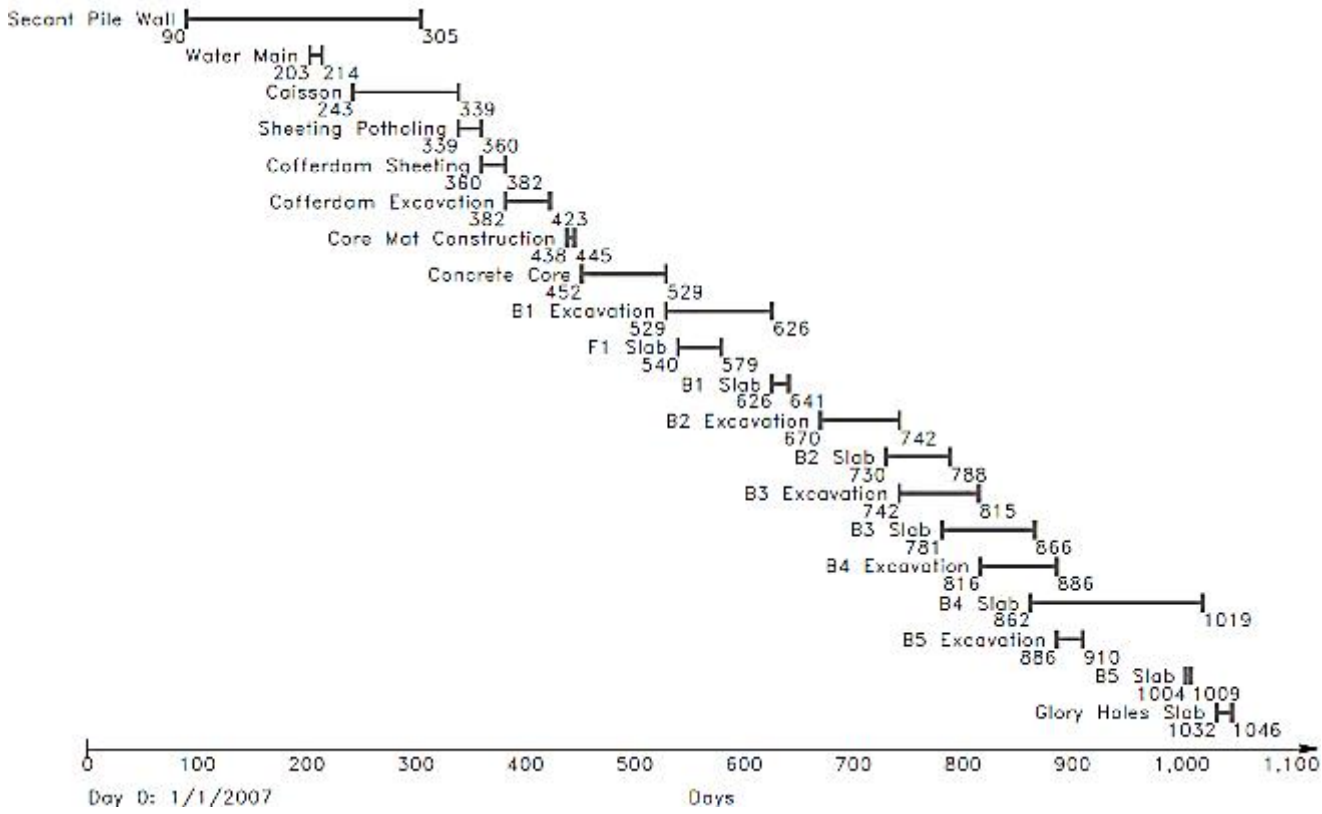

Figure 47. Constructive sequence of OMPW central core and basements. After (Sarabia 2012).

The temporary OMPW cofferdam had an effective height greater than 15 m, plus an embedment depth of 5.65 m reaching a total installation length of 20.65 m. The internal cofferdam diameter was about 24.25 m and was constructed with a PZC-18 sheet pile as shown in Figure 48. The sheet piles were driven from an elevation of 3.65 m CCD until a final elevation of -16.15 m CCD. To provide horizontal support, steel ring beams made of W14x176, W14x193, W14x211, and W14x257 steel sections were provided at elevations of 0.91, -1.83, -4.57, -7.92 m CC, respectively. Geometry details of the OMPW cofferdam are presented in Figure 48.

The construction process was as follow. Using heavy machinery the superficial fill was initially removed to an elevation of 3.7 m CCD in the area projected to be occupied by the cofferdam. From that level, the sheet pile wall was driven until an elevation of -16.15 m CCD as shown, in Figure 49 (a). Then, the bottom-up construction sequence began, by digging up to the projected elevation of the first metal bracing I (0.91 m CCD). At this level, the first steel ring beam was installed and the excavation continued to the next bracing

elevation. This process was repeated until the bottom of the excavation was reached. Once the foundation elevation was achieved, the caissons and the foundation mat were constructed. Finally, the central core was built. The cofferdam was uninstalled while the basements slabs were constructed. Figure 49 illustrates the construction activities for the OMPW project.

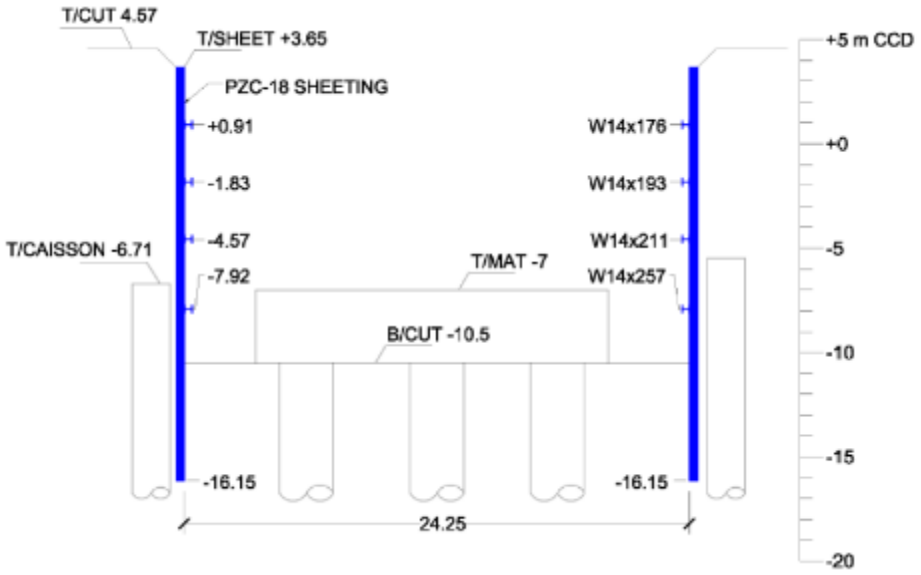

Figure 48. Schematic section of OMPW cofferdam. Measurements in meters. After (Arboleda-Monsalve 2014).

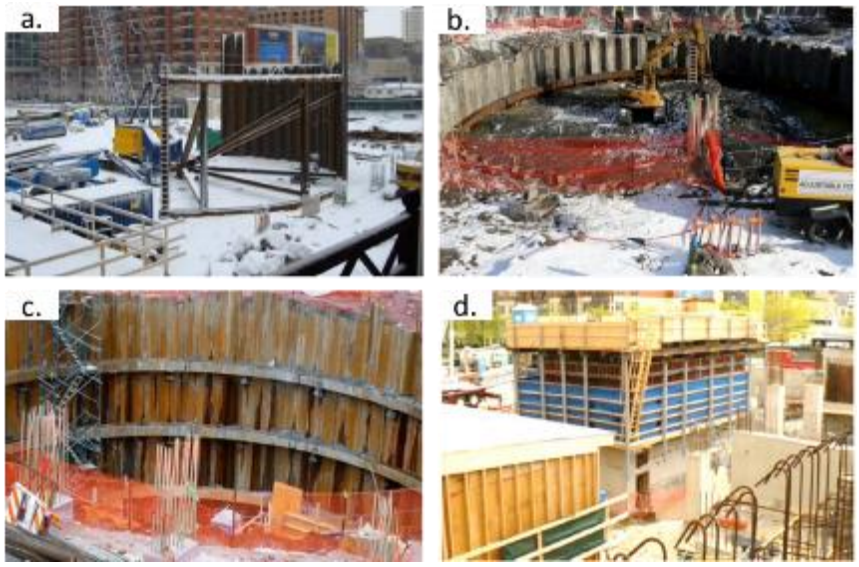

Figure 49. OMPW cofferdam construction sequence. Picture (a.) shows the sheet pile driving process. Picture (b.) shows the excavation from the first metallic bracing to the following. Picture (c.) shows the third metallic bracing installed and the excavation process. Picture (d.) shows the central core and basement slabs construction when cofferdam's work was done. After (Arboleda-Monsalve 2014).

3.1.2. Subsurface characteristics and geotechnical conditions

General conditions

Chicago city is located over a layered sedimentary formation, which is perhaps one of the most study soils in the world. The origin is explained as glacial soil strata resting over a rock base, four of these strata are from the oldest to the most recent Valparaiso, Tinley, Park Ridge and Deerfield as mentioned by (Chung and Finno 1992). The strata density and resistance is directly related with the glacial height when they were deposited, because of the drainage conditions, the permeability and the amount of time in which ice was on them (Chung and Finno 1992). Also, consolidating the strata in greater proportion with depth. The superficial strata, the urban fill and the Blodgett layer are very heterogeneous in their composition, as can be appreciated in the water content chart shown on Figure 50 and is a common condition in the area.

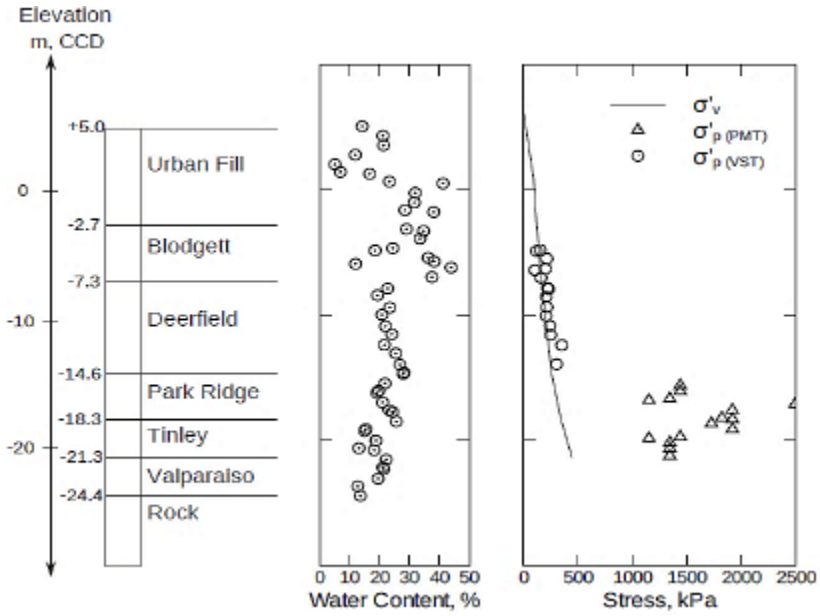

Figure 50. OMPW simplified subsoil profile. After (Sarabia 2012).

Local conditions

Based on the geotechnical exploration carried out on the site, the geology was interpreted and the stratigraphy defined. The exploration included drilling, sample recovery for visual inspection and basic laboratory tests. Additionally, field tests including vane shear and Menard pressuremeter were performed on the site (Sarabia 2012). The obtained results are summarized in Figure 51.

A second geotechnical exploration was completed to retrieve high quality soil samples to perform advance laboratory tests and to performed additional Menard pressuremeter and cross-hole tests (Sarabia 2012).

Based on the available information from the subsurface exploration, the subsoil characterization was done identifying a local stratigraphy as follows: a superficial urban fill, integrated by medium to dense sand with old debris. Is followed by different glacial deposits (Arboleda-Monsalve 2014). The first glacial deposits are the Blodgett and the Deerfield strata which are, mainly composed by clays with variable water content, strength and stiffness. The Blodgett layer is composed by a low plasticity clay of medium resistance, water contents in this layer fluctuate between 10 and 50 % and the undrained shear strength varies from 10 to 60 kPa from a minor to a major depth as shown in Figure 51.

The Deerfield stratum is composed by medium to stiff clays presenting a more uniform geotechnical conditions than the Blodgett layer due to its geological origin (Chung and Finno 1992). These conditions are shown in Figure 51, where it can be seen a water content of about 25 % and a undrained shear strength between 25 and 45 kPa. The Deerfield strata presents a normally consolidated condition proven by a shear strength normalized by the vertical effective stress ranging between to 0.20 to 0.25.

The Park Ridge deposit is composed by an overconsolidated clay with an OCR around of 1.5 according to (Arboleda-Monsalve 2014).

Subsequent deeper soils of larger resistance and stiffness are found. These soils are locally known as “hardpan” and are composed by overconsolidated stiff to very stiff silty clays of Tinley and Valparaiso strata (Arboleda-Monsalve 2014).

The rock was found at an elevation of -25 m CCD, consisting of weathered dolomite with high RQD (Rock Quality Designation). According to (Finno et al. 2014) RQD values can vary between 85 and 91 % classifying as a good to excellent quality rock according to (Deere 1989).

It is important to note that the bottom of the cofferdam reached the Deerfield stratum, while the embedment of the sheet piles reached Park Ridge material in search of greater stiffness.

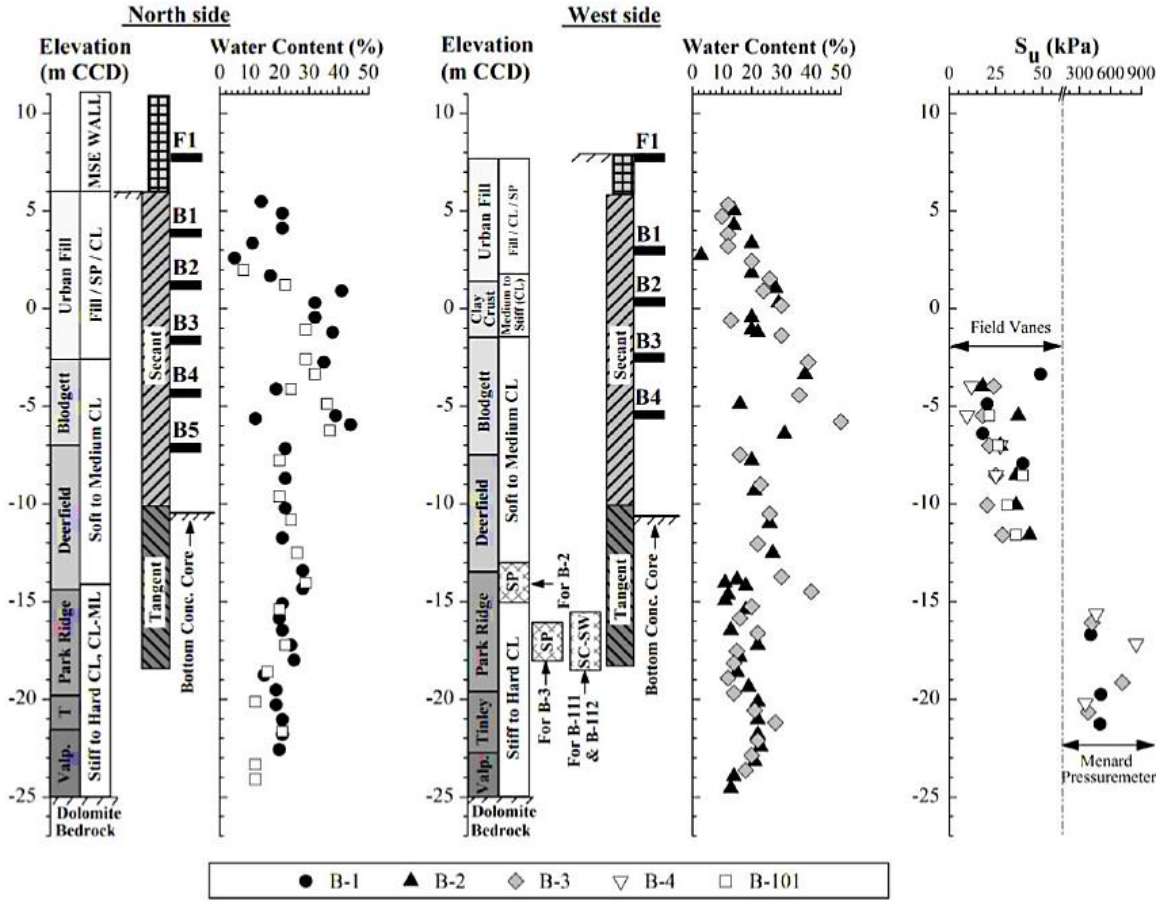

Figure 51. OMPW Local exploration results. After (Arboleda-Monsalve 2014).

Water Conditions

According to (Sarabia 2012) Lake Michigan, Chicago River and the underground structures such as hydraulic service lines and the Chicago Deep Tunnel highly influenced the subsoil water conditions in downtown Chicago. Lake Michigan and Chicago River define an elevated water table level close to the ground surface, while the underground structures generate a decrease in pore pressure over the bedrock creating a seepage condition from the surface to the underground structures. Measurements of this event have been made in different places of Chicago Loop between 1997 and 2008, supporting this premise and showing and average head elevation at -14 m CCD. As indicated by (Sarabia 2012) this approximately constant value indicates a relative equilibrium or steady state after the tunnels construction resulting in a drainage from the ground to these structures due to stresses differences between the ground pressure and the atmospheric pressure inside the

tunnels and the high permeability of the Valparaiso layer ($1x10^{-3}m/s$) according to a back-analysis performed by (Sarabia 2012) that can easily allowed into the tunnels.

Figure 52 shows a comparison between the hydrostatic pressure estimated from the Lake Michigan elevation and the head levels measured by piezometers installed at different elevations around downtown Chicago. The figure shows that the water pressures are controlled by a downward filtration product of the underground infrastructure built in the city (Sarabia 2012).

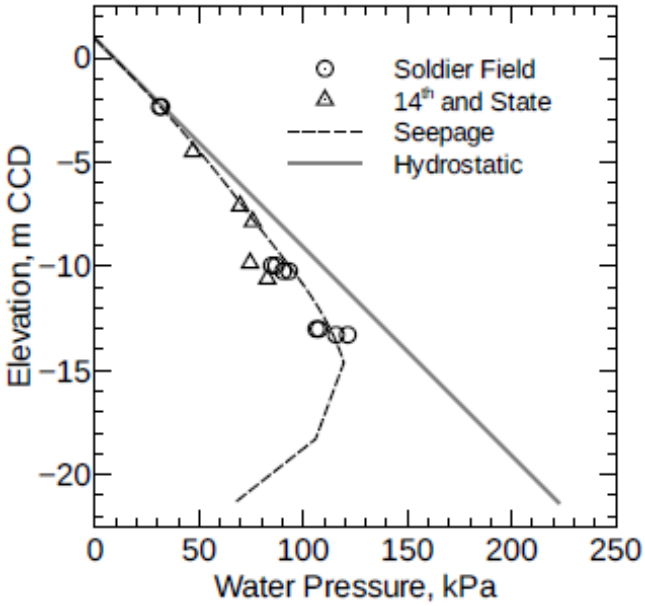

Figure 52. Pore pressure computed from Lake Michigan level Vs. Pore pressures measured from local piezometers. After (Sarabia 2012).

3.1.3. Observed performance

Cofferdam construction induced deformations were measured using inclinometers (for horizontal displacements) and settlement points (for vertical deformations). The location of the used instruments is shown in Figure 53. The continuous readings were taken during the entire construction process. Some instruments were damage during the process, but they were replaced and the monitoring was continually performed. According to Figure 47 the activities related to the central cofferdam construction took place between days 360 and 529. So, the instrumentation records presented in this research are limited by that time period.

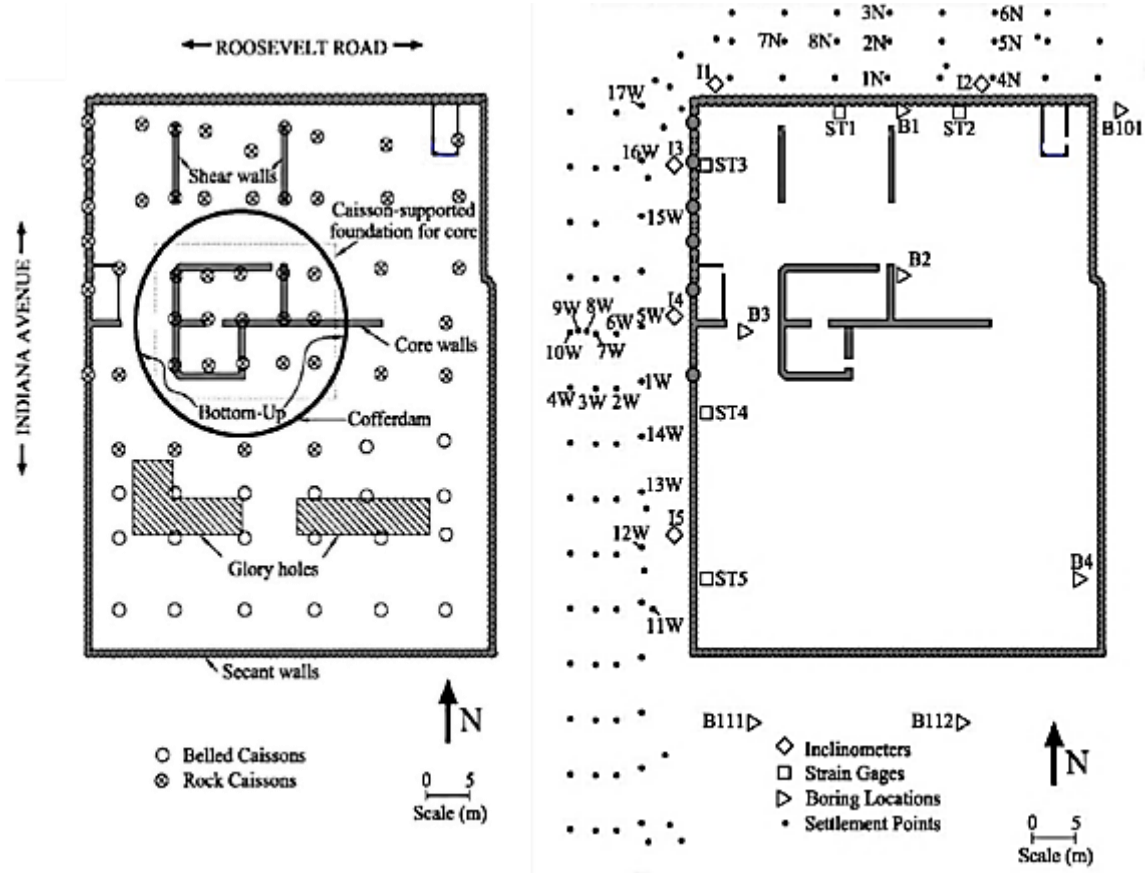

Figure 53. OMPW general plan and instrumentation location. After (Arboleda-Monsalve 2014).

The settlement points and inclinometers were installed around the perimeter wall as shown in Figure 53. The settlement points registered vertical ground movements caused by the internal excavation activities, which were used to plot a settlement contours as shown in Figure 56. The settlement points were sectored according to their position and performance. For example, some results in the northern sector are presented in Figure 54 showing a maximum deformation at the end of the concrete core construction activities of 27.4 mm, minimum value of 15.2 mm and an average magnitude of 24 mm (taking into account all northern results). It can be seen in Figure 54 that the settlement began to develop since the leveling activities and continue developing several increments until the excavation activities were completed and the mat foundation and central concrete core began to be build.

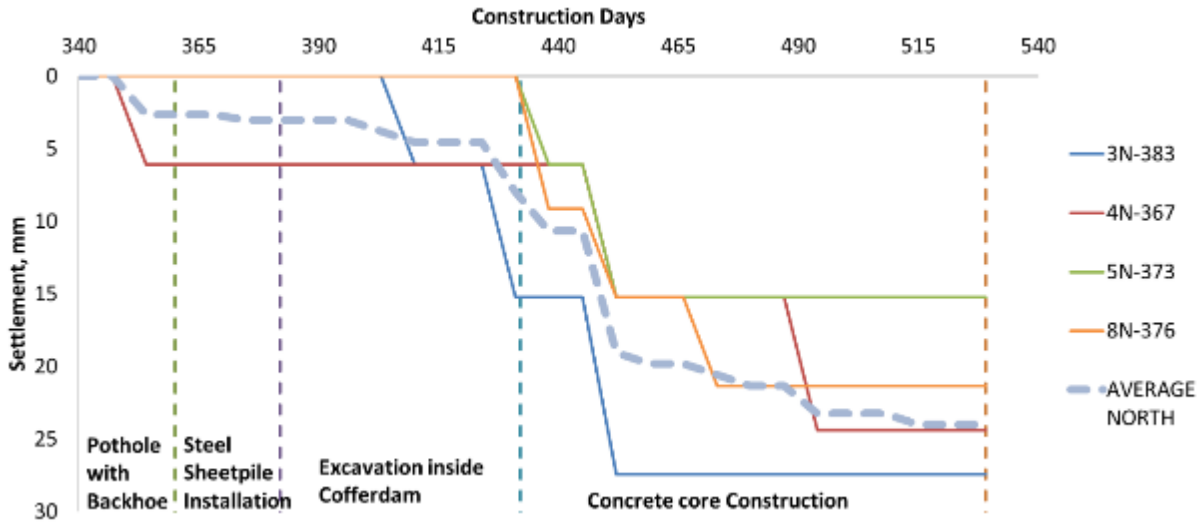

Figure 54. Northern settlement points of OMPW.

The vertical deformation behavior of some checkpoints in the western area is illustrated in Figure 55. This sector showed a similar behavior as the north side. However, the settlement points were located closer to the excavation resulting in larger deformations. For the western sector a maximum vertical deformation after day 529 of 45.7 mm was obtained, while the minimum and average settlement, taking into account all settlement point in this area, were 27.4 mm and 34.6 mm respectively.

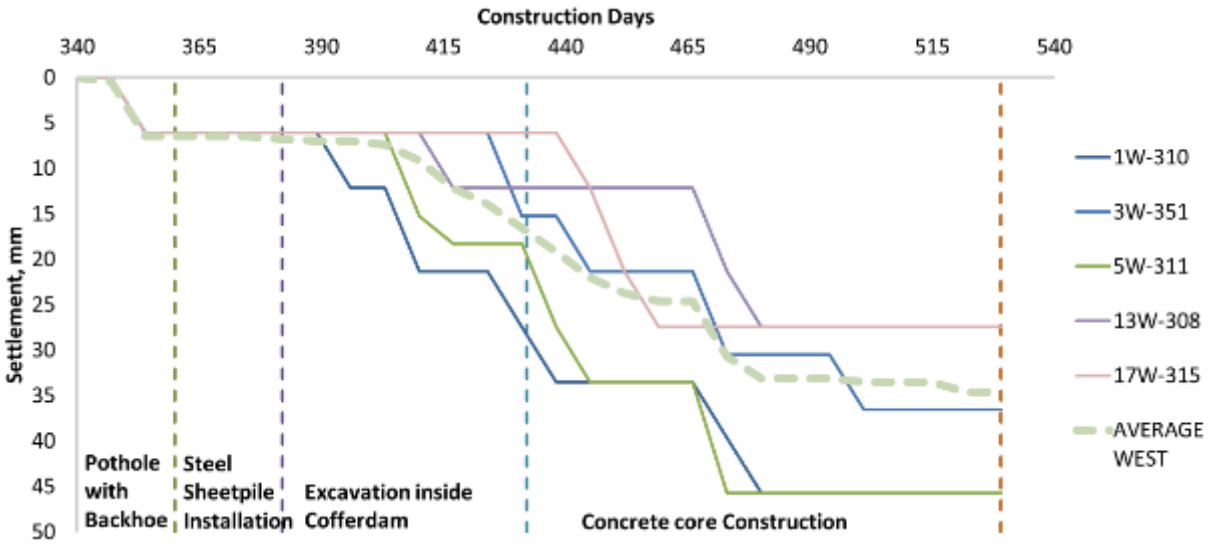

Figure 55. Western settlement points of OMPW.

As can be seen in Figure 55 the settlements began to develop as the leveling activities initiated, and continue increasing during the excavation activities inside the cofferdam. Settlements stop developing once the construction of the central concrete core began.

A settlement point contour was presented by (Arboleda-Monsalve 2014) on Figure 56 showing the influence of the excavation activities around the perimeter wall. It can also be seen in the figure how the settlement magnitude increased nearby the cofferdam reaching values between 45 and 50 mm. It shows the importance of considering the construction and performance of the temporary cofferdam structure on the final ground movements of the excavation.

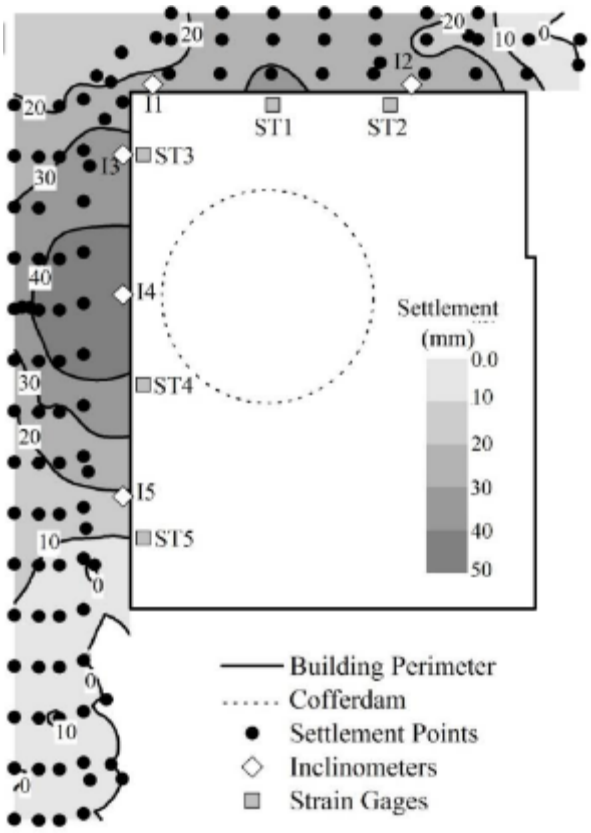

Figure 56. OMPW cofferdam excavation settlement curves. After (Arboleda-Monsalve 2014).

Regarding lateral ground movements, only inclinometers 2A and 4 were considered as they were the inclinometers installed closer to the cofferdam. The location of the considered inclinometers is shown in Figure 53 where they are labeled I2 and I4, respectively. Inclinometer I2 records deformations in the central northern area and inclinometer I4 (closer

to the cofferdam) captures lateral movements in the western area. Shortly after the cofferdam construction began, inclinometer I2 was damaged. It was reinstalled 1 m behind the perimeter wall and was relabeled as inclinometer 2A.

The horizontal displacement profiles obtained from inclinometer 2A are presented in Figure 57. Note that the end of the construction process a total lateral displacement at the surface of 2.1 cm was recorded in the inclinometer principal direction. This behavior was similar to the one characteristic of a passive structure with low props stiffness, and probably influenced by the secant pile wall installed between the cofferdam excavation and the inclinometer.

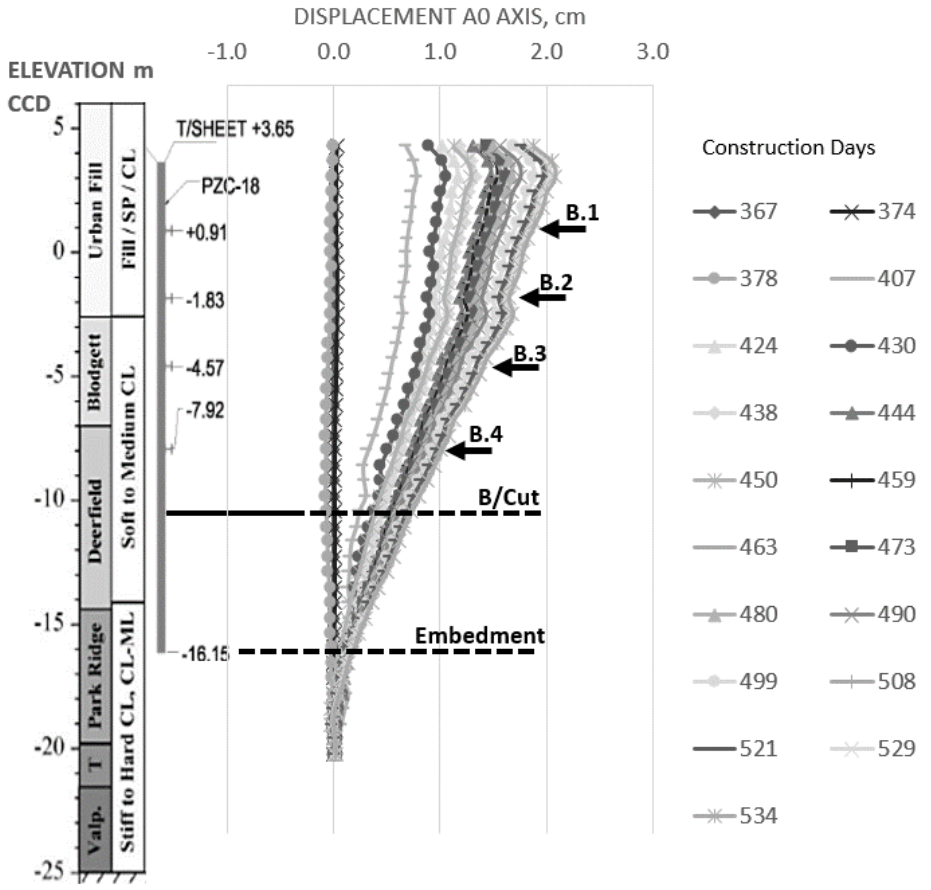

Figure 57. OMPW inclinometer 2A results. Soil profile adapted from (Arboleda-Monsalve 2014).

Lateral ground movement in the western side of the cofferdam were recorded with inclinometer 4 and are presented in Figure 58. Inclinometer 4 was installed 1 m behind the perimeter secant pile wall. The deformation pattern obtained with inclinometer 4 is similar

to the one capture with inclinometer 2A, showing a behavior characteristic of a passive structure with deformations allowed by lower braced stiffness, which is probably produced by the gap effect between braced elements and the sheet pile wall (Uribe-Henao and Arboleda-Monsalve 2016). Due to its proximity to the excavation, inclinometer 4 showed a lateral displacement of 4.5 cm in its principal direction at the elevation of the first steel ring beam (1 m CCD), where the urban fill and medium clay crust are encountered.

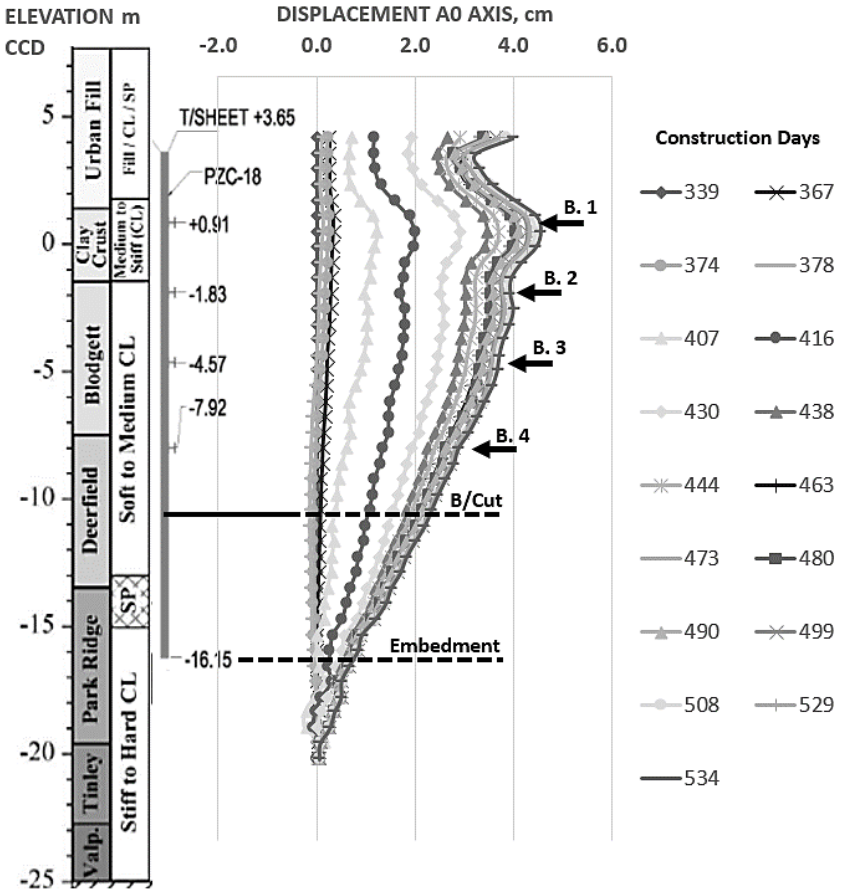

Figure 58. OMPW inclinometer 4 results. Soil profile adapted from (Arboleda-Monsalve 2014).

According to (Ou 2006) the shape of the vertical ground movements is affected by struts stiffness, preload magnitude, the safety of basal stability, excavation depth and the excavation width. As shown in Figure 59. Ou categorized vertical ground movements into two types: spandrel and concave. The type of settlement is controlled by the deformation of the retaining wall. For the OMPW case, the cofferdam excavation produced a cantilever type deflection, mostly generated during the first 100 days, and consequently inducing a

spandrel settlement shape. Additionally, if the OMPW excavation is advanced mostly in a sandy fill and soft to medium clay (urban fill, clay crust, Blodgett and Deerfield strata), then the spandrel shape is more likely to happen as argued by (Clough and O'Rourke 1990).

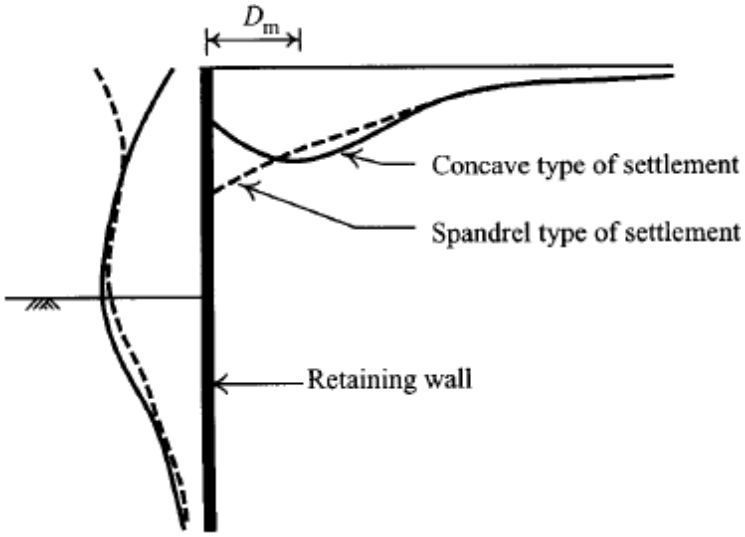

Figure 59. Types of horizontal and vertical ground deformations. After (Ou 2006).

Even though steel ring beams were installed and the recorded ground movements included the effects of the installation of the secant pile wall around the excavation perimeter. The magnitude and type of ground movements (similar to a cantilever wall) show that the OMPW excavation retaining system is not stiff enough to control ground deformations. New alternatives must be explored to increase cofferdam wall stiffness and to control, in a better way, ground displacements.

3.2 Chicago downtown Cofferdam

This project is located in the northern sector of Chicago loop where the Chicago River meets the Lake Michigan shore. This structure was projected to be the highest building in America with a total height of 610 m, but the 2008 economic crisis stopped the construction and only the temporary cofferdam needed to build the rigid central core, was completed.

The cofferdam area, as shown in Figure 60, is surrounded by water except on the west and east side where neighboring building and an urban viaduct are present. Due to these nearby infrastructure, a rigid excavation support system was design to control excessive ground movements and to avoid any damage on the nearby structures.

Figure 60. Chicago Downtown Cofferdam. (Google Earth 2016).

3.2.1. Constructive process

The building was planned to be built combining different methodologies as for the OMPW project. The rigid central core was conceived as a bottom-up sequence with a braced cofferdam, while the building basements were planned to be excavated and constructed using a top-down technique propping the perimeter wall with the basements floor slab. Seven to eight basements levels were initially planned reaching a record depth for habitational urban projects. Similar to the OMPW project, all the foundations were design as deep caissons extending to the bedrock the central core and to the hardpan stratum for all other elements., The project foundations distribution is illustrated in Figure 61, it is important to mention deep foundations allow the use of top-down methodologies.

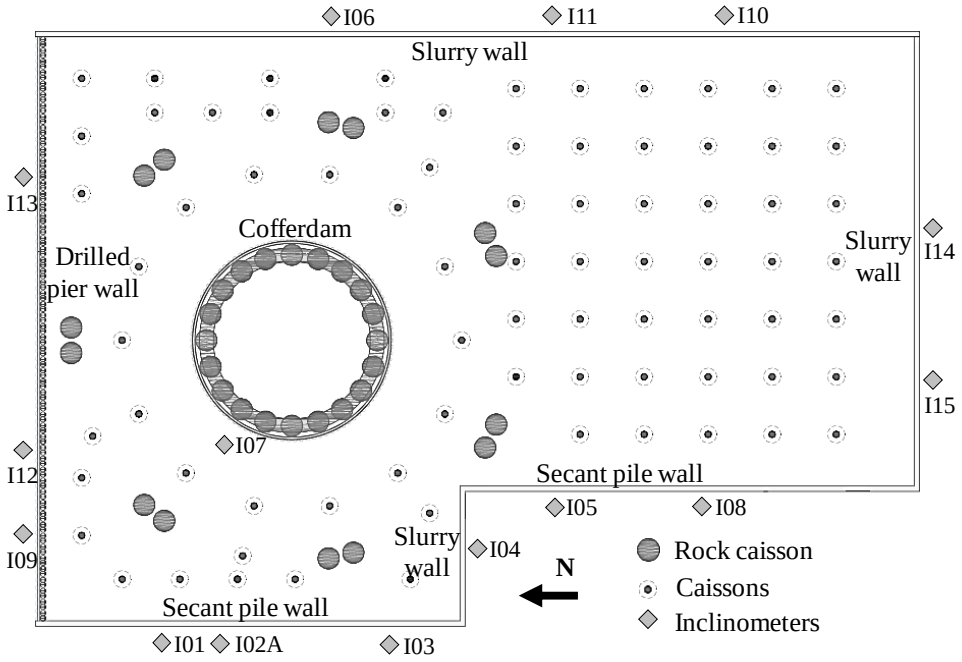

Figure 61. Chicago Downtown Cofferdam plan with foundation distribution, retaining structures and instrumentation.

Construction began by installing the perimeter retaining wall. It was composed by a drilled pier wall in the north side, a slurry wall in the south and east sides, and a secant pile wall in the west side as illustrated in Figure 61. Then, the temporary cofferdam was constructed following a bottom-up sequence using seven (7) reinforced concrete ring beams propping a sheet pile wall. Once the cofferdam was completed, the central concrete core caissons and mat foundation were built. Thereafter, a top-down sequence was planned to excavate the basements levels and construct the superstructure.

The main goal of this research work is to analyze the performance of the temporary cofferdam structure. For this reason, special focus is on its geometry and structural characteristics.

The cofferdam perimeter wall is made of steel sheet piles driven from 2.4 m CCD until a final elevation of -21 m CCD where competitive soil conditions (Chicago hardpan) were reached. The internal cofferdam diameter is approximately 33.2 m and it reaches and excavation depth of approximately 23.4 m. The lateral support was provided by seven reinforced concrete ring beams. They were poured in-situ as the excavation advanced to the mat foundation level at -20.7 m CCD. A cross-section of the cofferdam general geometry and employed concrete ring beams is shown in Figure 62. The steel sheet pile

section to form used to form the cofferdam wall was a PZ-27, while the concrete compressive strength specified for all the ring beams was 55 MPa (8000 psi). The concrete ring beams were welded to the sheet piles by their superior face with a steel profile and by the inner face as presented in Figure 63.

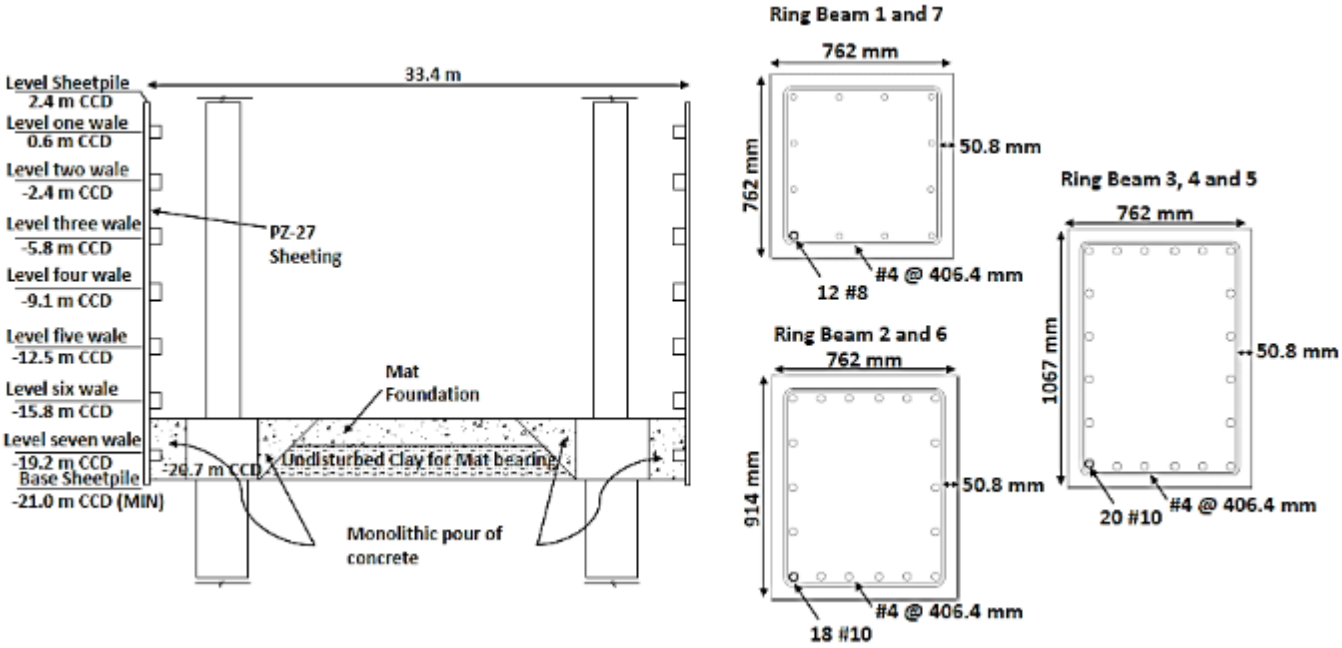

Figure 62. Cofferdam cross-section and concrete ring beams structural details.

The construction sequence for the installation of the urban cofferdam began by leveling the ground surface to an elevation of approximately 2.4 m CCD at which the sheet piles started to be driven. Simultaneously, the construction of the perimeter walls and foundations was undertaken. This process, as shown in Figure 64, started in the middle of October/2017 and finished early November/2017. Once the sheet piles were installed, the excavation activities inside of the cofferdam started and the first concrete ring beam was poured by the end of November/2017. It is important to mention that only 3 days after the first concrete ring beam was placed, the excavation and installation of the steel reinforcement of the second ring beam was completed. A similar sequence using very fast excavation and concrete ring beam placement rates was followed to complete the remaining of the excavation inside of the cofferdam.

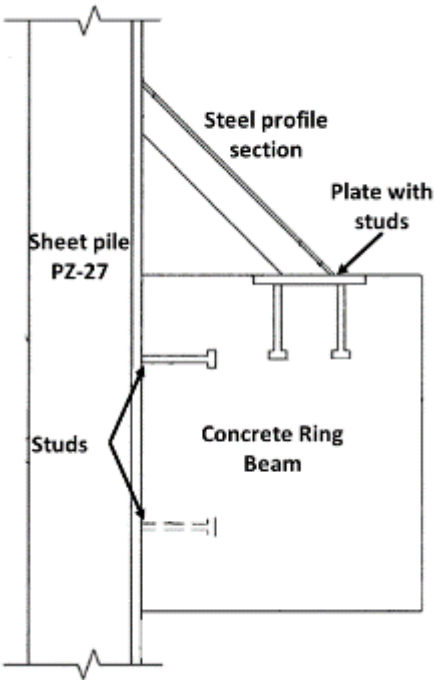

Figure 63. Picture of steel profile welded to the top face of the ring beams.

The cofferdam construction sequence is summarized in Figure 65. The reference day (0) was selected as the first day of sheet pile installation. The figure also shows the number of days necessary to complete each excavation and installation of concrete ring beam bracings. Note that twenty-nine days were necessary to complete the installation/pouring of sheet piles starting in October 12/2007, and the remaining of the excavation was completed in 80 days measured from the end of sheet pile driving to the end of excavation below ring beam 6. The excavation rate was reduced because of the installation of the concrete caissons necessary to support the concrete central core which were installed in about 200 days. The last picture in Figure 64 shows the installation of one of those rock-bearing caissons inside of the cofferdam. The concrete central core was never built and today the cofferdam remains as described and fill with water.

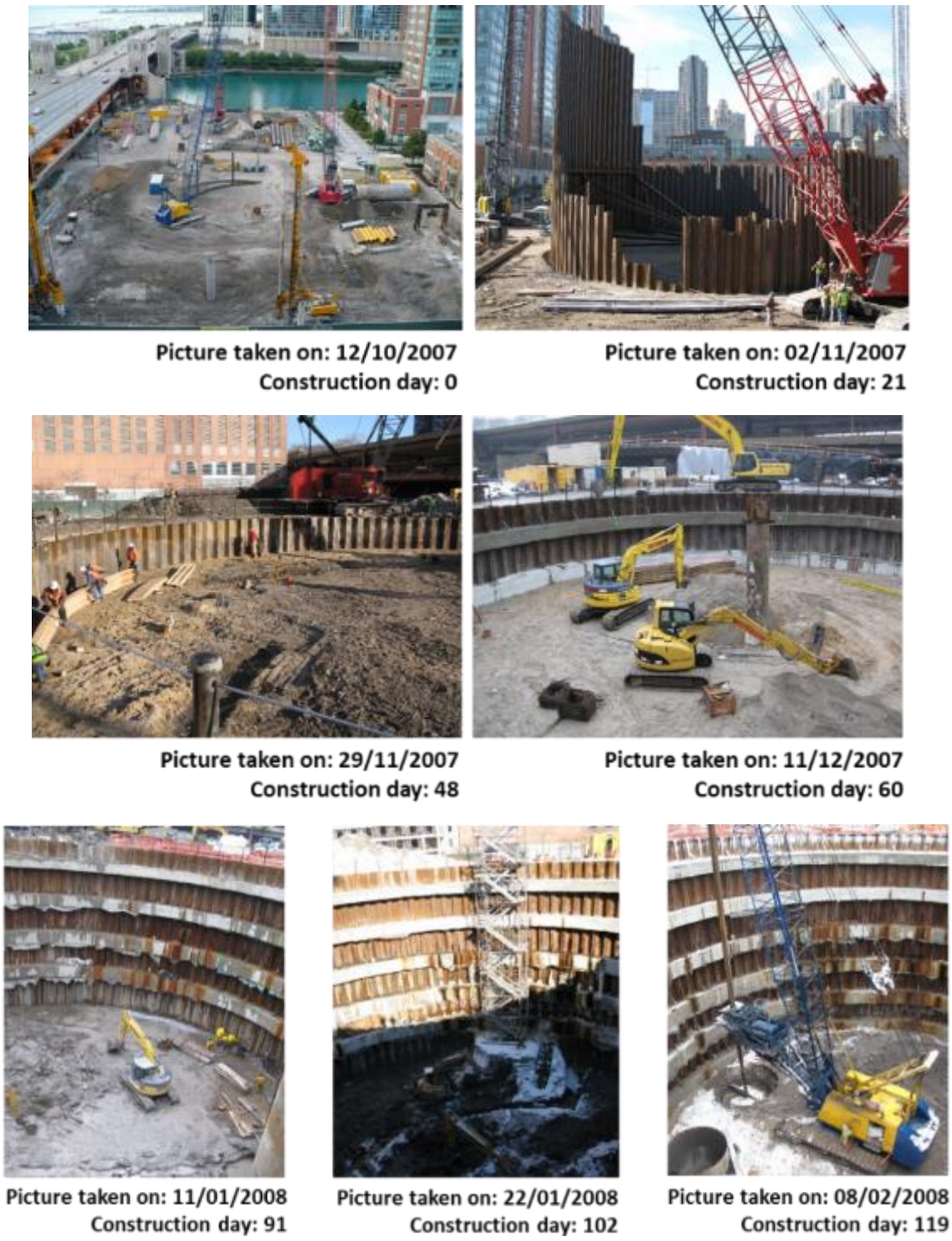

Figure 64. Construction sequence of the urban cofferdam: a) driving sheet piles, b) excavation and installation of the ring beams 1 and 2, c) subsequent excavation and bracing with concrete ring beam 3 to 6 including the beginning of rock-bearing caissons inside of the cofferdam.

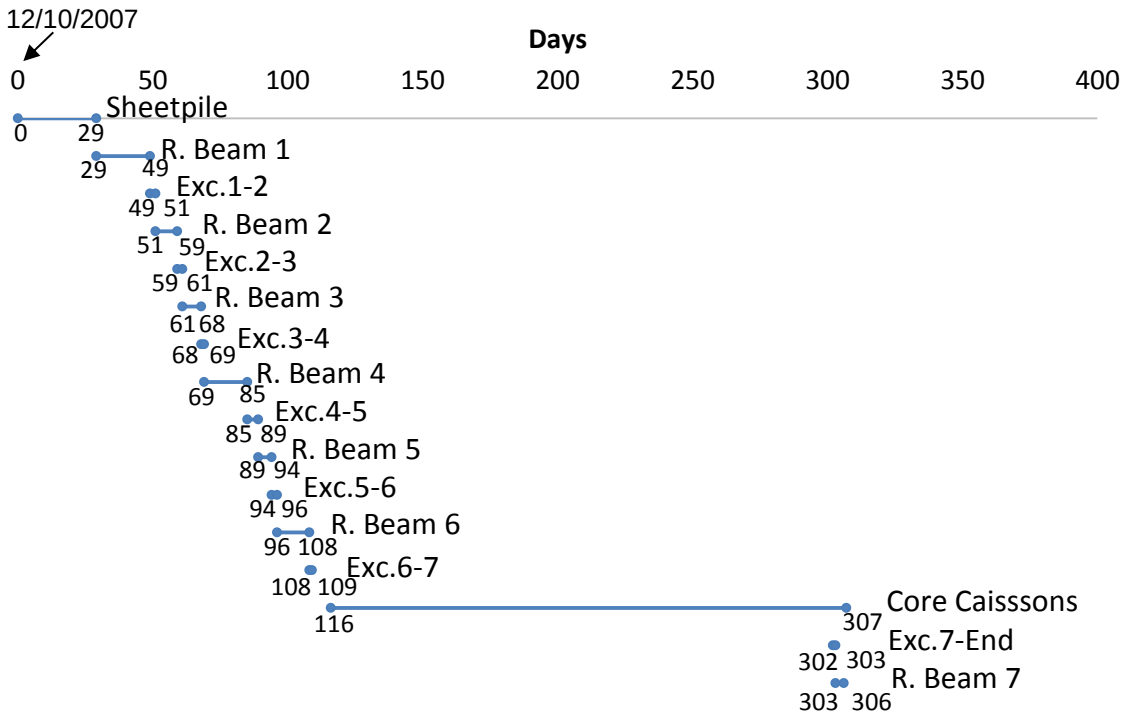

Figure 65. Sequence followed during construction of the urban cofferdam.

3.2.2. Subsurface characteristics and geotechnical conditions

The geotechnical exploration included 11 borings extending to depths between 31 and 43 m below the ground surface, and in-situ vane shear and pressuremeter tests. Additionally Goodman jack and Packer tests were performed in the bedrock to estimate stiffness and permeability properties of the intact rock mass. Piezometers were also installed at elevations of -27.7 and -28.7 m CCD to measure the ground water head on the top of the rock.

A basic stratigraphy characterization, including the results of the in-situ testing, is shown in Figure 66. The topmost stratum corresponds to an urban fill of variable thickness (1.5 to 4.6 m) composed mostly by granular soils with some gravels and interbedded layers of fine grained soils. Underlying the urban fill, a layer mainly composed of poorly graded sands and silty sands, including silts and gravels, is found. Below these sandy layers from -5 to -15 m CCD elevations, the field vane shear tests revealed the presence of lightly overconsolidated soft to medium clay layers with an undrained shear strength increasing with depth from 35 to 75 kPa. Stiff clays were found from -15 to -20 m CCD elevations which transitioned to hard clays up to an elevation of -24 m CCD. Undrained shear strength

obtained from pressuremeter tests performed in the hard clay layers varying from about 250 to 600 kPa (Bahar et al. 2013). An interbedded layer of silty sand and silty gravels of about 1.5 m in thickness was found underlying the hard clays. These granular materials transitioned to a moderately fractured dolomitic limestone at elevations of -28 to -32 m CCD with a Rock Qualify Designation (RQD) varying between 72 and 97%.

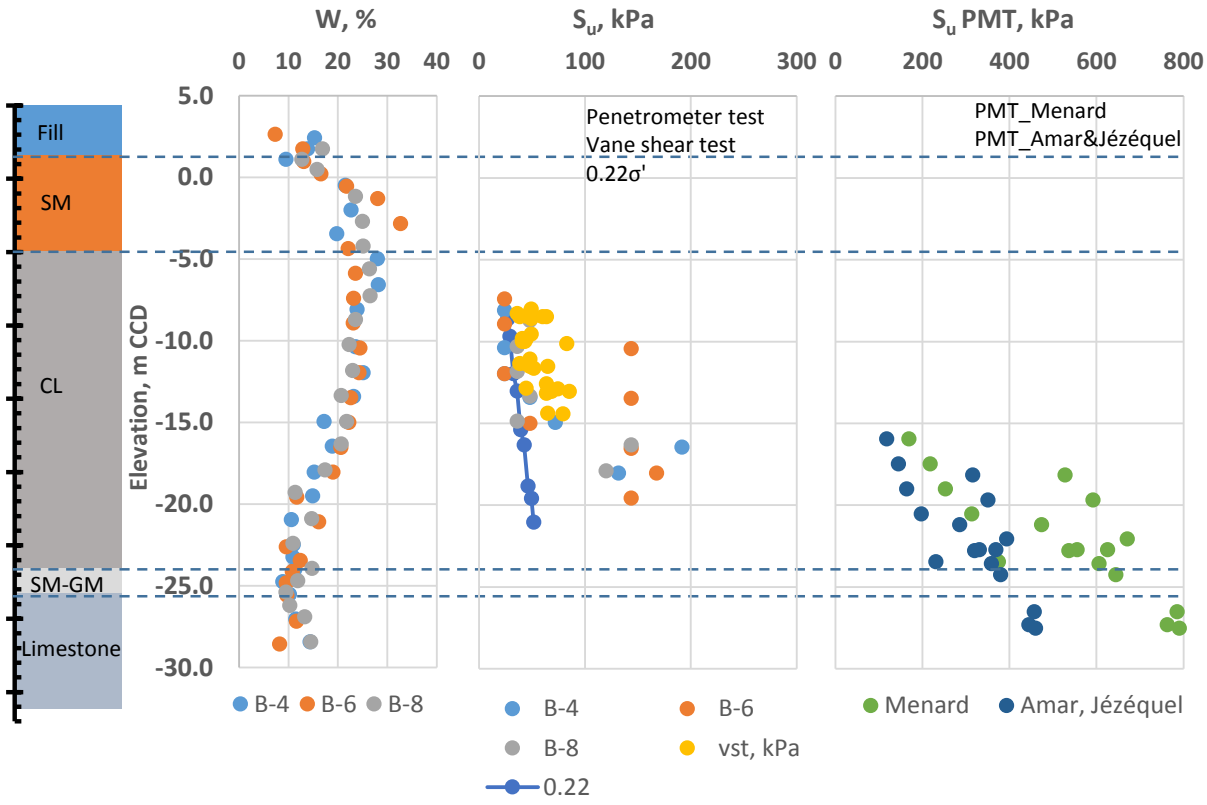

Figure 66. Subsurface conditions at the downtown cofferdam project site.

Regarding the ground water conditions at the project site, in addition to the ground water table located at an elevation of 1 m CCD, controlled by an adjacent Chicago river and Michigan Lake, piezometric readings taken at the site indicated the presence of an additional ground water head varying from -18.3 to -19.2 m CCD elevations. During the three months of monitoring, these piezometric readings were consistent along the site and might be caused by the presence of drainage tunnels that lowered the deep water table. These groundwater conditions suggest that the site is subjected to a steady state downward seepage toward the bedrock instead of hydrostatic conditions. Figure 67 presents the pore

water pressure measurements taken at the site and includes others presented by (Sarabia 2012) which were taken from nearby projects.

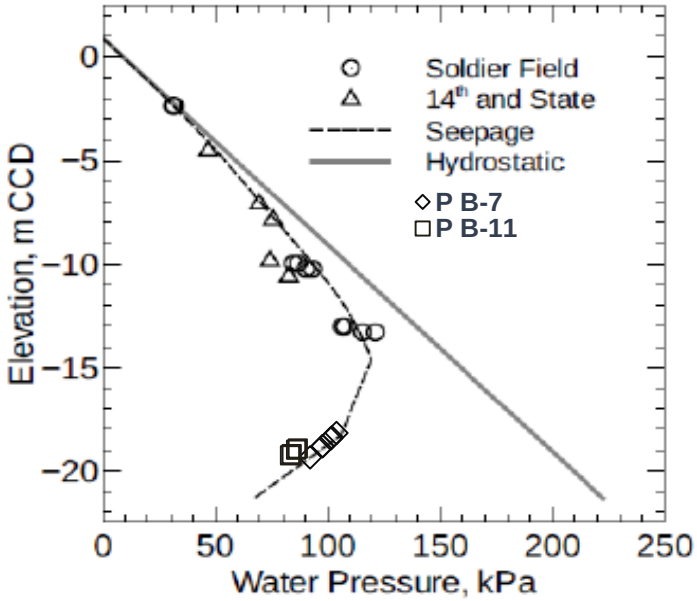

Figure 67. Comparison of pore water pressures measured at the project site (PB-7 and PB-11) with measurements from nearby projects. After (Sarabia 2012).

3.2.3. Observed performance

Lateral ground deformations at the site were monitored using inclinometers. The location of the inclinometers relative to the projected structure is shown in Figure 61. The cofferdam lateral deformations were directly measured with inclinometer 07, which was installed to a depth of 26.8 m, the other inclinometers shown in the figure were installed behind the perimeter slurry walls to monitor the lateral movements induced by the top-down excavation of the basement levels.

Readings at the inclinometer 07 were weekly basis starting on December 6th of 2007 during an approximated time period of 1600 days. Figure 68 presents data taken from Inclinometer 07 where an increase in the lateral displacements in response to the cofferdam inside excavation can be observed. The maximum lateral displacement was about 12 cm and took place around the elevation of the fourth concrete ring beam which is located in the soft to medium clay stratum. The deformation in the inclinometer secondary axis (i.e. in the perpendicular direction) reached a maximum of 4.8 cm and is, located at a slightly lower elevation than the principal one.

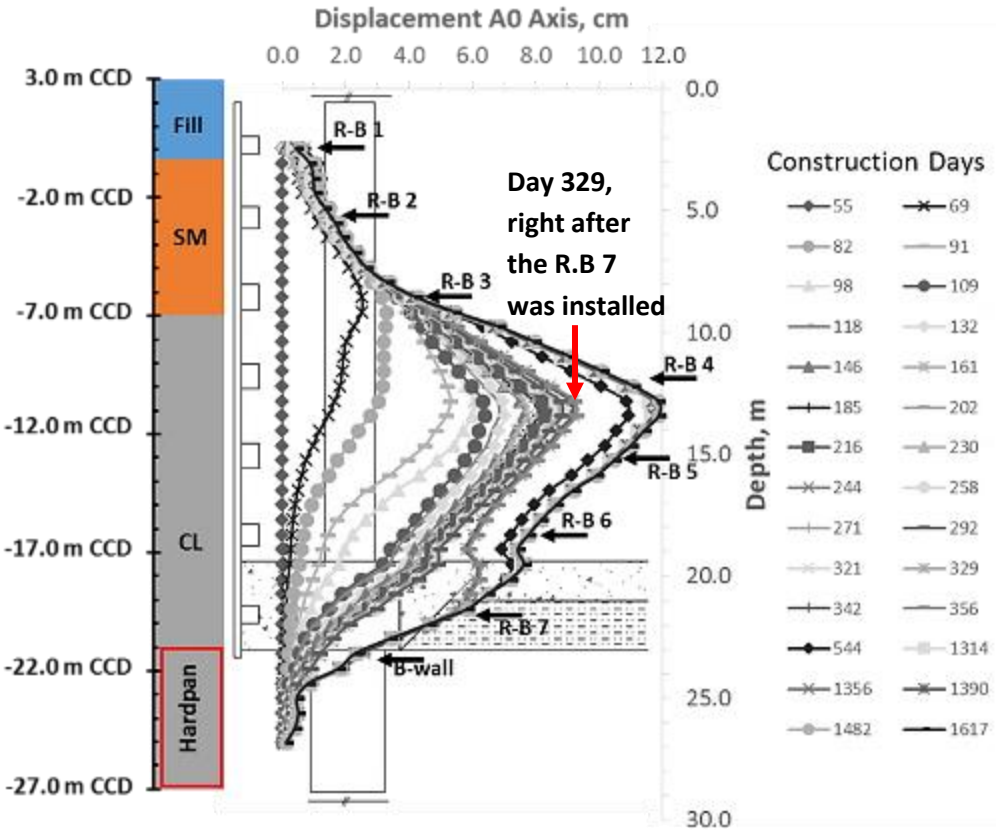

Figure 68. Lateral cofferdam movements in the principal axis measured with inclinometer 07.

Figure 69 presents the variation of lateral deformations with construction time, measured with inclinometer 07 for each ring beam, referenced from the inclinometer surface as: 2.4, 5.5, 8.8, 12.2, 15.5, 18.9, 22.3, 23.8, and 24.1 respectively from ring beam 1 to 7 and for the base cut and final sheet pile depth. The figure shows the excavation sequence in relation to construction days and construction activities. Most of the excavation sequence inside of the cofferdam was rapidly completed, in about 80 days. The lateral deformations tend to increase as the excavation between concrete rings beams occurred. This increase in the rate of deformation is evidenced by the steep slopes of the curves between days 60 and 100, coinciding with the excavations between the third and fifth concrete ring beam, which are located at elevations where soft to medium clay are present. Finally at day 307 (measured from the reference day: sheet pile driving), the foundations at the bottom of the cofferdam were constructed and the last excavation below the mat foundation level was completed to install the final concrete ring beam. These activities induced the last and final large horizontal displacements reaching almost 9 cm at the level

of the fourth concrete ring beam, and significantly increasing lateral movements below the sixth concrete ring beam.

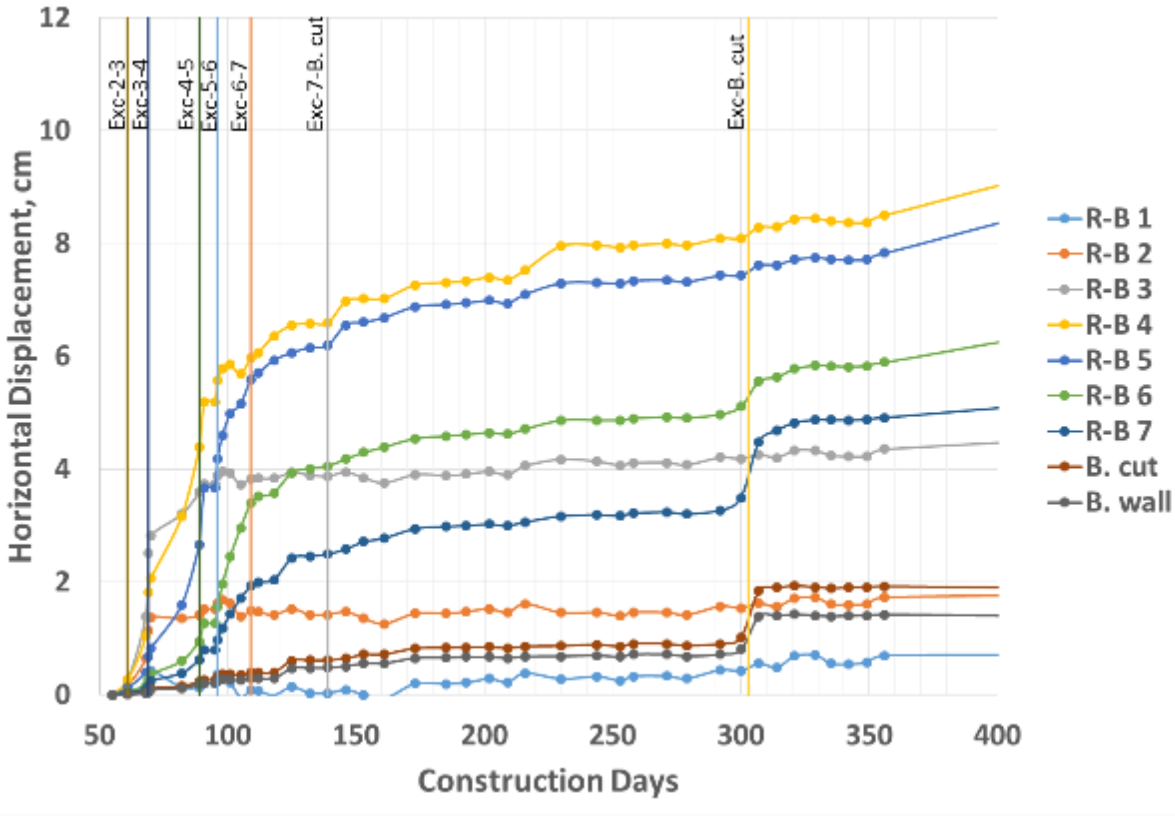

Figure 69. Cofferdam lateral movements measured with inclinometer 07 versus construction days (day 0: sheet pile driving).

Even though the reinforced concrete ring beams were designed and conceived as stiff structural members, the measured lateral deformations of the cofferdam were typical of low-stiffness braced excavations systems. This flexible cofferdam response, can be attributed to the very fast construction sequence. The short times between excavation and pouring, with an average of 2 days for excavations activities and concrete ring beams pouring times from 3 to 20 days. These time lengths for the construction activities might have impacted the concrete maturity of the ring beams affecting the gain in strength and stiffness of the concrete and the maximum load for each concrete ring beam without reaching a propping strength and stiffness. This effect was particularly accentuated during the excavations around the third and fourth concrete ring beams, where critical excavation conditions are encountered due to the presence of soft to medium clays.

Even though the construction activities for the Chicago Downtown Cofferdam took place in 329 days, lateral deformations with inclinometer 07 were measured for a period of 4.5 years which allowed to capture concrete and soil time and temperature dependency effects and not only horizontal deformations induced by excavation activities.

The ratio of maximum lateral deformation ($\delta_{hm} = 12\ cm$) to excavation depth ($H_e = 23.1\ m$) for the downtown cofferdam was about 0.52%, which is typical of excavations in soft clays as reported by (Ou 2006) ($\delta_{hm} = (0.2 - 0.5\%)H_e$). The upper limit (i.e. $\delta_{hm}/H_e = 0.5\%$) is the recommended value for excavations through clays. (Ou 2006) also mentioned that the lateral deformations can be larger when the support system is influenced by the time dependence effects of the concrete.

Table 9 presents excavation-induced ground movements for different types of retaining walls assuming good workmanship, and a retaining wall fully embedded on stiff clay. This table can only be used for excavations depths between 8 and 31 m, having a factor of safety against basal heave greater than 3. If the downtown cofferdam is analyzed as a “high support stiffness” structure taking into account the seven reinforced concrete ring beams, the expected ground induced movements should be approximately 0.15% of the excavation depth, value that was highly exceeded during construction, If the cofferdam is analyzed as a “low support stiffness” structure the recorded total ground displacements still exceed the values recommended in Table 9.

Table 9. Ground surface movements due to excavation of bored pile, diaphragm wall and sheet pile walls wholly embedded in stiff clay. Taken from (CIRIA C580 2003).

Movement type	**High support stiffness** (high propped wall, top-down construction)		**Low support stiffness** (cantilever or low-stiffness temporary props or temporary props installed at low level)	
	Surface movement at wall (per cent of max excavation depth)	**Distance behind wall to negligible movement** (multiple of max excavation depth)	**Surface movement at wall** (per cent of max excavation depth)	**Distance behind wall to negligible movement** (multiple of max excavation depth)
Horizontal	0.15	4	0.4	4
Vertical	0.1	3.5	0.35	4

Taking into account that the ground movements registered during the construction of the cofferdam largely exceed the expected or recommended, values by (Ou 2006) and Table 9, it can be concluded that either the quality of workmanship during the construction or the velocity of the works compromised the strength and stiffness of the concrete ring beam used as lateral bracings. Concrete stiffness is a parameter that develops with time as the material compressive strength increases, in this particular case, concrete strength was over dimensioned for soil and water lateral pressure, proof of that was the stability of the structure during its service life. However, the high construction sequence velocity caused an underdeveloped stiffness that affected the horizontal deformations by a more flexible response of the concrete ring beams than the estimated.

Other factor that might have contributed to increase the ground movements around the cofferdam was limited embedment depth of the sheet pile wall, only 0.3 m into the Chicago hardpan, increasing the pressure on the bottom concrete ring beams. It is expected that a larger embedment depth would stiffen the cofferdam bottom limiting deep seated movements. Additionally, the construction records show there was a period of time (1 to 2 days) in when the final excavation level was reached but the seventh concrete ring beam installation was delayed, leaving most of the ground and water pressure to be contained by the sixth concrete ring beam. This construction detail generated an important increment in ground displacements, which exceeded the expected empirical estimations.

Chapter 4

4. Concrete time and temperature effects

Concrete strength is developed with time depending upon the geometry of the structural member and the curing conditions of the concrete mix. Development of creep and shrinkage strains are also dependent on those curing conditions (Bazant and Baweja 2001). Under ideal temperature and humidity, it is expected that concrete will reach its design compressive strength in 28 days. However, these variables are not always controlled and could affect concrete maturity in a range varying from 20 days to 3 months. During the construction of the reinforced concrete ring beams for the downtown cofferdam, concrete cylinder tests were tested to evaluate the gain of concrete strength with time. The design 28-day concrete compressive strength was 55 MPa (8000 psi). The results of concrete compressive strength measured with cylinder tests were used along with the concrete mix properties, geometric configurations and environmental exposure of structural elements during construction, standard concrete practice approaches to determine shrinkage, creep, and aging of concrete for the downtown cofferdam. The standard concrete practice methods: (ACI 209 1997) and (CEB-FIP 1993) were employed and are also presented in this chapter.

4.1 Concrete strength and stiffness development with time

4.1.1 Development of concrete strength with time

According to (CEB-FIP 1993) the concrete compressive strength, f_{cm}, can be determined as:

$$f_{cm} = f_{ck} + \Delta f \tag{43}$$

where f_{ck} is the compressive strength below which 5% of all possible strength measurements for the specified concrete may be expected to fall, and Δf is a constant taken as 8 MPa. The variation of concrete compressive strength with time based on (CEB-FIP 1993) is as follows:

$$f_{cm}(t) = \beta_{cc}(t) f_{cm} \tag{44}$$

$$\beta_{cc}(t) = exp\left\{s_c\left[1 - \left(\frac{28}{t/t_1}\right)^{1/2}\right]\right\} \tag{45}$$

where $f_{cm}(t)$ is the average concrete compressive as a function of time in days, f_{cm} is the average concrete compressive strength at 20 days, $\beta_{cc}(t)$ is a coefficient variable as a function of the concrete age, t, in days, t_1 is a constant equal to 1 day, s_c is a coefficient that depends on the type of concrete (i.e., 0.2 for rapid hardening high strength cements, 0.25 for normal and rapid hardening cements, and 0.38 for slowly hardening cement).

Figure 70 presents the results of concrete cylinders tested under monotonically increasing compressive stresses for the downtown cofferdam. The tests are reported for all the concrete ring beams along with the reference values of concrete compressive design strength of 55 MPa. The figure presents the predicted variations for the 55 MPa concrete compressive design strength and for lower and upper bounds computed with 35 and 65 MPa, respectively. At the end of concrete tested records (about 56 days), large dispersion of the data from 30 to 80 MPa was measured with an average compressive strength of 56.5 MPa and a standard deviation of 12 MPa.

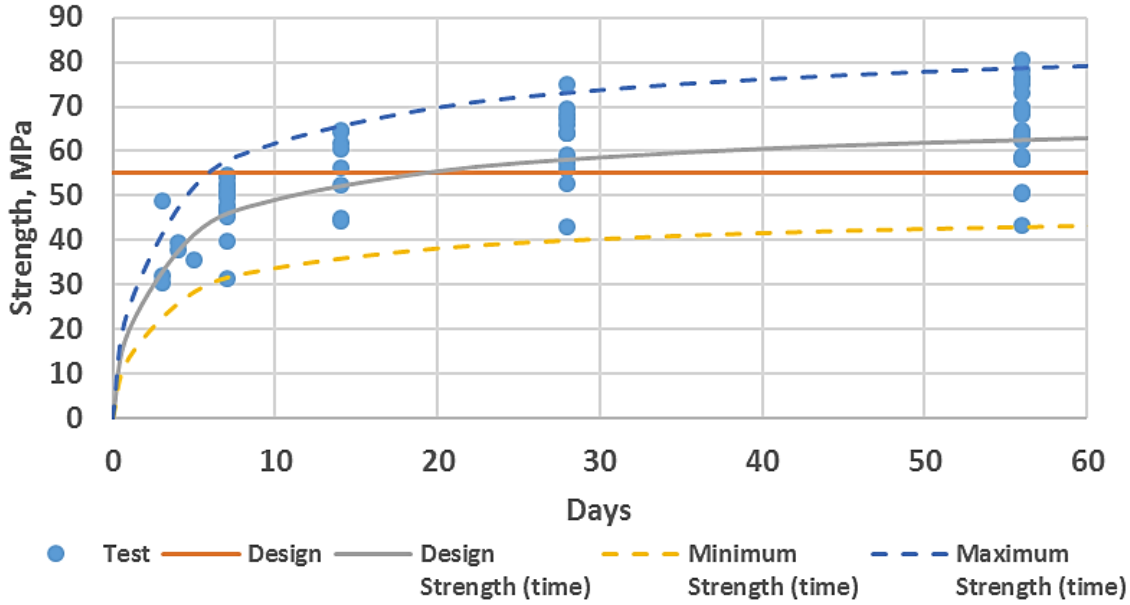

Figure 70. Development of concrete compressive strength with time computed with (CEB-FIP 1993) and measured with concrete cylinder tests.

The development of the compressive strength with time, according to (ACI 209 1997), follows the following hyperbolic function:

$$(f'_c)_t = \frac{t}{\alpha' + \beta t}(f'_c)_{28} \tag{46}$$

where, α and β are constants in days, $(f'_c)_{28}$ is the design compressive strength at 28 days, and t is the age of the concrete in days. Those constants are function of the type of concrete and the curing method and can vary from 0.05 to 9.25 and from 0.67 to 0.98 for α' and β, respectively.

Figure 71 presents the test results of compressive strength tests and the strength curves obtained with (ACI 209 1997) for a design strength of 55 MPa. The constants α and β were assumed equal to 2 and 0.9, respectively. Minimum and maximum compressive strength were estimated with the same methodology; variations were found from 40 to 70 MPa respectively.

The compressive strength after 10 days of maturity is less than the design strength which implies that concrete should not be subjected to loading arising from the excavation activities unless the structural element is designed to account for this overstress.

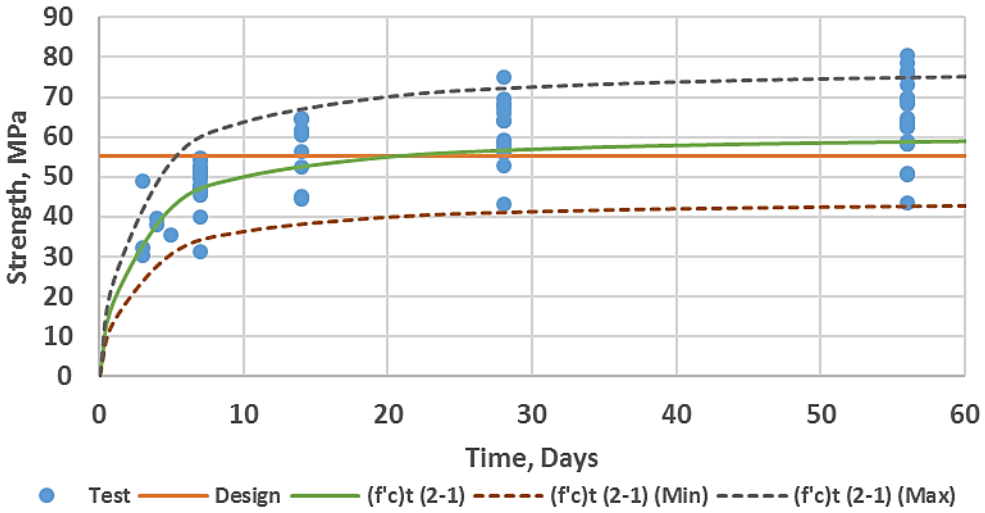

Figure 71. Development of concrete compressive strength with time computed with (ACI 209 1997) and measured with concrete cylinder tests.

Note that the concrete ring beams reached the design strength after 18 days, which is considered long term conditions. However, for the short term and depending upon the formwork removal and subsequent soil excavation, the ring beams might not have the required strength to support the lateral earth pressure induced by the excavation. It can be seen in Figure 71 that about 10 days after the concrete was placed, the strength was still below the design compressive strength, which is a critical condition as some excavation activities took place within four days of concrete placement. This is a contributing factor to explain the large deformations that occurred during the cofferdam construction. It is also important to mention that the concrete cylinders were cured and tested under controlled laboratory conditions, which are presumably different from the actual environmental conditions of the ring beams and thus, low concrete strength values are plausible due to the low temperatures experienced in actual field conditions.

4.1.2 Development of concrete modulus of elasticity with time

The elastic modulus for normal weight concrete can be determined as follows:

$$E_{ci} = E_{co}[(f_{ck} + \Delta f)/f_{cmo}]^{1/3} \quad (47)$$

where E_{ci} is the modulus of elasticity in MPa for a concrete age of 28 days, f_{ck} is the compressive strength below which 5% of all possible strength measurements for the specified concrete may be expected to fall, and f_{cmo} and E_{co} are constants taken as 10 MPa and 2.15 x10^4 MPa, respectively. For a given 28-day concrete compressive strength, the modulus of elasticity can be calculated as:

$$E_{ci} = E_{co}[f_{cm}/f_{cmo}]^{1/3} \quad (48)$$

where f_{cm} is the concrete compressive strength measured at 28 days. A modulus reduction of 15% can be applied when only elastic analyses are considered. The variation of the modulus of elasticity with time, based on (CEB-FIP 1993), is expressed as follows:

$$E_{ci}(t) = \beta_E(t)E_{ci} \quad (49)$$

$$\beta_E(t) = [\beta_{cc}(t)]^{0.5} \quad (50)$$

where $E_{ci}(t)$ is the evolution of concrete elastic modulus with time in days, $\beta_E(t)$ is a coefficient variable with time, and $\beta_{cc}(t)$ is the same coefficient shown for the variation of concrete strength with time.

Figure 72 presents the evolution of the modulus of elasticity based on the available results of concrete compressive cylinder tests using the (CEB-FIP 1993) expressions. The figure also includes the variation of the elasticity modulus for the design concrete compressive strength of 55 MPa along with the lower and upper bounds. A similar trend as the one depicted for the development of compressive strength was obtained for the modulus of elasticity. Note that five (5) days after the concrete was placed, it has not reached the required stiffness for the design compressive strength (55 MPa). This could also explain the large excavation-induced deformations registered by the inclinometer with four of the seven concrete ring beams working with an average curing period of 5 days.

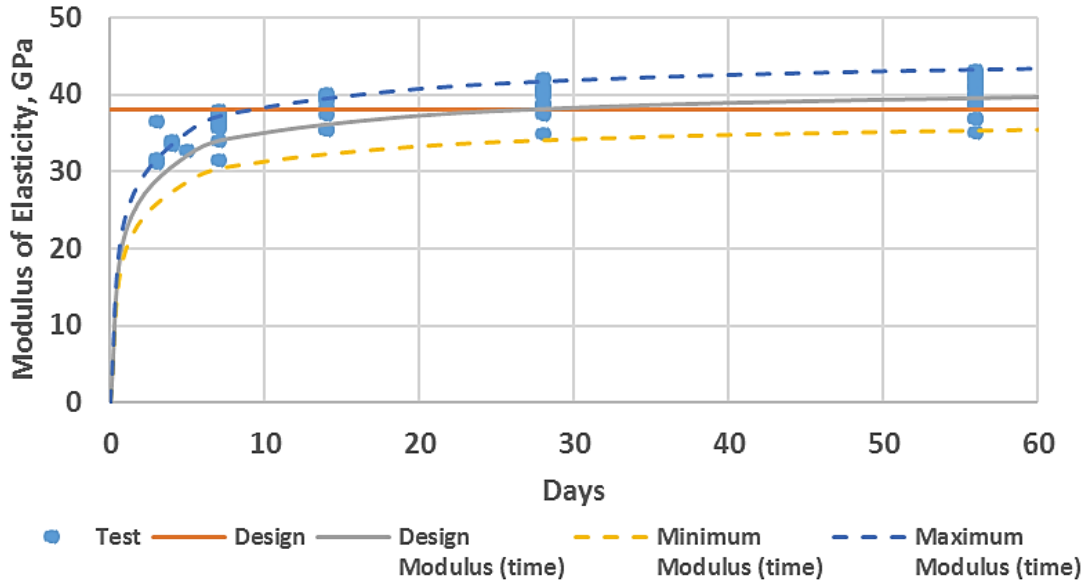

Figure 72. Variation of concrete modulus of elasticity with time based on (CEB-FIP 1993) and results of concrete cylinder tests.

The American building code (ACI 209 1997) recommends the following expression to define the development of concrete modulus of elasticity with time:

$$E_{ct} = g_{ct}[w^3(f'_c)_t]^{1/2} \quad (51)$$

where g_{ct} is a constant taken as 0.043, w is the concrete unit weight, and $(f'_c)_t$ is the compressive strength at a given time t. Figure 73 presents the development of the modulus of elasticity with time computed with (ACI 209 1997). Also included in the figure are the values based on the cylinder tests results. The figure shows a similar behavior as the one obtained for the development of concrete compressive strength, where after about 15 days of maturity the concrete reaches the design concrete strength and stiffness.

As mentioned before, stiffness did not reach the expected design value until 10 to 15 days after concrete had been poured for the (CEB-FIP 1993) and (ACI 209 1997) methodologies respectively. It may help to explain why ground displacements were larger than expected. Accelerated construction procedures did not wait the minimum require time to achieve proper strength and stiffness between excavations, that as presented before, in some cases took an average curing time of 5 days.

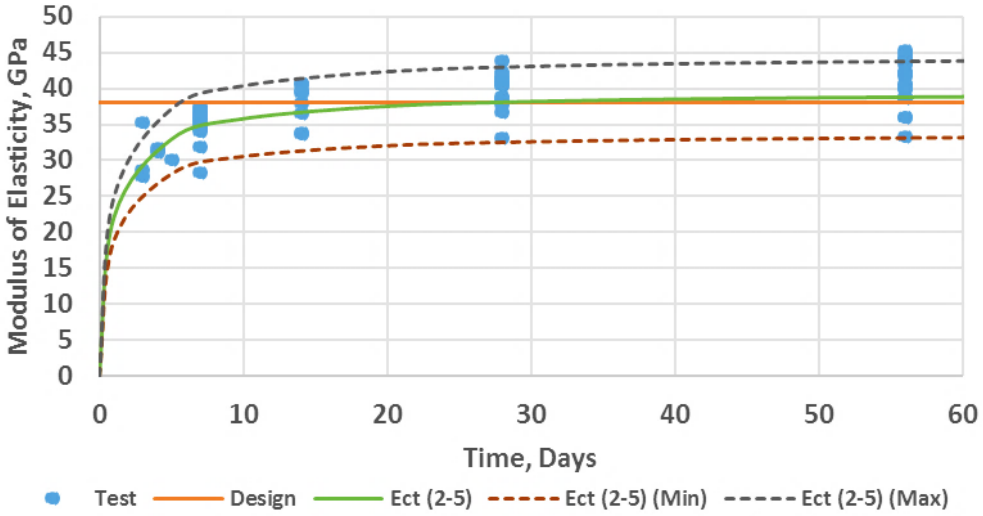

Figure 73. Variation of concrete modulus of elasticity with time based on (ACI 209 1997) and concrete cylinder tests results.

4.2 Concrete creep and shrinkage development with time

4.2.1 Concrete creep development with time

For stress levels under 40% of the concrete compressive strength, creep strains are assumed to vary linearly with the stress level. For a structural member under a constant applied load, the following expression is proposed by (CEB-FIP 1993) to estimate concrete creep strains:

$$\varepsilon_{cc}(t,t_0) = \frac{\sigma_c(t_0)}{E_{ci}}\phi(t,t_0) \tag{52}$$

where $\sigma_c(t_0)$ is the compressive strength at the time of loading which was assumed as $0.4f_{cm}(t_0)$ i.e. 22 MPa for a f_{cm} = 55 MPa, $\phi_{(t,t_0)}$ is a creep coefficient and E_{ci} is the concrete modulus of elasticity at 28 days. The creep coefficient based on (CEB-FIP 1993) can be evaluated as:

$$\phi(t,t_0) = \phi_0\beta_c(t-t_0) \tag{53}$$

where ϕ_0 is the notional creep coefficient, β_c is a coefficient to describe the development of creep with time after loading, t is the age of concrete in days, and t_0 is the age of concrete at loading. The notional creep coefficient based on (CEB-FIP 1993) recommendations can be expressed as follows:

$$\phi_0 = \phi_{RH}\beta(f_{cm})\beta(t_0) \tag{54}$$

where

$$\phi_{RH} = 1 + \frac{1 - RH/RH_0}{0.46(h/h_0)^{1/3}} \tag{55}$$

$$\beta(f_{cm}) = \frac{5.3}{(f_{cm}/f_{cmo})^{0.5}} \tag{56}$$

$$\beta(t_0) = \frac{1}{0.1 + (t_0/t_1)^{0.2}} \tag{57}$$

In the above equations $h = 2A_c/u$ is the notional size of the structural member in *mm*, A_c is the cross sectional area of the structural element, *u* is the perimeter of the member in contact with the atmosphere, f_{cm} is the concrete compressive strength at 28 days, f_{cmo}= 10 MPa, RH is the relative humidity of the ambient, and RH_0, h_0 and t_1 are constants taken as 100%, 100mm, and 1 day, respectively. The development of creep coefficient with time is given as:

$$\beta_c(t - t_0) = \left[\frac{(t - t_0)/t_1}{\beta_H + (t - t_0)/t_1}\right]^{0.3} \tag{58}$$

where

$$\beta_H = 150\left\{1 + \left(1.2\frac{RH}{RH_0}\right)^{18}\right\}\frac{h}{h_0} + 250 \leq 1500 \tag{59}$$

The dimensions of the concrete ring beams employed at the downtown cofferdam, necessary for the calculation of creep strains, are listed in Table 10. The cofferdam design considered larger ring beams around the middle of the excavation depth, corresponding to

the location of the soft to medium compressible clays where large excavation-induced movements were expected.

Table 10. Geometry of the concrete ring beam used in Chicago Downtown Cofferdam.

Ring Beam	Width (mm)	Height (mm)	Ac (mm^2)	U (mm)	h (mm)
RB 1 and 7	762	762	580644	2286	508.0
RB 2 and 6	762	914.4	696772.8	2438.4	571.5
RB 3, 4, and 5	762	1066.8	812901.6	2590.8	627.5

The calculation of creep strains using the abovementioned equations, for a design concrete compressive strength of 55 MPa, are presented in Figure 74. The calculations were performed until day 1600 which corresponds to the last day of lateral deformation measurements taken with the inclinometer.

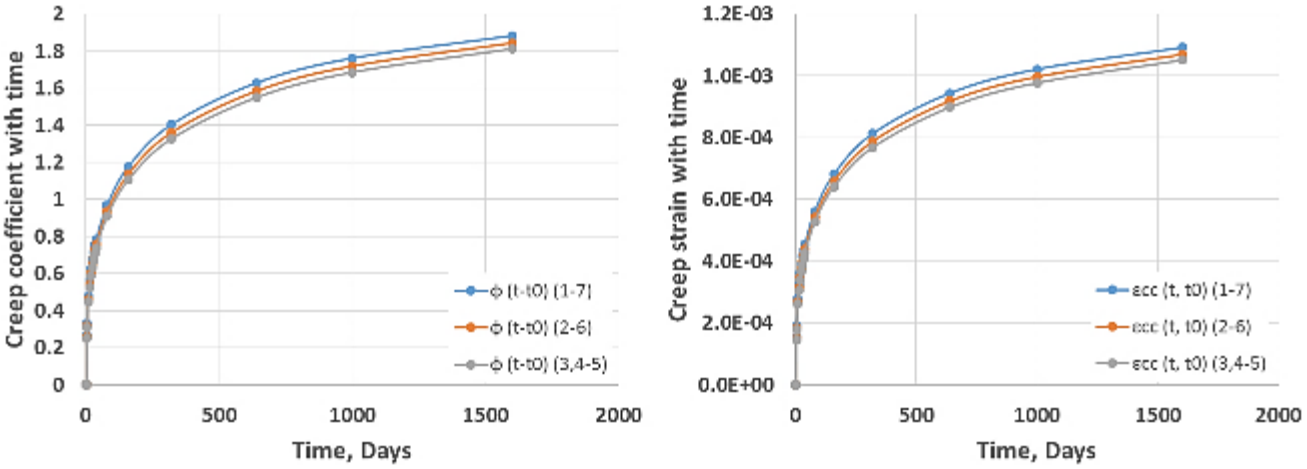

Figure 74. Computed development of creep for the concrete ring beams according to (CEB-FIP 1993): a) evolution of creep coefficient with time; and b) evolution of creep strains with time.

The American code (ACI 209 2008) suggests the following expressions to estimate the amount of creep strains that a structural member develops under sustained loading conditions.

$$\nu_t = \frac{t^{\Psi'}}{d + t^{\Psi'}} \nu_u \tag{60}$$

where ν_t is the concrete creep at a given time t, d is a time variable in days, ν_u is the ultimate creep coefficient, and Ψ' is a constant in function of the element shape. (ACI 209 2008) presents some ranges and typical values for these constants, as shown in Table 11.

Table 11. Range of variation of creep constants (ACI 209 1997).

Parameter	Min. value	Max. value	Recommended value
$\boldsymbol{\Psi'}$	0.4	0.8	0.6
$\boldsymbol{d}$	6	30	10.0
$\boldsymbol{\nu_u}$	1.3	4.15	2.4

(ACI 209 2008) proposed correction factors to account for environmental and shape conditions that differ from the values used to calibrate the code formulas. These correction factors are due to wet curing when the element is loaded after 7 days, relative humidity conditions above 40%, and size correction factors quantified in terms of the volume-surface ratio. These proposed corrections factors can be calculated as:

$$Creep\ \gamma_{la} = 1.25(t_{la})^{-0.118} \tag{61}$$

$$Creep\ \gamma_{\lambda} = 1.27 - 0.0067\lambda, for\ \lambda > 40\% \tag{62}$$

$$Creep\ \gamma_{vs} = \left({}^{2}/_{3}\right)[1 + 1.13exp(-0.0213\ {}^{v}/_{S})] \tag{63}$$

where, t_{la} is the loading time in days not less than 7, λ is the relative humidity in percentage, ${}^{v}/_{S}$ is the volume-to-surface ratio in *mm* computed with the surface corresponding to those faces of the element in contact with the atmosphere. For a rectangular prismatic member, it is the same ratio of cross-sectional area to effective perimeter ratio. The (ACI 209 2008) also suggests correction factors related to the concrete mix such as slump, fine aggregate content, and air content. The correction factors are expressed as follows:

$$Creep\ \gamma_{s} = 0.82 + 0.00264s \tag{64}$$

$$Creep\ \gamma_{\Psi} = 0.88 + 0.0024\Psi \tag{65}$$

$$Creep\ \gamma_{a} = 0.46 + 0.09a\ \geq 1 \tag{66}$$

where, s is the slump of the concrete mix in *mm*, Ψ is the ratio of fine aggregates from the total aggregates expressed in percentage from the total weight, and a is the air content also expressed in percentage. Table 12 shows the mix composition properties used and

correction factors computed with Equations (64) - (66) for the particular case of the downtown cofferdam.

Table 12. Creep correction factors based on the specific concrete mix used for the ring beams.

Property name	Variable	Value
Slump	S (mm)	130
	γ_s	1.16
Fine aggregates	Ψ (%)	50
	γ_Ψ	1.00
Air content	a (%)	8
	γ_α	1.18

Figure 75 presents the variation of creep coefficients with time using the expressions recommended by (ACI 209 2008) for the concrete ring beam bracings of this research. The concrete ring beams were made from the same concrete mix design and that's why the three curves are superposed. The figure also presents a comparison between this methodology and the one proposed by (CEB-FIP 1993). It is observed that the first 200 days depict the same behavior for all the ring beams regardless of the method used. Larger discrepancies in the long-term behavior were observed.

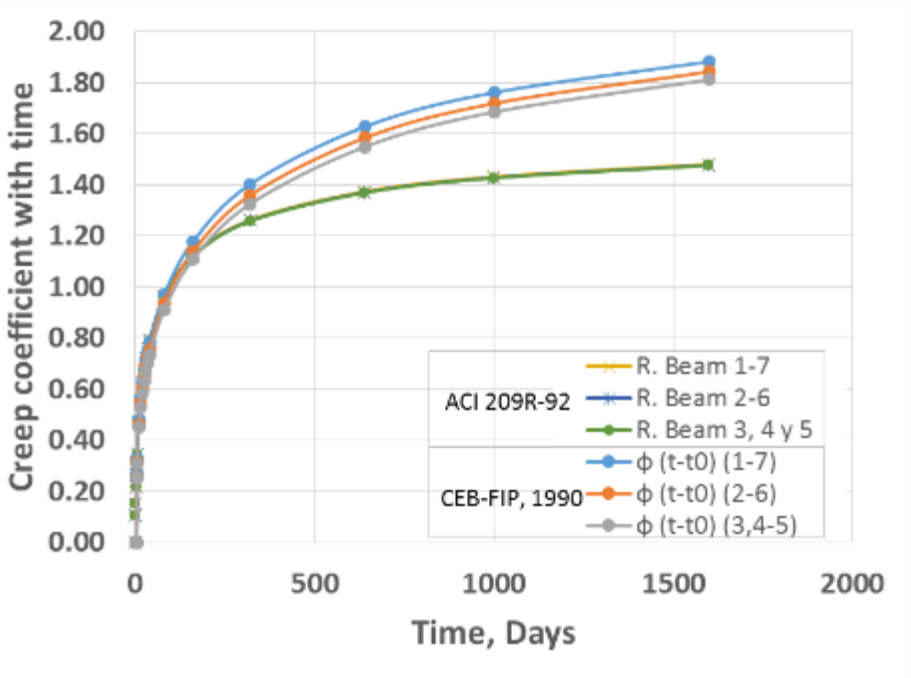

Figure 75. Development of creep coefficient with time according to (ACI 209 2008) with corrections by (ACI 209 2008) and compared with creep coefficients computed with (CEB-FIP 1993).

4.2.2 Concrete shrinkage development with time

Regarding the shrinkage in concrete, (CEB-FIP 1993) recommends the following expression to estimate shrinkage strains:

$$\varepsilon_{cs}(t, t_s) = \varepsilon_{cso}\beta_s(t - t_s) \tag{67}$$

$$\varepsilon_{cso} = \varepsilon_s(f_{cm})\beta_{RH} \tag{68}$$

$$\varepsilon_s(f_{cm}) = [160 + 10\beta_{sc}(9 - f_{cm}/f_{cmo})]\, x\, 10^{-6} \tag{69}$$

where ε_{cso} is the notional shrinkage coefficient, β_s is a coefficient to describe development of shrinkage with time, t is the age of concrete in days, t_s is the age of concrete at the beginning of shrinkage, f_{cm} is the average 28-day concrete compressive strength, f_{cmo} is a constant taken as 10 MPa, β_{sc} is a coefficient that depends on the type of cement (4 for slowly hardening, 5 for normal or rapid hardening, and 8 for rapid hardening high strength cements), and β_{RH} and β_{sRH} are given by:

$$\beta_{RH} = -1.55\beta_{sRH} \; for \; 40\,\% \leq RH < 90\,\% \tag{70}$$

$$\beta_{RH} = +0.25 \; for \; RH \geq 99\,\% \tag{71}$$

$$\beta_{sRH} = 1 - \left(\frac{RH}{RH_0}\right)^3 \tag{72}$$

The coefficient for shrinkage development with time, according to (CEB-FIP 1993), is given as:

$$\beta_s(t - t_s) = \left[\frac{(t - t_s)/t_1}{350(h/h_0)^2 + (t - t_s)/t_1}\right]^{0.5} \tag{73}$$

Figure 76 presents the development of concrete shrinkage for the ring beam bracings of the Chicago Downtown Cofferdam based on the equations proposed by (CEB-FIP 1993).

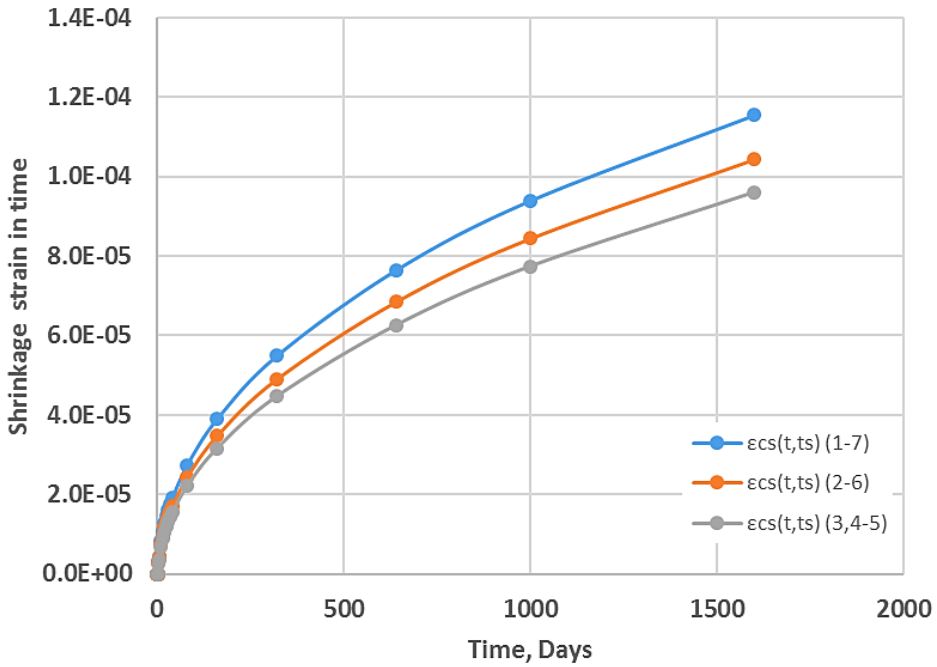

Figure 76. Computed shrinkage strains for the concrete ring beam bracings of the Chicago Downtown Cofferdam.

(ACI 209 2008) suggests the development of shrinkage strains in concrete elements based on ACI 209R-92 approach, that can be estimated as follows.

$$(\varepsilon_{sh})_t = \frac{t^{\alpha}}{f + t^{\alpha}} (\varepsilon_{sh})_u \quad (74)$$

where $(\varepsilon_{sh})_t$ is the concrete shrinkage strain at any time t, f is a time variable in days, $(\varepsilon_{sh})_u$ is the ultimate shrinkage strain coefficient, and α is a constant based on the element size. Typical variations and recommended values by (ACI 209 2008) are listed in Table 13.

Table 13. Range of variation of shrinkage constants (ACI 209 2008).

Parameter	Min. value	Max. value	Recommended value
α	0.9	1.1	1.0
f	20	130	35.0
$(\epsilon_{sh})_u$	4.15E-04	1.07E-03	7.80E-04

Additional corrections to estimate concrete shrinkage for conditions that differ from the ones used to derive the code expressions are proposed. Corrections arising from wet curing conditions different than 7 days are presented in Table 14.

Table 14. Correction factors for wet curing conditions different than 7 days (ACI 209 2008).

Duration of moist curing in days	Correction factor (γ_{cp})
1	1.20
3	1.10
7	1.00
14	0.93
28	0.86
90	0.75

The correction factors due to relative humidity values larger than 40% and size correction factors quantified in terms of the volume-to-surface ratios are proposed by (ACI 209 2008) as follows:

$$Shrinkage\ \gamma_{\lambda} = 1.40 - 0.0102\lambda, for\ 40\% \leq \lambda \leq 80\% \quad (75)$$

$$Shrinkage\ \gamma_{\lambda} = 3.00 - 0.030\lambda, for\ 80\% < \lambda \leq 100\% \quad (76)$$

$$Shrinkage\ \gamma_{vs} = 1.2\exp(-0.00472\,{}^{v}/_{s}) \quad (77)$$

The correction factors due to concrete mix composition related to concrete mix slump, amount of aggregate fines, cement content, and air content are proposed by (ACI 209 2008) and presented as follows:

$$Shrinkage\ \gamma_s = 0.89 + 0.00161s \tag{78}$$

$$Shrinkage\ \gamma_\Psi = 0.30 + 0.14\Psi\ for\ \Psi \leq 50\% \tag{79}$$

$$Shrinkage\ \gamma_\Psi = 0.30 + 0.14\Psi\ for\ \Psi \leq 50\% \tag{80}$$

$$Shrinkage\ \gamma_c = 0.75 + 0.00061c \tag{81}$$

$$Shrinkage\ \gamma_a = 0.95 + 0.008a \tag{82}$$

where, s is the slump of the mixture in mm, Ψ is the ratio of fine aggregates to total weight in percentage. c is the content of cement in kg/m^3, a is the air content express in percentage. Table 15 summarizes the correction factors for shrinkage calculations arising from concrete composition.

Table 15. Shrinkage correction factors based on the specific concrete mix used for the ring beams.

Property name	Variable	Value
Slump	S (mm)	130
	γ_s	1.10
Fine aggregates	Ψ (%)	50
	γ_Ψ	1.00
Cement content	c (kg/m^3)	362*
	γ_c	0.97
Air content	a (%)	8
	γ_α	1.01

* The cement content may vary from a range of 279-445 for this an average value was selected.

Figure 77 shows the development of shrinkage strains with time for each concrete ring beam of Chicago Downtown Cofferdam using the (ACI 209 2008) method. The results are compared with those obtained from (CEB-FIP 1993) equations. Note that larger shrinkage strains are obtained with the method proposed by (ACI 209 2008).

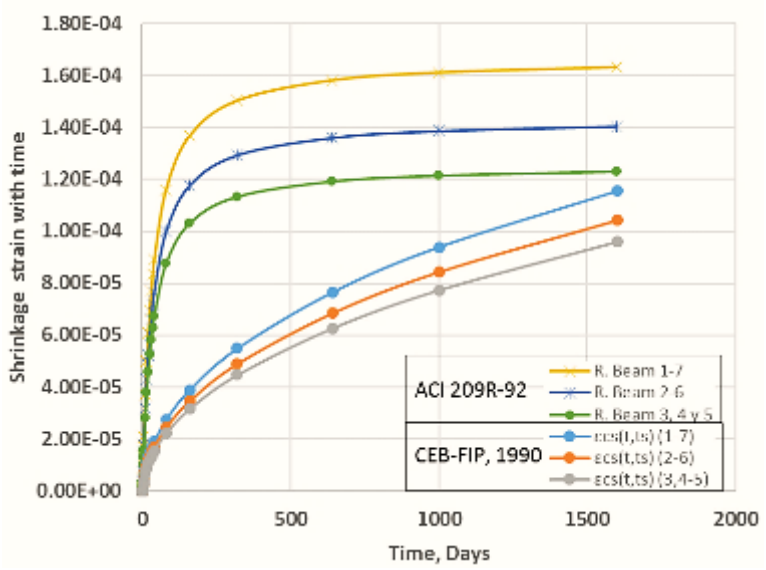

Figure 77. Development of shrinkage strains with time according to ACI 209R-92 and updated by (ACI 209 2008) compared with shrinkage strains by (CEB-FIP 1993).

The results presented in Figure 77 match the overall trend of shrinkage values presented by (ACI 209 2008) in Figure 78, in which those methods are compared, that comparison also including others methods.

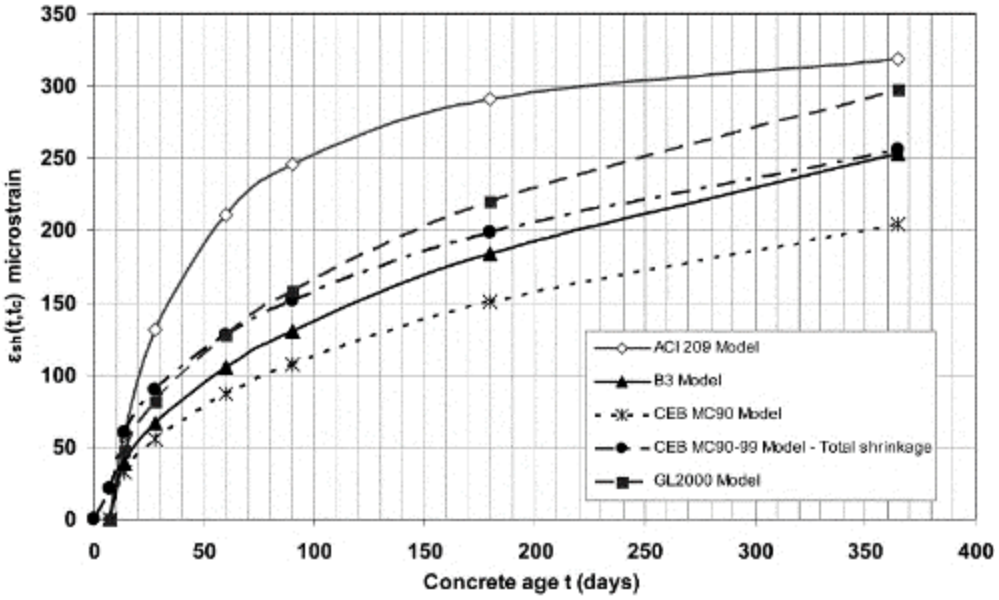

Figure 78. Comparison of different methodologies to estimate the development of shrinkage with time. Taken from (ACI 209 2008).

In the short-term large differences are obtained between (CEB-FIP 1993) and (ACI 209 2008) shrinkage methodologies, with almost twice the microstrains between them.

However, with time the difference decreases (Figure 77). When a short-term shrinkage analysis is performed, this huge difference must be considered, for example when evaluating Chicago Downtown Cofferdam which most of the strains happened in less than a year according to the inclinometer.

4.3 Influence of ambient temperature on concrete maturity

The previous models for compressive strength, modulus of elasticity, creep and shrinkage do not take into account the effect of temperature during aging. Changes in temperature through the day or even between seasons can induce significant deviations in the predictions under a constant temperature of 20°C. In this section temperature corrections are made and the concrete time effects recalculated.

4.3.1 Maturity of concrete

Concrete maturity is directly affected by temperature changes, which caused an increase or decrease in the hydration process between cement and aggregates. (CEB-FIP 1993) presents the following expression to estimate concrete aging including temperature changes:

$$t_T = \sum_{i=1}^{n} \Delta t_i \exp\left[13.65 - \frac{4000}{273 + T(\Delta t_i)/T_0}\right] \quad (83)$$

where, t_T is the age time adjusted by temperature, Δt_i is an interval of time in days for a temperature T in °C, and $T_0 = 1°C$.

The maturity of each cofferdam ring beam was estimated using Eq. (83). Figure 79 shows the daily Chicago average temperature measured from 1st October 2007 to 4th November 2008. Also, include in the figure are the dates when the concrete rings were cast.

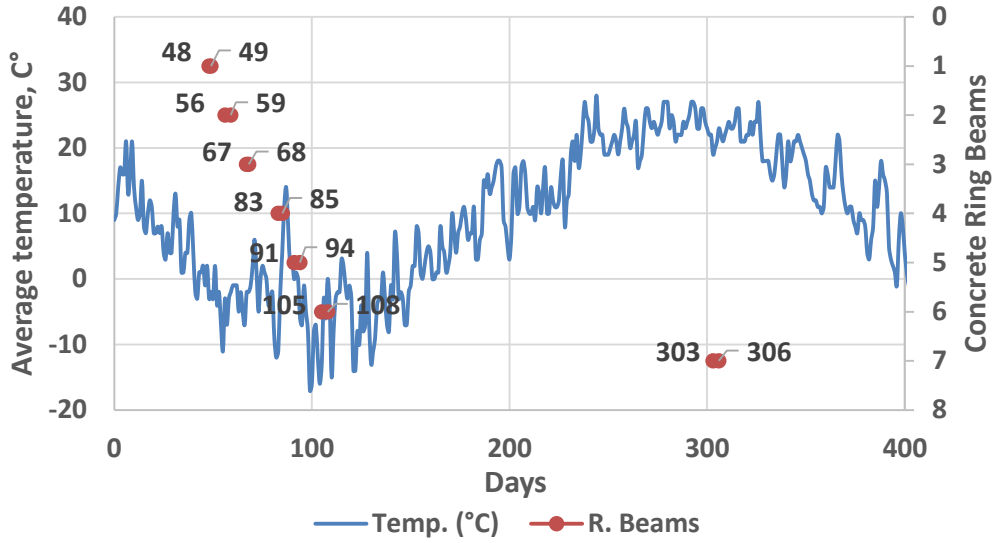

Figure 79. Chicago average temperature variation from 01/10/2007 to 04/11/2008 and the initial and final ring beams pouring dates (in construction days).

According to Eq. (83) and Figure 79, the time needed to reach maturity considering temperature changes was adjusted (see Figure 80). Note that the first six ring beams installed during winter did not reach maturity in 28 days and needed at least 80 days to achieve a working age. On the other hand, the last ring beam (ring 7), which was poured during summer under medium and high environmental temperatures, only needed 25 days to reach the maturity.

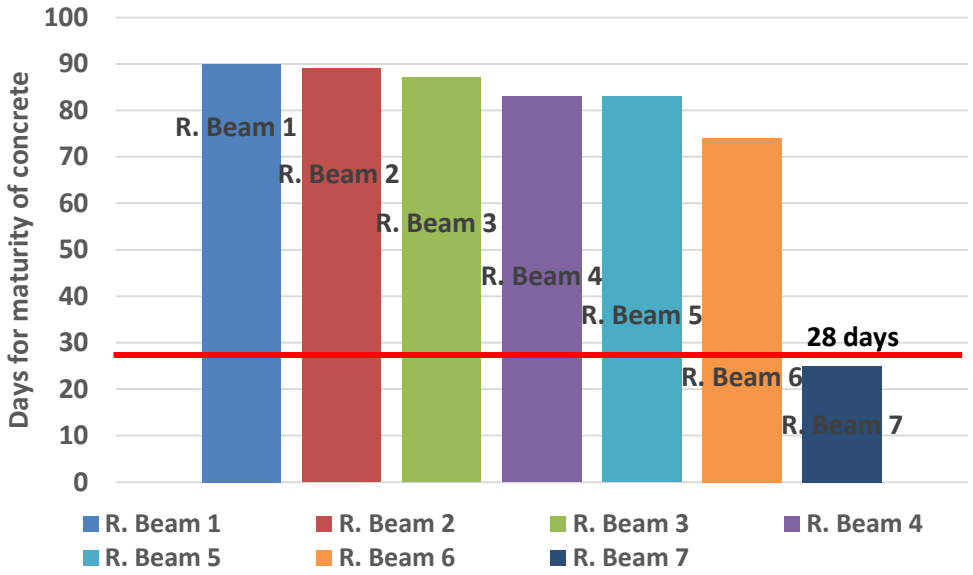

Figure 80. Time needed to reach the maturity according to the environmental temperature.

Figure 81 shows average temperature variation in Chicago, the dates when the concrete ring beams were cast and the adjusted time for temperature effects required to reach working conditions. This figure shows the importance of temperature for concrete maturity. For this particular case, the low Chicago temperatures did not allow a normal hydration process delaying the normal curing time from 28 days to 80 or 90 days. These estimates were made taking into account a constant relative humidity and a wet curing process.

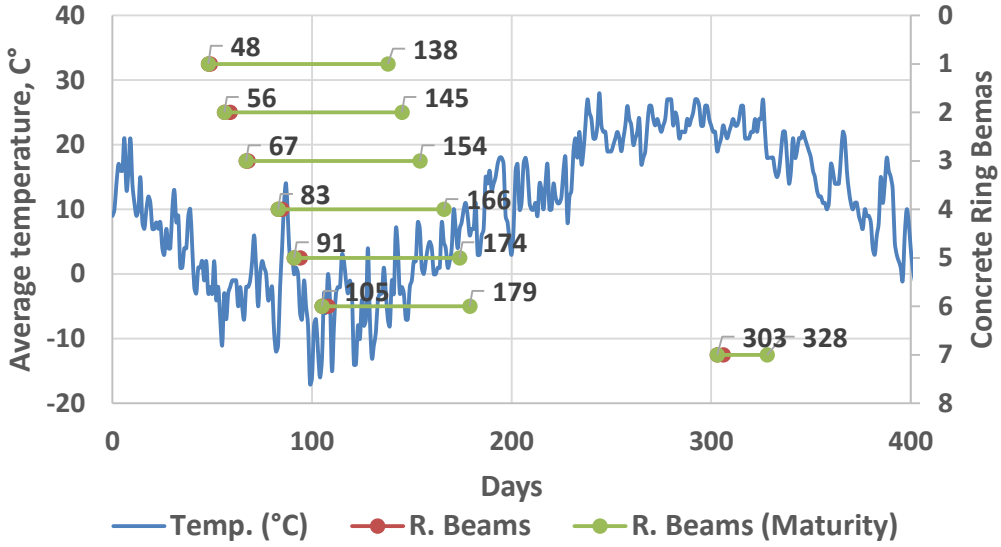

Figure 81. Average Chicago temperature from 01/10/2007 to 04/11/2008, and time in days needed for the concrete ring beams to reach maturity taking into account temperature effects.

4.3.2 Effects of Temperature on the development of concrete strength and stiffness

As discussed in Section 4.3.1, concrete maturity can be delayed by low temperatures. This effect is directly reflected on concrete compressive strength and stiffness as longer curing times are needed to reach design values.

Using the corrected times for temperature, the development in time of compressive strength and stiffness was estimated for each concrete ring beam as shown in Figure 82 and Figure 83. Note that temperature delays the development of both strength and stiffness, reaching the design values in a longer period of time, and resulting in larger discrepancies with laboratory tests results which are showed in the same figure (blue dots) under the design magnitude for a period of time under ten days.

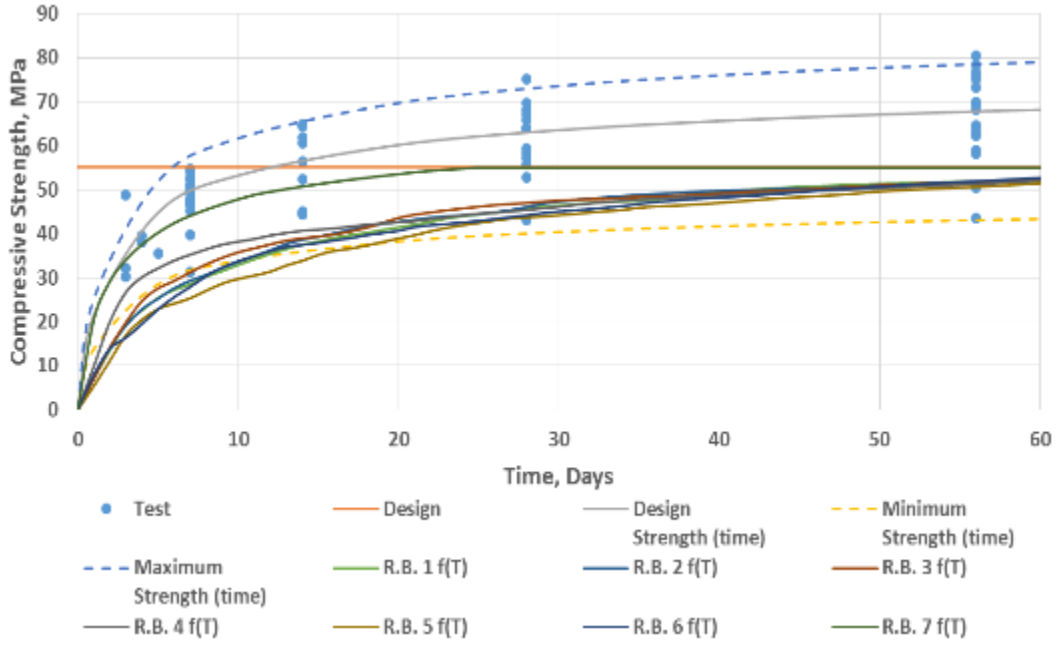

Figure 82. Compressive strength with time including temperature effects according to (CEB-FIP 1993).

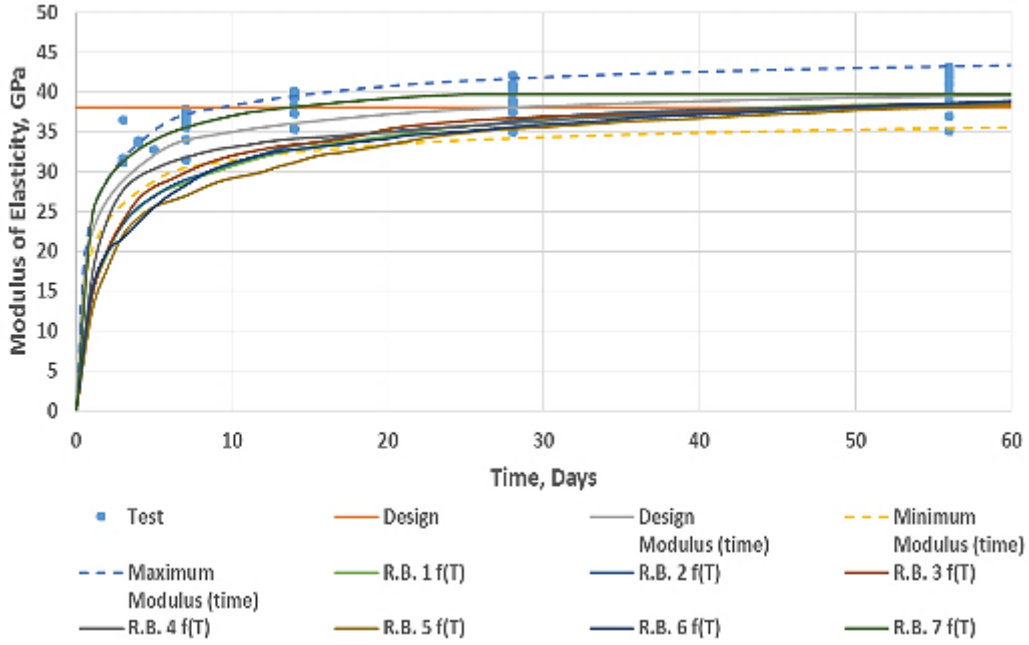

Figure 83. Modulus of elasticity with time including temperature effects according to (CEB-FIP 1993).

Alternatively, the concrete maturity corrected for temperature can be estimated according to Arrhenius maturity function defined by ASTM C 1074 as:

$$t_e = \sum_{0}^{t} e^{\frac{-E}{R_g}\left[\frac{1}{273+T_c}-\frac{1}{273+T_r}\right]} * \Delta t \tag{84}$$

where, t_e is the equivalent age at the reference curing temperature, T_c is the average concrete temperature in (°C) for a given time interval, T_r is reference temperature (usually 20 or 23°C), E is activation energy in *J/mol*, R_g is the universal gas constant, and Δt, is the time interval in hours.

Once the concrete maturity is corrected for temperature, a strength-maturity relationship can be used. (Carino and Lew 2001) recommends three relationships between concrete strength and maturity: the exponential function, the logarithmic function and the hyperbolic function. The last one, according to the author, describes better the concrete strength gain. This function, considering the maturity correction, is as follows:

$$S = S_u \frac{k_c(t - t_0)}{1 + k_c(t - t_0)} \tag{85}$$

where, S is the compressive strength at time, t, S_u is the limiting compressive strength, t is the time interval (in *hours*), t_0 is the time when strength development is assumed to begin (in *hours*), and k_c is the rate constant, initial slope of strength-age curve, (*1/hour*). (Carino and Lew 2001) and later (Wade et al. 2006) reported values of t_0 and k_c based on regressions taking into account the type of concrete and temperature.

The concrete modulus of elasticity was calculated based on the ACI code section 8.5.1.(ACI 1980), which relates the compressive strength of a normal weight concrete with the modulus of elasticity as:

$$E_c = 4700\sqrt{f'_c} \tag{86}$$

where, f'_c is the concrete compressive strength, in SI units [MPa] and the E_c is also in [MPa].

Figure 84 and Figure 85 show compressive strength and stiffness development with time corrected for the maturity of concrete according to Arrhenius maturity function and ACI (1980), respectively. As expected, the low temperatures during Chicago's winter season have a direct impact on concrete strength and stiffness as longer curing times are needed to reach design values. The blue dots in the figures show the laboratory tests results which

were under the design magnitude for a period time less than ten days as well as the estimated strength and stiffness for each concrete ring beam.

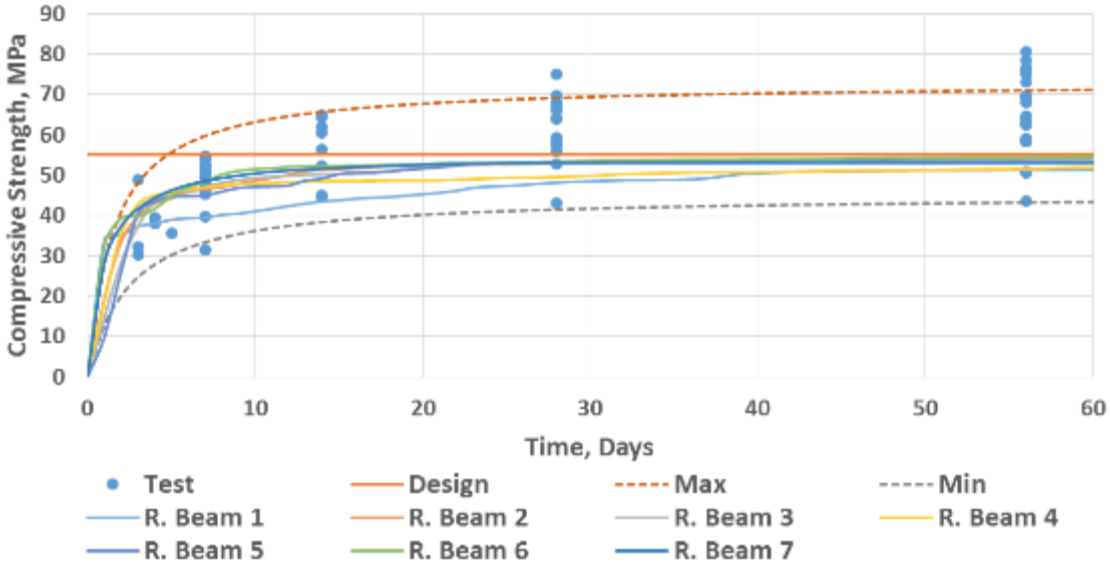

Figure 84. Compressive strength with time including temperature effects according to (ASTM C 1074).

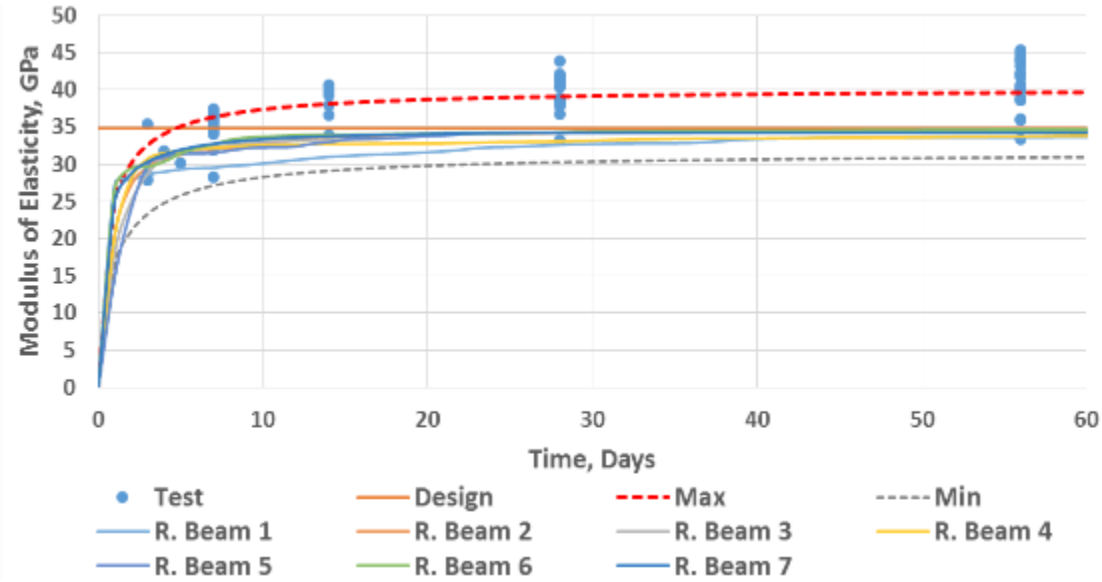

Figure 85. Modulus of elasticity with time including temperature effects according to (Carino and Lew 2001) and (ACI 1980).

The concrete elements were affected during curing by the low temperatures of the winter season, needing more time to reach the design magnitudes, and if at these effects

we add the short time between pouring and excavation cycles in the construction process, we might observe a unexpected performance influenced by concrete low strength and stiffness of the elements as show in chapter 3.

Both American and European methodologies, presented above show similar behavior between concrete compressive strength and stiffness when affected by aging under low temperatures. Always showing compressive strength and stiffness under the tested cylinders results for the first 5 days. That when comparing with Chicago Downtown Cofferdam construction process indicates that there were not enough strength and stiffness in the first service days of some of the concrete ring beams when they were stressed the most, right after the excavation below the ring beam was performed.

4.3.3 Effects of Temperature on the development of concrete creep and shrinkage

The (CEB-FIP 1993) specifies the following corrections to take into account the effect of variable temperature in the prediction of creep and shrinkage strains with time:

$$\beta_{H,T} = \beta_H \beta_T \tag{87}$$

$$\beta_T = exp[1500/(273 + T/T_0) - 5.12] \tag{88}$$

where $\beta_{H,T}$ is a temperature dependent coefficient that replace β_H in the equation (58), and $T_0 = 1°C$.

For the creep coefficient (CEB-FIP 1993), specifies:

$$\phi_{RH,T} = \phi_T + (\phi_{RH} - 1)\phi_T^{1,2} \tag{89}$$

$$\phi_T = exp[0.015(T/T_0 - 20)] \tag{90}$$

where, $\phi_{RH,T}$ is a temperature dependent coefficient that replace ϕ_{RH} in equation (54), and $T_0 = 1°C$.

Figure 86 shows significant differences for the fourth concrete ring beam when the creep coefficient is calculated for a constant temperature of 20°C and when it is computed taking into account a variable temperature.

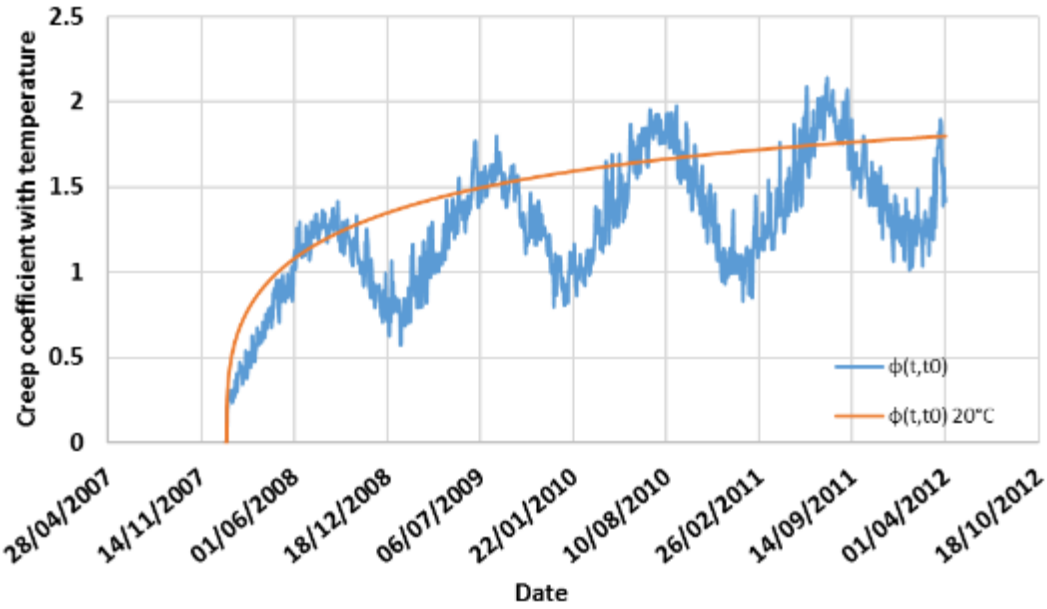

Figure 86. Fourth concrete ring beam creep coefficient vs. time. Orange line represents constant temperature; blue line takes into account temperature effects.

The temperature effects on shrinkage strains can be directly evaluated, according to (CEB-FIP 1993), by using the above coefficients in the following expression:

$$\alpha_{sT}(T) = 350\left(\frac{h}{h_0}\right)^2 exp[-0.06(T/T_0 - 20)] \tag{91}$$

where, $\alpha_{sT}(T)$ is a temperature dependent coefficient that replace the product of $350(h/h_0)^2$ in equation (73), $h_0 = 100\,mm$, and $T_0 = 1°C$.

(CEB-FIP 1993) also takes into account the temperature effect on the computation of the conceptual shrinkage coefficient via the following expressions:

$$\beta_{RH,T} = \beta_{RH}\beta_{sT} \tag{92}$$

$$\beta_{sT} = 1 + \left(\frac{8}{103 - 100\,RH/RH_0}\right)\left(\frac{T/T_0 - 20}{40}\right) \tag{93}$$

where, $\beta_{RH,T}$ is a temperature dependent coefficient that replaces β_{RH} in equation (68), $RH_0 = 100\,\%$, and $T_0 = 1°C$.

Figure 87 shows the variation in time of shrinkage strains for the fourth concrete ring beam of the downtown cofferdam. Similar to Figure 86, results under a constant temperature of 20°C are compared to those obtained under a variable temperature.

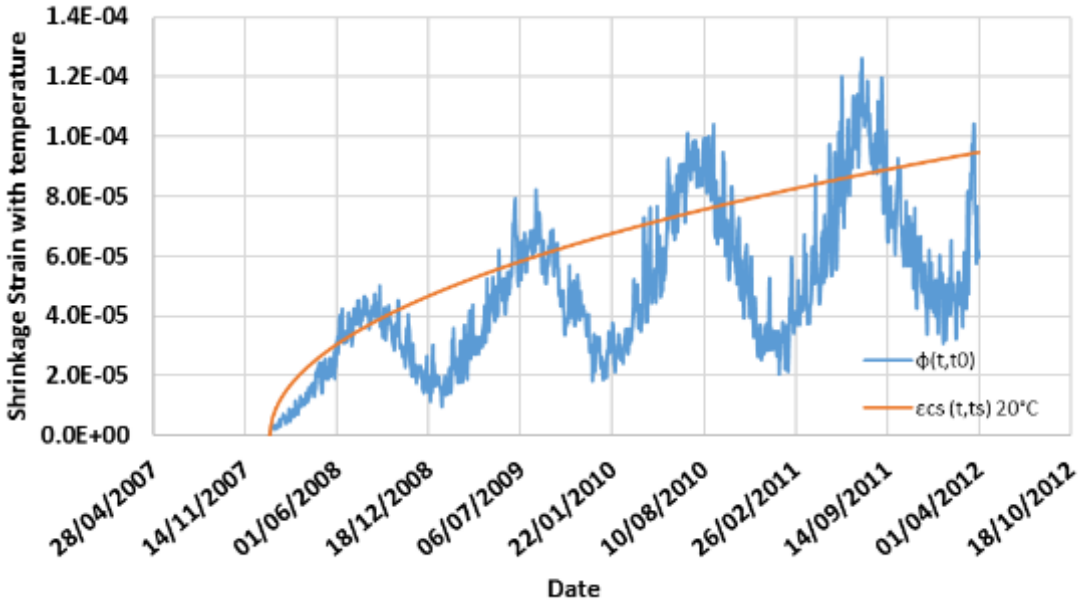

Figure 87. Fourth concrete ring beam shrinkage strains vs. time. Orange line represents constant temperature; blue line takes into account temperature effects.

The commonly used approach of assuming concrete as a linear elastic material without temperature effects can generate differences between what is computed and what is measured during construction. These differences can be larger if temperature fluctuations are neglected. As presented in Figure 86 and Figure 87 for creep and shrinkage effects, respectively, temperature variations can induce larger strains than those assumed at a constant temperature value. These differences are even larger when typical structural software are used and models always accumulate displacements.

Temperature variations must be considered in cases where concrete strains and excavations displacements are critical so a more reliable prediction can be achieved.

Chapter 5

5. Performance analysis

This chapter is divided in two sections. In the first part of the chapter a comparison of the field performance between the One Museum Park West (OMPW) and Chicago Downtown Cofferdams is presented. In the last section of the chapter, a back-analysis of the Chicago Downtown Cofferdam is presented. The proposed numerical model takes into account the non-linear behavior of concrete under variable physical and environmental conditions. By comparing both cofferdam performances, numerical results and field performance data, conclusions are drawn and recommendations given regarding field performance and construction procedures.

5.1 Differences between OMPW and Chicago Downtown cofferdams

The OMPW and Chicago Downtown Cofferdams are located about 2.5 km away from each other presenting similar subsoil conditions as illustrated in Figure 88. As described in chapter 3, both cofferdam construction were conceived for similar purposes: to support the building rigid concrete core in deep competent soil. In general, both projects followed a similar construction sequence, combining top-down construction with an initial “central” cofferdam constructed using a bottom-up sequence. It eliminated the excavation activities from the critical path for the project construction.

As shown in Figure 88, the cofferdams dimensions are significantly different. While the OMPW cofferdam had an internal diameter of 24.25 m and a 14.15 m excavation depth, the Chicago Downtown Cofferdam was larger and deeper, presenting an internal diameter of 33.2 m and a total excavation depth of 23.1 m. Note also that OMPW had a significantly larger embedment wall length compared to the Chicago Downtown Cofferdam which only reach 0.3 m. It means that OMPW cofferdam always presented a larger passive resistance during each excavation cycle. The short embedment length employed at the Chicago Downtown Cofferdam means that for the last excavation cycle, all the lateral stresses had to be taken by the seven concrete ring beams.

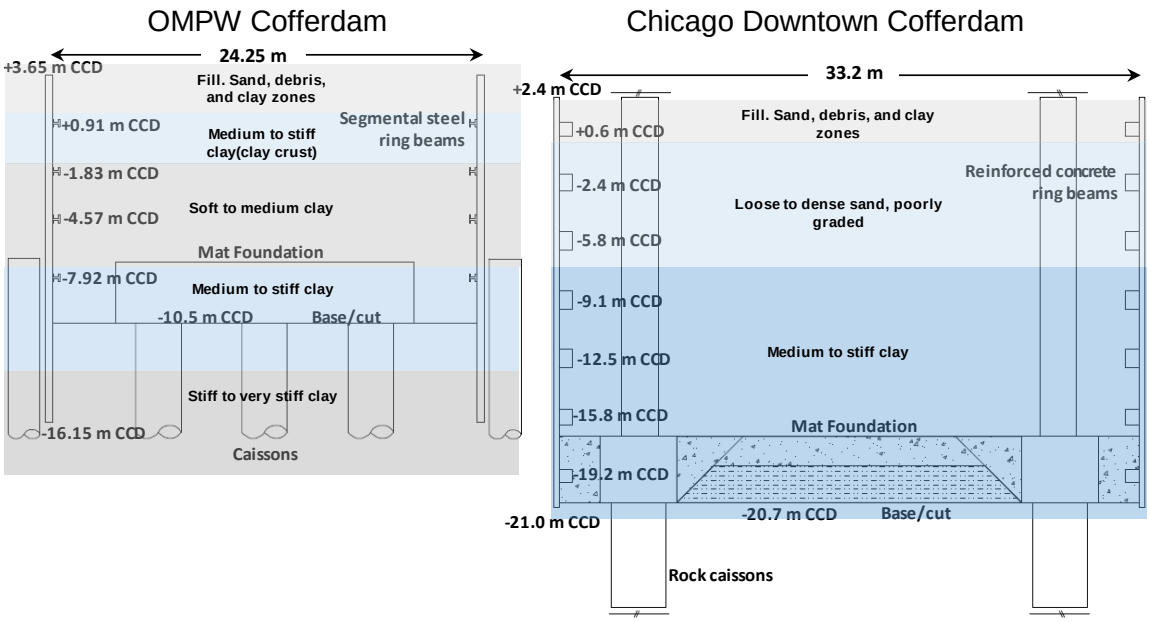

Figure 88. Scheme and subsoil strata OMPW and Chicago Downtown Cofferdam.

The principal difference between the two cofferdams is the employed lateral braced system. The OMPW cofferdam was constructed with segmental steel ring beams, while the Chicago downtown Cofferdam employed cast in place concrete ring beams (see Figure 89). As presented in Chapter 3, these lateral braced systems have a direct impact on the soil-structure interface response and consequently on the induced ground movements.

OMPW Cofferdam **Chicago Downtown Cofferdam**

Figure 89. OMPW cofferdam with segmental steel braces and Chicago Downtown Cofferdam with cast-in-place reinforced concrete ring beams.

5.1.1 Lateral deformation

As presented in Chapter 3, the Chicago cofferdam is much deeper and included 3 more lateral support levels, (7 in total), than the OMPW cofferdam. Then, to have a direct comparison on the performance of both lateral braced systems Figure 90 was prepared showing the measured lateral deformations of the OMPW cofferdam when it reached the design excavation level (i.e., 14.15 m) and those for the Chicago Downtown cofferdam when the excavation reached the elevation of the fifth concrete ring beam (i.e., 14.9 m) and only 4 lateral support levels were installed.

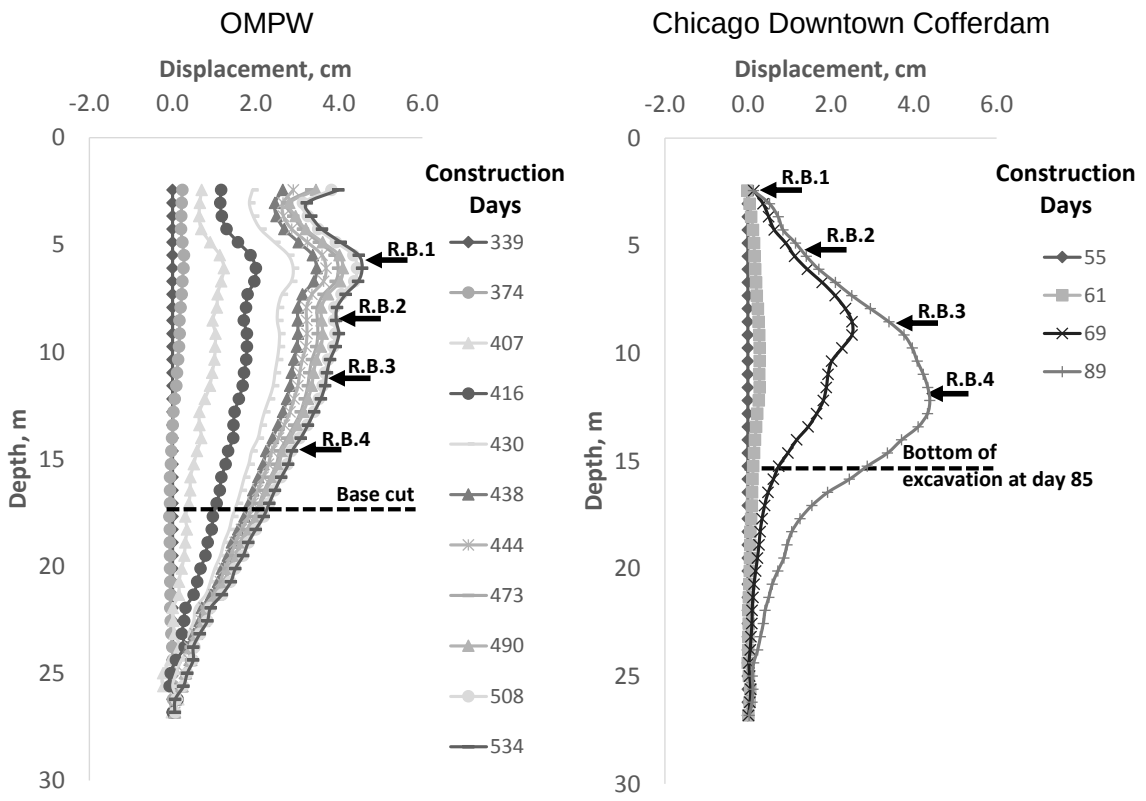

Figure 90. Lateral displacements: OMPW cofferdam at final excavation elevation and Chicago Downtown Cofferdam at an elevation of 14.9 m.

Note that for the conditions illustrated in Figure 90, both cofferdams developed a total lateral displacement of about 4.5 cm. However, the lateral deformation pattern is different. While the OMPW cofferdam presented displacements similar to a cantilever wall (including the perimeter secant pile wall between the cofferdam and the inclinometer), the Chicago Downtown cofferdam presented a deep inward deformation pattern, typical of low stiffness strutted walls. It must be mentioned that the lateral deformations recorded for the Chicago Downtown cofferdam do not account for the excavation and installation of concrete ring beam 1 as because the inclinometer was not in service, resulting in an apparent stiffer response.

The cantilever wall movement registered at the OMPW cofferdam is mainly due to the gap between the segmental steel ring beams and the sheet piles, which are considered a flexible wall because of the interlock gap at the connections. On the other hand, the Chicago Downtown cofferdam lateral deformation pattern was controlled by the stiffness of the concrete ring beams, which were directly poured against the sheet piles eliminating the gap

between the lateral bracing and the retaining wall and presumably reducing the interlock gap between sheet pile sections. However, as presented in Chapter 4, the accelerated construction times for the Chicago Downtown cofferdam, added to the low temperatures during concrete pouring, compromised concrete maturity and lead to an initial low strength and stiffness gain that induced larger lateral deformations during the cofferdam construction. Long-term or post construction ground movements around the cofferdam were also induced by concrete and soil time-dependent effects: concrete creep and shrinkage, and soil consolidation and creep. Figure 91 shows the measured lateral deformations at key construction times for the downtown cofferdam. Note that during two relatively long periods of time, between construction days 112 to 307 and 307 to 1617, no removal of soil took place, but ground movements were still induced. These continue lateral deformations are attributed to concrete and soil time-dependent effects. However, it is important to mention that these deformations could have also being associated to alternative construction works such as caissons excavation and mat foundation construction.

The advantage of using concrete ring beams over segmental steel ring beams was blighted by the construction process, because even though the strains at the beginning were restricted by a well installed concrete ring beam the following activities were performed very fast and under low temperatures causing an initial low strength and stiffness response and deformations 4 times larger than the maximum values estimated at the end of 4.4 years of service due to time-dependent effects, such us creep and shrinkage. Figure 92 shows details about the concrete ring beam construction that support the hypothesis about the detrimental effect of low temperatures on the cofferdam performance. In the pictures, exposed steel rebar and accumulation of snow directly over the recently cast concrete can be observed. As explained in Chapters 2 and 4, it compromised the maturity process leading to slower hydration of the cementitious paste and causing premature shrinkage and a slow strength and stiffness gain, which resulted in unforeseen immediate deformations, and in long-term conditions additional shrinkage strains.

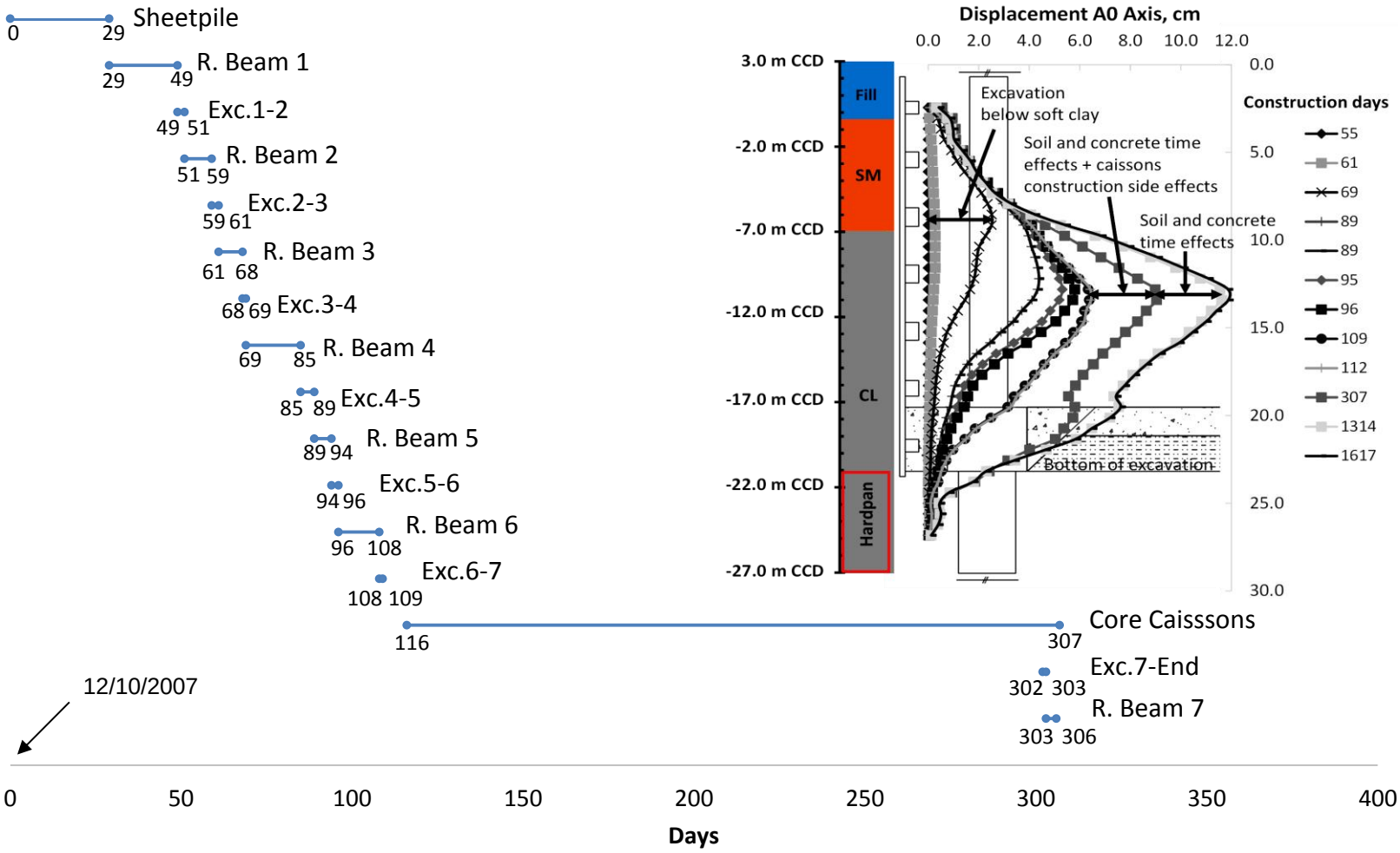

Figure 91. Chicago Downtown Cofferdam lateral displacements (inclinometer 07) associated with some construction activities and materials time-dependent effects.

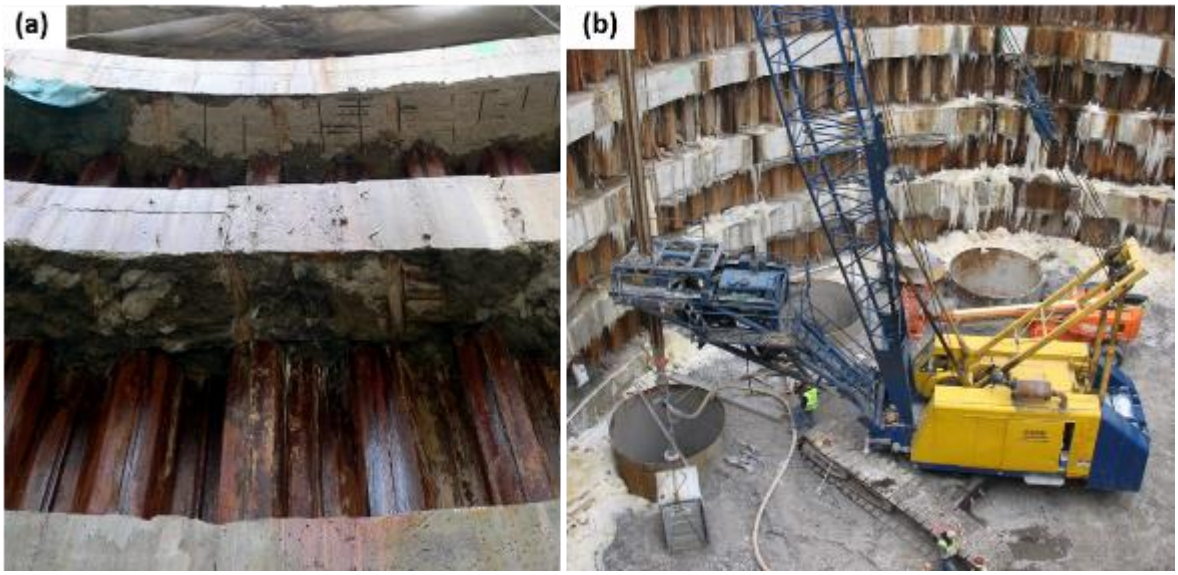

Figure 92. Pictures showing concrete ring beam conditions during construction: (a) exposed rebar, (b) concrete ring beams cover with snow.

It is well known that time-dependent movements are not only function of the retaining elements and materials. They are always present in soil-structure interaction problems. Time-dependent movements in cohesive soils are typically related to consolidation and creep when a sustained load is applied. These creep effects may be larger in soft soil excavations as discussed by (Martin and Clough 1990). Additionally, ancillary activities, such as perimeter wall installation, construction of soil and rock caissons, removing of casings and even removing of existing foundations and structures around or within the excavation, can affect ground movements and increase the estimated values (Finno et al. 2014).

A comparison of cofferdam performance, in terms of the maximum lateral deformation versus excavation depth, with available empirical correlations was conducted. Figure 93 shows an approximate linear relation between maximum lateral deformation, δ_{hm}, and excavation depth, H, where δ_{hm}/H= 0.25% to 0.28% was obtained for OMPW cofferdam and Chicago Downtown Cofferdam respectively. The last two excavation stages (days 307 and 1617) of the Chicago Downtown Cofferdam were not taken into account as no soil removal was performed and most likely were highly affected by concrete time-dependent effects. As expected, the maximum lateral deformation directly increase with excavation depth (Clough and O'Rourke 1990), (Moormann 2004), (Wang et al. 2009), (Finno 2010) and (Tan and Li 2011) The obtained relationship ($\delta_{hm}/H = 0.25\ to\ 0.28\%$) is similar to the

upper range proposed by (Clough and O'Rourke 1990) for typical excavations in medium to stiff soils, δ_{hm}/H= (0.05 to 0.25)%, which for soft clays can reach values up to δ_{hm}/H= 3.2%. (Moormann 2004) found from its worldwide database that the relation between δ_{hm} and H in soft clays presents a large dispersion. However, for stiff clays an average relation of δ_{hm}/H= 0.25%, similar to the value presented here for both cofferdam excavations, was reported. Deep excavations in Shanghai (Tan and Li 2011) presented δ_{hm}/H between 0.1 and 0.5%, which is also similar to the ratio found for OMPW and Chicago Downtown cofferdams.

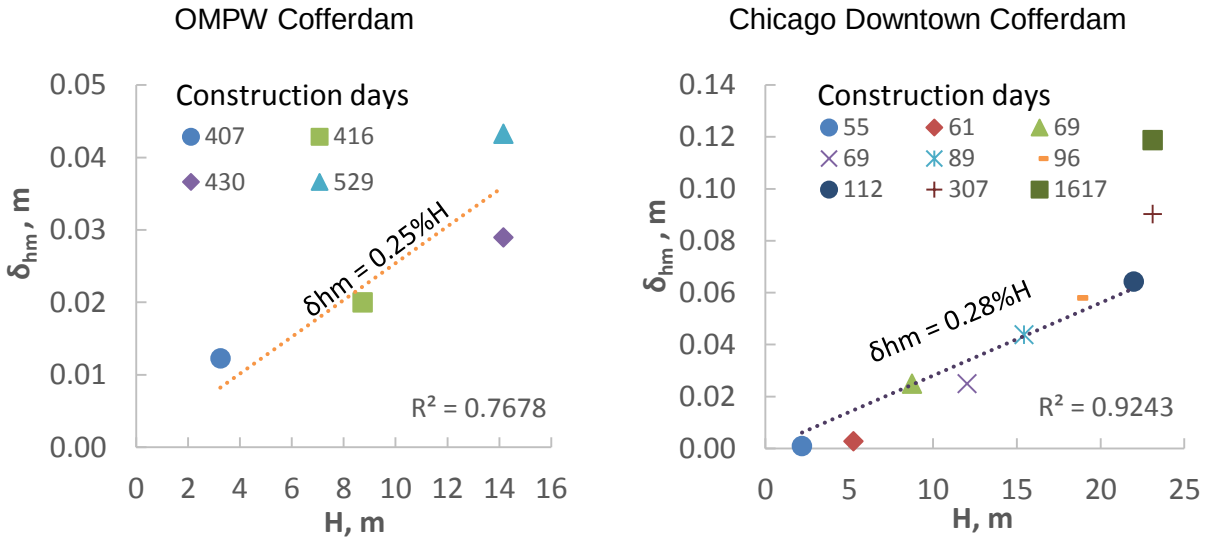

Figure 93. Maximum lateral deformation vs. excavation depth.

It must be mentioned that these available empirical relations are based on diverse geotechnical conditions, types of retaining structures and constructions methodologies. For example, when the top-down construction method is employed with an uppermost slab placed close to the original ground surface, the normalized horizontal movement (δ_{hm}/H) is approximately (0.14 to 0.2)% (Finno et al. 2013). Filtrating the Shanghai case history database by excavation procedure, the bottom-up method showed an average value of 0.41%, as reported by (Wang et al. 2009). Additionally, cofferdam excavations differ from typical rectangular excavations subjected to 3d conditions in that earth and water pressures are resisted by the structure retaining bracers as hoop compressive stresses, obeying to axial symmetric conditions, these compressive stresses are easy provided by rigid concrete or steel sections and consequently differences in performance are expected.

By using (Bryson and Zapata-Medina 2012) methodology the lateral deflections of Chicago Downtown cofferdam were estimated with a relative stiffness ratio, by assuming a relative inertia of the structure estimated as an equivalent section of the sheet piles and the stiffness modulus only in function of the concrete ring beams quality. The maximum horizontal displacement expected for the entire excavation (23.1 m depth) will be around 9.4 cm. By the other hand, if the method is used with an affected stiffness due to not enough maturity and concrete exposed to low temperature, with modulus magnitudes such as the ones exposed in chapter 4, the maximum lateral deformation will be 11.2 cm. These results show a great correlation with the field performance (inclinometer 07) presented in Figure 68 and again in Figure 91.

Chicago Downtown cofferdam achieved larger lateral deformations than the ones estimated Figure 91**¡Error! No se encuentra el origen de la referencia.**, which were computed with a maximum lateral displacement of 3 cm for the total excavation depth, and less than 2 cm for a partial depth of 14.9 m. The exceeded values obtained during the construction process can be attributed in great proportion to accelerated construction process and time and temperature effects of concrete ring beams, which started their useful life with low strength and stiffness due to an incomplete maturity, and finally worked for a long time, which allowed the development of creep and shrinkage strains. Otherwise, soil time-dependent effects must also contribute in the final cumulative displacement achieved by Chicago Downtown Cofferdam.

5.1.2 Settlements

Figure 94 presents the correlation between the maximum lateral deformation and maximum vertical settlement based on performance data recorded at different stages of the OMPW cofferdam construction. The obtained relation, $\delta_{vm} = 1.04\delta_{hm}$, is similar to the one proposed by (Moormann 2004) that varies between (0.5 to 1.0)δ_{hm} for most of the soil conditions, with some rare cases reaching values of $2\delta_{hm}$.

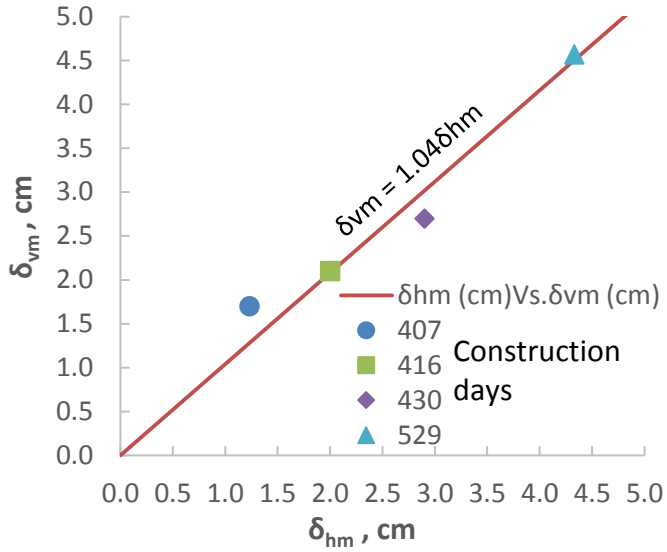

Figure 94. Maximum lateral deformation vs. maximum vertical settlement during the OMPW cofferdam excavation process.

Also by comparing the vertical ground deformations registered in the central zone of the west side of the excavation, which were the larger deformations during the excavation process as presented in Figure 55. These vertical deformations were found within the Peck's (1969) and (Clough and O'Rourke 1990) settlement envelopes and influence distance. Based on the measured lateral deformation profile, in the settlement behavior in time and the recommendations given by Hsieh and Ou (1998), the OMPW presented a concave type pattern for the western side as presented in Figure 95.

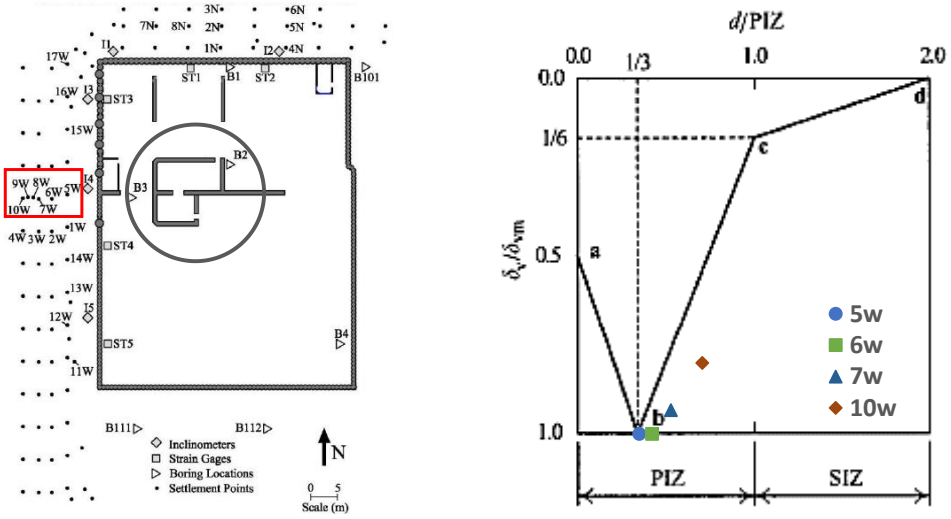

Figure 95. a) OMPW settlement point plan; b) west central settlement with Hsieh and Ou (1998) proposed settlement profile.

The Chicago Downtown cofferdam presumably presented a concave settlement distribution estimated by Hsieh and Ou (1998) methodology with a concave settlement, which for an excavation depth of 14.9 m was estimated of 2.7 cm and is presented in Figure 96.

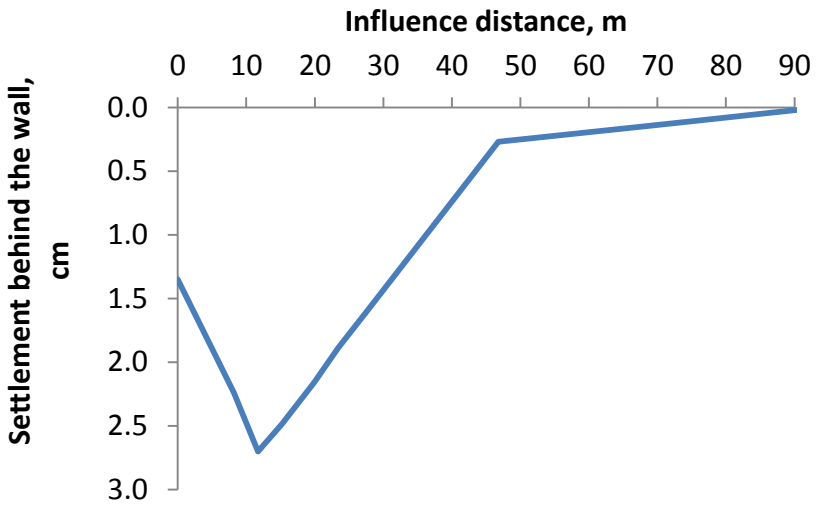

Figure 96. Settlement distribution behind the retaining wall, using (Ou 2006).

The minimum and maximum settlement registered in OMPW were 1.5 and 4.5 cm respectively, while for Chicago Downtown Cofferdam the maximum settlement estimated assuming an excavation depth of 14.9 m was 2.7 cm (Figure 96). The Chicago downtown cofferdam estimated settlement is within the minimum and maximum vertical deformation measured at OMPW cofferdam, presenting similar vertical to lateral deformation ratio.

In both cases, the cofferdam installation was just a preliminary step of the principal top-down excavation of the building project. However, this previous activity already generated deformations near the limit established by the city of Chicago, leaving no “room” for additional ground deformations. These situations evidence the necessity of detailed specifications for construction during the design process to account or eliminate time effects.

5.2 Chicago Downtown cofferdam back-analysis

In this section, a back-analysis for the Chicago Downtown Cofferdam was performed to evaluate temperature and concrete time effects. Lateral deformations, measured via inclinometer 07, are used as the comparison criteria. The numerical calculations were conducted using the Finite Element Method (FEM) in the commercial software SAP2000 V.18, whose focus is structural analysis and design, and consequently presents significant limitations for soil behavior modeling. However, it allows for staged construction and the modeling of concrete time and temperature effects, which most FEM geotechnical software failed to capture. The main objective of the proposed back analysis is to separate and quantify the effects of: i) stress relief due to soil excavation, ii) temperature and maturity, iii) concrete strength and stiffness gain with aging, and iv) concrete creep and shrinkage.

5.2.1 Earth pressures and soil representation

As presented in chapter 3, the local subsoil conditions basically consist in sedimentary soils covered by a superficial fill. A summarized geotechnical characterization and homogenized stratigraphy are presented in Table 16. In the table, “Nspt”, is the corrected standard penetration test blows, “w”, is the natural water content, “γ”, is the material specific unit weight, “S_u”, is the undrained shear strength, “ϕ’”, is the internal friction angle, “c’”, is the drained cohesion intercept, and “k” is the soil modulus employed with the p-y curve method.

Table 16. Chicago Downtown Cofferdam basic geotechnical characterization and stratigraphy.

N.F. elevation 1 m CCD

Material	USCS	Initial elevation (CCD)	Final elevation (CCD)	Nspt	w (%)	γ (kN/m³)	Su (kPa)	φ' (°)	c' (kPa)	k (MN/m³)
Fill 1	SG	2.4	1.0	22	12	19.0	-	29	-	32.6
Fill 2	SG	1.0	-0.6	27	16	20.0	-	32	-	23.5
Loose to dense sand	SM	-0.6	-7.4	34	25	20.8	-	35	-	34
Soft clay	CL	-7.4	-11.0	-	23	19.9	50	26	25	66.5
Soft to medium Clay	CL	-11.0	-13.8	-	20	20.5	80	28	35	130.2
Stiff clay	CL	-11.0	-18.0	-	16	21.2	190	33	40	399

Stiffer clay	CL	-18.5	-21.0	-	11	21.8	250	36	60	552

The geotechnical parameters listed in Table 16 were used to estimate the lateral earth pressures acting against the cofferdam structure. Initially, K_0-conditions, which were compared with typical values and pressuremeter tests results. Active earth pressure conditions, estimated using the Rankine (1857) theory were also used to establish pressure limit conditions. The K_0-condition was used as the initial soil pressure acting against the cofferdam before the excavation activities began and represents to upper pressure limit, while the active state was considered as the minimum earth pressure under a full mobilized condition.

The established earth pressure conditions are associated to the sheet piles flexible behavior, which initially generates a mobilize soil shear resistance and wall deflections (Clough and Kuppusamy 1985). Sheet piles are flexible system that allows the soil to change its confining stress relation while it deforms and mobilize soils shear resistance. The earth pressure behind the wall changes from the at-rest earth pressure state to an active pressure while the soil pressure below the bottom cut reaches a higher state near the passive pressure as presented in Figure 97. This cycle initially repeats until a full interlock between the sheet pile sections is achieved. After that, the retaining system behavior is mainly controlled by construction procedures and excavation sequence.

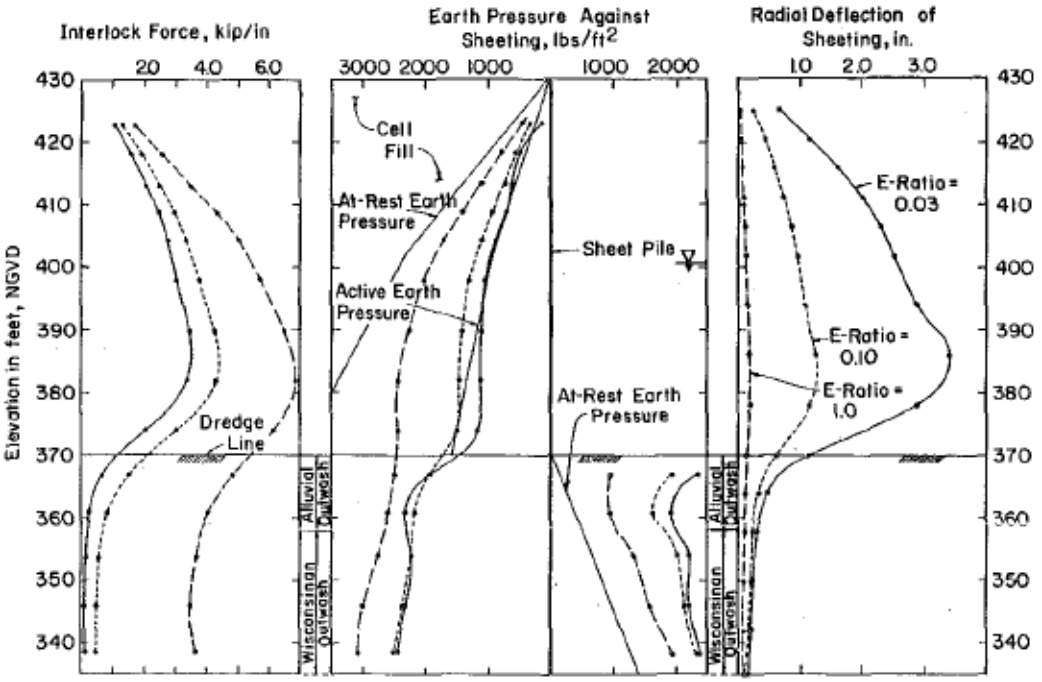

Figure 97. Interlock force, earth pressure against sheeting and radial sheet pile deflection (Clough and Kuppusamy 1985).

These earth pressure boundaries along with the considered water pressure distribution acting over the structure are illustrated in Figure 98. The water pressure distribution was estimated based on the water table location and the piezometers information presented in Section 3.2.2 and Figure 67 and again in Figure 98 (b). These conditions were used to estimate the total pressure acting against the cofferdam structure during the stage construction sequence followed in the numerical model.

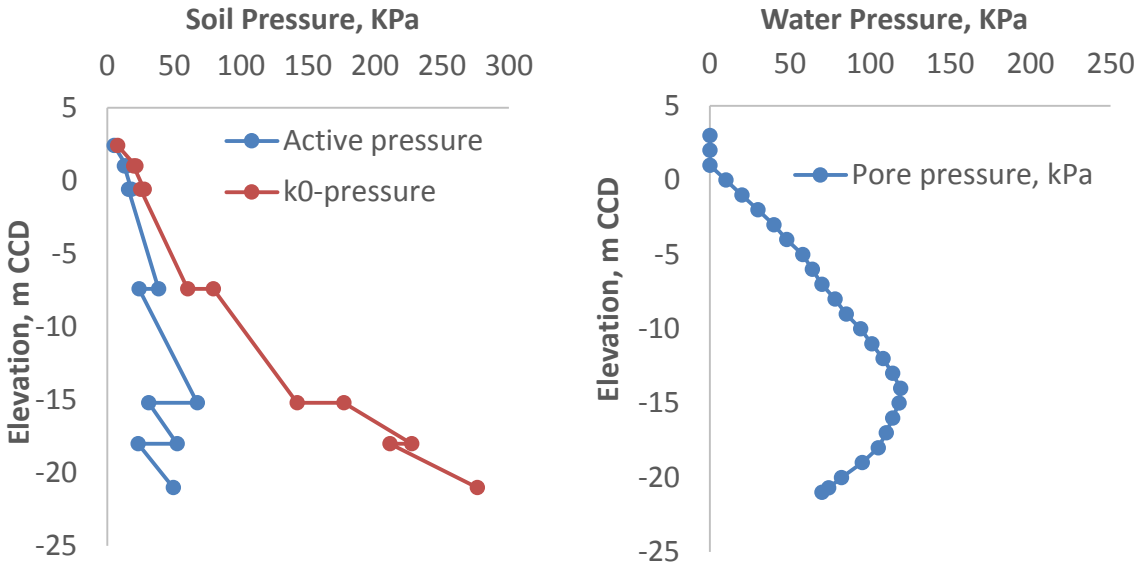

Figure 98. Pressures acting over the cofferdam: (a) earth pressure; and (b) water pressure.

The soil behavior and stiffness inside the cofferdam (i.e. passive side) is numerically represented by a series of nonlinear springs, which were calibrated based on the parameters presented in Table 16 and the methodology proposed by Matlock and Reese (1960). The “soil spring” response in terms of force versus displacement is presented in Figure 99, Figure 100, Figure 101 and Figure 102 for each of the soil layers considered. The spring’s constants were degraded during the stage construction simulation to take into account the characteristic soil softening due to stress relief. At each construction stage, a new set spring constants was input in the model replacing the ones still in the inner bottom of the cofferdam as proposed by (Uribe-Henao and Arboleda-Monsalve 2016). This discrete nonlinear “soil spring” model is a practical way to model, in a structural FEM software package, the characteristic change in soil stiffness that takes place during an excavation process.

Fill 1 **Fill 2**

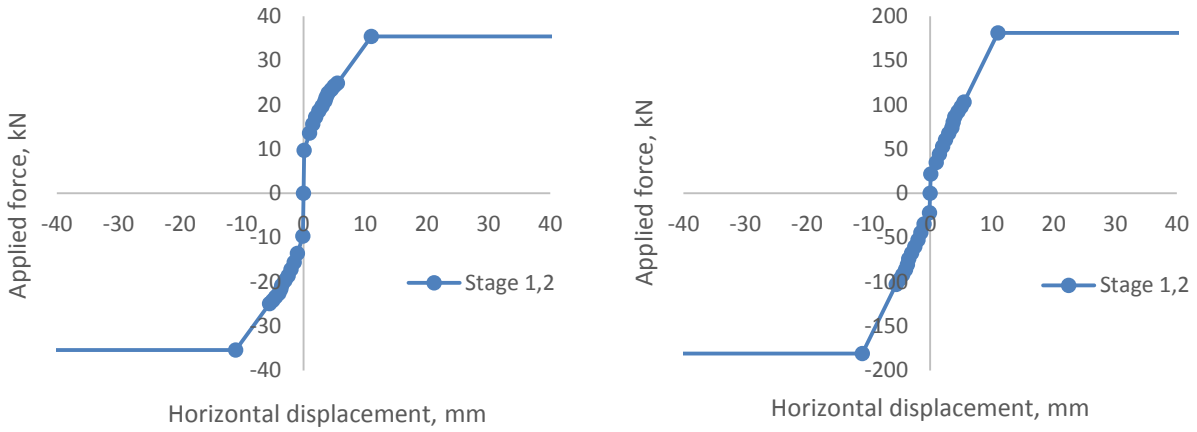

Figure 99. Fill 1 and Fill 2 springs used to during the simulation process, including a degradation in stiffness used to simulate softening due to vertical stress relief.

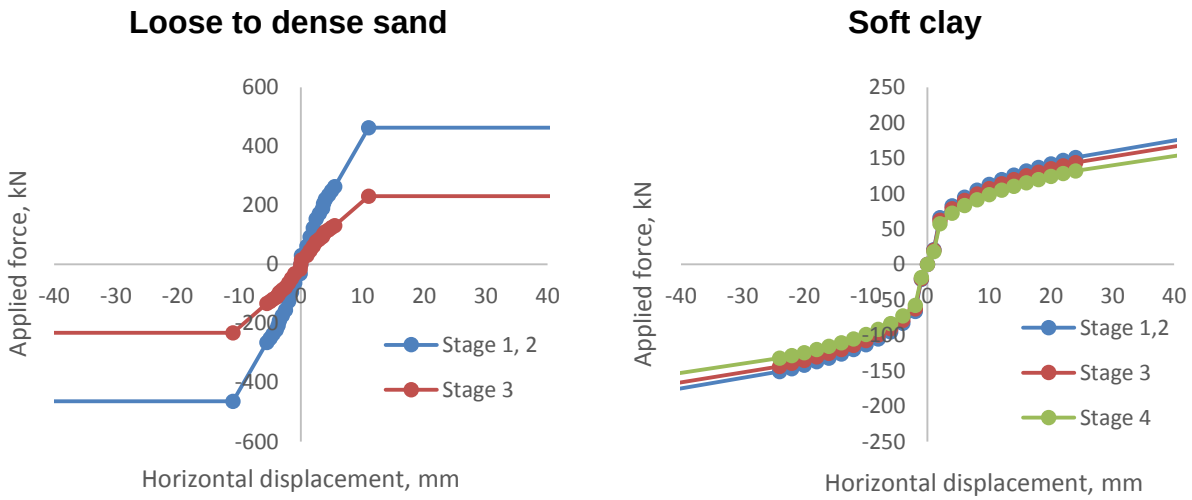

Figure 100. Loose to dense sand and soft clay springs used to during the simulation process, including a degradation in stiffness used to simulate softening due to vertical stress relief.

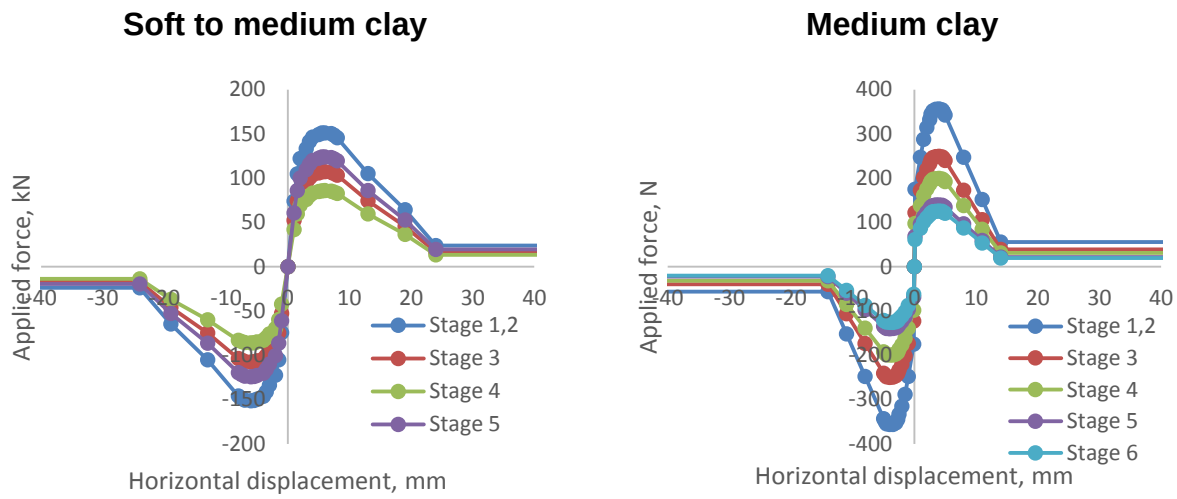

Figure 101. Soft to medium clay and medium clay springs used to during the simulation process, including a degradation in stiffness used to simulate softening due to vertical stress relief.

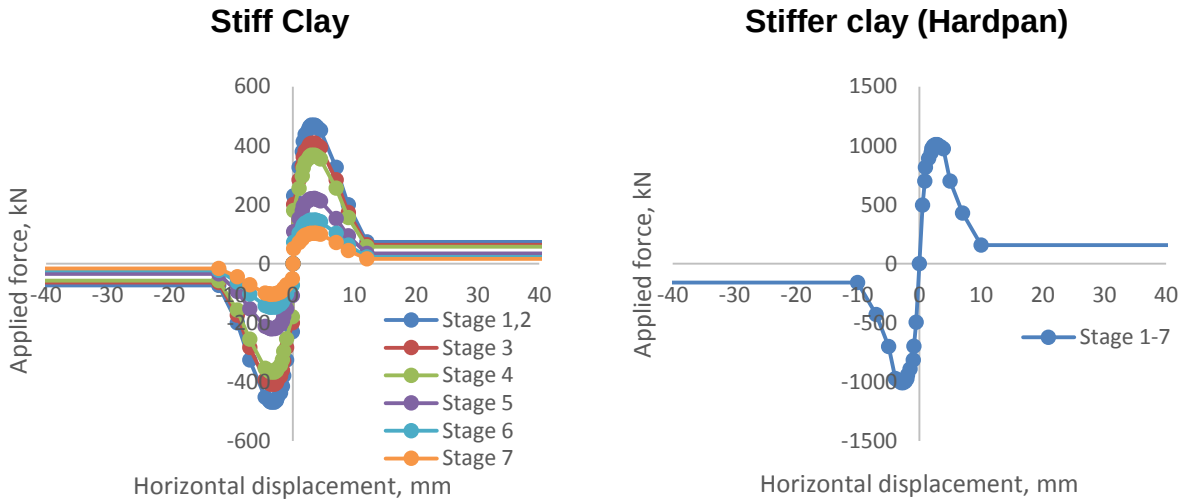

Figure 102. Stiff clay and Hardpan springs used to during the simulation process, including a degradation in stiffness used to simulate softening due to vertical stress relief.

5.2.2 Structural elements

Two issues were specially treated during the modeling process: the interlock gap between the sheet pile sections and the time and temperature dependent effects of the concrete ring beams.

- **5.2.2.1 Sheet pile wall**

Sheet pile walls were modeled as shell-thin elements with multi-linear elastic links at the interlock space. The shells are composed by 34040 points and 24840 areas, following the exact geometry of a sheet pile PZ-27. The base of the cofferdam model was only restricted in the vertical direction. Additionally, the concrete ring beams were fixed to the sheet piles simulating the welded constructed condition presented in Figure 63.

The interlock gap between sheet pile sections has been classically addressed by two limit conditions: fully fixed with full transfer of shear stress between sheet pile sections, and fully-free where each sheet pile sections acts as an individual structural member without shear stress transfer between them (Williams, S.G.O.; Little 1992). The operating moment of inertia of a sheet pile group can varied between 0.28 and 0.43 of the usually combined value used during the design process. Additionally, the deflection of a sheet pile retaining wall is associated with the shear force transmission between them. Shear force not only depends on the relative displacement between sheet piles interlock, but also on "*(i) load history of the penetration forces (driving), (ii) load history from penetrating neighboring piles, (iii) the bending history of the wall, (iv) changes of the soil properties in the clogged voids, and (v) the behavior of the wall over time*" (Schmieg and Vielsack 2002). Because of the above factors, sheet pile wall interlocks are uncertain, and therefore a conservative recommendation for their modeling is to consider sheet piles walls as individual members without a complete coupling between them.

The existing design methods for sheet pile walls are composed by free body diagrams that implicitly assume the structure reaches maximum tension during the construction between elements. FEM back-analyses of different case histories have shown good correlation with field performance data and laboratory tests. However, a large limitation of the design methods is that the elastic modulus of the structure is far from being the manufacturer recommended value where a constant maximum tension between sheet piles is assumed (Wissmann et al. 2003). Recently, (Uribe-Henao and Arboleda-Monsalve 2016) model a sheet pile interlock subjected to compressive stresses under K_0 conditions. Stress increments were applied to close the gap at the interlock, which is assumed to be filled with soil, and fully engage the sheet pile sections. An interlock stiffness modulus was proposed to represent the deformation response of typical Chicago soils under in-situ confining

pressures for the interlock behavior until it reaches a total closure. This relation is presented in Figure 103 and was used to model the sheet pile interlock in the back-analysis model.

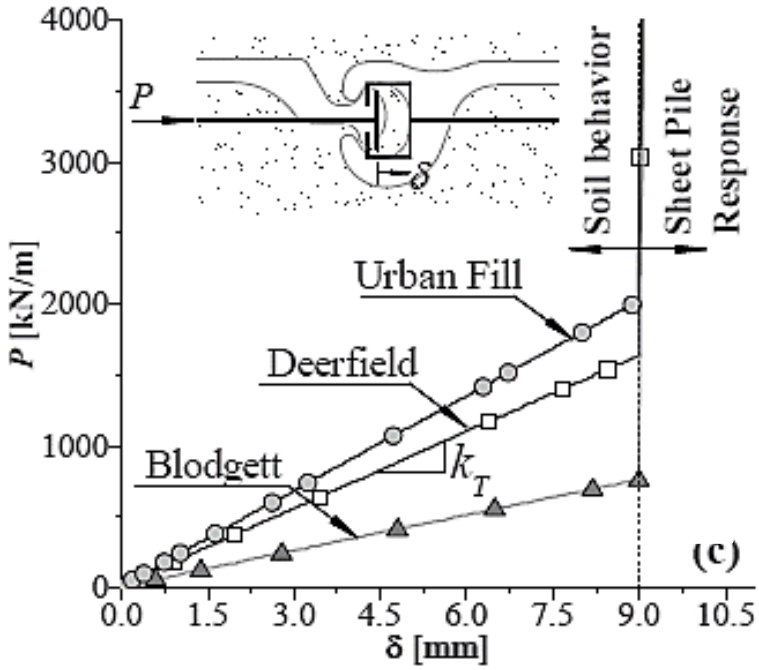

Figure 103. Force-deformation curves for sheet piles interlock response computed for different soil layers. Taken from (Uribe-Henao and Arboleda-Monsalve 2016).

- **5.2.2.2 Concrete ring beams**

The concrete ring beams were modeled as frame sections with 1610 points and frames, without any restriction and fixed to the sheet piles as they were welded during the construction (Figure 63).

The material concrete of the ring beams was modeled according to the time and temperature dependence effects presented in chapter 4 taking into account the construction sequence of the project. For the back-analysis the concrete ring beams properties were divided into four categories according to the (CEB-FIP 1993) models, the ring beams section, and temperature conditions. The first group is presented in Figure 104 and was used for concrete ring beam 1; the second is illustrated in Figure 105 and was employed for concrete ring beams 2 and 6; the third group presented in Figure 106 and was used for concrete ring beams 3, 4 and 5; and the last set presented in Figure 107 was

used for concrete ring beam 7. All figures present concrete compressive strength, modulus of elasticity, creep coefficient and shrinkage strain versus time. These properties were calculated according to each ring beam effective cross section and standardized by a cement type coefficient of 0.25 that stands for normal concrete, a constant relative humidity of 75%, a shrinkage coefficient of 5, and shrinkage start age of 3 days. An average loading age of 7 days was assumed based on the available construction records where after 7 days from the initial pouring the next excavation level was completed and the recently installed concrete ring beam was loaded. This last aspect does not fully represent reality but the available information about this topic was not detailed enough.

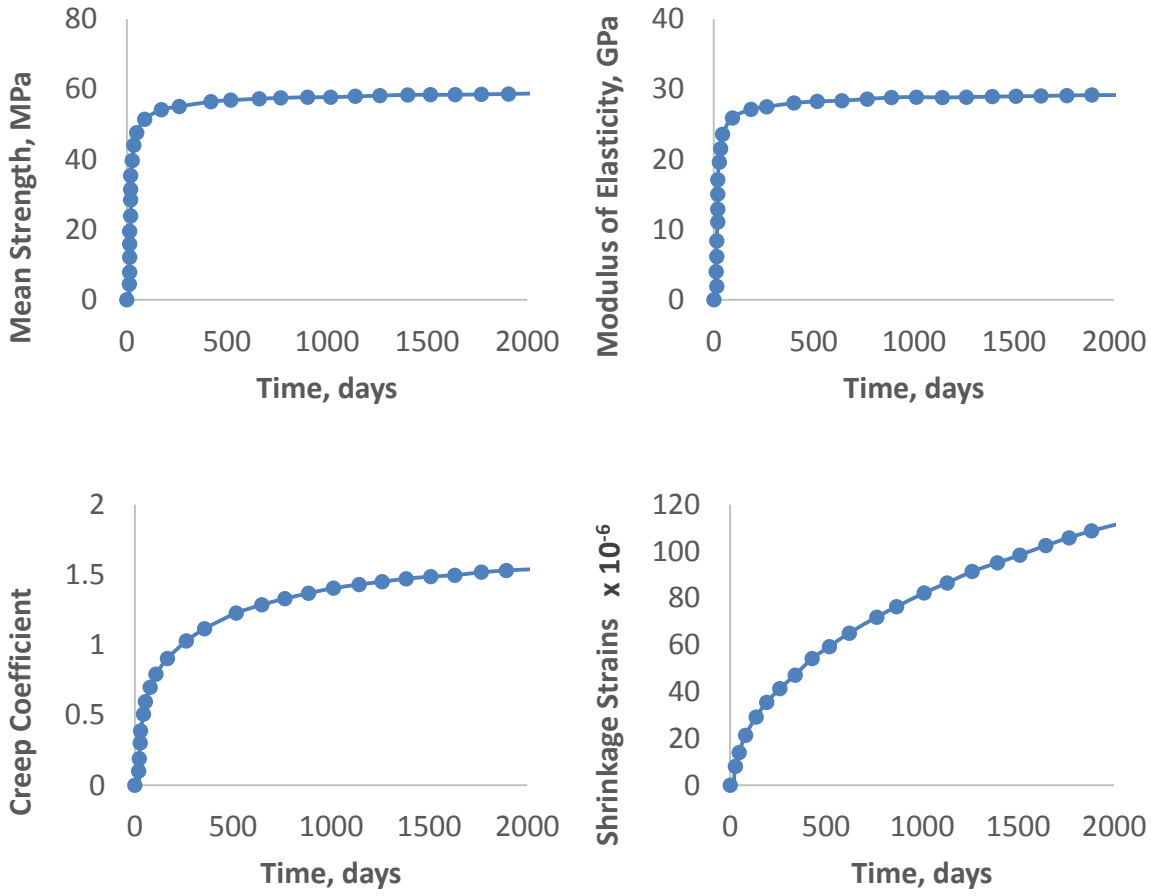

Figure 104. Concrete time dependent effects according to (CEB-FIP 1993) and affected by concrete maturity (temperature), used for ring beam 1.

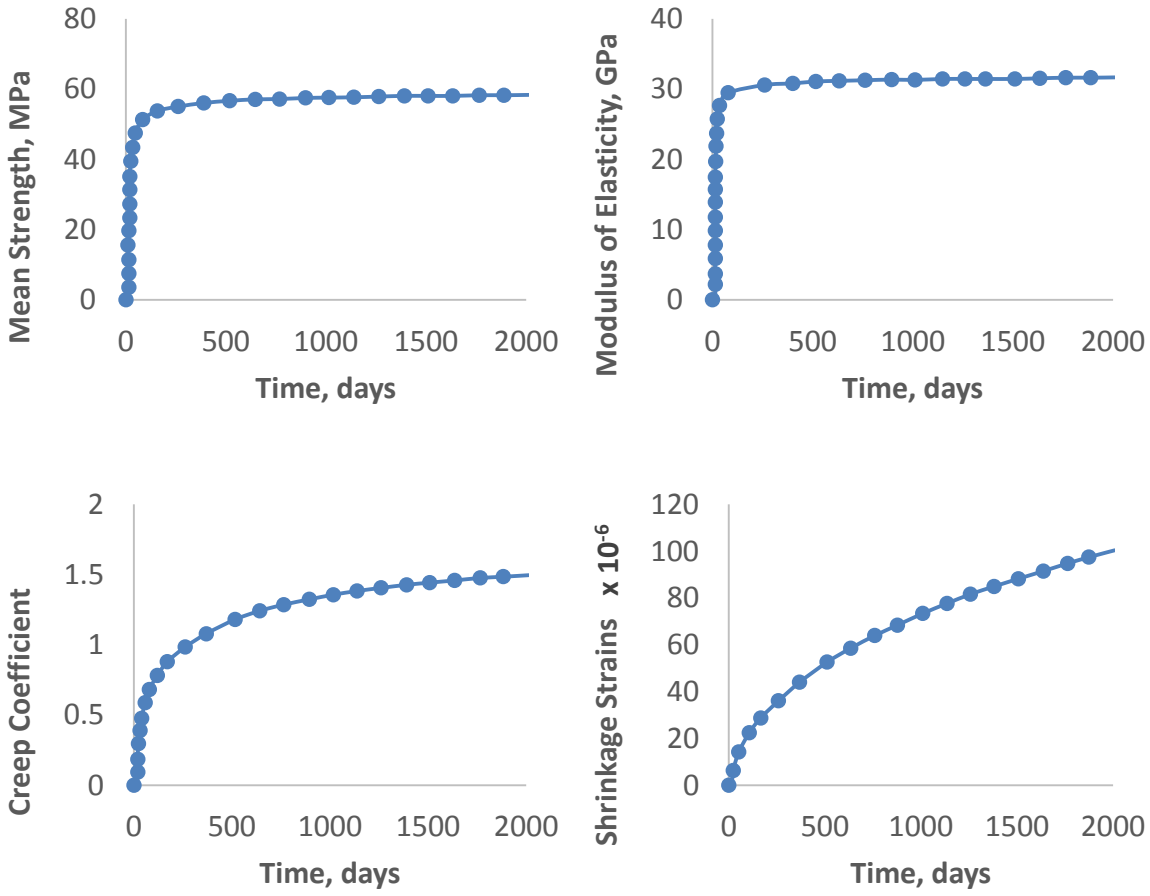

Figure 105. Concrete time dependent effects according to (CEB-FIP 1993) and affected by concrete maturity (temperature), used for ring beam 2 and 6.

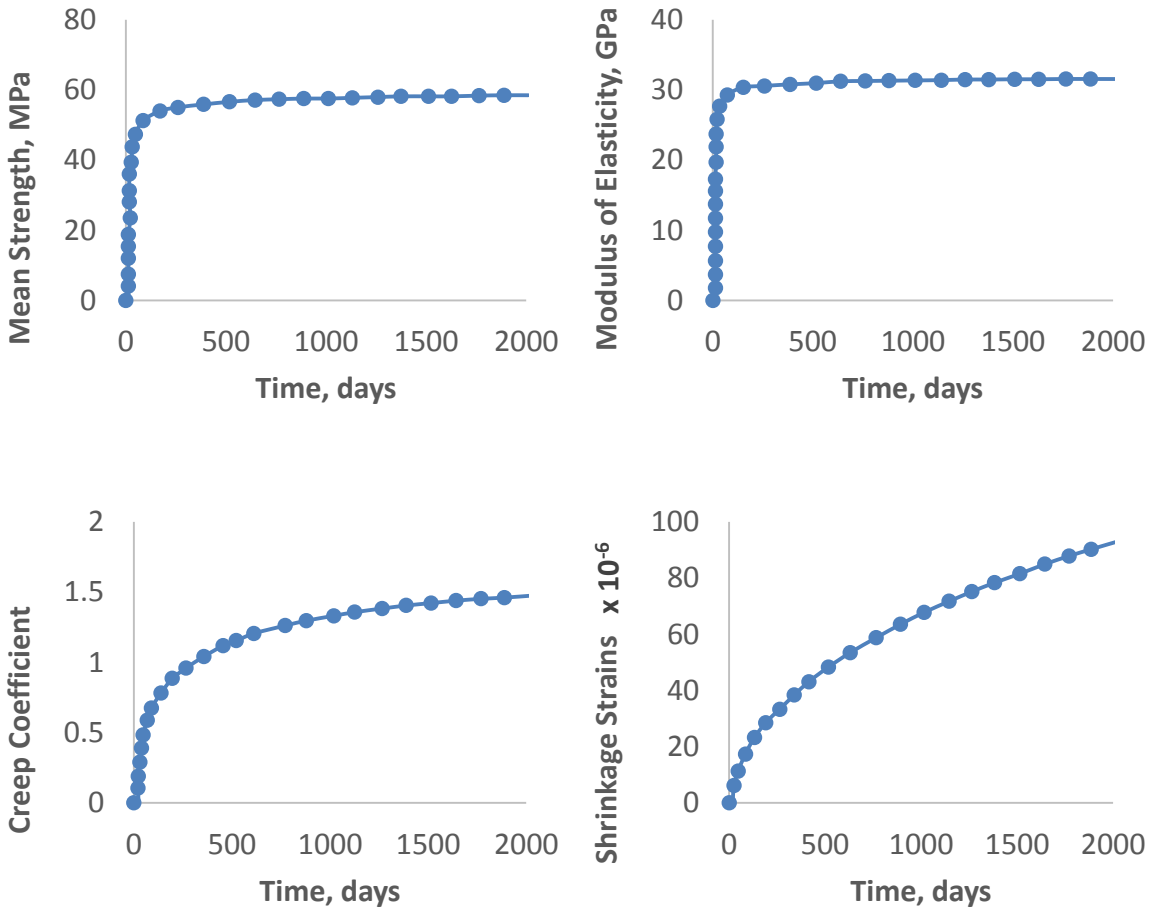

Figure 106. Concrete time dependent effects according to (CEB-FIP 1993) and affected by concrete maturity (temperature), used for ring beam 3, 4 and 5.

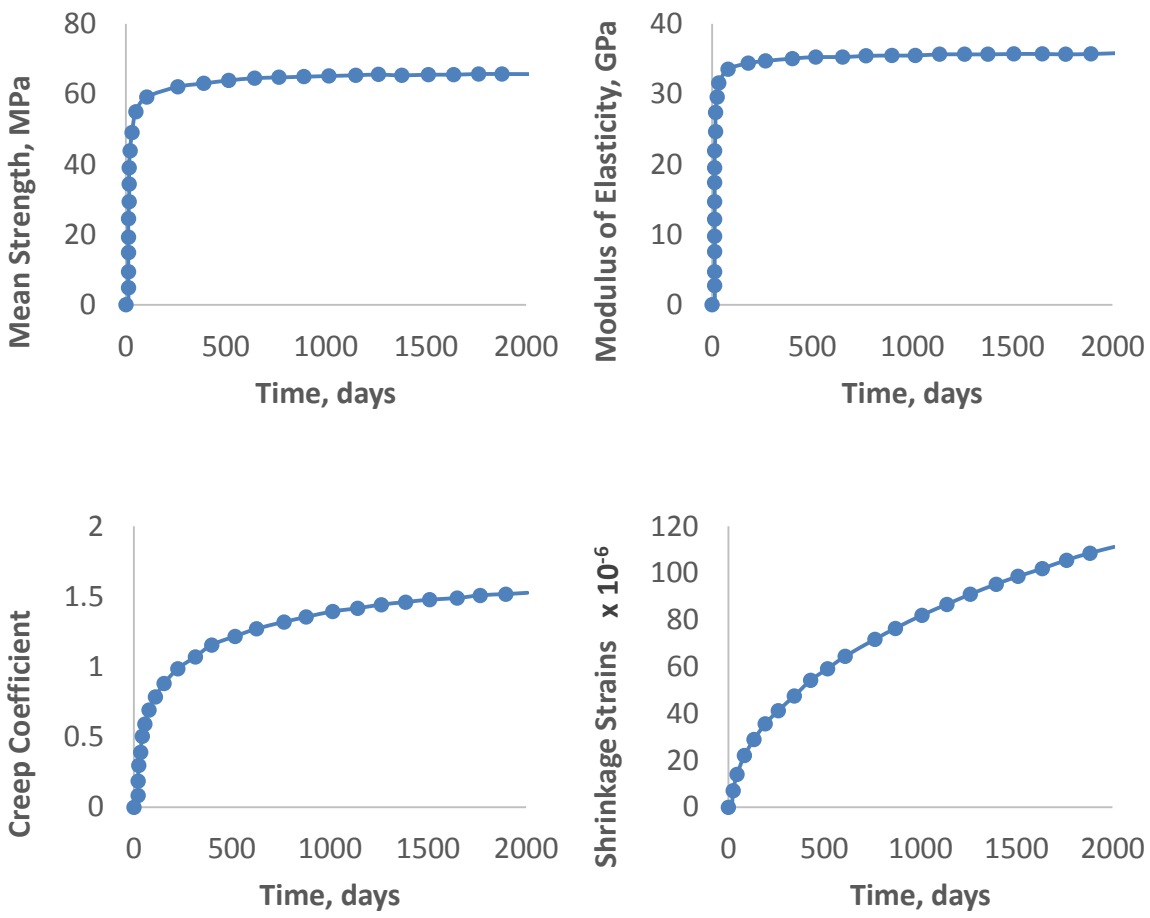

Figure 107. Concrete time dependent effects according to (CEB-FIP 1993) and affected by concrete maturity (temperature), used for ring beam 7.

A scalar factor was used as a coefficient to limit the hyperbolic curves that define ultimate compressive strength, stiffness, creep coefficient and shrinkage strain values. These scalar factors were based on temperature effects, which took into account concrete maturity according to (CEB-FIP 1993) and ACI methodologies updated by (Carino and Lew 2001) and (Wade et al. 2006). From these procedures, a scalar factor for each concrete ring beam was estimated according to the average temperature records during curing time and a constant relative humidity of 75 %.

5.2.3 Staged construction sequence

The SAP2000 back-analyses followed a staged construction sequence matching closely the construction days and completed activities during the actual cofferdam excavation (see Table 17). The staged construction sequence used in the back-analysis is presented in Figure 108.

Lateral deformations were measured for 4.5 years even though the excavations activities took place in a period of time of 329 days. This information allowed the back-analyses to simulate concrete time dependent effects, and evaluate their impact in lateral deformations for a temporary structure as will be presented ahead.

Table 17. Construction day with completed excavation activities information and inclinometer 07 controls.

Construction day	Completed activity	Inclinometer reading
55	• Sheet pile was driven • R.B.1 was installed • Exc.1-2 was done	Installation
61	• R.B.2 was installed • Exc.2-3 was done	Second
69	• R.B.3 was installed • Exc.3-4 was done	Third
89	• R.B.4 was installed • Exc.4-5 was done	Sixth
95	• R.B.5 was installed	Eight
96	• Exc.5-6 was done	Ninth
109	• R.B.6 was installed	Thirteen
112	• Exc.6-7 was done	Fourteen
307	• Exc.7-end was done • R.B.7 was installed	Thirty-sixth
1314	• Without changes	Forty-sixth
1617	• Without changes	Fifty-two

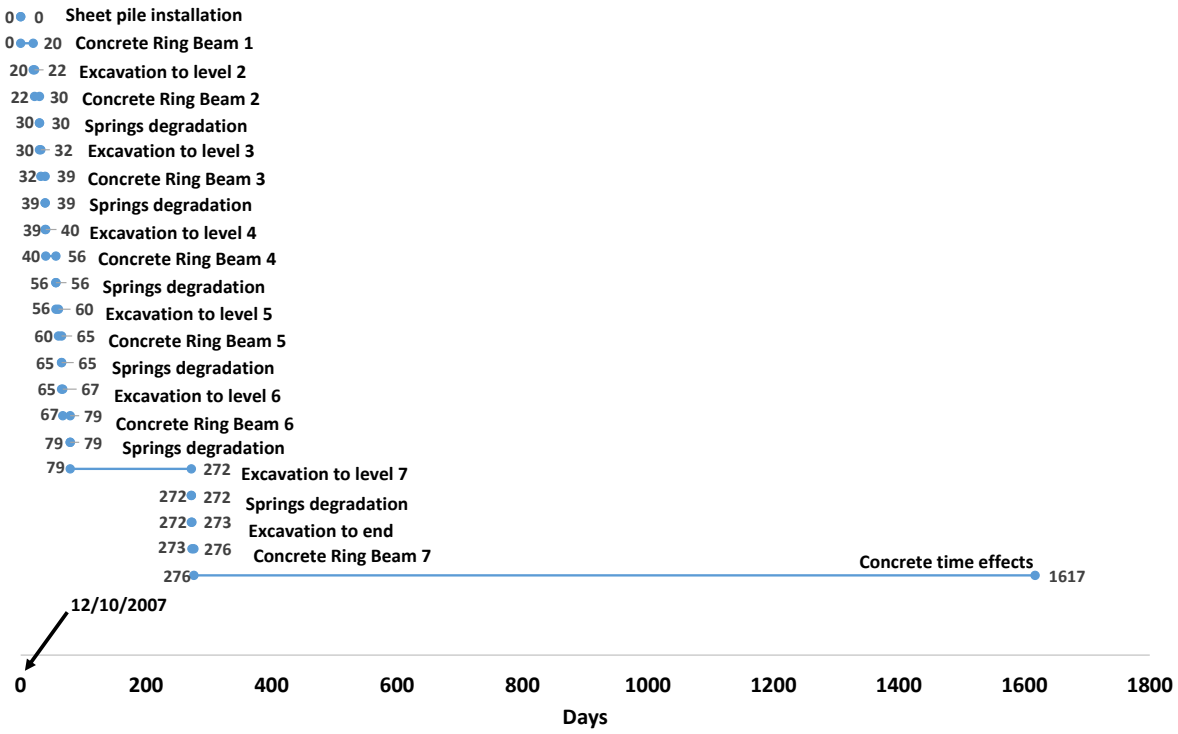

Figure 108. Staged construction sequence followed in SAP2000 V.18.

5.2.4 Employed mesh

The mesh for the base model in SAP2000 is presented in Figure 109. The concrete ring beam are simulated by frame sections elements while the sheet pile wall is included as shell-thins elements following the exact geometry conditions of a PZ-27 section with a structural steel grade of A992Fy50. The cofferdam base was only restricted to vertical displacements as the sheet piles were embedded into Chicago hardpan. For the interlock gap, multi-linear elastic springs, as the ones presented in section 5.2.2.1, were employed. The springs simulate a gradual development of tension stress between the sheet piles as the construction sequence advances. The cofferdam inner passive resistance was modeled with multi-linear elastic springs as explained in Section 5.2.1, while the outer face of the cofferdam structure is loaded by a distributed load representing K_0 and/or active earth pressures. In summary, the model was constructed with 46690 points, 1610 frames, 24840 areas, and 32430 links. All set as multi-linear elastic.

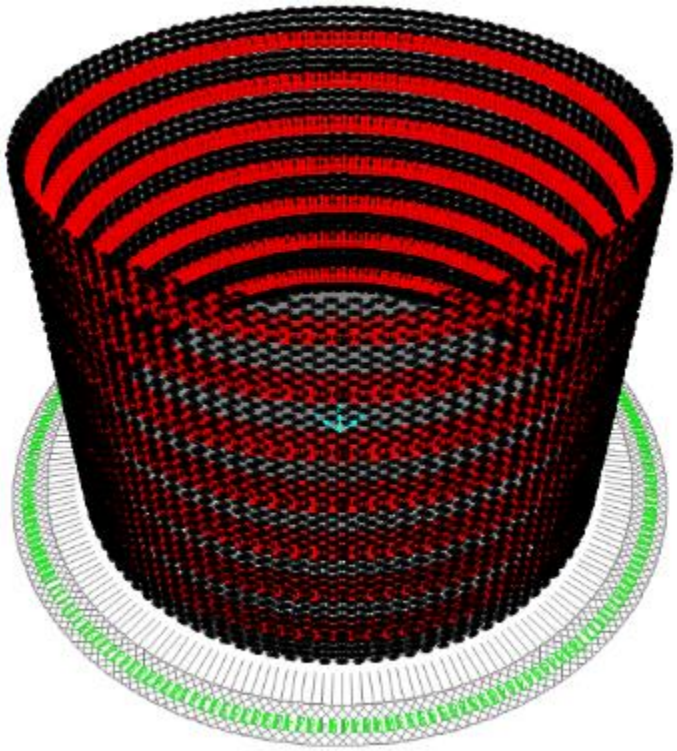

Figure 109. Mesh of the base model in SAP2000 V.18.

5.2.5 Results of the base model

The results from the SAP2000 back-analysis are presented for different cases. Initially, including all concrete time and temperature effects; then, considering each effect individually; and finally neglecting concrete time dependent and temperature effects and modeling the concrete as normally done in practice, i.e., as a liner elastic material with constant properties.

- **5.2.5.1 All concrete time and temperature dependent effects.**

The first back-analyses was performed including all concrete time dependent effects such as compressive strength, modulus of elasticity (stiffness), creep, and shrinkage. The numerical results are compared with the inclinometer records and are presented in Figure 110. The comparison of numerical and observed lateral deformations is done for the excavation stages summarized in Table 17. The deformed 3D model after construction day 1617 is presented in Figure 111.

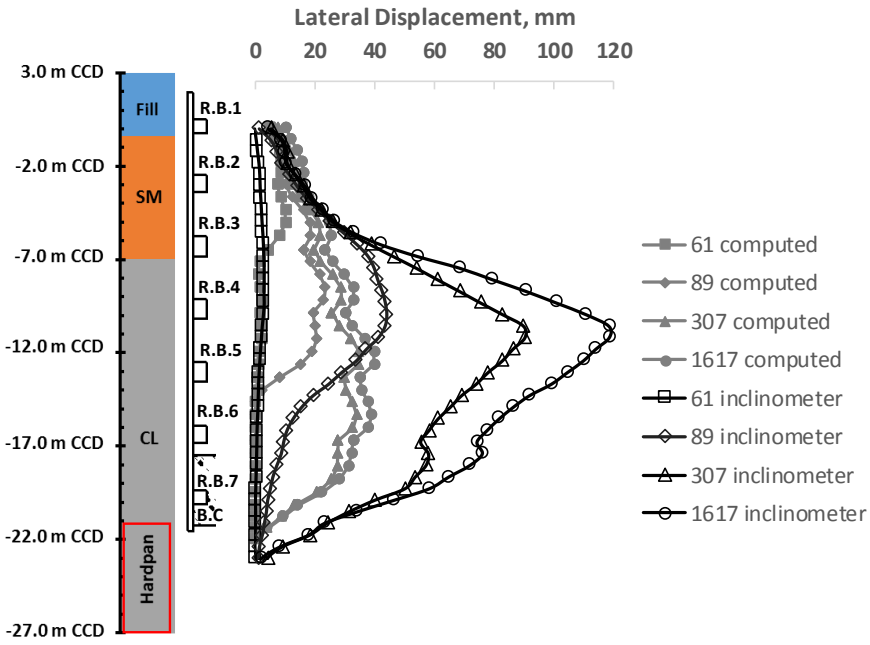

Figure 110. Cofferdam lateral displacements vs. depth including all time and temperature concrete effects.

Figure 111. Cofferdam deformed shape including all concrete time and temperature effects.

From Figure 110 it is clear that the maximum lateral deformation (about 40 mm) computed with the SAP2000 back-analysis underestimates the cofferdam field performance. The main reason for this difference lies in the way soil was simulated

neglecting any soil time effect during the construction stages. In other words, simplified “soil springs” were used inside the cofferdam to model the passive resistance inside the structure, so that reasonable lateral displacements arising from concrete time and temperature effects could be obtained. A SAP2000 model, without any passive resistance in the inner side, would yield excessive ground movements and results that are inconsistent with observed lateral deformation patterns. The soil springs only can model soil stiffness behavior and fall short to capture the characteristic soil time dependent behavior or changes in stress path due to excavation activities. It is well known that SAP2000 is a FEM software intended for structural analysis that presents many limitations for soil behavior modeling. In addition, the simplified construction sequence employed for the computations, where all construction details that took place during the excavation could not be included, affected the computed results yielding significant differences with respect to the field inclinometer. However, the objective of this research is to study the concrete time dependent effects and their influence on a cofferdam braced with concrete ring beams. In that sense, SAP2000 allows for good representation of structural and concrete behavior, so that a parametric study can be performed analyzing concrete time effects individually and coupled with other factors.

- **5.2.5.2. Concrete compressive strength and stiffness as an aging and low temperature effect**

A new analysis was performed to evaluate concrete aging-dependent properties: compressive strength and modulus of elasticity. All other effects such as creep and shrinkage were neglected so that the compressive strength and stiffness effects with time and low temperature conditions can be individually estimated and their impact over the cofferdam performance evaluated. The computed lateral displacement vs. depth response, compared with inclinometer data recorded during the excavation stages, is presented in Figure 112.

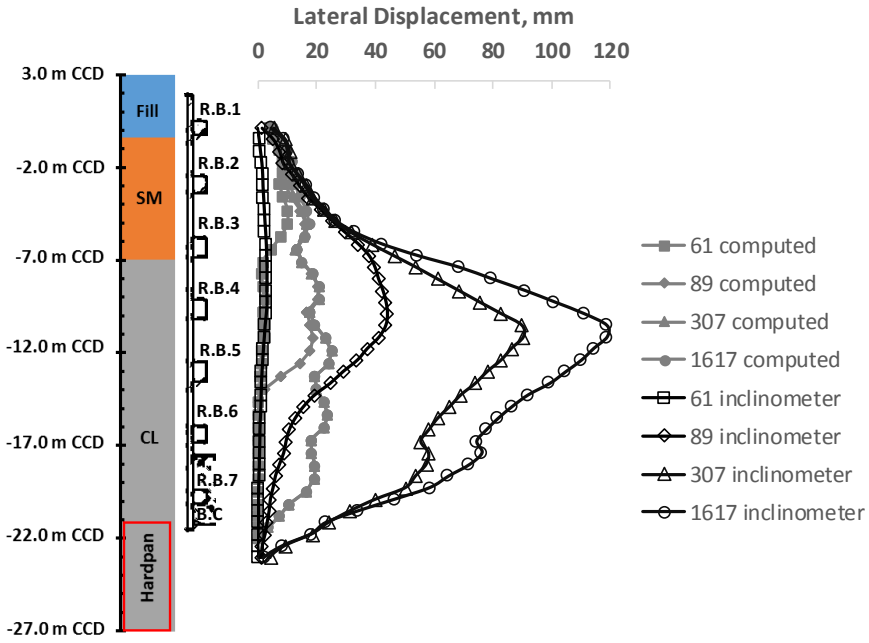

Figure 112. Cofferdam lateral displacements vs. depth including variable compressive strength and stiffness with time and temperature.

Under the abovementioned conditions the maximum computed lateral deformation is about 2.5 cm and is located between the fourth and fifth concrete ring beams. It represents 10.3 % of the maximum lateral deformation including all effects (time and temperature) (see Table 18). The location agrees with the recorded maximum displacement which is located just below the fourth concrete ring beam. When compared with field instrumentation records, the difference between maximum lateral deformations is about 9.5 cm. However, the deformation distribution is similar during the initial staged construction, i.e. before day 89. When the excavation depth reaches the clay layers, the cofferdam performance is highly influenced by changes in soil stiffness, from medium-stiff to soft, and the decrease of the factor of safety against basal heave. These two aspects have been identified as major controlling factors of ground deformations around excavations support systems ((Terzaghi et al. 1996), (Clough and O'Rourke 1990), (Ou et al. 1993), (Bolton et al. 2010) and (Bryson and Zapata-Medina 2012)).

It is important to mention that the inclinometer was installed behind the sheet pile wall within the soil mass. Then, its readings do not entirely represent the actual sheeting lateral

deformation pattern and magnitude. It can explain to a certain degree the differences between the compute sheet pile wall deformation and the observed one.

- **5.2.5.3. Effect of concrete creep on lateral deformations of the cofferdam**

A simulation including concrete as a linear elastic material except for concrete creep and temperature effects was carried out to isolate their impact on the cofferdam response. The computed lateral deformation vs. depth during the excavation simulation is presented in Figure 113. For this case, the maximum computed lateral displacement, at construction day 1617 and for an excavation depth equal to 23.1 m, was about 3.1 cm. This magnitude represents 26.2 % of the maximum computed lateral deformation obtained when all concrete time and temperature effects are included in the analysis (4.0 cm) (see Table 18).

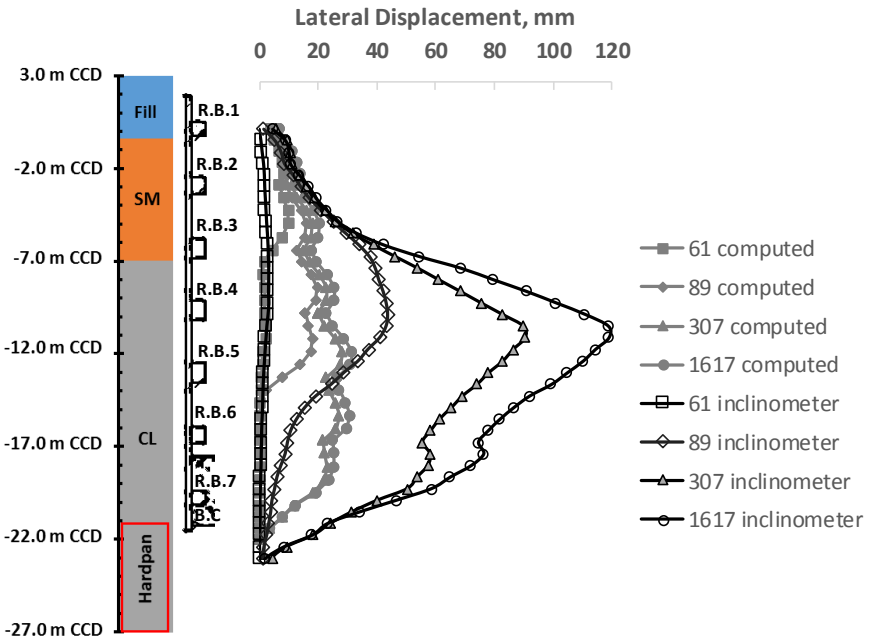

Figure 113. Cofferdam lateral displacements vs. depth including variable creep with time and temperature.

In Figure 113, creep-induced lateral deformations between construction days 307 and 1617 are appreciable (about 3 mm) when compared to those computed for the same dates in Figure 112 where only concrete aging and temperature effects were considered. Creep is a time-dependent effect that theoretically increases with time following a continuous hyperbolic function, unlike the strength and stiffness affected by aging, where the difference between these construction days is basically none. It is because hyperbolic curves defined

for concrete compressive strength and modulus of elasticity reach an early asymptote zone, without significant changes after a 100 days.

- **5.2.5.4. Effect of concrete shrinkage on lateral deformations of the cofferdam**

Similarly to the above case, a simulation including only concrete shrinkage effects over time was performed to individually evaluate shrinkage effects. The computed lateral deformation response, compare to inclinometer data, is presented in Figure 114. The maximum computed lateral deformation, including only shrinkage effects at the construction day 1617 was about 2.1 cm with almost none influence between days 307 and 1617.

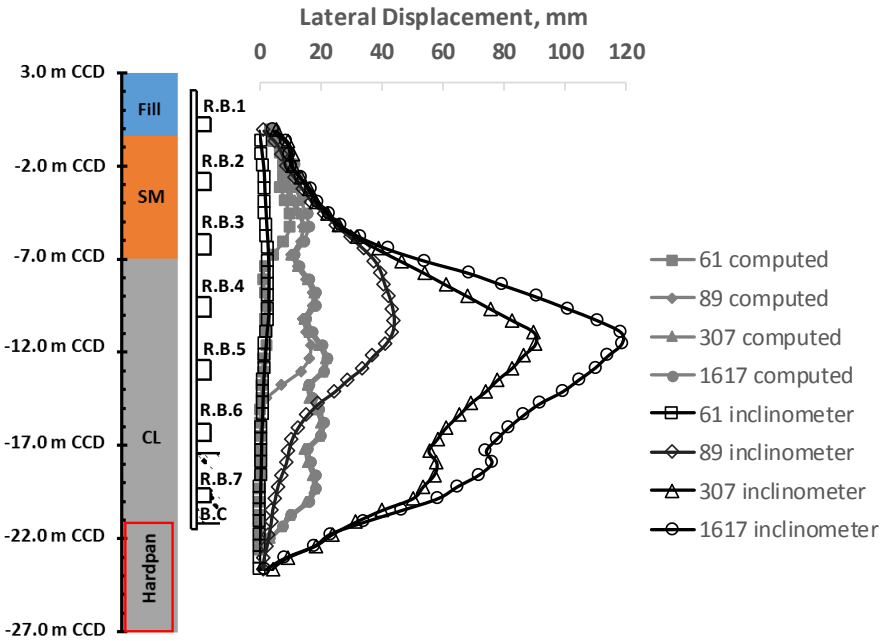

Figure 114. Cofferdam lateral displacements vs. depth including variable shrinkage with time and temperature.

- **5.2.5.5. Effect of modelling concrete as a linear elastic material**

Finally, a numerical simulation of the cofferdam construction was carried out assuming the concrete as a linear elastic material with constant compressive strength and stiffness. Creep and shrinkage over time effects were neglected as done in common practice. The numerical lateral displacements vs. depth are presented in Figure 115. The maximum lateral deformation was 2 cm at the same excavation depth obtained for previous cases.

As expected, there is no change in the computed cofferdam response between construction days 307 and 1617, as creep and shrinkage effects were neglected and the soil was modeled in an elastic way with discrete springs.

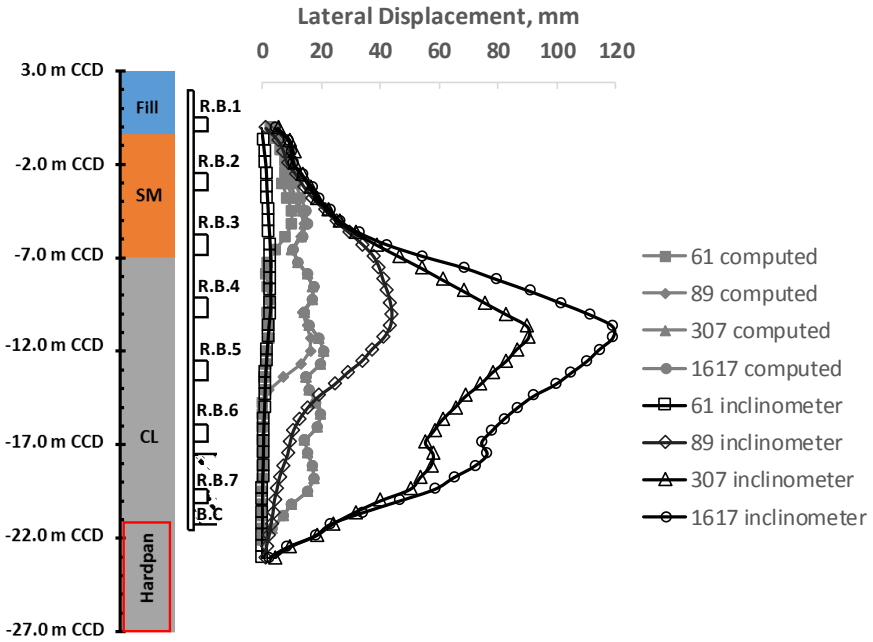

Figure 115. Cofferdam lateral displacements vs. depth assuming concrete as a linear elastic material with constant properties.

- **5.2.5.6. Discussion of isolated and coupled effects**

The maximum computed lateral deformation profile for each of the evaluated scenarios is presented in Figure 116. It can be seen in the figure that all cases present a similar deformation pattern. It is because the lateral soil profile is mainly function of the followed construction stages ((Clough and O'Rourke 1990), (Moormann 2004) and (Finno 2010)) and the multi-linear elastic characteristics defined for the soil springs. So, concrete time and temperature dependent effects only affect the lateral displacement magnitude while the deformation distribution remain almost the same.

Table 18 summarizes the maximum displacement for each computed condition, and the percentage of each effect among over the total displacements where all the concrete time and temperature dependent effects were taken into account. Where δ_{hm} is the maximum horizontal displacement for each simulated case and $\Delta\delta_{hm}$ is the maximum horizontal

displacement difference for each analysis setting respect the case without any concrete time and temperature effect.

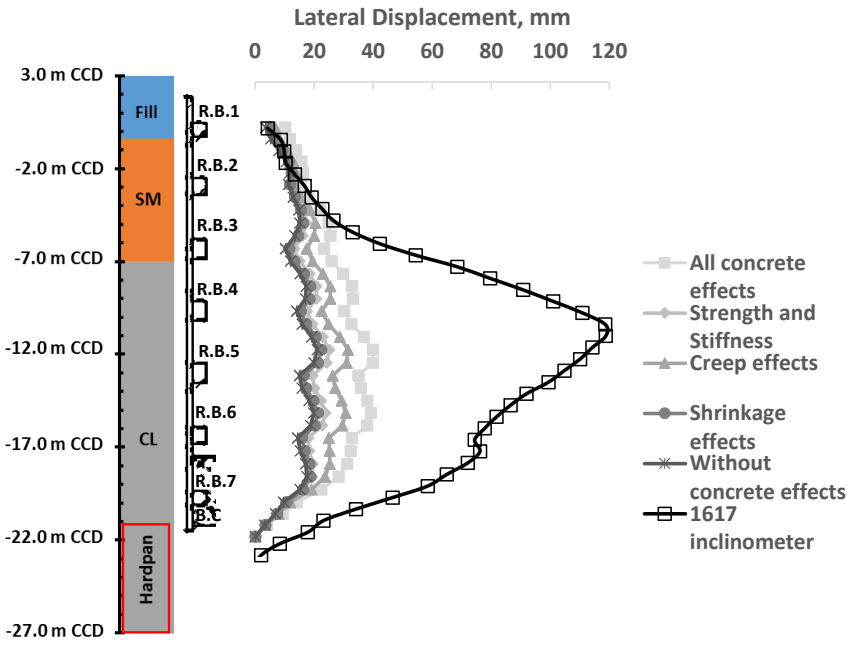

Figure 116. Maximum lateral deformations computed at construction day 1617 for the different considered scenarios.

Table 18. Maximum displacement results from the computed cases.

Computed condition	δ_{hm}, mm	$\Delta\delta_{hm}$, mm	$\Delta\delta_{hm}/\delta_{hm\_max}$
Without concrete time effects	21.0	21.0	52.7%
Strength and Stiffness with aging	25.1	4.1	10.3%
Creep time dependent effects	31.4	10.4	26.2%
Shrinkage time dependent effects	22.4	1.4	3.6%
All concrete time dependent effects	39.8	18.9	-

*All time dependent effects were affected by low temperature conditions.

There is a small difference, about 7.3%, between the computed maximum displacement considering a model with all concrete time and temperature effects and the sum of lateral movements obtained by individually evaluating each effect. This is because the material effects are non-linear and the temperature coefficient does not act in the same scalar way for each computed condition.

In terms of lateral deformation magnitude, we can see from the results summarized in Figure 116 and Table 18 significant differences between the considered cases. Note that for the evaluated cofferdam structure, creep is the most significant concrete time dependent effect with a maximum computed deformation of about 3.1 cm, followed by time variations in concrete compressive strength and stiffness with a maximum lateral displacement of 2.5 cm. It is also important to mention that shrinkage effects only increased lateral displacements in about 1.4 mm, presenting a small contribution to the total lateral movements. Note also that the classical approach employed in the state-of-practice, i.e., assuming concrete as a lineal elastic material with no time-dependent effects, underestimates the induced lateral deformation in about 50% with respect to the simulation including all concrete effects.

It is interesting to note that concrete shrinkage presents a low to negligible impact on the maximum lateral deformations of the considered cofferdam structure. It is contrary to previous results in top-down excavations where shrinkage had the larger impact on the total lateral deformations when concrete time-dependent effects were included (Arboleda-Monsalve and Finno 2015). As shown in Section 4.2.2, shrinkage is a concrete time-dependent effect that is function of the concrete compressive strength, cement type, environmental relative humidity, concrete age, and the notional size of the element. These parameters can be relatively well defined. Then, the difference between the obtained results and those presented by (Arboleda-Monsalve and Finno 2015) for top-down excavations may be attributed to the geometrical properties of the concrete elements employed for lateral support, which are significantly different in cofferdams and top-down excavation support systems. There is an evident difference between a concrete slab and a concrete ring beam size, which directly affects the notional size parameter and therefore the shrinkage strain magnitude. Additionally, concrete ring beams present a large hoop stiffness under compression, limiting the contraction in the inner direction.

To confirm the above results, concrete ring beam 4 was individually evaluated using the software SAP2000 V.18 under isolated creep and shrinkage effects as shown in Figure 117, Figure 118 and Figure 119, respectively. The simulations were run considering (CEB-FIP 2013) and (ACI 209 2008) models and the same earth and water pressures so that the comparison between individual effects can be performed under the same conditions. Creep is presented with strains due to the surrounding pressure and creep itself, and also the

difference by taking away the initial elastic strains. Also, shrinkage of the concrete ring beam was analyzed without any pressure applied to the element to estimate the resultant strain over 1600 days. The obtained results are presented in Figure 117, Figure 118 and Figure 119 and summarized in Table 19.

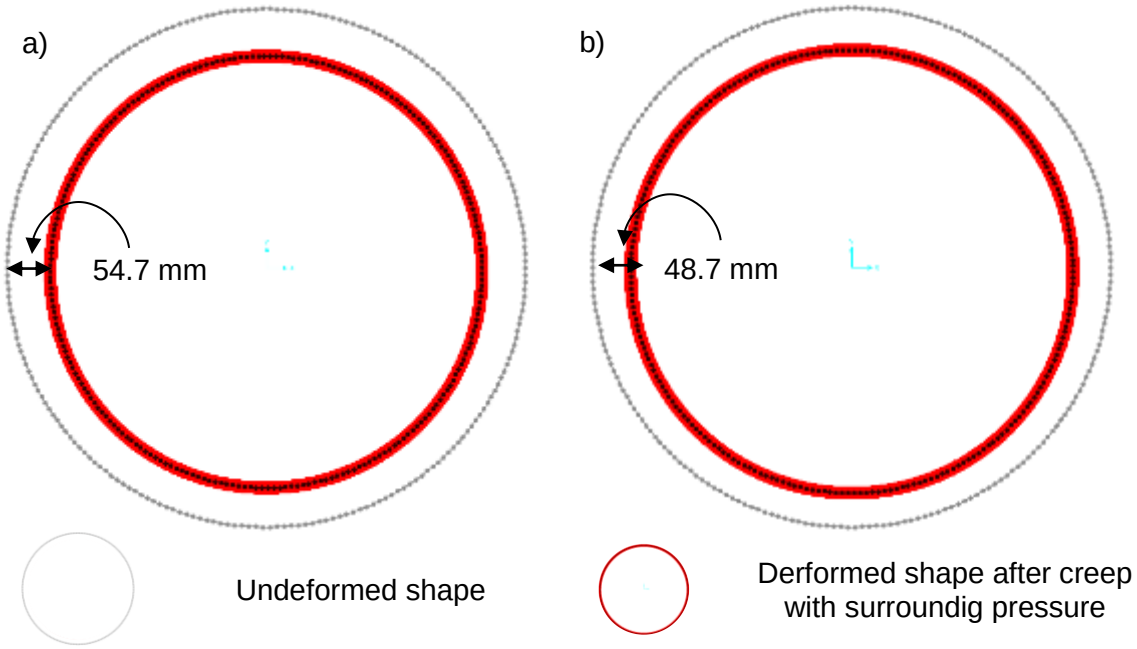

Figure 117. Creep effects over 1600 days with soil and water pressure. a) Fourth concrete ring beam modeled with (CEB-FIP 1993). b) Fourth concrete ring beam modeled with (ACI 209 2008). SAP2000 V.18.results, scale 1:50.

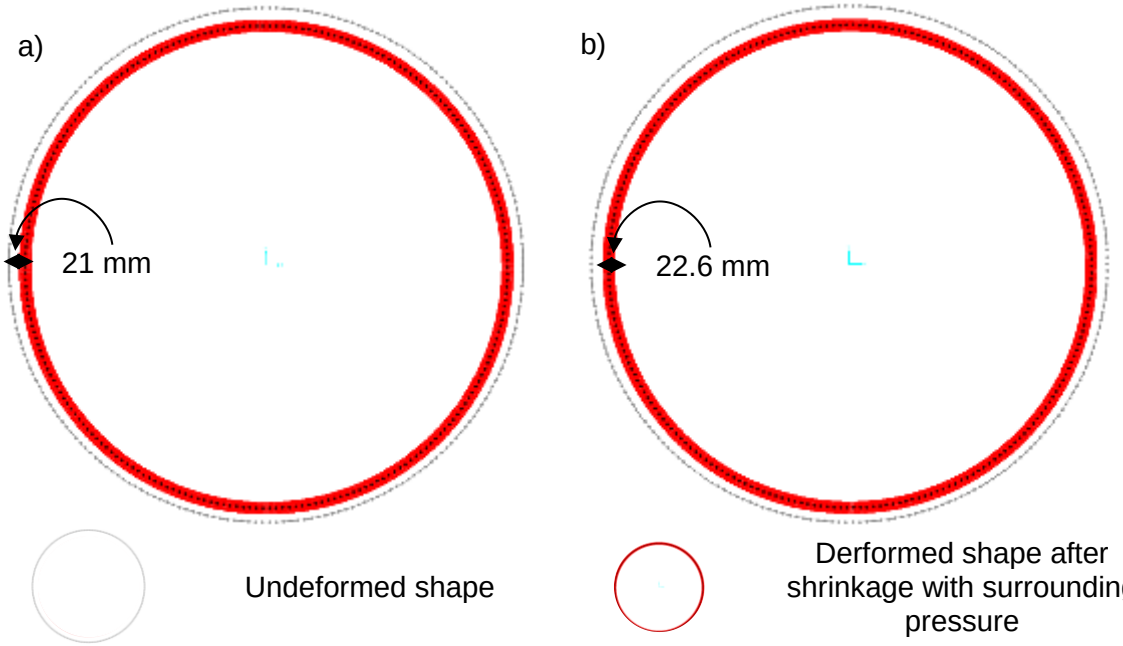

Figure 118. Shrinkage effects over 1600 days with soil and water pressure. a) Fourth concrete ring beam modeled with (CEB-FIP 1993). b) Fourth concrete ring beam modeled with (ACI 209 2008). SAP2000 V.18.results, scale 1:50.

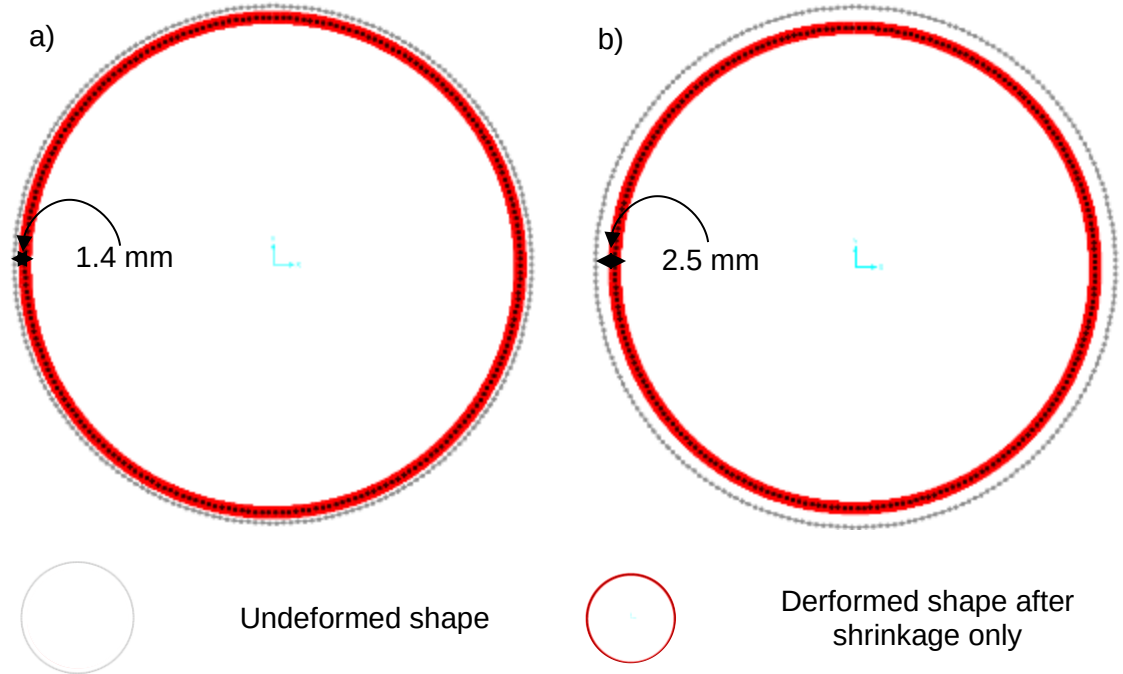

Figure 119. Shrinkage effects over 1600 days without soil and water pressure. a) Fourth concrete ring beam modeled with (CEB-FIP 1993). b) Fourth concrete ring beam modeled with (ACI 209 2008). SAP2000 V.18.results, scale 1:500.

Table 19. Single concrete ring beam analyzed for isolated creep and shrinkage effects in a timer period of 1600 days.

Fourth concrete Ring Beam	Lateral deformation, mm	
	CEB-FIP, 2010	ACI209, 2008
Creep with pressure	54.7	48.7
Creep without initial elastic strain	35.7	29.7
Shrinkage with pressure	21	22.6
Shrinkage without pressure	1.4	2.5

From the single ring beam creep and shrinkage analyses subjected to the same pressure conditions, a clear difference between the computed lateral deformations is observed. These results correlate well with the previous back-analyses where creep effect had a larger impact on lateral displacements than shrinkage, 26 and 3.6 %, respectively. Note also that creep and shrinkage models based on (CEB-FIP 1993), (CEB-FIP 2013) and (ACI 209 2008) methodologies yield similar results. However, as these are time-dependent effects, small differences between them are expected. The results of the analysis of shrinkage under no lateral pressure agree with the initial cofferdam back-analysis, where shrinkage only affects the resultant maximum displacement in 3.6 % of the total displacements computed taking into account all concrete time and temperature effects.

The above results support the premise that the circular geometry of the concrete ring beams adds a stiffer hoop effect on the cofferdam structure that limits shrinkage effects and their resultant deformations. Conversely, creep directly affects the concrete ring beam stiffness by reducing the modulus of elasticity of the material, which could result in larger deformations around the cofferdam under an imposed load.

In comparison with results from top-down analyses as the ones presented by (Arboleda-Monsalve and Finno 2015), these effects have a larger impact on concrete slabs than concrete ring beams due to the volume/surface ratio parameter, which is much smaller in slabs than ring beams causing larger creep and shrinkage effects. In addition, the creep effect in the case of top-down excavations propped with floor slabs is less important than shrinkage as the slabs are extremely rigid in the axial direction to support earth an water pressure, while the ring beams are equally reinforced among their cross-section.

- **5.2.5.7. Analysis closure**

The back-analyses results presented above considered almost all the factors exposed by (Kung 2009) and summarized in Section 2.2, inherent factors were known due to the exploration and the geotechnical characterization performed for the projects initial design process. Design-related factors were also known because the structural elements used for the cofferdam were fully described in the project information. However the construction related-factors were truly a difficult issue to consider during the back-analysis process, although the construction method was clear, prior and simultaneously construction near the excavation was not, for example, from construction reports and pictures is known that the perimeter wall and caissons were constructed while the excavation activities were in process but their construction timing were unclear and impossible to associate with the registered field performance.

For “A” quality predictions and high quality back-analyses, all factors mentioned before should be known in detail, so the difference between computed results and field performance data may be “unquestionable” and discrepancies may be associated with unresolved issues of material behavior.

After the field performance analysis and the computed excavation process, the construction related-factors are considered to be extremely important factors. A misunderstood, a mistake or a bad process can change everything and even compromise the excavation performance or even its stability. For example, the evaluated case history had two important construction related-factors: a very fast construction process and low temperatures, which affected the resultant lateral deformations yielding values larger than the predicted at the final depth of excavation. On the other hand, the design process had an important design-related factor, in which the assumption of concrete as a linear elastic material compromised the estimated excavation performance with large differences from the registered in the field during the construction.

In the previous analyses several factors that affect the excavation performance were simplified and others just not taken into account to simplify the modeling conditions. The presented results still have to be confirmed via a fully coupled analysis where the characteristic soil behavior can be modeled in a more realistic way, time dependent concrete effects can be included, and a detailed construction sequence followed.

Nonetheless, they indicate that in low temperatures and without a proper concrete maturity, excavation-induced deformations larger than expected can develop.

Chapter 6

6. Conclusions and recommendations

The evaluation of the performance of the two case histories presented in this work supports the understanding and prediction of soil-structure behavior for different types of earth support systems. As exposed by (CIRIA C580 2003), the technical literature contains insufficient high-quality data on the performance of retaining structures, making it urgent to collect measurement of more case histories with different soil conditions and support systems. The field performance data presented in this work will help to understand the soil-structure behavior of cofferdam structures. Additionally, the numerical analyses combined with the field performance will help to establish relationships between excavation geometrical factors and resulting wall and ground deformations.

6.1 Conclusions

6.1.1 Concrete time and temperature dependent effects

Based on concrete time and temperature effects computed using (ACI 209 1997), (ACI 209 2008), and (CEB-FIP 1993) models, the following conclusions can be drawn:

- Both ACI and CEB-FIP presented models in their guidelines to estimate compressive strength, stiffness, creep, and shrinkage strains taking into account temperature effects. The evaluated creep and shrinkage models show a good agreement between them for short-term analyses, but for evaluations during long

periods of time they show incremental discrepancies over time. For example for long-term evaluations the ACI formulation predicts twice as much strains than the CEB-FIP model. So these differences should be considered when shrinkage time-dependent effects are evaluated during short or long-term conditions.

- (CEB-FIP 1993) creep and shrinkage models have a great dependency on the notional size of the concrete element and the environmental relative humidity, while ACI models weight more on curing method, maturity and mix specifications.
- Concrete compressive strength and stiffness are function of maturity or aging. If low temperatures are presented, the strength gaining would be compromised and the concrete element would need a longer period of time to reach the designed values. For this condition there are methods to estimate concrete maturity as a function of temperature which is related to aging and therefore compressive strength and stiffness. All the maturity methodologies evaluated in this research estimated a similar behavior and reached similar aging days.
- Curing and testing of concrete cylinders on laboratory installations are far from representing field conditions, especially for projects constructed under extreme temperature and humidity environments. These test must be performed under similar field conditions.

6.1.2 Instrumentation and field performance

Based on the settlement and lateral deformations recorded during the OMPW temporary cofferdam excavation the following conclusions can be drawn:

- The recorded maximum lateral deflection, vertical settlement and ground movement distributions are consistent with the range of values presented for braced excavations (Clough and O'Rourke 1990), (Ou et al. 1993), (Moormann 2004), and (Wang et al. 2009). These ground movements were significant and at some point reach critical limit values based on Chicago city regulations (maximum allowable deformation is 50 mm, (Finno 2010)).Then, cofferdam-induced ground movements, which are commonly neglected because of the temporary nature of the cofferdam structure, must be taken into account to obtain reliable predictions of ground movements.

- The connection Interlock gap between sheet pile sections, which affects the stiffness of the retaining wall, and the gap between the steel ring beams and the sheet piles have an important effect in increasing ground movements and changing the expected lateral wall deflection shape from deep seated to cantilever type. Their coupled effect with soil behavior and other excavation elements is complex and require to be studied in more detailed.

Based on the field performance of the Chicago Downtown cofferdam excavation the following conclusions can be drawn:

- The recorded lateral wall deflections are consistent with the range of values presented for typical braced excavations (Mana and Clough 1981) (Clough and O'Rourke 1990), (Ou et al. 1993), (Moormann 2004), (Wang et al. 2009) and (Bryson and Zapata-Medina 2012). Similar to the OMPW project, the cofferdam-induced ground movements were significant and must be taken into account to obtain reliable predictions of ground movements.
- Accelerated constructions times between concrete ring beam pouring and subsequent soil excavation may have compromised concrete maturity yielding lower compressive strength and stiffness than those considered in the design, and consequently generating additional ground movements.
- Similar to braced and anchored excavations, workmanship quality, construction sequence and associated construction activities highly influence the behavior of cofferdams supported by concrete ring beams. Among them are the accelerated excavation cycles through soft materials and the construction of concrete core foundation caissons at the bottom of the cofferdam which may have decreased the passive resistance and produced secondary side effects such as clay squeeze and piping (Finno et al. 2014).

Based on the OMPW and Chicago Downtown cofferdam field performance comparison the following conclusions can be drawn:

- Under similar soil conditions and excavation depths, both cofferdams, one braced with segmental ring beams and other braced with concrete ring beams, recorded a similar maximum lateral deformation of about 4.5 cm and showed a linear relationship between the maximum lateral displacement and excavation depth.

- The main difference was observed in the measured lateral wall deformation profile. OMPW cofferdam presented a deformation shape similar to a cantilever structure, while Chicago downtown cofferdam showed a deep inward deformation pattern meeting Moormann (2004) premise always presenting its maximum value near the center height of the excavation.
- The cantilever wall movement registered at the OMPW cofferdam is mainly attributed to the gap between the segmental steel ring beams and the sheet piles. The Chicago Downtown cofferdam lateral deformation pattern is controlled by the stiffness of the concrete ring beams which were directly poured against the sheet piles eliminating the gap between the lateral bracing and the retaining wall. Then, it was expected that a cofferdam braced with concrete ring beams would yield smaller ground movements. However, similar deformation magnitudes were recorded as additional movements were induced by delayed concrete maturity, which lead to slow strength and stiffness gain, and concrete time-dependent effects such as creep and shrinkage.
- For Downtown Chicago cofferdam case history, the apparent advantage of using stiffer concrete ring beams over segmental steel ring beams to brace the structure and control ground movements was blighted by an accelerated construction sequence, low concrete curing temperatures, and the inherent time-dependent behavior of concrete. All these combined effects resulted in deformations 4 times larger than the maximum values estimated during design.

6.1.3 Concrete nonlinear behavior associated with excavation procedures

Based on concrete time and temperature effects computed with (CEB-FIP 1993) models and the Chicago Downtown Cofferdam back-analyses the following conclusions can be drawn:

- The concrete stiffness used for the ring beams has a larger impact on computed excavation deformations than soil stiffness, which in this case was represented by multi-linear springs. For large variations in soil-spring stiffness, the computed deformations just varied within millimeters. Conversely, for relatively small

variations in the concrete elasticity modulus, computed lateral deformations varied within centimeters.

- A simplified approach to account for temperature and concrete time-dependent effects is to apply a reduction scalar coefficient to the design compressive strength and therefore stiffness. In this way, compressive strength and stiffness affected by maturity with variable temperature conditions can be obtained.
- Time dependent effects were evidenced in the recorded field performance of the Downtown Chicago cofferdam between long periods of waiting time. Based on field performance data of top-down excavations, (Ou 2006) showed that time dependent effects increase ground deformations between waiting time periods. Direct comparison between field observations and numerical analyses is difficult because the registered ground movements included both, concrete and soil time dependent effects. The employed numerical tool in this work (SAP2000) does not allow for quantification of time-dependent effects in the soil mass.
- The numerical analyses performed for the Chicago Downtown cofferdam showed that concrete time-dependent effects (creep and shrinkage) contribute about 30 % of the total lateral displacements. This result agrees with values reported by (Ou 2006) and (Arboleda-Monsalve and Finno 2015) for top-down excavation where these effects contribute between 30 and 35% of total measured lateral deformations. It is important to mention that field instrumentation always capture a coupled behavior associated with excavation cycles, soil and concrete time dependent effects. These effects are very difficult to estimate and their quantification requires the implementation of complex numerical and coupled analyses.
- The concrete time-dependent effect that most affected the cofferdam horizontal wall displacements was creep. It induced 10.4 mm representing about 26% of the maximum computed lateral deformation.
- Concrete aging, expressed as a reduced compressive strength and stiffness, has also a significant impact on computed lateral displacements. As shown in this work, an accelerated construction sequence resulted in concrete ring beams loaded without reaching their full maturity. It induced a lateral wall deflection of 4.1 mm, which represents about 10 % of the total computed lateral deformations. These deformations correspond to an elastic analysis affected only by a lower stiffness.

This is always valid when concrete elements are not cracked. If cracking is to be considered, larger lateral deformations can be expected.

- Shrinkage only affected the maximum lateral displacement in 1.4 mm, corresponding to about 4% of the total maximum displacement, presenting a low to negligible impact on the maximum lateral deformations of the considered cofferdam structure. It is contrary to previous results in top-down excavations where shrinkage had the larger impact on the total lateral deformations when concrete time-dependent effects were included (Arboleda-Monsalve and Finno 2015). The difference between the obtained results and those presented by (Arboleda-Monsalve and Finno 2015) for top-down excavations may be attributed to the geometrical properties of the concrete elements employed for lateral support, which are significantly different in cofferdams and top-down excavation support systems. There is an evident difference between a concrete slab and a concrete ring beam size, which directly affects the notional size parameter and therefore the shrinkage strain magnitude. Additionally, concrete ring beams present a large hoop stiffness under compression, limiting the contraction in the inner direction. The evaluation of the single concrete ring beam showed that the ring geometry adds a stiffer hoop effect that limits shrinkage effects and their induced deformations. Conversely, creep directly affects the concrete ring beam stiffness by reducing the modulus of elasticity of the material, which result in larger deformations of the retaining structure. This is the fundamental reason for the obtained differences between an axisymmetric cofferdam structure and plane strain excavations supported by concrete ring beams and floor slabs, respectively. In addition, there is the volume/surface ratio parameter which is much smaller for concrete slabs than concrete ring beams causing larger creep and shrinkage effects in slabs than in concrete ring beams.
- For excavations where stability and ground movements are mainly controlled by the concrete quality, as in the case of temporary cofferdams employing a low stiffness retaining wall and concrete ring beams, the nonlinear behavior of the concrete and its time-dependent behavior affect in large proportion the system performance, as shown for the Chicago Downtown cofferdam where the back-analyses yield an increment of about 90 % in the lateral wall deflection.

6.2 Recommendations

Based on a detailed literature review, the observed performance of both case histories and the numerical analyses of the Chicago Downtown cofferdam, the following recommendations are given:

- When concrete elements are constructed under low temperature conditions, ASTM and ACI recommendations during the curing process should be followed so that the concrete can undergo a correct hydration process and reach a properly maturity. Additionally, when significant variations in the concrete normal temperature (20°C) are expected, the design process should explicitly considered these variations to estimate maturity and resulting strength and stiffness values. This is especially critical for bottom-up excavations where retaining elements are directly exposed to the environmental conditions.
- When accelerated construction is required, standardized maturity methods can be used to check concrete strength, stiffness and quality so accelerated constructions cycles can be properly accounted for. However, actual concrete conditions should always be monitored by geotechnical and structural engineers during construction so that expected and actual cofferdam behaviors do not deviate and jeopardize the stability of the excavation and adjacent infrastructure.
- In most of the numerical analysis and available design methodologies, an over average workmanship quality is assumed. In cases where workmanship quality is unknown or under average quality expected, additional factors of safety or even the use of conservative design parameters are suggested. In addition, always install instrumentation to verify design assumptions, control and monitor stresses and ground movements, confirm excavation performance, or take corrective action if necessary. This is an essential part of a geotechnical project, especially when ground movements are critical due to adjacent infrastructure.
- Empirical and semi-empirical correlations available in the technical literature can be used to initially size the elements of urban cofferdams structures and estimate excavation-induced deformations. However, if sensitive infrastructure is located nearby the excavation site, detailed numerical analyses are required for a suitable prediction of ground deformations around the excavation. The employed numerical model should:

i) include an “advanced” constitutive soil model that can correctly represent excavations stress path changes, inherent soil incrementally non-linear behavior which includes a high and constant stiffness at very small strains and a rapid decrease of stiffness with increasing strains.
ii) model material time-dependent effects such as fully couple consolidation analyses for soils; and creep and shrinkage for concrete.
iii) include a detailed construction sequence including activities such as wall installation, deep foundation construction, consolidation, swelling, removal of existing structures and foundations,
iv) consider variable temperature effects in concrete and the resulting maturity, strength and stiffness gain with time.
v) detail in a proper way structural elements and their connections, changes in sections, and stiffness variations.

7. References

ACI. (1980). *ACI Manual of Concrete Practice Part 1 - 1980*. *Manual*, Detroit.

ACI 209. (1997). *ACI 209R-92 Prediction of creep, shrinkage, and temperature effects in concrete structures*. *American Concrete Institute*.

ACI 209. (2008). *Guide for Modeling and Calculating Shrinkage and Creep in Hardened Concrete*. *ACI Committee 209*.

ACI 209.1R. (2005). "Report on Factors Affecting Shrinkage and Creep of Hardened Concrete." American Concrete Institute.

ACI 306R. (2010). "Guide to Cold Weather Concreting." American Concrete Institute, FarmingtonHills.

Arboleda-Monsalve, L. G. (2014). "Performance, Instrumentation and Numerical Simulation of One Museum Park West Excavation." Northwestern University.

Arboleda-Monsalve, L. G. (2015). "RUI: Effects of Pre-excavation Activities on the Performance of Urban Cofferdams."

Arboleda-Monsalve, L. G., and Finno, R. J. (2015). "Influence of Concrete Time-Dependent Effects on the Performance of Top-Down Construction." *Journal of Geotechnical and Geoenvironmental Engineering*, 141(4), 4014120.

ASTM C469-02. (2002). "ASTM C469-02: Standard Test Method for Static Modulus of Elasticity and Poisson's Ratio of Concrete in Compression." *ASTM Standard Book*, 4, 1–5.

Bahar, R., Alimrina, N., and Ouarda, B. (2013). "Interpretation of a pressuremeter test in cohesive soils." *International Conference on Geotechnical Engineering*, (1957), 1–10.

Bazant, Z., and Baweja, S. (2001). "Creep and Shrinkage Prediction Model for Analysis and Design of Concrete Structures : Model B3." *Adam Neville Symposium: Creep and Shrinkage—Structural Design Effects*, 83, 38–39.

Bolton, M. D., Lam, S. Y., and Vardanega, P. J. (2010). "Predicting and controlling ground movements around deep excavations." *Keynote Lecture in Geotechnical Challenges in Urban Regeneration, 11th Int. Conf. DFI-EFFC*, (May), 26–28.

Bowles, J. E. (1997). *Foundation Analysis and Design*. (I. The McGraw-Hill Companies, ed.), The McGraw-Hill Companies, Inc., Peoria.

Braja M., D. (1987). *Theoretical Foundation Engineering*.

Bryson, L. S., and Zapata-Medina, D. G. (2012). “Method for Estimating System Stiffness for Excavation Support Walls.” *Journal of Geotechnical and Geoenvironmental Engineering*, 138(9), 1104–1115.

Budhu, M. (2010). “Soil Mechanics and Foundation.” *John Wiley & Sons, INC.*

Carino, N. J., and Lew, H. S. (2001). *The Maturity Method: From Theory to Application*. USA.

CEB-FIP. (1993). “CEB-FIP model code 1990.”

CEB-FIP. (2013). *FIB Model Code for Concrete Structures 2010*. Lausanne.

Chung, C. K., and Finno, R. J. (1992). “Influence of depositional processes on the geotechnical parameters of Chicago glacial clays.” *Engineering Geology*, 32(4), 225–242.

CIRIA C580. (2003). “Embedded retaining walls.”

Clayton, C. R. I., Woods, R. I., Bond, A. J., and Milititsky, J. (2014). *Earth Pressure and Earth-Retaining Structures*. CRC Press.

Clough, G. W., and Kuppusamy, T. (1985). “FINITE ELEMENT ANALYSES OF LOCK AND D A M 26 COFFERDAM the need for costly high-strength sheet piles along the common wall , the Mississippi River interior cell walls , earth pressures acting on the cells , and cell-wall de- flections . Many of the parame.” *Journal of Geotechnical Engineering*, 111, 521–541.

Clough, G. W., and O’Rourke, T. D. (1990). “‘Construction Induced Movements of Insitu Walls’ Design and Performance of Earth Retaining Structures.” Geotechnical Special publication No. 25.

Clough, G. W., Smith, E. M., and Sweeney, B. P. (1989). “Movement Control of Excavation Support Systems by Iterative Design.” Current Principles and Practices. Foundation Engineering Congress, ASCE.

Command Naval Facilities Engineering. (1971). *Design Manual DM-7*.

Cummings, E. M. (1957). “Cellular Cofferdams and Docks.” *Journal of the Waterways and Harbors Division*, 83(3), 1–29.

Deere, D. U. (1989). *Rock Quality Designation (RQD) After Twenty Years*. Washingon.

FHWA. (1999). *Ground Anchors and Anchored Systems*. (Federal Highway Administration, ed.), Atlanta.

FHWA. (2005). “Micropile Design and Construction - Reference Manual.” FHWA.

FHWA. (2010). *Drilled Shaft: Construction Procedures and LRFD Design Methods*. *FHWA*

NHI-10-016.

Finno, R. J. (2010). “Recent Trends in Supported Excavation Practice.” Evaston.

Finno, R. J., Arboleda-Monsalve, L. G., and Sarabia, F. (2014). “Observed Performance of the One Museum Park West Excavation.” *Journal of Geotechnical …*, (1991), 1–11.

Finno, R. J., Arboleda, L., Kern, K., Kim, T., and Sarabia, F. (2013). “Computed and observed ground movements during top-down construction in Chicago.” Paris.

Gallant, A. p. (2011). “A Parametric Study of Open Cell Cofferdam Construction at the Port of Anchorage Marine Terminal Redevelopment Project.” Northwestern University.

Hansen, B. J. (1953). “Earth Pressure Calculation.” *The Institution of Danish Civil Engineers. The Danish Technical Press of Copenhagen*.

IQBAL, Q. (2009). “The Performance of Diaphragm Type Cellular Cofferdam.” *Proc. Int. Joint Conf. Biometrics*, University of Southampton.

ITACUS. (2011). *Sustainable Underground Development*. Switzerland.

Kim, J.-K., Moon, Y.-H., and Eo, S.-H. (1998). “Compressive Strength Development of Concrete with Different Curing Time and Temperature.” *Cement and Concrete Research*, 28(12), 1761–1773.

Kung, G. T. (2009). “Computers and Geotechnics Comparison of excavation-induced wall deflection using top-down and bottom-up construction methods in Taipei silty clay.” *Computers and Geotechnics*, Elsevier Ltd, 36(3), 373–385.

Lacroix, Y., Esrig, M., and Luscher, U. (1970). “Design, Construction, and Performance of Cellular Cofferdams.” *ASCE 1970 Specialty Conference on Lateral Stresses in the Ground and Design of Earth-Retaining Structures*, 271–328.

Mana, A. I., and Clough, G. W. (1981). “Prediction of Movements for Braced Cut in Clay.” *Journal of Geotechnical Engineering Division ASCE*, 107, 759–777.

Martin, J. R., and Clough, G. W. (1990). *A Study of the Effects of Differential Loadings on Cofferdams*. Vicksburg, Mississippi.

Mikkelsen, P. E. (2003). “Advances in Inclinometer Data Analysis.” 13.

Moormann, C. (2004). “Analysis of Wall and Ground Movements Due To Deep Excavations in Soft Soil Based on a New Worldwide Database.” *Soils and Foundations*, 44(1), 87–98.

Murthy, V. N. S. (2007). *Advanced Foundation Engineering*. CBS Publishers & Distributors, Bangalore, India.

Neville, A. M., and Brooks, J. J. (2010). *Concrete Technology*.

Ou, C.-Y., Hsieh, P.-G., and Chiou, D.-C. (1993). “Characteristics of ground surface settlement during excavation.” *Canadian Geotechnical Journal*, 30(5), 758–767.

Ou, C. Y. (2006). “Deep Excavation, Theory and Practice.”

Ovensen, N. K. (1962). “Cellular Cofferdmas, Calculation Methods and Model Tests.” *The Danish Geotechnical Institute, Copenhagen*, 14.

Packshaw, S. (1962). “Cofferdams.” *ICE Proceedings*, 21(6588), 367–398.

Puller, M. (1996). *Deep Excavations a Practical Manual*. Thomas Telford Publishing, London.

Reese, L. C., Wang, S. T., Isenhower, W. M., Arréllaga, J. A., and Hendrix, J. (2005). “A Program for Analysis of Single Piles Under lateral Load, Version 5.0.18.” Ensoft, Inc., Austin, Tx.

Reese, L., Van Impe, W., and Holtz, R. (2002). *Single Piles and Pile Groups Under Lateral Loading*. *Applied Mechanics Reviews*.

Robert Holtz ; William Kovacs. (1986). “An Introduction to Geotechnical Engineering.” *Engineering Geology*.

Santhosh, H. P., Swamy, H. M. R., and Prabhakara, D. L. (2014). “Construction of Cofferdam -a Case Study.” *Journal of Mechanical and civil engineering*, 2014(34), 45–50.

Sarabia, F. (2012). “Hypoplastic Constitutive Law Adapted to Simulate Excavations in Chicago Glacial Clays.” NorthWestern University.

Schmieg, H., and Vielsack, P. (2002). “Transmission of Shear Forces in Sheet Pile Interlocks.” *October*, (April), 292–297.

Schroeder, W. L., and Maitland, J. K. (1979). “Cellular Bulkheads and Cofferdams.” *Journal of Geotechnical and Geoenvironmental Engineering,* 105, 823–837.

Slope-Indicator. (2006). “Digitilt inclinometer Probe 503 02599.” Washington.

Tan, Y., and Li, M. (2011). “Measured performance of a 26 m deep top-down excavation in downtown Shanghai.” *Canadian Geotechnical Journal*, 48(5), 704–719.

Terzaghi, K., Peck, R. B., and Mesri, G. (1996). “Soil Mechanics in Engineering Practice, Third Edition.” *Wiley-Interscience Publication, John Wiley and Sons, Inc.*, 664 pp.

Uribe-Henao, A. F., and Arboleda-Monsalve, L. G. (2016). “Sheet Pile Interlocks and Ring Beam Installation Effects on the Performance of Urban Cofferdams.” Long Beach.

US Army Corps of Engineers. (1989). *Design of Sheet Pile Cellular Structures Cofferdams and Retaining Structures*. Washington.

Wade, S. A., Schindler, A. K., and Barnes, R. W. (2006). “EVALUATION OF THE

MATURITY METHOD TO.” (1).

Wang, J. H., Xu, Z. H., and Wang, W. D. (2009). “Wall and Ground Movements due to Deep Excavations in Shanghai Soft Soils.” *Journal of Geotechnical and Geoenvironmental Engineering*, 136(7), 985–994.

Westerberg, B. (2008). “Time-dependent effects in the analysis and design of slender concrete compression members Tidsberoende effekter vid analys och.”

Williams, S.G.O.; Little, J. A. (1992). “Structural Behavior of Sheet Piles Interlocked at the Centre of Gravity of the Combined Section.” *Structures & Buildings*, 94, 229–238.

Wissmann, K. J., Filz, G. M., Mosher, R. L., and Martin, J. R. (2003). “Sheet Pile Tensions in Cellular Structures.” *J. Geotech. Geoenviron. Eng.*, 129(3), 224.

Zapata-medina, D. G. (2007). “Semi-Empirical Method for Designing Excavation Support Systems Based on Deformation Control.” University of Kentucky.